SECOND GENERATION ADVANCED REBURNING FOR HIGH EFFICIENCY NOx CONTROL

Phase I Final Report

Project Period: October 1, 1995 - September 30, 1997

Prepared by:
Vladimir M. Zamansky, Peter M. Maly, Loc Ho, Mark S. Sheldon, David Moyeda,
Blair A. Folsom, W. Randall Seeker, William C. Gardiner, Jr. and Vitaly V. Lissianski

July 31, 1997

Submitted by:
Energy and Environmental Research Corporation
18 Mason, Irvine, CA 92618

ABSTRACT

This project develops novel Advanced Reburning (AR) concepts for high efficiency and low cost NO_x control from coal fired utility boilers. AR technologies are based on combination of basic reburning and N-agent/promoter injections. Phase I demonstrated that AR technologies are able to provide effective NO_x control for coal fired combustors. Three technologies were originally envisioned for development: AR-Lean, AR-Rich, and Multiple Injection AR (MIAR). Along with these, three additional technologies were identified during the project: reburning plus promoted SNCR, AR-Lean plus promoted SNCR, and AR-Rich plus promoted SNCR. The promoters are sodium salts, in particular sodium carbonate. These AR technologies have different optimum reburn heat input levels and furnace temperature requirements. For full scale application, an optimum technology can be selected on a boiler-specific basis depending on furnace temperature profile and regions of injector access.

The experimental program included combustion tests in 20 and 200 kW facilities. Pilot scale studies in the 200 kW combustor demonstrated the ability of the AR technologies to achieve NO_x reductions of 95+% during gas firing and 90+% during coal firing. Byproduct emissions were found to be lower than those generated by commercial reburning and SNCR technologies.

A detailed reaction mechanism was developed to model the AR chemical processes. The mechanism (355 reactions of 65 species) includes the following submechanisms: GRI-Mech-2.11, SNCR chemistry, sodium chemistry with Na_2CO_3 decomposition reactions, SO_2/SO_3 reactions, and interaction of HCl with flue gas components. Modeling provided insight into the controlling factors of the process and qualitatively described the observed reaction trends. Modeling predicted and explained the effect of sodium promotion under both fuel-rich and fuel-lean conditions. The sensitivity analysis revealed the most significant elementary reactions affecting formation and destruction of NO and other N-containing compounds in the reburning and burnout zones.

The AR design methodology was updated by using experiments and analytical models to include the second generation improvements. This methodology was then used for application of the novel AR concepts to a 100 MW tangentially fired utility boiler, and to predict the impacts of the AR systems on boiler performance and NO_x emissions. A parallel AR-Lean demonstration (outside the scope of this project) provided an opportunity to test several novel AR components in the field.

Economic analysis demonstrates a considerable economic advantage of AR technologies in comparison with existing commercial NO_x control techniques, such as basic reburning, SNCR, and SCR. Particularly for deep NO_x control, AR results in 2-3 times lower costs (in $/ton of NO_x removed) than SCR for the same level of NO_x control. The market for AR technologies is estimated to be above $1.5 billion.

TABLE OF CONTENTS

LIST OF FIGURES

LIST OF TABLES

1.0 EXECUTIVE SUMMARY

In this project EER is developing second generation enhancements to Advanced Reburning (AR). AR is an NO_x control technology which integrates reburning with injection of a nitrogen reducing agent (N-agent), two well known commercial NO_x control technologies. Reburning involves injection of a hydrocarbon fuel above the burners to produce a fuel rich zone where NO_x is reduced to elemental nitrogen. Overfire air is added to burn out combustibles. Reburning can typically achieve about 60% NO_x reduction in full scale applications. N-agent injection involves the injection of an N-agent such as ammonia or urea into high temperature gases in the convective pass of a boiler where is reduces NO_x to elemental nitrogen. The commercial version of this system is termed Selective Non-Catalytic Reduction (SNCR) and typically achieves 20-40% NO_x reduction in full scale applications.

EER's original configuration of AR (now termed AR-Lean) was developed prior to this project and is currently being demonstrated at full scale. AR-Lean is expected to achieve NO_x reduction in the range of 75-85% in compatible boiler designs. This project is developing second generation AR (SGAR) systems which increase the NO_x reduction to over 95% and broaden applicability to a wide range of boiler designs. This family of SGAR technologies includes various combinations of the following elements:

- Injection of a reburning fuel to produce slightly fuel-rich conditions in the reburn zone where a portion of the NO_x reduction occurs.
- Injection of overfire at a lower temperature range than conventional reburning, typically (1250-1420°K).
- N-agent injection at one or multiple locations: in the reburning zone, with overfire air, and downstream of the overfire air injection to provide the remainder of the NO_x reduction.
- Addition of water soluble promoter additives which enhance the effectiveness of the N-agent NO_x reduction.

By selecting various combinations of these elements, the SGAR systems can be tailored to site specific boiler characteristics to achieve NO_x control ranging from about 60% for reburning alone to as high as 95% for the most complex SGAR system. These SGAR systems can meet the most stringent NO_x control requirements of Title 1 of the Clean Air Act Amendment at considerably less cost than Selective Catalytic Reduction, the only commercial NO_x control technology which can achieve comparable NO_x reduction. In addition, SGAR avoids the massive duct modifications and catalyst replacement/disposal problems of SCR.

At the beginning of the project, EER proposed the development of three SGAR systems differing in the way in which the N-agent injection is integrated with reburning:

- <u>Promoted Advanced Reburning - Lean (AR-Lean)</u> -- This is the original AR configuration but with a promoter added to the N-agent. The N-agent and promoter are injected with

the overfire air.

- <u>Advanced Reburning - Rich (AR-Rich)</u> -- Here, the N-agent is injected into the reburning zone with or without a promoter. This provides increased flexibility in locating the overfire air ports to match the boiler convective pass configuration.

- <u>Multiple Injection Advanced Reburning (MIAR)</u> -- This involves two stages of N- agent injection with promoters: in the reburning zone and with the overfire air. NO_x reduction as high as 95% is achieved by three stages: reburning, rich injection of the N-agent and lean injection o the N-agent.

During the project, the family of SGAR systems was expanded with three additional configurations:

- <u>AR-Lean + SNCR</u> -- This is the integration of the AR-Lean with conventional SNCR where the N-agent is injected downstream of the overfire air with a promoter.

- <u>AR-Rich + SNCR</u> -- This is the integration of AR-Rich with conventional SNCR where the N-agent is injected downstream of the overfire air with a promoter.

- <u>Reburning + Promoted SNCR</u> -- This is basic reburning followed by the promoted SNCR process.

This family of six SGAR configurations allows the NO_x control system to be tailored to site specific requirements. Also, components can be added in building block fashion to increase NO_x reduction as the NO_x regulations become more stringent over time.

This project is being conducted in two phases: Phase I -- Development of a Design Methodology, and Phase II -- Process Optimization and Scale-up.

Phase I consists of the following six tasks:

Task 1.1	Project Coordination and Reporting/Deliverables
Task 1.2	Kinetics of Na_2CO_3 Reactions with Flue Gas Components
Task 1.3	0.1×10^6 Btu/hr Optimization Studies
Task 1.4	1.0×10^6 Btu/hr Process Development Tests
Task 1.5	Mechanism Development and Modeling
Task 1.6	Design Methodology and Application

This report presents the results of Phase I which was conducted over a period of two years. The objectives of Phase I were as follows:

1.   Develop an understanding of the mechanisms through which promoter additives improve N-agent effectiveness.

2.   Develop a kinetic analytical model of the Promoted and Multiple Injection AR technologies.

3.   Optimize the SGAR processes using the analytical model and bench and pilot scale experiments under controlled mixing conditions.

4.   Upgrade EER's AR design methodology to include the second generation advances.

The following Phase I technical performance goals were established in the Project Management Plan:

• NO_x emissions from the 1.0 x 10⁶ Btu coal fired Boiler Simulator Facility should be controlled to less than the requirements for post-RACT NO_x control in the Northeast Ozone Transport Region for the year 2003.

•   The total estimated cost of controlling NO_x emissions based on the 1.0 x 10⁶ Btu/yr coal fired tests should be less than that currently projected for SCR NO_x control systems.

•   SGAR should not cause a significant reduction in boiler efficiency or significant adverse environmental impacts compared to basic reburning and SNCR technologies.

All Phase I objectives and technical performance goals have been met or exceeded, and it was demonstrated that AR technologies can achieve high efficiency and low cost NO_x control.

Initial parametric screening tests were conducted in a bench scale facility, followed by pilot scale developmental studies. Experimental work was paralleled by kinetic modeling which provided a scientific understanding of the process, including the activity of N-agent promoters. Simultaneously, an experimental study was conducted to define the high-temperature chemistry of sodium carbonate under simulated flue gas conditions. The results were used for updating the kinetic model. The modeling used experimental data to define key process parameters, culminating in a design methodology for the eventual scale-up and implementation of the technologies.

A kinetic study on thermal decomposition of Na_2CO_3 was conducted in Task 1.2 using a flow system with Gas Chromatography (GC) and Mass-Spectrometry (MS) analysis of products. It was found that significant decomposition of Na_2CO_3 occurs on a one second time scale at temperatures between 900 and 1300 K. The main decomposition products were identified as CO_2, Na atoms, and Na_2O. The rate of Na_2CO_3 decomposition was measured as functions of temperature, residence time, and initial Na_2CO_3 concentration. The decomposition of Na_2CO_3

from 900 to 1190 K was described kinetically in terms of two irreversible and one reversible reactions: $Na_2CO_3 \rightarrow Na_2O + CO_2$; $Na_2O + CO_2 \rightarrow Na_2CO_3$; and $Na_2O + H_2O <=> 2NaOH$.

In Task 1.3, 0.1×10^6 Btu/hr combustion tests were conducted with natural gas as main and reburning fuel. The promoted AR-Lean process achieved about 86% NO_x reduction at 10% reburning fuel heat input and only 15 ppm Na_2CO_3 in flue gas. The promoted AR-Rich process achieved 88% NO_x reduction at 10% reburning fuel and 15 ppm Na_2CO_3. Thus, the presence of Na_2CO_3 promotes the effect of both "lean" and "rich" N-agent injection. Several sodium compounds (Na_2CO_3, $NaHCO_3$, and $NaOH$) were tested and achieved comparable promotion effectiveness. In AR-Rich, NO_x reduction was enhanced when the N-agent was injected into the reburning zone with a delay time after injection of the reburning fuel. The MIAR process achieved 90-91% NO_x reduction in these bench scale tests and was expected to improve at larger scales since the injectors adversely affected the temperature profile in these small scale tests.

Task 1.4 involved 1.0×10^6 Btu/hr tests in a Boiler Simulator Facility (BSF). Initial experiments were performed with natural gas firing. In AR-Lean, injection of urea or ammonia with OFA provided 45-82% NO reduction depending on the injection temperature. This was consistent with previous EER research. Addition of 15 ppm of Na_2CO_3 promoter to the N-agent greatly improved NO_x reduction. Performance was about equal for ammonia and urea with maximum of 89-94%. In AR-Rich, similar NO_x reduction was obtained for injection of ammonia and urea, 70-77%. However, addition of 15-25 ppm Na_2CO_3 significantly improved NO_x reduction, up to 94- 95%. Two N-agent injections (MIAR) demonstrated 78-82% NO_x reduction without sodium and up to 98% NO_x reduction, with 15 ppm Na_2CO_3. This was the maximum NO_x reduction achieved by AR systems.

Experiments were also conducted with coal firing. The results showed that the AR technologies can provide up to 95% NO_x control for a high-sulfur coal-fired combustor. The NO_x reduction due to N-agent injection was higher, but the effect of sodium promotion was lower in comparison with gas firing. Na_2CO_3 was found to promote performance only by 5-8 percentage points when added at 75 ppm. Maximum NO_x reductions achieved by the promoted AR technologies with coal firing were 90% for AR-Lean, 93% for AR-Rich, and 95% for MIAR. Three other AR modifications: AR-Lean+Promoted SNCR, AR-Rich+Promoted SNCR, and Reburning+Promoted SNCR, provided up to 95, 92, and 93% NO_x reduction, respectively.

A separate study was then conducted to evaluate byproducts emissions from different AR variants in comparison with basic reburning and SNCR. The following emissions were characterized: NO_x, CO, CO_2, O_2, SO_2, N_2O, total hydrocarbons, NH_3, HCN, SO_3, fly ash mass loading, size distribution, PM10, PM2.5, and carbon in ash. The results showed that in most configurations AR technologies have less byproduct emissions than basic reburning and SNCR processes under similar operating conditions.

In Task 1.5, a reaction mechanism, including 355 reactions of 65 chemical species, was developed to characterize the chemical processes of reburning and AR. The mechanism consists of C-H-O-N submechanism (GRI-Mech-2.11, no variation of rate constants) and submechanisms describing SNCR chemistry, and reactions of sodium, sulfur, and chlorine. Modeling was performed using three kinetic programs: Chemkin-2, Senkin (developed by Sandia National Laboratories) and EER's One Dimensional Flame code (ODF). Modeling was capable of predicting major reaction trend, qualitatively describing AR processes, and, in some cases, was close to quantitative process description. Modeling explained why the delayed ammonia injection into the reburning zone is capable of reducing NO concentration and why certain additives, such as oxygen and active radicals, can promote the NO-NH$_3$ interaction in the reburning zone. Modeling also described the NO-NH$_3$ interaction in the burnout zone. A sensitivity analysis was conducted which revealed the most significant elementary reactions affecting formation and destruction of fuel-N compounds in the reburning zone under various conditions. Modeling with different mixing times demonstrated the importance of delayed mixing modes for efficient NO$_x$ reduction. Modeling explained the effect of sodium promoters under both fuel-rich and fuel-lean conditions. Sodium reactions can affect NO$_x$ control by decreasing or increasing the radical pool when it is needed. The radicals in turn can react with NH$_3$ to form NH$_2$ species which reduce NO to molecular nitrogen. The effect of promoters is most pronounced in systems with long characteristic mixing times, as is typical in full-scale industrial applications.

In Task 1.6, EER's reburning design methodology was expanded to SGAR and an economic and market assessment was conducted. To demonstrate the applicability of the methodology, it was applied to a typical 100 MW coal-fired utility boiler with tangentially firing burners, resulting in development of conceptual designs for several second generation AR systems, and predictions of their impacts on boiler NO$_x$ emissions and operating performance. Thermal performance models were used to evaluate the impacts of implementing AR processes on the thermal performance of the boiler. For implementation of AR-Lean, AR-Rich, or MIAR processes, the reburning fuel would be injected into the lower furnace and the overfire air would be injected into the upper furnace in a cavity between the first two tube banks of the convective pass. The overall boiler efficiency for operation with an AR system is similar to that for operation with a basic gas reburning system. The results of the analysis are specific to the boiler configuration evaluated and should not be generalized to other boiler designs. The results of injection system analysis indicate that good mixing of the process streams necessary to implement advanced reburning (AR-Lean, AR-Rich, and MIAR) on the case study boiler can be achieved. Natural gas can be injected from each wall in a pattern which achieves good distribution of the reburning fuel. Overfire air injection into a cavity in the convective pass, needed for implementation of each of the AR processes under consideration, can be achieved using high pressure wall jets. For the AR-Lean and MIAR processes, these ports can also be used to inject the reagent. Injection of reagent into the upper furnace, needed for the AR-Rich and MIAR processes, can be achieved using a lance-based system. Full scale NO$_x$ reduction level is predicted to be above 90% and can be additionally increased with the use of promoters.

The original work scope for this task was based on applying the design methodology to a hypothetical case study; however, it was hoped that an initial AR demonstration could be developed in parallel with Phase I (outside the scope of this DOE project) to allow application to a real unit and evaluation of some of the SGAR elements. EER was successful in developing an initial AR demonstration project. In 1995 EER installed AR-Lean on a 105 MW tangentially fired boiler. Initial AR testing was conducted in 1996 and will continue through 1998. This unit was used as the basis for extending the design methodology. AR-Lean tests on the boiler showed that stratification within the reburn zone could adversely affect the performance. Regions of inadequate CO in the reburning zone reduced the N-agent NO_x control and caused NH_3 slip. While modifications were successful in reducing stratification, this experience shows the importance of mixing and scale up, two factors to be evaluated in Phase II. In addition to these AR-Lean tests, opportunity was taken to obtain preliminary larger scale data on several of the SGAR components including N-agent injection into the reburning zone, N-agent injection downstream of the reburning zone in an SNCR mode, and N-agent injection into the reburning zone and with the overfire air.

An economic analysis was conducted comparing SGAR technologies using gas and coal as reburning fuels with SCR for two representative Title 1 CAAA applications: a cyclone fired boiler and a wall fired boiler equipped with low NO_x burners. The analysis was based on the EPRI Technology Assessment Guide (TAG) methodology which evaluates the total annual levelized cost including capital and operating cost components ($/ton). The unit cost of NO_x control ($/ton) is also calculated. Depending on the specific application, SGAR offers total cost reductions of 48 to 69% over SCR. The market for AR technologies is estimated to be above $1.5 billion.

Additional work is needed in Phase II to move the technology to a demonstration stage. In particular, the following steps are necessary to optimize and scale up the SGAR technologies:

- Identify alternative promoters based on the promotion mechanisms developed in Phase I.
- Identify and test coal mineral compounds responsible for the increased NO_x reduction in AR-Rich and MIAR with coal firing (about 10% higher than for gas firing).
- Optimize mixing (reburn fuel, N-agents, OFA) via combined chemistry/mixing models.
- Optimize N-agent injection to maximize NO_x reduction with negligible ammonia slip.
- Evaluate the effect of N-agent/promoter mixing times representative of full scale.
- Optimize SGAR with new promoters and mixing regimes at 1×10^6 Btu/hr scale.
- Scale up and confirm the design methodology via 10×10^6 Btu/hr Proof-of- Concept tests and limited component tests during the ongoing boiler AR tests.
- Update the economic and market analysis to confirm the advantages of SGAR.

2.0 INTRODUCTION

This project develops a family of novel Advanced Reburning (AR) NO_x control technologies, which have the potential to achieve 95% NO_x control in coal fired boilers at a significantly lower cost than Selective Catalytic Reduction (SCR). AR systems integrate basic reburning and N-agent injection (typically ammonia or urea). Specific features of the new AR systems in comparison with basic reburning include:

- Low heat input of reburn fuel to provide slightly fuel-rich conditions in the reburning zone.
- N-agent injection at one or two locations, including in the reburning zone, along with overfire air, and/or downstream of the overfire air injection.
- Low temperature of overfire air injection (1250-1400 K).
- Injection of promoter additives which enhance the effectiveness of the N-agent.

Phase I consists of six tasks:

Task 1.1	Project Coordination and Reporting/Deliverables
Task 1.2	Kinetics of Na_2CO_3 Reactions with Flue Gas Components
Task 1.3	0.1×10^6 Btu/hr Optimization Studies
Task 1.4	1.0×10^6 Btu/hr Process Development Tests
Task 1.5	Mechanism Development and Modeling
Task 1.6	Design Methodology and Application

The project is currently in schedule, about 94% of the planned activities are completed, and all project objectives and technical performance goals have been met or exceeded. The project work under Tasks 1.2 and 1.6 is underway, however, these results will not change the main conclusions.

Figure 2.1 summarizes the nomenclature for the various regions of the Second Generation Advanced Reburning (SGAR) process. The region upstream of the reburning fuel injection is referred to as the "primary zone" or the main combustion zone. The primary zone Stoichiometric Ratio (SR_1) was maintained at $SR_1=1.1$ for all tests and the initial NO concentration in this zone is referred to by a subscript "i". The region between the reburning fuel and overfire air (OFA) injection is referred to as the "reburning zone" or reburn zone and is maintained at stoichiometry SR_2. The reburning fuel is injected at a temperature of T_1. An N-agent (A_1) can be introduced into the reburn zone at T_2 with a Nitrogen Stoichiometric molar Ratio $NSR_1=A_1/NO$. The NO concentration for NSR calculations is the local amount at the point of N-agent injection. All N-agents can be injected with or without promoters. The rich side N-agent and promoter (Pr_1) are injected with a t_1 delay time after reburn fuel injection. Overfire air is injected at T_3. OFA can serve as a carrier gas for injecting an N-agent (A_2) and promoter Pr_2. A_2 is injected with $NSR_2=A_2/NO$. The downstream region of OFA injection is referred to as the "burnout zone". Stoichiometric ratio in this zone is SR_3. An N-agent (A_3) can also be injected (with or without promoter Pr_3) downstream of the OFA injection location (t_2 delay time, $NSR_3=A_3/NO$) into the burnout zone under conditions of the Selective Non-Catalytic Reduction process (SNCR).
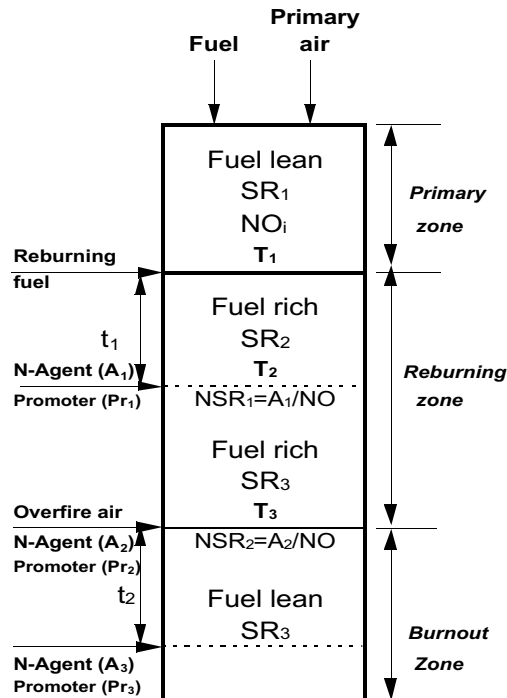
Figure 2.1 SGAR schematic - definitions.

3.0 BACKGROUND

3.1 High Efficiency NO_x Control under Title 1 of the CAAA

Title 1 of the Clean Air Act Amendment (CAAA) of 1990 requires NO_x controls in ozone non-attainment areas. The initial Title 1 regulations, implemented over the last few years, required Reasonably Available Control Technologies (RACT). In most areas, the NO_x levels for RACT are based on Low NO_x Burners (LNB) and are in the range of 0.4 to 0.5 lb/10^6 Btu. As a result, there has been little industry demand for higher efficiency and more expensive NO_x controls such as reburning, SNCR, and SCR. However, the current RACT requirements are not the end of NO_x regulations. Much more stringent NO_x control will be required to bring many of the ozone non-attainment areas into compliance, particularly in the Northeast. The post-RACT requirements are based, to a large extent, on SCR, the commercial technology with the highest NO_x control efficiency.

With SCR, NO_x is reduced to N_2 by reactions with N-agents on the surface of a catalyst. The SCR process effectively uses the N-agent. Injection at a NSR of 1.0 typically achieves about 80% NO_x reduction (i.e., 80% N-agent utilization). SCR is fully commercial in Europe and Japan and there are a few US installations. This is the reason for its extensive use as the basis of NO_x control requirements for post-RACT.

Since the post-RACT NO_x control requirements are largely based on SCR, achieving the required NO_x levels with SCR is relatively easy. However, SCR is far from an ideal utility solution. There are several important problems, and cost leads the list. SCR requires a catalyst in the flue gas exhaust stream. This large catalyst, and its related installation and boiler modifications, are expensive. As SCR technology has advanced over the last decade, the cost has decreased; however, at present, the initial cost of an 80% NO_x control SCR system for a coal fired boiler is

still about a factor of four greater than that of LNB. Increasing the NO_x control to 95% approximately doubles the SCR system cost.

In addition, the SCR catalyst life is limited. Catalyst deactivation, through a number of mechanisms, typically limits catalyst life to about 4 years for coal fired applications. SCR catalysts are also toxic and, therefore, pose disposal problems. Since the catalyst is the major cost element in the SCR system, catalyst replacement and disposal contributes heavily to the total cost of NO_x control.

Thus, there is a need for a high efficiency, low cost NO_x control which utilities could apply to meet post-RACT NO_x control requirements without the problems of SCR discussed above. Ideally, such a technology would meet the following requirements:

1. NO_x control comparable or greater than SCR;
2. Low capital cost compared to SCR;
3. Total cost of NO_x control ($/ton) low compared to SCR and ideally comparable to LNB;
4. Compatible with all types of coal fired units (wall, tangential and cyclone fired);
5. Minimal plant modifications and no requirement to re-route and treat the entire flue gas stream;
6. No major components with limited life (such as the SCR catalyst);
7. No additional emissions of air toxics, criteria pollutants, or toxic solid or liquid waste materials;
8. Ability to integrate with technologies for controlling other pollutants, such as SO_2, air toxics and with projected CO_2 control strategies;
9. Minimal impact on boiler efficiency and operations; and
10. Flexibility to achieve the required level of control with potential to readily implement add-on controls to reach more stringent control levels if required.

3.2 Limitations of Available NO_x Control Technologies for Post-RACT Applications

The suitability of AR for post-RACT applications can best be appreciated by comparing it with the currently available NO_x control technologies. Table 3.1 shows the typical performance for a range of conventional NO_x controls applied to a pulverized coal fired boiler with baseline emissions of 1.0 lb/10^6 Btu. Both the applicability of specific NO_x controls and their performance depend heavily on site specific factors. While the values in the table are generally representative of state of the art performance, each installation will be different.

Table 3.1. Performance of NO_x control technologies.

Technology	Nominal Performance For Baseline NO_x 1.0 lb/10^6 Btu	
	NO_x Reduction (%)	NO_x Emission (lb/10^6 Btu)
Low NO_x Burners	30-50	0.5-0.7
Low NO_x Burners + Overfire Air	50-60	0.4-0.5
Reburning	50-70	0.3-0.5
Selective Non-Catalytic Reduction (SNCR)	40-70	0.3-0.6
Selective Catalytic Reduction (SCR)	80	0.2
AR systems (projected)	80-95	0.05-0.2

Low NO_x burners and overfire air (OFA) provide only modest NO_x control. However, their capital costs are low and, since no reagents are required, their operating costs are near zero. This has made them the technologies of choice for the modest NO_x control required under Title 4 and the initial RACT under Title 1 of the CAAA. However, alone, they cannot approach the NO_x control required for post-RACT or the 90-95% NO_x control goal of the near future.

For deeper NO_x control, reburning, SNCR or SCR can be added to low NO_x burners and OFA, or

installed as stand alone systems. Reburning controls NO_x via fuel staging. The main portion of the fuel is fired through the conventional burners with a small portion of the fuel injected into the furnace above the burners. The result is a fuel rich "reburning zone" where NO_x is reduced by reactions with active radicals formed during interaction of the reburn fuel and oxygen from the main combustion zone. Reburning, alone, can achieve only 50-70% NO_x control and, hence, may not be a candidate for most post-RACT applications.

The reaction of N-agents with NO_x can proceed without a catalyst at high temperatures. This is the SNCR process. It is effective over a narrow "temperature window" centered about 1250 K where the N-agent forms NH_2 radicals which react with NO. The NH_2 radicals are formed from the N-agent via interaction with radicals, e.g.

$$NH_3 + OH \rightarrow NH_2 + H_2O \text{ and } NH_3 + H \rightarrow NH_2 + H_2$$
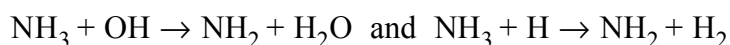
The NH_2 species can reduce NO to molecular nitrogen

$$NH_2 + NO \rightarrow N_2 + H_2O$$
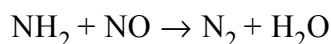
Under ideal laboratory conditions, deep NO_x control can be achieved; however, in practical, full scale installations, the non-uniformity of the temperature profile, difficulties of mixing the N-agent across the full boiler cross section, limited residence time for reactions, and ammonia slip, limit SNCR's effectiveness to about 40%. For typical SNCR conditions with a NSR of 1.5 and 40% NO_x control, the N-agent utilization is only 27%. Thus, while SNCR does not require a catalyst, and, therefore, has a low capital cost compared to SCR, it requires about four times as much N-agent resulting in higher operating costs.

In summary, the NO_x control technologies listed above all have limitations which may prevent

them from successfully achieving cost effective post-RACT compliance.

3.3 Advanced Reburning

The conventional AR process is an EER patented (Seeker et al., 1992) synergetic integration of basic reburning and N-agent injection. In this process, an N-agent is injected along with the OFA and the reburning system is adjusted to optimize the NO_x reduction due to the N-agent. By adjusting the reburning fuel injection rate to achieve near stoichiometric conditions (instead of the fuel rich conditions normally used for reburning), the CO level is controlled and the temperature window for selective NO_x reduction is broadened and deepened. The reburning fuel is reduced from about 20 to about 10% which has considerable economic benefits (the incremental cost of gas for gas reburning and the cost of the coal pulverization equipment for coal reburning). With AR, the NO_x control due to reburning is somewhat reduced, however, this reduction is offset by the significant enhancement of the N-agent NO_x control.

The AR process was developed by EER as part of a DOE program (Chen et al., 1989) focusing on the optimization of basic reburning. Tests were conducted over a range of scales (up to 10 x 10^6 Btu/hr) and achieved above 80% NO_x control. An AR design methodology was developed by extending EER's reburning design methodology. Conventional AR is now being demonstrated at the NYSEG 105 MW Greenidge Station.

3.4 Second Generation Advanced Reburning (SGAR)

Improved versions of the conventional AR process are under development at EER since 1993. They were first predicted by kinetic modeling and then confirmed by 300 kW combustion tests via EER in-house R&D funds. The SGAR systems have the potential to achieve 95% NO_x control on all types of coal fired boilers without massive hardware changes, without increasing air toxic and toxic waste problems, and at a cost for NO_x control on the order of half that of SCR.

These systems will provide flexible installations that allow NO_x levels to be lowered as new elements of the technology become available. The SGAR systems incorporate several improvements over conventional AR, such as:

- N-agent injection into the reburning zone;
- Promoter additives which enhance the effectiveness of the N-agent; and
- Injection of N-agents with or without promoters at two locations.

Sodium salts, in particular sodium carbonate (Na_2CO_3) were identified as effective AR promoters. By integrating these improvements with conventional AR, NO_x control can be increased to 90-95% for cyclone units and even higher for pulverized coal fired units (wall and tangentially fired) where AR can be further integrated with low NO_x burners and overfire air. This family of AR technologies is intended for post-RACT applications in ozone non-attainment areas where NO_x control in excess of 80% is required.

Three SGAR systems were originally proposed to DOE under the 1994 PRDA solicitation. They include:

- <u>Promoted Advanced Reburning - Lean (AR-Lean)</u> - conventional AR (N-agent injected with the OFA) which can be used with a promoter added to the agent.
- <u>Advanced Reburning - Rich (AR-Rich)</u> - N-agent injection with or without a promoter into the reburning zone.
- <u>Multiple Injection Advanced Reburning (MIAR)</u> - N-agents with promoters injected in two locations: within the reburning zone and with the OFA.

4.0 PHASE I PROGRAM OBJECTIVES

The overall objective of Phase I was to demonstrate the effectiveness of the SGAR technologies at bench and pilot scale over a sufficiently broad range of conditions to provide all of the information needed for process optimization and scale up. The Phase I program is conducted over a two year period. Specific program objectives were as follows:

1. Develop an understanding of the mechanisms through which promoter additives improve N-agent effectiveness;
2. Develop a kinetic analytical model of the Promoted and Multiple Injection AR technologies;
3. Optimize the SGAR processes using the analytical model and bench and pilot scale experiments under controlled mixing conditions; and
4. Upgrade EER's AR design methodology to include the second generation advances.

Phase I project determines the ability of the SGAR technologies to meet the following technical performance goals:

* NO_x emissions from the 1×10^6 Btu/hr coal fired Boiler Simulator Facility controlled to less than the requirements for post-RACT NO_x control in the NESCAUM area for the year 2003;
* Total estimated cost of controlling NO_x emissions based on the 1×10^6 Btu/hr coal fired tests less than that currently projected for SCR NO_x control systems; and
* No significant reduction in boiler efficiency or significant adverse environmental impacts when compared to current reburning and SNCR technologies.

Figure 4.1 shows the task structure and the major milestones for the program. Task 1.1, Project Coordination and Reporting/Deliverables, coordinates the efforts of the Key Personnel involved with the project so that the objectives of this project are met: on time, on specification, and on budget. Phase I experimental work started from parametric screening tests at a bench scale facility (Task 1.3), followed by pilot scale developmental studies (Task 1.4). The Phase I program utilized two EER test facilities providing nominal thermal capacities of 0.1 and 1×10^6 Btu/hr. The experimental work was paralleled by kinetic modeling (Task 1.5) which provided a scientific understanding of the process, including the activity of N-agent promoters. A detailed reaction mechanism of the SGAR processes was developed based on available combustion chemistry data. Simultaneously, an experimental study (Task 1.2) was conducted at the University of Texas to

define high-temperature chemistry of sodium carbonate under simulated flue gas conditions. The results were used for updating the kinetic model. The modeling used experimental data to define key process parameters, culminating in upgrading EER's existing design methodology for conventional AR to include the second generation improvements (Task 1.6).

Project Initiation:
Detailed Work Plan
Kick-off Meeting at FETC, 12/95

10/01/95

**Sodium Kinetics
Task 1.2**

**Optimization Tests
Task 1.3**

**Kinetic Modeling
Task 1.5**

Project Review Meeting
at FETC, 7/96

**Development Tests
Task 1.4**

**Design/Applications
Task 1.6**

Project Review Meeting
at FETC, 7/97

7/31/97

7/31/97

9/30/97

**Phase II
Proposal**

**Draft
Final
Report**

**Approved
Final
Report**
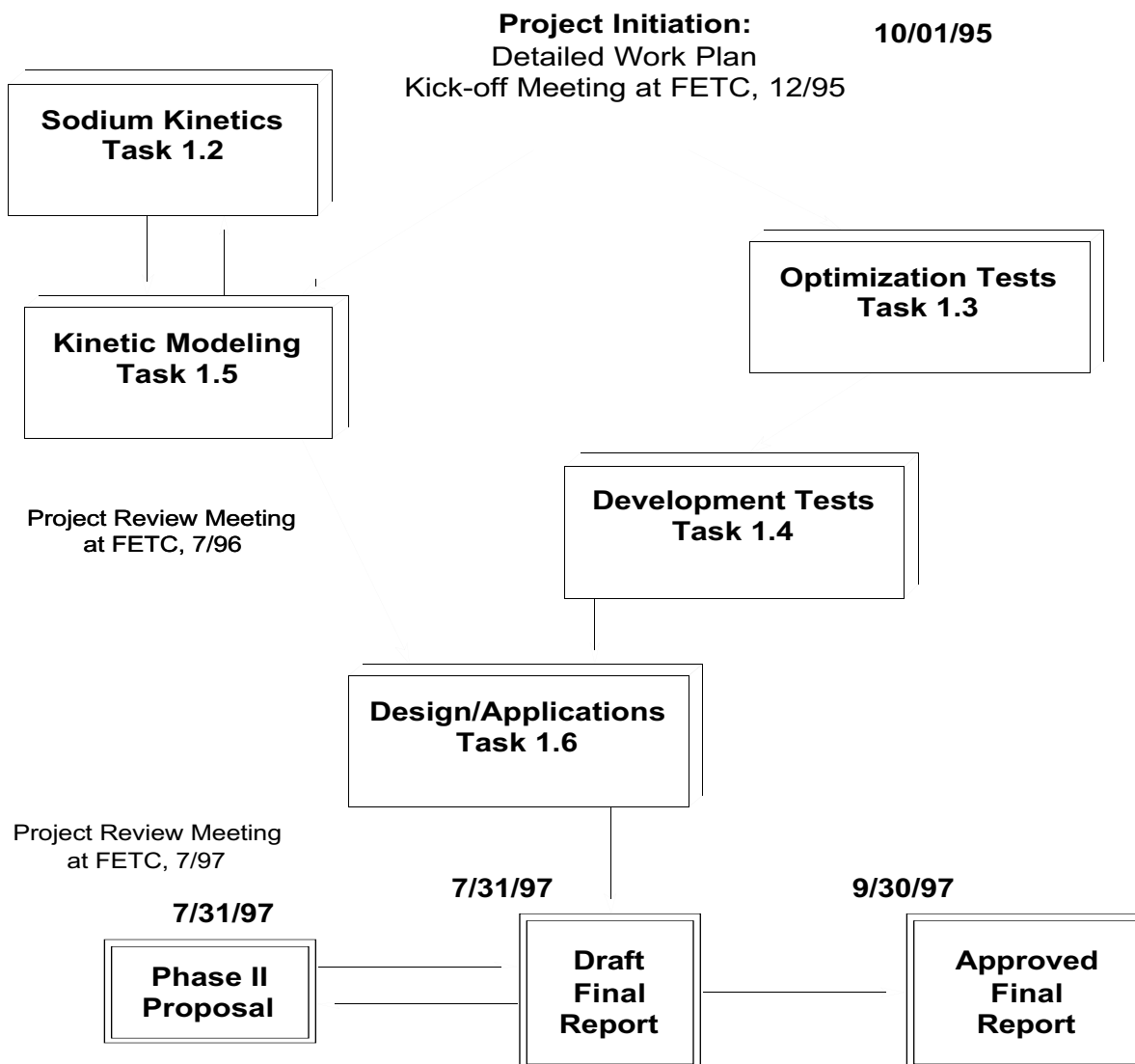
Figure 4.1. Phase I task structure and major milestones.

4-2

5.0 KINETICS OF Na_2CO_3 REACTIONS WITH FLUE GAS

5.1 Literature Review

Although salts of alkali metals have long been used as flame inhibitors (Mitani and Nioka, 1984; Jensen and Jones, 1982), the chemical mechanism of their decomposition at high temperatures is not well known. On the other hand, decomposition of sodium bicarbonate $NaHCO_3$, (Wu and Shih, 1993; Heda et al., 1995) sodium carbonate perhydrate $Na_2CO_3 \cdot 1.5H_2O_2$ (Galwey and Hood, 1979) and double salts which occur in the $Na_2CO_3 \cdot NaHCO_3 \cdot H_2O$ system (Ball et al., 1992) at low temperatures has been studied intensively, primarily because thermal decomposition of these salts can produce a highly porous Na_2CO_3 product which can be used for SO_2 removal from waste gases. It was found that decomposition of these salts starts at around 350 K; by 500 K they are practically completely converted into Na_2CO_3 and H_2O

$$NaHCO_3 \rightarrow 0.5Na_2CO_3 + 0.5CO_2 + 0.5H_2O \qquad (5.1)$$

$$Na_2CO_3 \cdot 1.5H_2O_2 \rightarrow Na_2CO_3 + 1.5H_2O + 0.75O_2 \qquad (5.2)$$

$$6(Na_2CO_3 \cdot NaHCO_3 \cdot 2H_2O) \rightarrow 9Na_2CO_3 + 3CO_2 + 15H_2O \qquad (5.3)$$
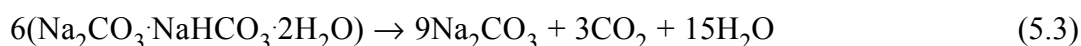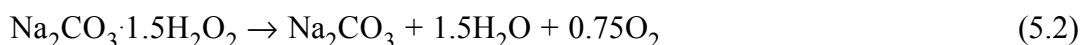
Decomposition of Na_2CO_3 thus determines rate of decomposition of other salts of Na and carbonic acid at still higher temperatures, and very little is known about the decomposition mechanism of Na_2CO_3. It was found that the time scale for flame inhibition by Na_2CO_3 is about 10 ms at 1200 K and 0.5 ms at 1800 K, which is thought to correspond to the decomposition time of Na_2CO_3. (Mitani and Nioka, 1984) The inhibiting effect of salts on flame was attributed (Jensen and Jones, 1982) to catalytic removal of H atoms and OH radicals in the chain

$$NaOH + H \rightarrow Na + H_2O \qquad (5.4)$$

$$Na + OH + M \rightarrow NaOH + M \qquad\qquad (5.5)$$

While Na atoms in flames have been studied for years, (Carabetta and Kaskan, 1968; Hynes et al., 1984; Srinivasachar et al., 1990; Schofield and Steinberg, 1992) their reaction mechanisms are not well understood, and the rate coefficients of some important reactions are not known. Apparently Na, NaO, NaO_2, and NaOH are coupled to one another in flames by fast reactions which rapidly interconvert one species to another as conditions vary. (Hynes et al., 1984; Schofield and Steinberg, 1992) Analysis of Na influences on $H_2-O_2-N_2$ flames led to the conclusion that the Na chemistry is largely controlled by

$$Na + H_2O \rightarrow NaOH + H \qquad\qquad (5.6)$$

$$Na + O_2 + M \rightarrow NaO_2 + M \qquad\qquad (5.7)$$

$$NaO_2 + H \rightarrow NaO + OH \qquad\qquad (5.8)$$

$$NaOH + OH \rightarrow NaO + H_2O \qquad\qquad (5.9)$$

At temperatures above 2300 K the main channel for Na disappearance is reaction (5.6). As temperature decreases, however, the importance of NaO_2 increases and the predominant depletion of sodium is via reaction (5.7). Kaskan (1971) concluded that reaction (5.7) is the dominant Na oxidation process in lean $H_2-O_2-N_2$ flames at temperatures from 1400 to 1700 K. Other observations also support NaO_2 as an important intermediate species at temperatures below 1900 K. (McEwan and Phillips, 1966) However, contradictory values of the rate coefficient for the reaction (5.7) have been reported. (Kaskan, 1971; McEwan and Phillips, 1966; Husain and Plane, 1982)

Ho et al. (1993) and Chen et al. (1993) considered the feasibility of using sodium (a representative alkali metal) salts to control N_2O emissions from combustion sources. Perry and Miller (1996) investigated this process by dynamic modeling and concluded that the key reaction

is

$$Na + N_2O \rightarrow NaO + N_2 \qquad (5.10)$$

where sodium atoms are produced by the reverse of reaction (5.6). This explanation, however, is not the only possible one. The same effect of N_2O removal could be explained by the reaction

$$N_2O + OH \rightarrow N_2 + HO_2 \qquad (5.11)$$

since sodium hydroxide additive enhances production of active species like OH (reaction (5.5)) already present in exhaust gases.

The literature review thus shows that practically no information is available about the rate of Na_2CO_3 decomposition at high temperatures. The active species formed during decomposition are not well defined either, and as a result the mechanism of Na_2CO_3 influences on high temperature chemistry is essentially unknown.

5.2 Thermodynamics of Sodium in Combustion Flue Gas

5.2.1 The Solid to Gas-Phase Transition

Sodium carbonate melts at 1120 K and is relatively stable at still more elevated temperatures—according to a textbook of inorganic chemistry (Bailar et al. 1973) it does not decompose until 1220 K. Thermodynamic calculations based on the EER thermochemical data base show that $\Delta_r G°$ for the reaction

$$Na_2CO_3 \leftrightarrow Na_2O + CO_2 \qquad (5.12)$$

changes sign from positive to negative in the temperature range 2400–2500 K (Figure 5.2.1), making reaction (5.12) "spontaneous" only at temperatures above 2400 K. Since the most common way to supply Na_2CO_3 is as an aqueous solution, one also has to consider the spontaneity of

$$Na_2CO_3 + H_2O \leftrightarrow 2NaOH + CO_2 \qquad\qquad (5.13)$$

Figure 5.2.1 shows that reaction (5.13) becomes spontaneous (in the sense that P_{CO2} is greater than P_{H2O}) at temperatures above 2000 K. Thermodynamic calculations thus show that reactions (5.12) and (5.13) for all species in their standard states are not spontaneous at temperatures normally achieved in the flow system, i.e., less than 1400 K. This statement does not mean, however, that at low Na_2CO_3 concentrations significant conversion of Na_2CO_3 to products can not be achieved. The equilibrium partial pressure of CO_2 in reaction (5.12) over the surface of liquid or solid Na_2CO_3 calculated using values of $\Delta_r G^\circ$ from Figure 5.2.1 is equal to 0.01 Torr at 1400 K. The statement "reaction (5.12) is not spontaneous at 1400 K" means that Na_2CO_3 decomposes at that temperature only until the partial pressure of CO_2 reaches 0.01 Torr. Thus if the amount of Na_2CO_3 is very small, all of it might decompose and the partial pressure of CO_2 still be less than 0.01 Torr. Figure 5.2.2 illustrates this idea by showing how Na_2CO_3 to CO_2 conversion (based on equation (5.13)) at chemical and phase equilibrium at a total pressure of 1 atmosphere depends on temperature at initial Na_2CO_3 concentrations of 100, 300 and 500 ppm, typical concentrations used in our flow system experiments and proposed for pollution control in flue gas. The assumed amount of H_2O in the mixture is 20%, the rest is N_2. Conversion in Figure 5.2.2 is defined as the concentration ratio $[CO_2]/[Na_2CO_3]_0$, where $[Na_2CO_3]_0$ is the initial concentration of sodium carbonate. The calculations were performed using the EER thermochemistry data base and the NASA program CET89 (Feitelberg, 1994), which calculates chemical equilibrium compositions taking into account both gaseous and condensed-phase reactants and products. It is clear from Figure 5.2.2 that significant decomposition of Na_2CO_3

occurs in the temperature range from 1000 to 1500 K even though reaction (5.12) is not spontaneous at these temperatures in the ordinary thermochemical sense. The dependence of conversion on the initial amount of Na_2CO_3 is evident—as the initial concentration decreases, fractional conversion of Na_2CO_3 to CO_2 is more complete.
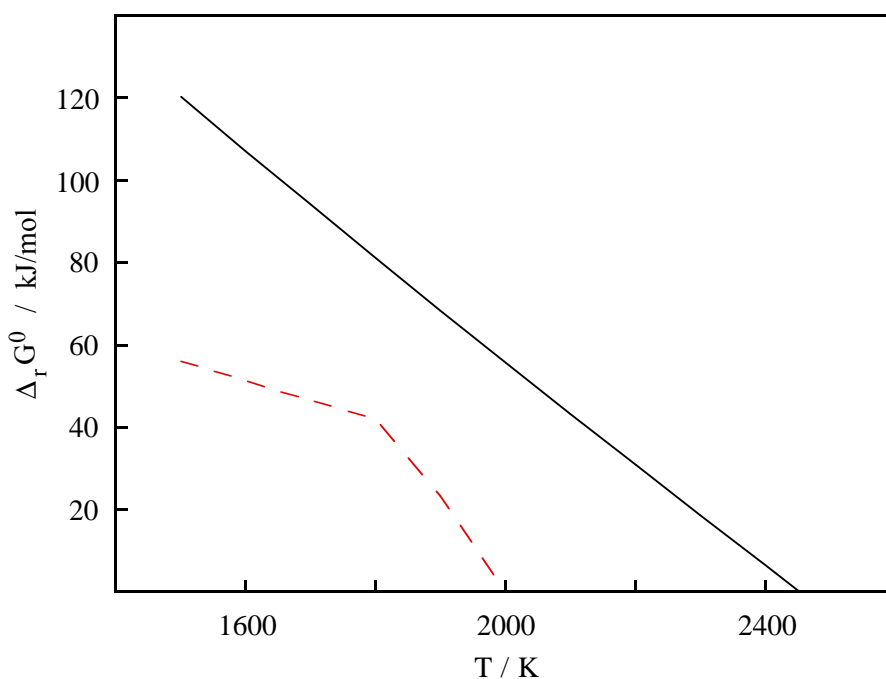
Figure 5.2.1. Dependence of $\Delta_r G°$ (EER thermochemistry) for $Na_2CO_3 \leftrightarrow Na_2O + CO_2$ (solid) and $Na_2CO_3 + H_2O \leftrightarrow 2NaOH + CO_2$ (dashed) on temperature. The break in the dashed line corresponds to the melting temperature of NaOH.
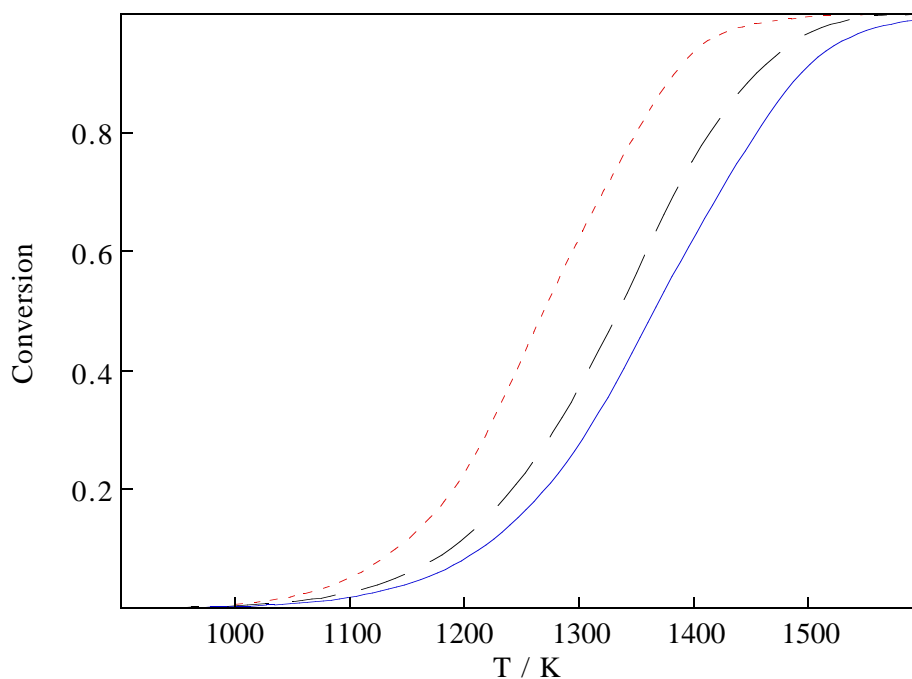
Figure 5.2.2. Dependence of Na_2CO_3 to CO_2 conversion according to equation (5.13). Solid line corresponds to an initial Na_2CO_3 concentration of 500 ppm in the gas phase, the dashed line to 300 ppm, and the dotted line to 100 ppm.

These simple one-reaction calculations for conditions typical of the experiments thus confirm that significant fractional decomposition of Na_2CO_3 in the presence of water is thermochemically favored beginning at temperatures slightly above 1000 K.

Our flow system experiments, however, show significant Na_2CO_3 decomposition also at temperatures below 1000 K. Figure 5.2.3 shows a comparison between calculated equilibrium conversions and those derived from experimental profiles at long residence times. It indicates that at the conditions of our experiments the Na_2CO_3 decomposition reaction is not equilibrated as predicted by the thermochemistry used. Because we felt that the thermochemical model was uncertain, particularly for its gas-phase Na_2CO_3 component, and could not explain the experimental decomposition profile, and because reaction (5.13) oversimplifies a complex process that involves many chemical reactions, we composed a dynamic model to fit the data. For the

conditions of our experiments Na_2CO_3 decomposition can be described as consisting of two opposed irreversible steps

$$Na_2CO_3 + H_2O \rightarrow 2NaOH + CO_2 \qquad (5.14)$$

$$2NaOH + CO_2 \rightarrow Na_2CO_3 + H_2O \qquad (5.15)$$

occurring in the directions indicated. An alternative model of Na_2CO_3 decomposition is

$$Na_2CO_3 \leftrightarrow Na_2O + CO_2 \qquad (5.12)$$

that can also proceed in irreversible steps

$$Na_2CO_3 \rightarrow Na_2O + CO_2 \qquad (5.16)$$

$$Na_2O + CO_2 \rightarrow Na_2CO_3 \qquad (5.17)$$

which in presence of water can be followed by NaOH formation

$$Na_2O + H_2O \leftrightarrow 2\ NaOH \qquad (5.18)$$

making the ultimate effect of model (5.12) identical to model (5.13).
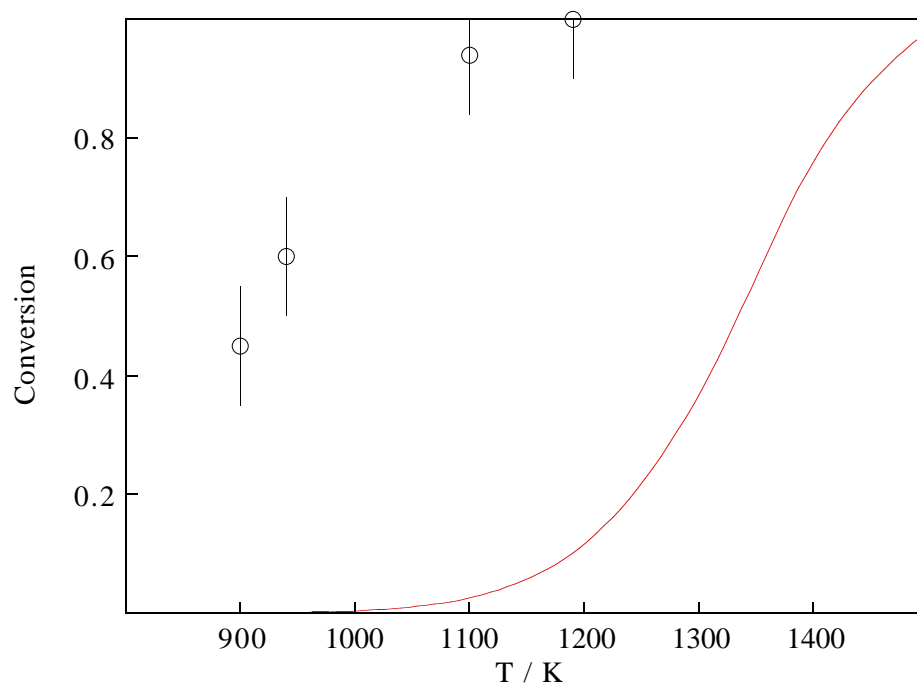
Figure. 5.2.3. Comparison between experimental and calculated (Feitelberg, 1994) equilibrium conversions of Na_2CO_3 to CO_2. The initial concentration of Na_2CO_3 was 300 ppm.

5.2.2 Available Thermodynamic Data on Sodium in the Gas-Phase

The documented gas-phase thermochemistry of sodium compounds is sparse. The 1985 JANAF table provides for non-halogen neutral compounds the information shown in Table 5.2.1. The tabulated enthalpy of formation values for 1500 K can be combined with the 1500 K values for the radicals H, O, OH and CN and the stable molecules HCN, H_2, H_2O and H_2SO_4 to derive the bond strengths of the sodium bonds in these molecules and the enthalpy changes of reaction for the key atom exchange reactions that establish the equilibrium composition of high temperature systems containing sodium. The JANAF values for these species at 1500 K are summarized in Table 5.2.2.

Table 5.2.1. JANAF standard enthalpies of formation at 298 and 1500 K.

Species	$\Delta_f H_{298}$ (kJ)	$\Delta_f H_{1500}$ (kJ)	Error @ 298 K	Source
Na	107.3	0	± 0.7	Vapor pressure data at 298 K; reference state above 1170.5 K.
Na_2	142.07	−75.2	± 1.2	Spectroscopic bond dissociation energy value.
NaO	83.68	−23.7	± 41.8	Estimated bond dissociation energy from $k_e r_e D°$= constant and spectroscopic D° for LiO.
Na_2SO_4	−1033.6	−1294.5	± 25.1	Thermo of solid and average of various vapor measurements.
NaH	124.26	15.6	± 19.2	Spectroscopic measurement of D°.
NaOH	−197.76	−303.7	± 12.6	Complex but secure thermochemical cycles
$(NaOH)_2$	−607.5	−822.5	± 25.1	Mass-spectrometric study of vapor-phase dissociation equilibria
NaCN	94.27	−12.8	± 2.1	Vapor pressure and composition measurements, thermo of crystal
$(NaCN)_2$	−8.8	−213.2	± 13	1200 K vapor composition.

Table 5.2.2. JANAF standard enthalpies of formation at 298 and 1500 K.

Species	$\Delta_f H_{1500}$ (kJ)	Species	$\Delta_f H_{1500}$ (kJ)
H	224.8	H_2	0
O	254.2	H_2O	−250.3
OH	124.8	H_2SO_4	−788.8
CN	259.7	HCN	132.1

The dissociation reactions breaking off the Na atom can then be compared with one another and with the corresponding reactions for breaking off a hydrogen atom at 1500 K as shown in Table 5.2.3.

Table 5.2.3. Thermochemistry for breaking Na–X bonds at 1500 K.

Reaction	$\Delta_r H_{1500}$ (kJ)	$\Delta_r H_{1500}$ (kJ) for Na = H	Difference between H and Na
$Na_2 \rightarrow Na + Na$	75.2		
$NaH \rightarrow Na + H$	208.2	449.6	241.4
$NaCN \rightarrow Na + CN$	272.5	352.4	79.9
$NaO \rightarrow Na + O$	277.9	354.2	75.3
$NaOH \rightarrow Na + OH$	428.5	599.9	171.4
$NaOH \rightarrow NaO + H$	504.8	599.9	95.1

The sense of the results is not surprizing: The strength of the Na–X bond increases with increasing electronegativity difference between Na and X, and Na bonds to other atoms and radicals less strongly than does H. The numerical comparisons shown in the fourth column are disappointing, however, in that there is neither consistency nor an understandable trend in the comparison to be seen in the compounds for which there is data to analyze this way.

Another way to compare sodium bonding with hydrogen bonding is through an isodesmic reaction series, in which sodium trades partners with hydrogen in a reaction that conserves the number and type of chemical bonds. The following linearly independent reactions illustrate the results of this alternative analysis style for HCN as the trading partner.

$$NaOH + HCN \rightarrow \quad NaCN + H_2O \qquad\qquad -91.5 \text{ kJ}$$

$$NaO + HCN \rightarrow \quad NaCN + OH \qquad\qquad 3.6 \text{ kJ}$$

$$Na_2SO_4 + 2\,HCN \rightarrow \quad 2\,NaCN + H_2SO_4 \qquad\qquad 100.7 \text{ kJ}$$
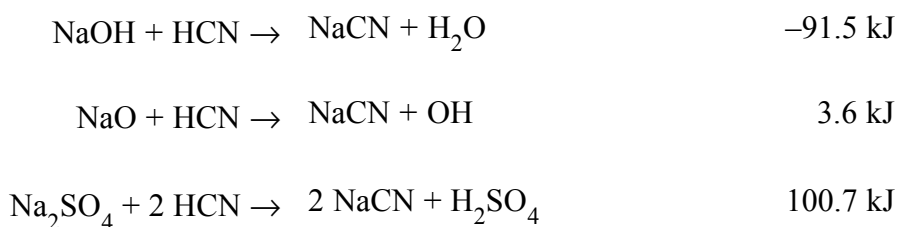
In all three cases an Na atom (2 of them in the third reaction) trades bonding to an O for bonding to CN. The trade is exothermic if the O is a hydroxyl O atom, essentially thermoneutral for a lone O atom, and endothermic for a sulfate O atom.

Two conclusions emerge from the foregoing overview of gas-phase sodium thermochemistry.
The first is an assessment of the available high temperature thermochemical data base: It is too small, and has too-large error bounds, to permit reliable estimation of the energetics of other sodium-containing species by an analog of the group additivity methods that have proved to be successful in correlating the thermochemistry of gas-phase molecules (Cohen, 1996) and radicals (Lay et al., 1995). Neither the bond dissociation energies nor the isodesmic reaction series that can be constructed from the available information suffice for extrapolation purposes.

The second is that while sodium bonding is characteristically weaker than bonding of its Group I fellow hydrogen in all gas phase species, this bonding is not so weak that only the most stable sodium species need be considered for modeling purposes. As example, formation of the O–H bond in NaOH provides 505 kJ/mol, implying that NaO is readily able to abstract H atoms from most of the H-containing species present in flue gas. It is thus necessary to estimate thermochemical and kinetic parameters for many more sodium-containing species than the

JANAF set if one is to hope for adequate dynamic modeling of sodium chemistry under flue gas conditions.

Mention should be made of two other gas phase sodium species that have been discussed. The first is the sodium analog of water, Na_2O, for which thermochemical data have been generated based on the experiments of Hildenbrand and Murad (1970). As shown below, the binding of the second Na atom is sufficiently weak that very small amounts of it are formed at low total sodium concentrations. The second species is the superoxide NaO_2, which has been invoked to explain Na concentration measurements in flames, Knudsen cells and flow reactors. The thermochemical inferences show disappointingly large scatter, i.e., dissociation energy values in kJ/mol of <115, >145, 163± 21, <184, <195, >202, 234±13, 230±5, and 243 ±21. (Marshall et al., 1990 and references cited therein.) Theoretical values of 150, 151, 156, 185, 196 and 199 kJ/mol have been reported for various levels of theory (Partridge et al., 1992 and references cited therein). The experimental and theoretical values are consistently large enough to demonstrate that NaO_2 has to be considered as an intermediate in high-temperature sodium chemistry, but its thermochemistry is clearly as much or more a problem as that of NaO.

Taking the available thermochemical data all together permits one to generate more complete overviews of the species expected to be present at chemical equilibrium than is seen in the foregoing more narrowly targeted discussion. Leaving out the uncertain NaO_2 and solving the equilibrium at 1 atm pressure over the temperature range of interest here provides the overviews shown below. Figure 5.2.4 shows an equilibrium composition chart for the conditions of our laboratory experiments, in which the only source of CO_2 was the small addition of Na_2CO_3, and Figure 5.2.5 shows the corresponding distribution for conditions that can be encountered at flue gas compositions, when there is an exogenous source of CO_2 corresponding to an equivalence ratio of 1 for a fuel containing equimolar amounts of C and H.
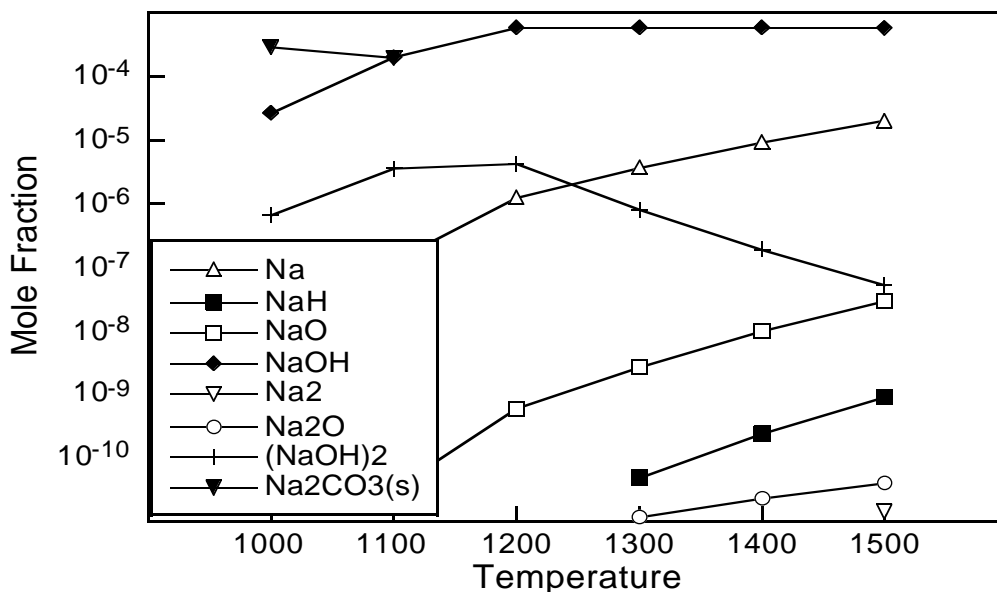
Figure 5.2.4. Equilibrium distribution of sodium-containing species at 1 atm pressure in 80% N_2, 20% H_2O and 300 ppm Na_2CO_3. The only condensed phase stable for these conditions is solid Na_2CO_3 below 1100 K.
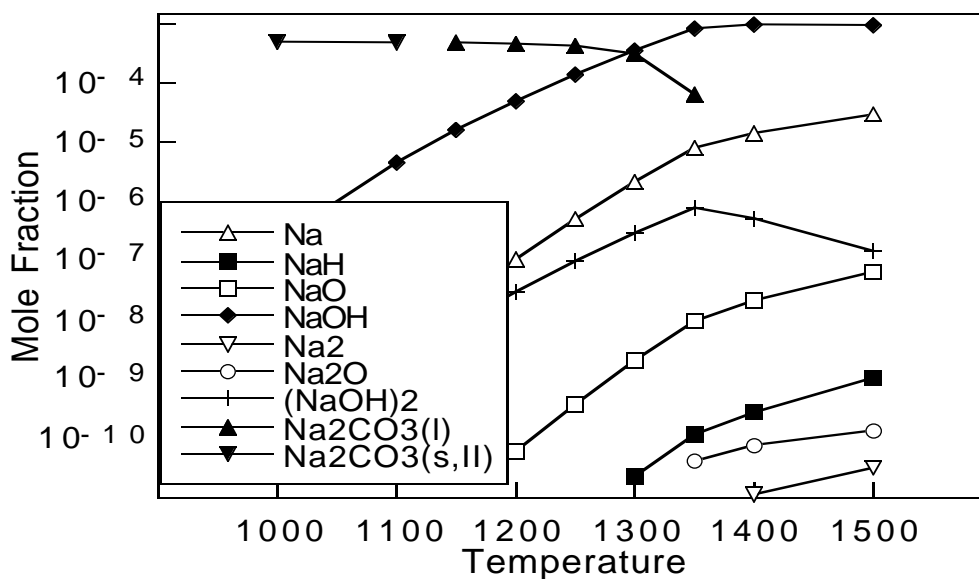
Figure 5.2.5. Equilibrium distribution of sodium-containing species at 1 atm pressure in a flue-gas-like mixture with 300 ppm of added Na_2CO_3. The assumed fuel had C:H and equivalence ratios of 1. The high concentration of CO_2 forces the condensed phase to be solid or liquid sodium carbonate rather than the intrinsically more stable hydroxide. Aside from this difference the composition is quite similar to that of the CO_2-free case, especially at higher temperatures.

Based upon the JANAF species and NaO_2, one can start to model flue gas conditions to examine the basic flow of sodium chemistry. Such models have been composed for example by Plane (1991) and Schofield and Steinberg (1992). In these mechanisms additional species are advanced, with provision of estimated, if any, thermochemical data. The additional species include NaO_3, $NaHCO_3$, and $NaCO_3$ in the Plane (1991) model, designed to describe sodium chemistry in the mesosphere, and NaS, $NaSH$, NaS_2, $NaOS$ and $NaSO_2$ in the Schofield and Steinberg (1992) model, designed to describe sodium-sulfur interactions in flames; the latter authors describe structural and thermochemical estimation procedures in detail. Calculations using the Chemkin program and these reactions are in progress.

It is clear that the JANAF species and NaO_2 do not suffice to give a complete picture of the interactions of sodium species with the advanced reburning process. The strength of sodium bonds to other prominent radicals (as we have calculated, but not reported here) at the 6-31G(d)++/MP2 level with isodesmic series) is sufficient to enable many such species to interact with not only the common flame radicals but also with the ones that are specific to the AR chemistry, such as the NH_i species. Translating our molecular electronic structure results for these species into temperature-dependent thermodynamics for these species is in progress. We assume that the results of simulations that include these species will support the basic conclusion of our Phase I research—that the sodium enhancement effect arises from general increased radical availability—but until the main candidate sodium species relevant to the advanced reburning environment are tested in simulations, as Plane and coworkers did for the atmospheric case and Schofield and coworkers did for the sulfur-interactions, this conclusion must remain tentative.

5.3 Experimental Methods

Most of our experiments on Na_2CO_3 decomposition were done in a flow system over the

temperature range from 900 to 1300 K. These experiments provided information about the rate of Na_2CO_3 decomposition and reactions of Na_2CO_3 with components of flue gas. In place of our early intention to identify gas-phase species by shock tube experiments, we decided to substitute mass spectrometric ones in order to get a broader range of information about the product distribution resulting from high temperature Na_2CO_3 decomposition.

The following sections give descriptions of the experimental apparatus used in our work.

5.3.1 Flow System

The flow system used for our experiments is shown in Figure 5.3.1. Our efforts began with the construction of the flow and gas handling systems for our gas chromatograph (GC). The gas handling system was made with a combination of glass and metal components so as to enable both high and low pressure operation. A new reactor for the flow system was constructed that took advantage of an ultrasonic atomizing nozzle system supplied by EER, which provided a reliable way to spray aqueous Na_2CO_3 solution with salt concentrations up to 15% by weight. The reactor was initially horizontal and later rearranged in a vertical orientation to suppress deposition of Na_2CO_3 on the walls. The second design also included preheating the carrier gas to temperatures in the range 300–400 $^\circ$C and use of a ceramic adapter between the nozzle system and the reactor. The adapter allowed mixing hot carrier gas with the spray from the nozzle without overheating the nozzle itself. (The specified working temperature range of the nozzle is up to 200 $^\circ$C). The original GC columns were replaced with new ones packed with molecular sieve and HAYESEP Q to enable measurements of CO_2 and surrogate components of flue gas. The sensitivity of the GC to CO_2 was enhanced by use of high-sensitivity thermal conductivity filaments and by prolonged pretreatment of the columns at 200 $^\circ$C. These modifications resulted in a sensitivity level of 50 ppm of CO_2 and permitted us to work with the flow system at Na_2CO_3 levels close to those used by EER in their field experiments.

Preliminary experiments showed that temperature measurements taken inside of the reactor were significantly different from measurements taken in the furnace area that originally were used for temperature determinations. To enable correct temperature measurements, the construction of the flow reactor was changed to enable a thermocouple to be inserted directly into the gas flow. Measurements showed that by adjusting the current through each of three segments of the furnace a uniform temperature distribution inside of the reactor can be created with temperature variations within ±10 degrees.
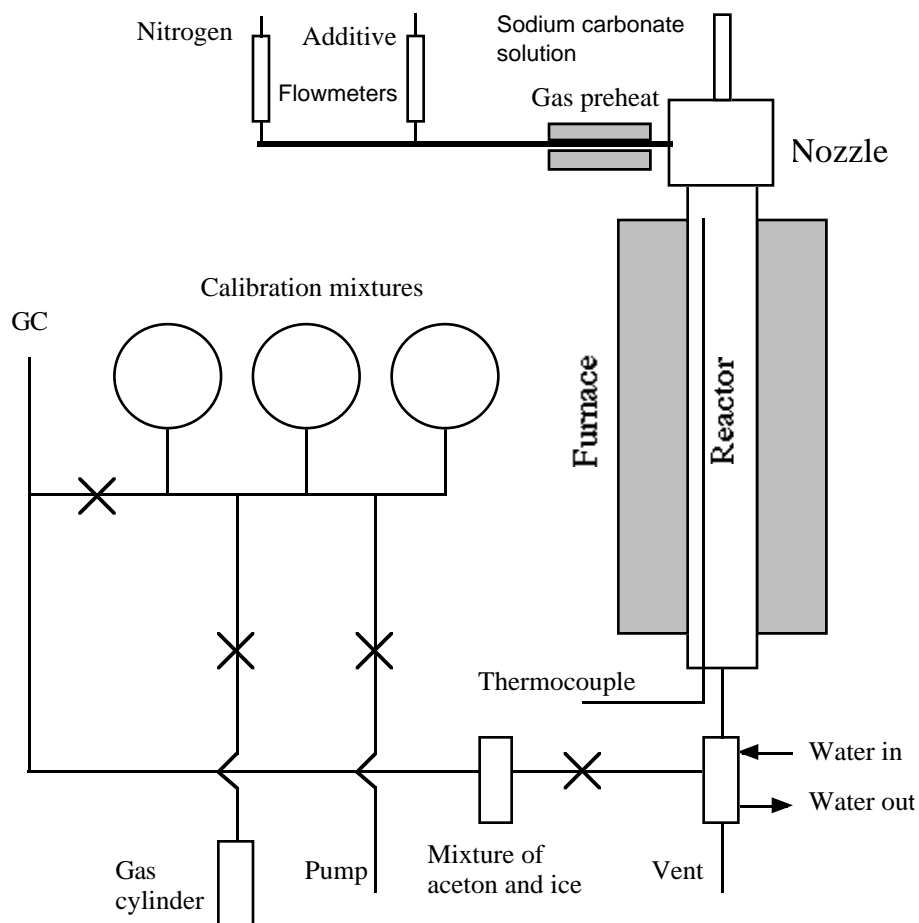
Figure 5.3.1 Flow system diagram.

Two drying systems were installed to dry gas after passing through the reactor. The first system was used to separate most of the water so as to prevent condensation in communication lines. The second system used acetone and dry ice to dry gas before taking a sample for GC analysis.

The second system protected the sensitive GC columns from being destroyed by the basic solution formed from Na_2CO_3 decomposition.

5.3.2 Mass Spectrometric Analysis

The products of Na_2CO_3 thermal decomposition were identified using a Finnigan MAT TSQ 70 mass spectrometer in thermal, electron bombardment and chemical ionization modes. Small amounts of aqueous Na_2CO_3 solution were heated on a Nichrome wire until the water evaporated and the solid or liquid Na_2CO_3 started to decompose. In electron ionization mode, used in most experiments, the gas phase was bombarded at electron ionization (EI) energies of 70, 25, 12 volts. In chemical ionization mode (CI), the gas pressure in the ion source was increased to typically 10^{-3} mbar of CH_4; the dominant initial CH_4^+ ions collide with molecules M and transfer a proton to give MH^+ ions with little excess initial energy and therefore little tendency to fragment. Thus, whereas the EI spectra contained peaks corresponding to both molecular and fragment ions, the CI spectra were simpler, mostly having predominantly parent ion peaks. Both EI and CI modes were used in our experiments. In auxiliary experiments the Nichrome wire was replaced by lower-melting metals in order to identify, by the melting temperature, the effective temperatures where changes in the ion patterns appeared.

5.4 Rate of Sodium Carbonate Decomposition

5.4.1 Sodium Carbonate Decomposition in Nitrogen

Experiments on Na_2CO_3 decomposition were done in quartz and stainless steel reactors. It was found that reactors made from different materials produced similar results. It is known, however, that sodium carbonate reacts with silicon oxide, the main component of quartz, to form silicates

$$Na_2CO_3 + SiO_2 \rightarrow Na_2SiO_3 + CO_2 \qquad (5.19)$$

Reaction (5.19) becomes spontaneous in the temperature range 500–600 K (Chase et al., 1985). That reaction (5.19) does occur for the conditions of our experiments is supported by the observation that after passing Na_2CO_3-containing test gas through the quartz reactor for 18 to 20 hours the surface of the reactor roughened, and after running for still longer times the reactor was virtually destroyed. The observed rate of Na_2CO_3 decomposition was the same in a fresh reactor and in a reactor with surface exposed to Na_2CO_3 for several hours, which suggests that reaction (5.19) does not contribute significantly to CO_2 production on the time scale of our experiments. This observation is supported by a study of reaction (5.19) undertaken by Terai et al. (1968). Using thermogravimetry, x-ray diffraction, and radioactive tracing they studied the sodium carbonate-silica reaction in the temperature range from 1000 to 1100 K and reported that the reaction is not controlled by diffusion of Na in silica. The diffusion coefficient calculated from the penetration rate of Na into fused silica was determined to be $D = 5.0 \times 10^{-11}$ cm^2/s. This value of D actually shows how fast the reaction between sodium carbonate and silica is and can be used to estimate the rate of reaction (5.19), which then can be compared with rate of the reaction in the gas phase as follows. Since the gas volume in the reactor is $V = 100$ cm^3 and typical concentrations of CO_2 were about 1×10^{-7} mol/cm^3, the total amount of CO_2 produced is 1×10^{-5} mol per second. For a reactor with diameter 2.5 cm, length 40 cm and wall thickness 0.1 cm the total amount of silica in the reactor is 0.5 mol. From this data, the time required to produce 1×10^{-5} mol of CO_2 in reaction (5.19) can be computed and compared with typical residence time 0.5 second. Production of 1×10^{-5} mol of CO_2 results in consumption of $1 \times 10^{-5}/0.5 = 2 \times 10^{-5}$ volume of silica. For our reactor it gives penetration distance $l = 0.1 \times (2 \times 10^{-5}) = 2 \times 10^{-6}$ cm. Values of l and diffusion coefficient D give a simple estimation of reaction time t in the solid phase through the Einstein equation

$$t = l^2/D \tag{5.4.I}$$

Using $l = 2\times10^{-6}$ cm and the value of D measured by Terai et al. (1968), formula (5.4.I) gives $t = 8$ s, much larger than the 0.5 s characteristic times of our experiments.

An alternate line of reasoning leading to the same result is this. The entire reactor contains about 0.5 mol of silica; as the observed production rate of CO_2 is about 10^{-5} mol/s, the entire reactor would be lost to form sodium silicate in only 5×10^4 seconds (14 hours) if all of the CO_2 would originate in heterogeneous reaction (5.19) to form sodium silicate. Our observations show however that the lifetime of the quartz reactor is at least 30 hours. Thus reaction (5.19) does not contribute significantly to CO_2 production on the time scale of our experiments.

Experimental study of Na_2CO_3 decomposition at temperatures from 900 to 1300 K and pressure 1 atm was done in the flow system. Details of the experimental procedure are given below. An aqueous solution of Na_2CO_3 was sprayed into preheated flow of N_2; the mixture then passed through the quartz reactor and cooled. Sample taken from exhaust gases passed through additional cooling system to get rid of water traces and then analyzed by GC. The flow rate of N_2 and the rate of solution consumption were measured and used to calculate the residence time of the mixture in the reactor. These calculations were done assuming ideal behavior of N_2 and H_2O vapor formed upon evaporation of water in the reactor. Initial concentrations of Na_2CO_3 in the mixture were varied in the range from 300 to 1000 ppm. Since both reactions (5.12) and (5.13) give stoichiometric ratio $CO_2/Na_2CO_3 = 1$, this ratio can be used to determine degree of Na_2CO_3 decomposition. Concentrations of CO_2 measured in samples taken from the outlet of the reactor were used to compute the degree of Na_2CO_3 decomposition (Figure 5.4.1). Experiments in the flow system show that at temperatures above 900 K significant amounts of CO_2 are formed. The scatter of the data is significant, especially at short residence times, probably due to insufficiently controlled mixing. At residence times longer that 0.1 s a distinct temperature influence on CO_2 production can be observed. At temperatures around 900 K the maximum conversion of Na_2CO_3 to products is about 0.5 even at the longest residence times. As

temperature increases the reaction becomes faster and at 1190 K it takes only about 0.12 s for complete decomposition of Na_2CO_3. The observations show a rate of reaction proportional to $[Na_2CO_3]^{1.5}$, indicating that reaction does not occur in one step but rather in a complex mechanism. Assuming that the rate of the total reaction has Arrhenius dependence on temperature, an effective energy of activation can be determined as follows. For fixed degree of Na_2CO_3 decomposition the time required for decomposition is a measure of the rate of the reaction, and effective energy of activation can be determined from the slope of the plot that shows dependence of this time on inverse temperature. Figure 5.4.2 shows the dependence of the time required for 30% decomposition on the reactor temperature. The effective energy of activation determined from this plot is 86 kJ/mol.
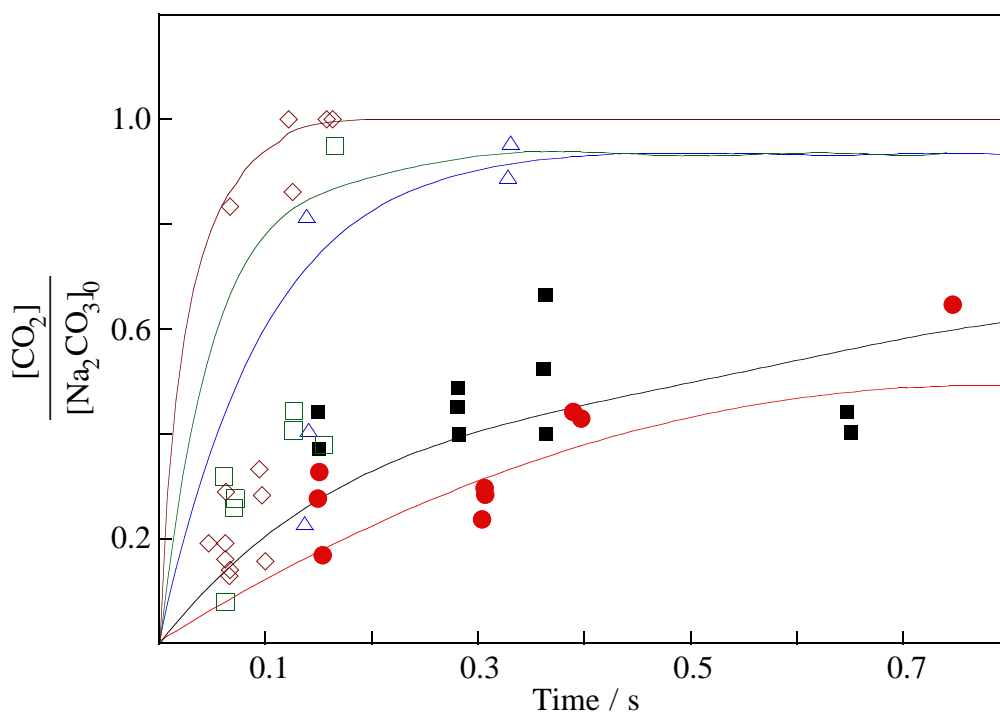
Figure 5.4.1 Comparison of experimental (symbols) and calculated (lines) Na_2CO_3 conversion profiles. Mixture 0.03% Na_2CO_3 + 20.00% H_2O + 79.97% N_2 at P = 1 atm.
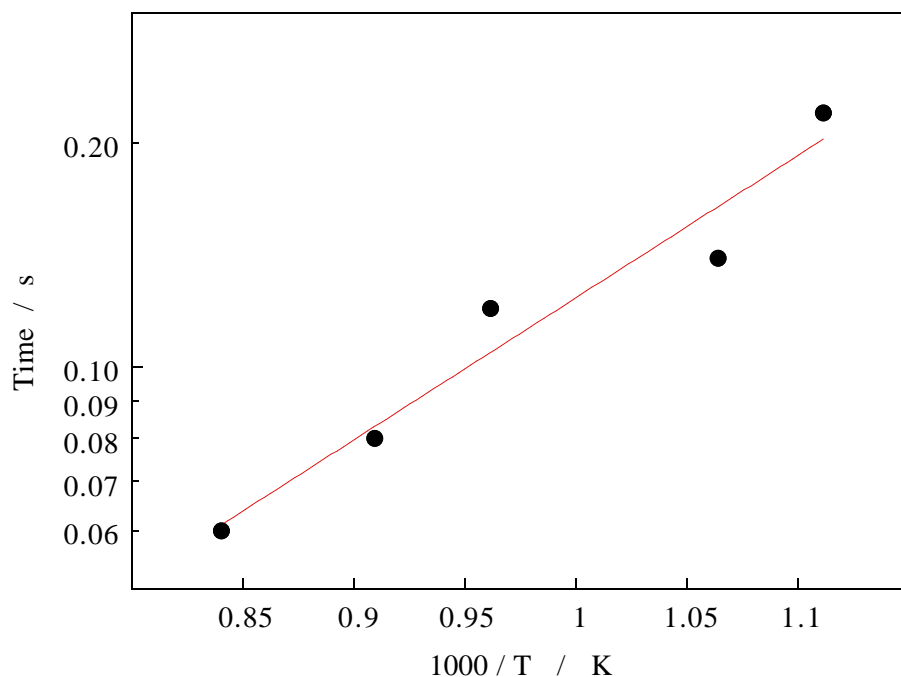
Figure 5.4.2   Temperature dependence of the decadic logarithm of time required for decomposition of 30% of the initial amount of Na_2CO_3.

To model irreversible (see section 5.2) Na_2CO_3 conversion, we used reactions (5.16, 5.17) and

$$Na_2O + H_2O \leftrightarrow 2NaOH \tag{5.20}$$

with reactions (5.16) and (5.17) being irreversible and reaction (5.20) being possible in both directions. The rate coefficient of reaction (5.20) was estimated as that of

$$CaO + H_2O \leftrightarrow Ca(OH)_2, \tag{5.21}$$

measured by Cotton and Jenkins (1971) to be $9.18 \times 10^{12} \exp(-3120/RT)$. Estimates show that the characteristic lifetime of CaO in the reaction (5.21) at 1000 K, 1 atm and 20% H_2O is less than 1 µs, much less than the characteristic time of our experiments. This suggests that for the conditions of our experiments Na_2O is practically instantaneously converted to NaOH, and thus

the value of the rate coefficient of reaction (5.20) is not really important. All calculations were made using the Chemkin-II modeling program (Kee et al., 1992) under constant pressure and temperature constraints. Thermochemical data for all species but Na_2O were taken from Zamansky and Maly (January 1997); thermochemical data for Na_2O were taken from the NASA database (McBride et al., 1993).

Sensitivity calculations (Figure 5.4.3) show that the rate coefficient of reaction (5.16) affects both initial and equilibrium conversions of Na_2CO_3 to CO_2, while that of reaction (5.17) mainly affects the equilibrium value. The rate coefficients of reactions (5.16) and (5.17) were adjusted for the conditions of our experiments (0.03% Na_2CO_3 + 20.00% H_2O + 79.97% N_2 at 1 atm). The rate coefficient of reaction (5.16) was varied to match the initial part of the profiles at 900, 940, 1040, 1100 and 1190 K, while the rate coefficient of reaction (5.17) was changed until the final calculated conversion was equal to the experimental value. Figures 5.4.4 and 5.4.5 show the dependence of rate coefficient of reactions (5.16) and (5.17) on temperature as derived from matching the experimental conversion profiles. The rate coefficient of reaction (5.16) follows a simple Arrhenius dependence, while that of reaction (5.17) decreases with temperature, possibly due to limitation of the reaction rate by CO_2 transport. Least square fits to all data give next expressions for k_5 and k_6

$$k_{16} = 2.54 \times 10^6 \exp(-13040/T) \tag{5.4.II}$$

$$k_{17} = 1.11 \times 10^5 \exp(7580/T) \tag{5.4.III}$$
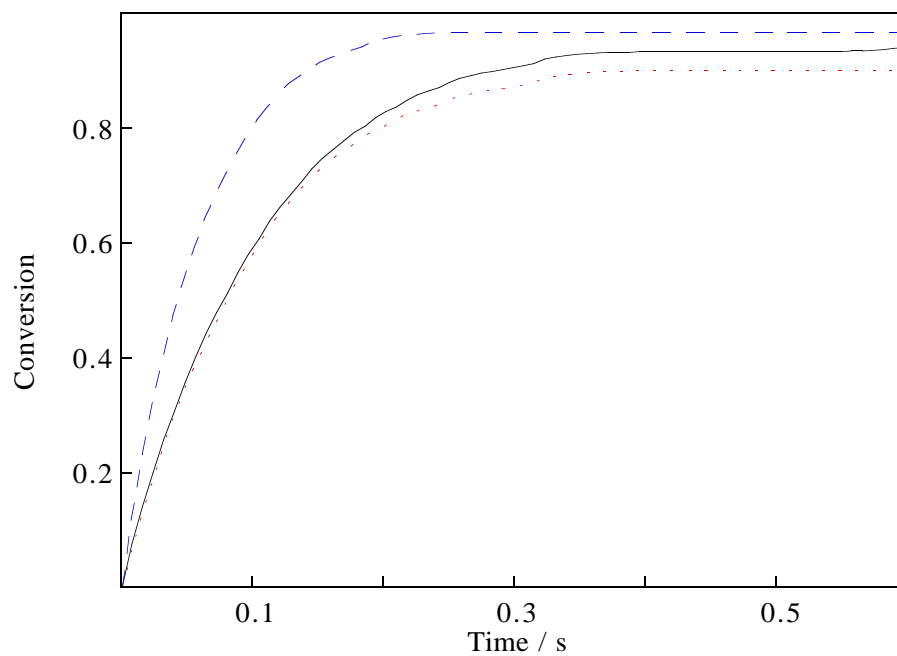
Figure 5.4.3 Sensitivity spectrum for decomposition of Na_2CO_3. The dashed line represents calculations with a doubled rate coefficient of reaction (5.16), the dotted line a doubled rate coefficient of the reaction (5.17).
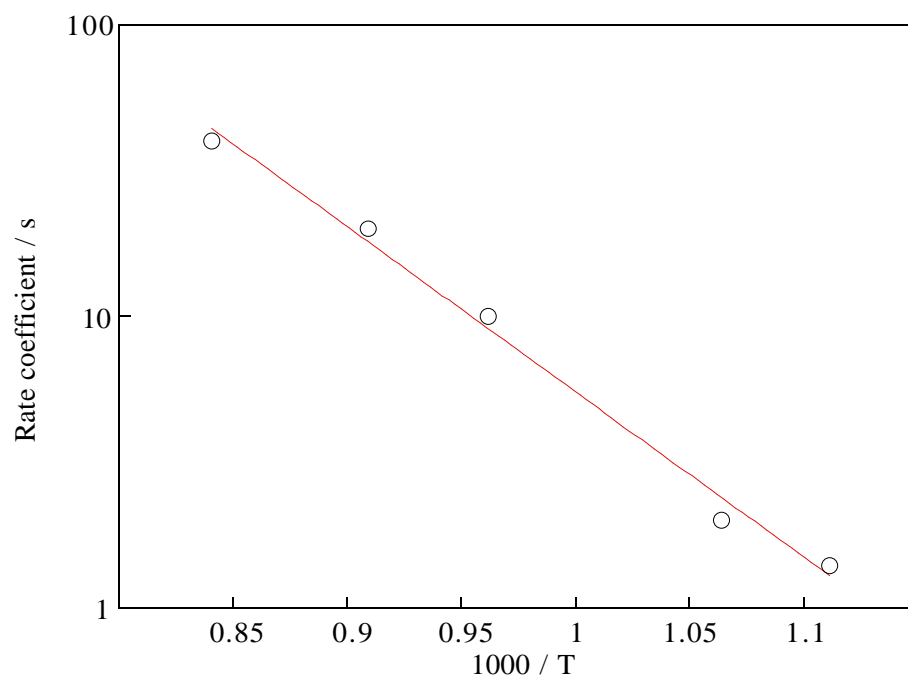
Figure 5.4.4 Rate coefficient inferred for $Na_2CO_3 \rightarrow Na_2O + CO_2$ (5.16).
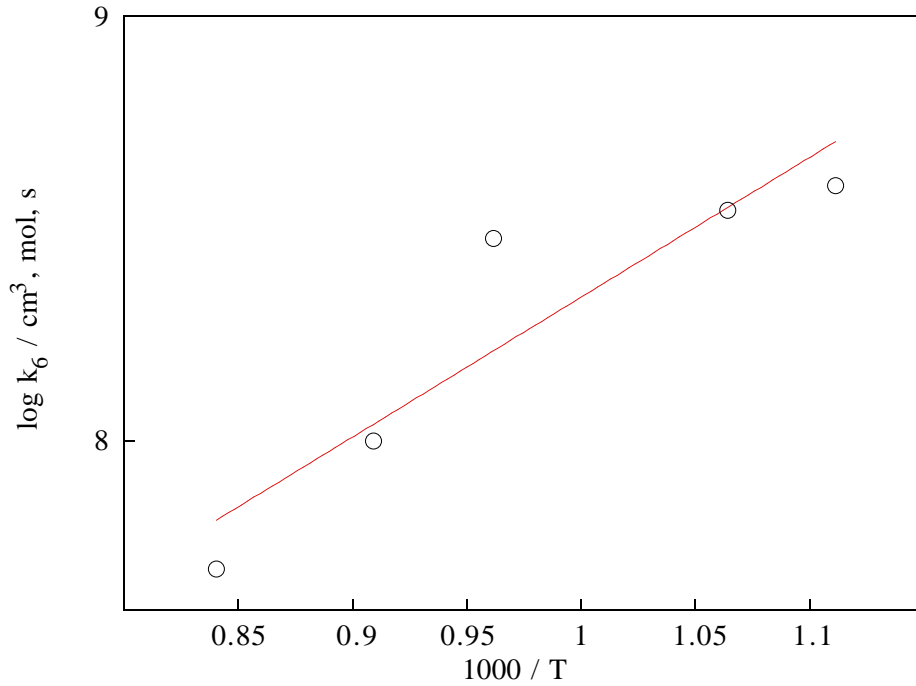
Figure 5.4.5 Rate coefficient inferred for $Na_2O + CO_2 \rightarrow Na_2CO_3$ (5.17).

The total uncertainties (TU) in rate coefficient of reactions (5.16) and (5.17) were determined through the formula

$$TU_i = ((a_i \times U_{exp})^2 + U^f_i{}^2)^{0.5}$$

where U_{exp} is the uncertainty of the experimental data (20%), a_i is the sensitivity of the rate coefficient of the reaction (i) to the experimental data, and U^f_i is the uncertainty associated with the least square fit to all data points for the rate coefficient of reaction (i). Sensitivity coefficients a_i were defined as $a_i = 1.4\ln(C/C_0)$, where C and C_0 are computed conversions for doubled and for reference values of the rate coefficient of the reaction (i), and are equal to 0.46 for reaction (5.16) and 0.1 for reaction (5.17). The values of U^f_i were found to be 10 and 25% for k_{16} and k_{17}. Based on these data, values of TU_{16} and TU_{17} were calculated to be 14 and 25 %.

Figure 5.4.1 shows a comparison between experimental and calculated conversion profiles based

on the above expressions. At higher temperatures complete decomposition of Na_2CO_3 occurs within 0.2 s, while at low temperatures conversion at long times reaches a maximum value and then stays constant. Taking into account the significant scatter of the experimental data, the agreement between measured and calculated profiles is good.

These results for the rate of Na_2CO_3 decomposition thus show that at temperatures higher than 1400 K Na_2CO_3 decomposes relatively quickly to produce NaOH and CO_2, suggesting that Na_2CO_3 and NaOH should have practically the same efficiencies as NO_x control agents.

5.4.2 Reactions of Sodium Carbonate with Components of Flue Gas

The flow system was used to measure the rate of reaction between the decomposition products of Na_2CO_3 and CH_4, H_2, CO, and NO. These experiments were done at 1150 K and a residence time of 2 s in mixtures containing $0.5\%Na_2CO_3 + 1.7\%H_2O + N_2$ with 0.5% additive. In each case the concentration of additive in the mixture after passing through the reactor was measured; measurements were done by GC for CH_4, H_2, CO, and O_2 additive and with the chemiluminescence analyzer for NO. In the first set of experiments pure water was sprayed through the nozzle while a mixture of additive and nitrogen passed through the reactor and the concentration of additive in the outlet gas was measured. In the second set of experiments the gas and liquid flow conditions were the same as in the first one except that the water was replaced with a solution containing 5% Na_2CO_3 by mass. Comparison of two runs showed no detectable changes in additive concentrations. We conclude that there is no chemical reaction with observable rate between the decomposition products of Na_2CO_3 and CH_4, H_2, CO, and NO under the conditions studied. It was also observed that the concentration of NO stayed constant when O_2 and Na_2CO_3 were injected into the mixture at the same time.

Experiments with ammonia injection to evaluate the reactions of NO and NH_3 in the presence of

Na are under way.

5.5 Mass Spectrometry of Decomposition Products

Mass spectrometric analysis was used to identify the species formed during decomposition of Na_2CO_3. Figure 5.5.1 shows time histories of ions with mass/charge (m/z) ratios 44 (mostly CO_2^+) and 106 ($Na_2CO_3^+$) and total ion current for EI = 70 eV. The temperature during the run rises from room temperature (0 on the x-axis) to the final temperature, which corresponds to red hot nichrome. The first peak on the total ion current curve corresponds to the temperature at which all water evaporates. Peak heights are on a relative scale assuming the height of the largest one (in this case m/z = 44) to be 100. Figure 5.5.2 shows all detected ions for the moment when m/z = 44 reaches its maximum value (62 on the x-axis). It reveals the presence of H_2O^+ (18), Na^+ (23), CO_2^+ (44), very small amounts of $NaOH^+$ (40) and $Na_2CO_3^+$ (106). The peak with m/z = 28 corresponds to CO^+ and N_2^+ present as residual gas; the other peaks are difficult to identify. As the EI energy decreases (Figure 5.5.3) the contribution of Na^+ becomes more prominent compared to other ions because of its very low ionization energy: Figure 5.5.4 show a mass spectrometric analysis with EI = 0, i.e., with all ions arising from thermal ionization of Na_2CO_3 on the wire. This mass spectrum shows Na^+ (23) and a species with m/z = 129 ($Na_3CO_3^+$). (The species with m/z = 39 corresponds a background peak, probably K^+ (39), and always appear in analyses with low EI).

```
CHRO: M25GR0580 ver 4 on UIC 2 2      25-MAR-97 Elapse: 00:01:04      62
Samp: NA2CO3                                    Start : 14:42:34      76
Comm: EI   ELEN=-70V
Mode: EI +Q3MS HMR UP LR
Oper: RR                                        Inlet :
Peak: 1000.00 mmu     Label wndw: 1 > 76        Masses: 10 > 250
Area: 0, 4.00         Baseline  : 0, 3          Label : 0, 40.00
```
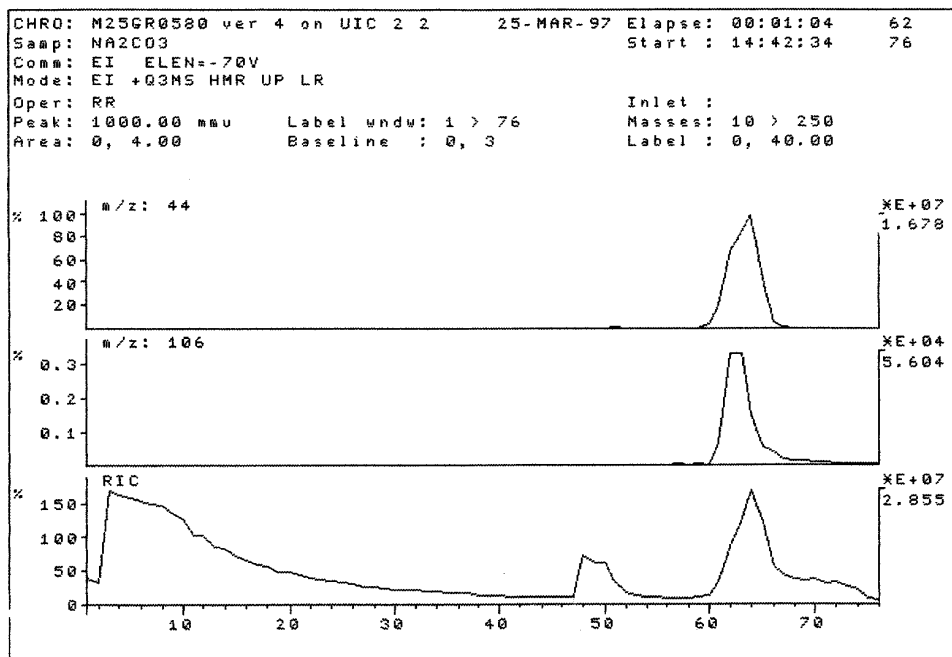
Figure 5.5.1 Time histories of ion currents at *m/z* = 44 and 106 and total ion current. EI = 70 eV, nichrome wire. The x-axis gives the heating time in seconds.


```
SPEC: M25GR0580 ver 4 on UIC 2 2      25-MAR-97 Elapse: 00:01:04      62
Samp: NA2CO3                                    Start : 14:42:34      76
Comm: EI   ELEN=-70V
Mode: EI +Q3MS HMR UP LR
Oper: RR                                        Inlet :
Base: 43.9            Inten : 11275129          Masses: 10 > 250
Norm: 43.9            RIC   : 14275138          # peaks: 230
Peak: 1000.00 mmu
```
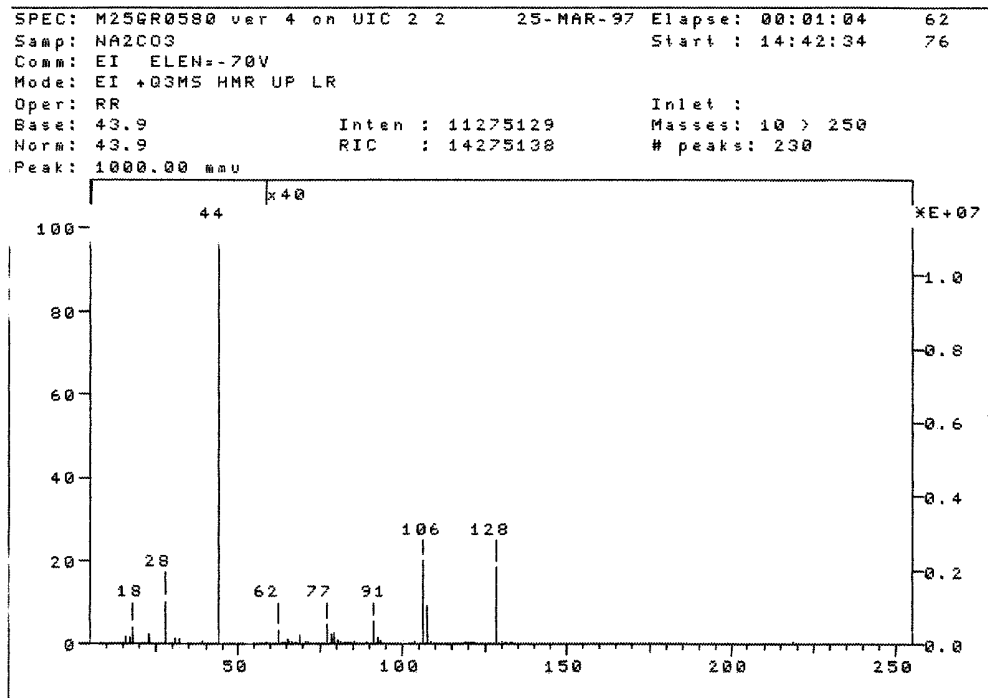
Figure 5.5.2 Mass spectrum at 62 s on the x-axis of Figure 5.5.1. *m/z* = 18 corresponds to H_2O^+, 28 CO^+ to 44 CO_2^+ to 62 Na_2O^+ to 106 $Na_2CO_3^+$ and 128 to $Na_3CO_3^+$.

5-27

```
SPEC:  M25GR0580 ver 6 on UIC 2 2      25-MAR-97 Elapse: 00:00:31   30
Samp:  NA2CO3                                    Start : 15:12:24   41
Comm:  EI ELEN=-12V
Mode:  EI +Q3MS HMR UP LR
Oper:  RR                                        Inlet :
Base:  22.5                 Inten : 1947315      Masses: 10 > 250
Norm:  22.5                 RIC   : 4194778       # peaks: 263
Peak:  1000.00 mmu
```
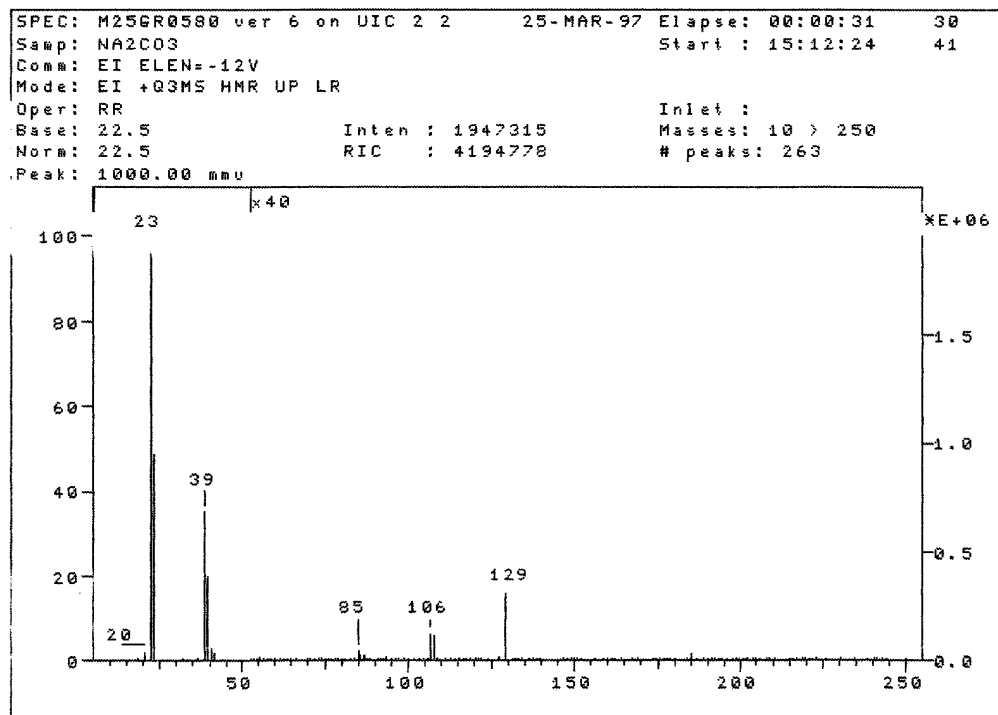

Figure 5.5.3 Mass spectrum at the time *m/z* = 23 reaches its maximum. EI = 12 eV.

```
SPEC:  M25GR0580 ver 7 on UIC 2 2      25-MAR-97 Elapse: 00:00:44   42
Samp:  NA2CO3                                    Start : 15:20:48   51
Comm:  EI ECURR=0
Mode:  EI +Q3MS HMR UP LR
Oper:  RR                                        Inlet :
Base:  22.7                 Inten : 919310       Masses: 10 > 250
Norm:  22.7                 RIC   : 1830766       # peaks: 264
Peak:  1000.00 mmu
```
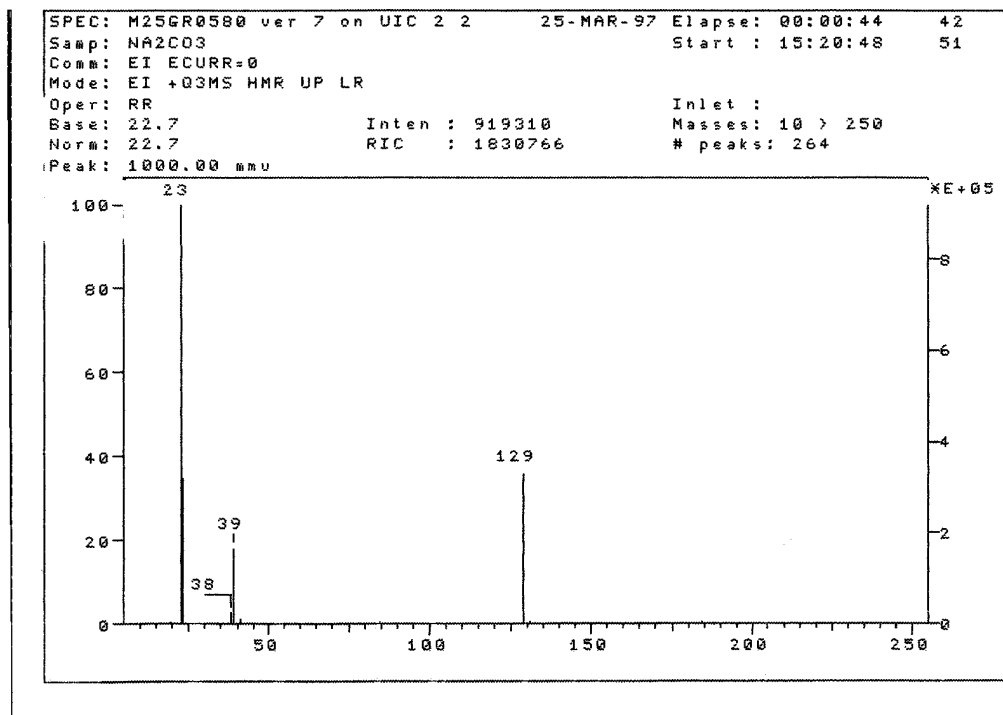

Figure 5.5.4 Mass spectrum at the time *m/z* = 23 reaches its maximum in thermal ionization mode.

Figure 5.5.5 shows results of mass spectrometric analysis of an Na_2CO_3 sample in chemical ionization mode. The product distribution (Na^+, CO_2^+, $Na_2CO_3^+$) is the same as in electron ionization mode with a few new species; among them $m/z = 53$ in greatest amount.


```
Samp: NA2C03/HI CONC.                      Start : 10:19:53    25
Comm: CI/CH4   P=2TORR
Mode: CI -Q3MS HMR UP LR
Oper: RR                                   Inlet :
Peak: 1000.00 mmu     Label undw: 1 > 25   Masses: 10 > 250
Area: 0, 4.00         Baseline  : 0, 3     Label : 0, 40.00
```
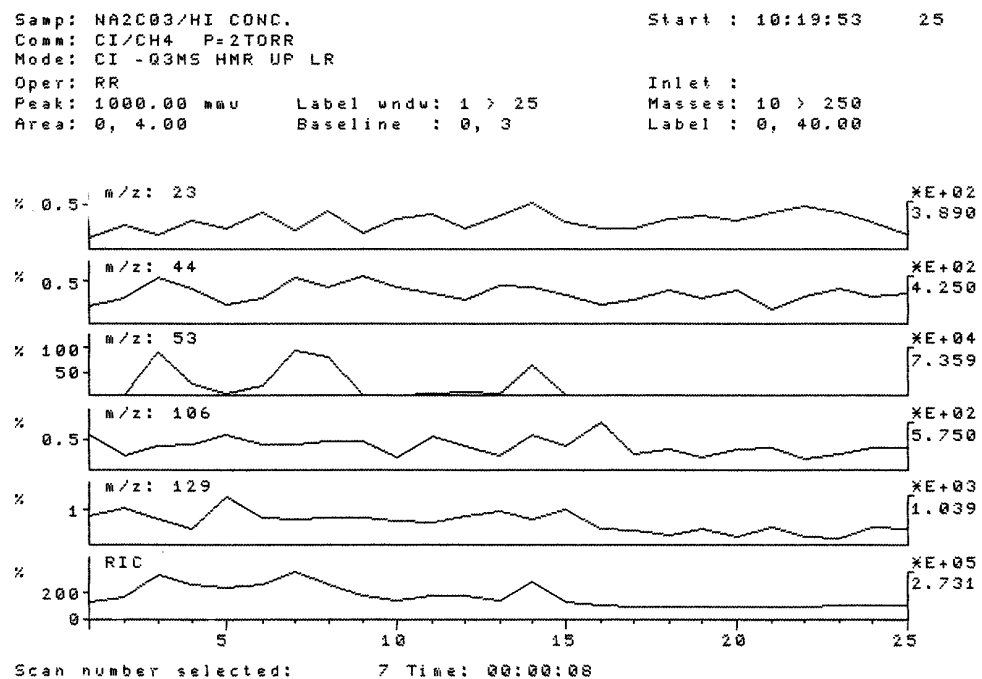
Figure 5.5.5 Time histories of ions with $m/z = 23$ (Na^+), 44 (CO_2^+), 53 ($Na_2CO_3^{++}$), 106 ($Na_2CO_3^+$), 129 ($Na_3CO_3^+$), and total ion current. Chemical ionization mode, Nichrome wire.

A general disadvantage of mass spectrometric measurements is that they do not provide continuous recording of the sample temperature. It is therefore not possible to correlate mass spectra closely with the temperature at which active species are formed and/or decomposition of Na_2CO_3 occurs. It is possible, however, to correlate some moments on the time scale with corresponding temperatures when in place of standard nichrome wire, which melts at very high temperature, wire made from a metal with lower melting temperature is used. The moment when such a wire melts is detected as a maximum in the total ion current and corresponds to the melting temperature of the metal. Since Ag has melting point of 1235 K, within the temperature range of our interest, we conducted some experiments using Ag wire instead of nichrome. These were done in EI mode with an ionization energy of 70 eV and in thermal ionization mode (EI = 0). The

time of Ag occurrence in the mass spectrum (Figure 5.5.6) (which also corresponds to the maximum in total current) corresponds to the moment of time when temperature of the wire is 1235 K (39 s). The mass spectrum (Figure 5.5.7) at this temperature shows CO_2^+ (44), $NaOH^+$ (40), $Na_2CO_3^+$ (106) and many other species. Some of them are easily identifiable (H_2O^+ and N_2^+), while secure identification of others requires additional (i.e., high-resolution) analysis. Figure 5.5.7 does not indicate the presence of Na atoms. To find out if Na atoms are present in the system at 1235 K we repeated experiments with an Ag wire in thermal ionization mode (Figs. 5.5.8 and 5.5.9). Figure 5.5.8 shows that one of the maximums in Ag^+ (109) concentration corresponds to the maximum in total ion current (22 s on x-axis) at the temperature 1235 K. The mass spectrum (Figure 5.5.9) at this temperature shows Na^+ (23) and species with $m/z = 39$ and 129.
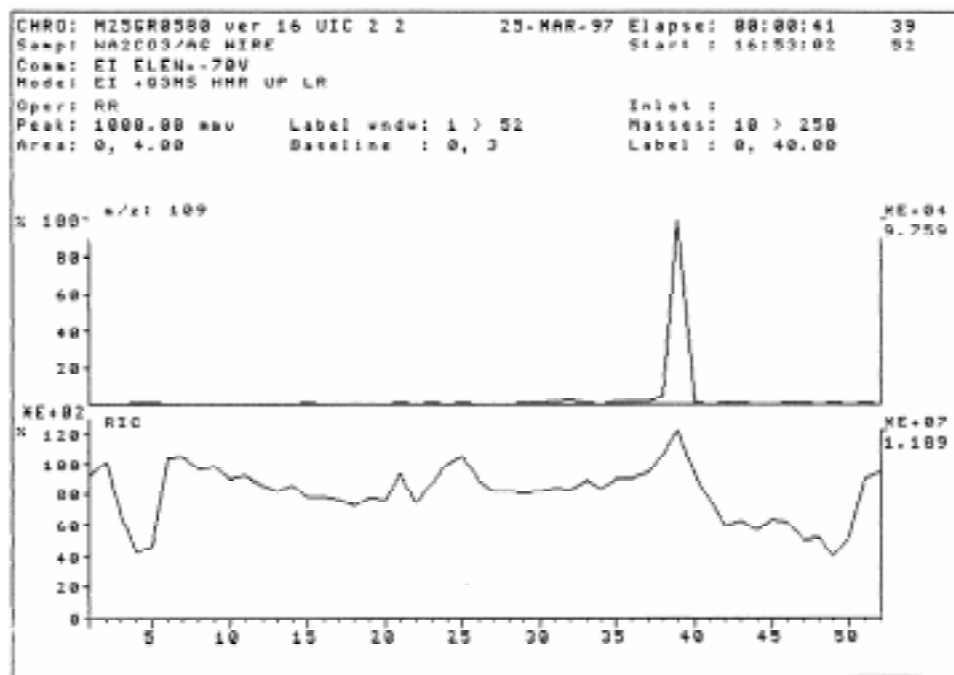
Figure 5.5.6 Time histories of Ag^+ (109) and total ion current for experiments with Ag wire. EI = 70 eV. Time 39 s corresponds to 1235 K.
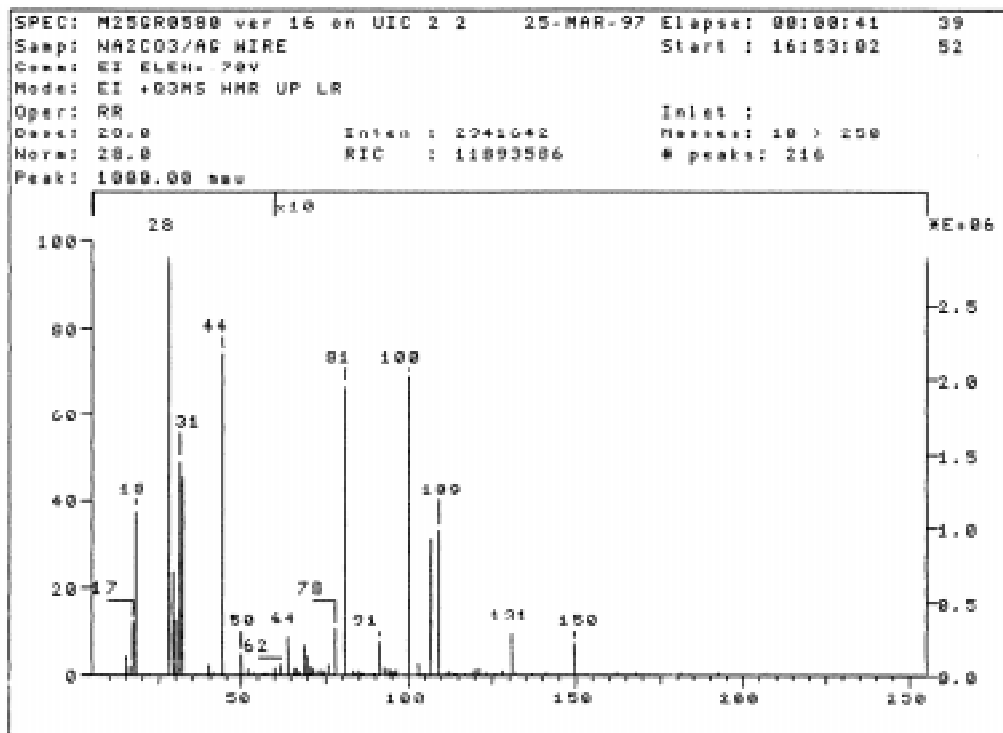
Figure 5.5.7 Mass spectrum at 1235 K. EI = 70 eV.
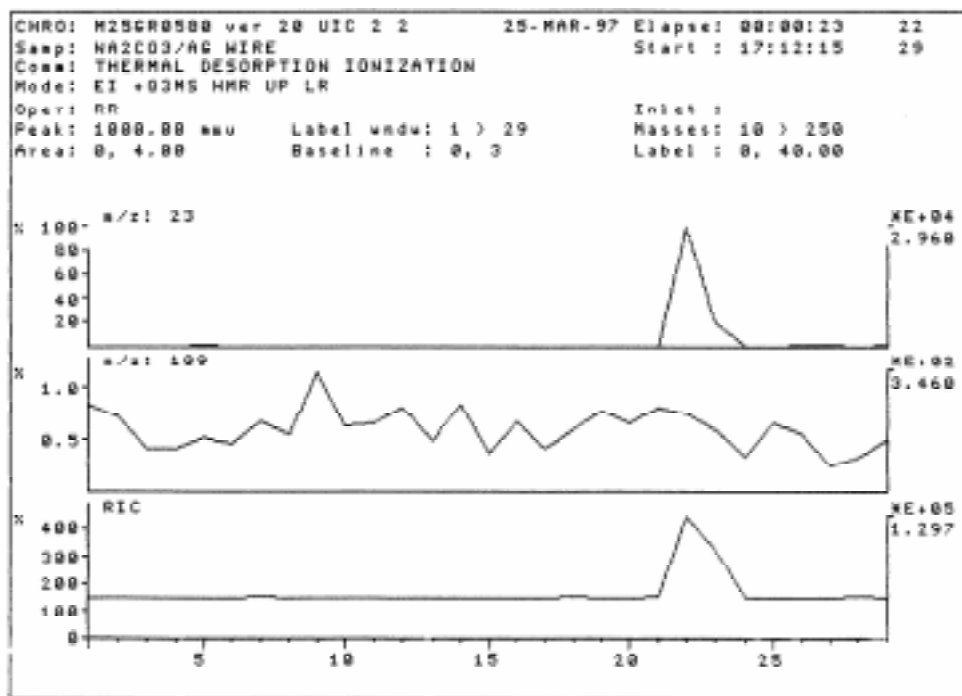
Figure 5.5.8 Time histories of ions with $m/z = 23$ (Na$^+$) and 109 (Ag$^+$), and total ion current through the detector for thermal ionization mode.
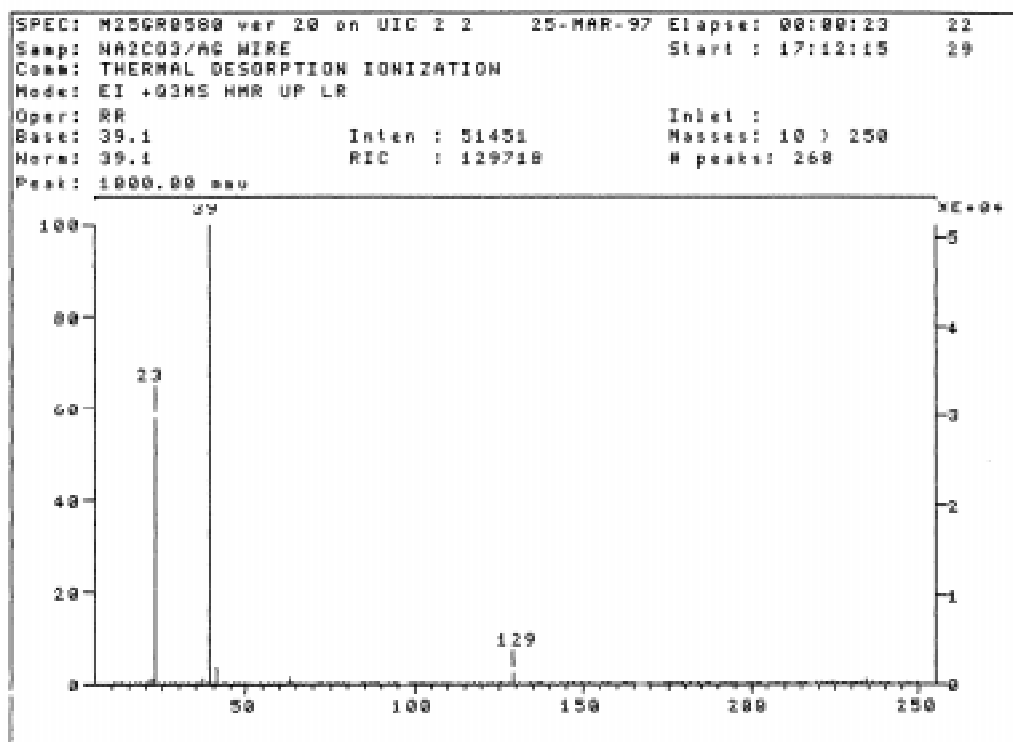
Figure 5.5.9 Mass spectrum corresponding to the moment of burnout of Ag wire for thermal ionization mode.

Mass spectrometric analysis of products of Na_2CO_3 decomposition thus confirms that the primary gas-phase decomposition products are Na, NaOH and CO_2. Experiments with temperature control show formation of Na atoms at 1235 K.

5.6 Kinetics of Na_2CO_3 Reactions: Conclusions

1. Decomposition of Na_2CO_3 was studied in a flow system over the temperature range from 900 to 1190 K. An aqueous solution of sodium carbonate was sprayed into a flow of N_2 such that the concentration of Na_2CO_3 injected into the test gas ranged from 100 to 500 ppm. The observed decomposition rate of Na_2CO_3 can be described kinetically in terms of two irreversible Na_2CO_3 $\rightarrow$ $Na_2O + CO_2$ (5.16) and $Na_2O + CO_2 \rightarrow Na_2CO_3$ (5.17) and one reversible $Na_2O + H_2O \leftrightarrow$

2NaOH (5.20) chemical reactions. The corresponding rate coefficients k_{16} and k_{17} were adjusted to describe the measured rate of Na_2CO_3 decomposition, while the rate coefficient of reaction (5.20) was estimated from kinetic data for the similar reaction of CaO. Least square fits to all data gave $k_{16} = 2.54 \times 10^6 exp(-13040/T)$, $k_{17} = 1.11 \times 10^5 exp(7580/T)$ $cm^3 mol^{-1} s^{-1}$.

2. Mass spectrometric analysis of products of Na_2CO_3 decomposition confirms that the primary gas-phase products of decomposition are Na, NaOH and CO_2. Experiments with temperature control show formation of Na atoms at temperature 1235 K.

3. Extrapolating the results of our flow system experiments to higher temperatures shows that Na_2CO_3 decomposition at temperatures over 1400 K produces NaOH and CO_2 very quickly . NaOH then decomposes more slowly. According to Westley et al. (1994), the characteristic time of NaOH decomposition at 1500 K to produce Na and OH is 160 ms; extrapolation of our data for Na_2CO_3 decomposition to that temperature gives an Na_2CO_3 decomposition time of 2.3 ms. These observations suggest that Na_2CO_3 and NaOH should have practically the same efficiencies as pollution control agents.

4. Flow system experiments at 1150 K show no chemical reaction between Na_2CO_3 decomposition products and H_2, CO, CH_4 or NO. This experiment indicates that the effect of NO removal by Na_2CO_3 is mainly due to promotional effect that Na_2CO_3 additive has on the concentrations of atoms and radicals already present in flue gas at high temperature, in particular OH and H. Enhancement of radical concentrations in the presence of Na_2CO_3 can occur through NaOH thermal decomposition

$$NaOH + M \rightarrow Na + OH + M$$
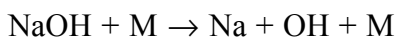
and in further reactions of Na atoms, which were observed among the products of Na_2CO_3

decomposition in mass spectrometric analysis. H-atoms, for example, are produced by

$$Na + H_2O \rightarrow NaOH + H$$
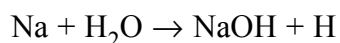
These two reactions provide for continuous flow of radicals into the system and thus account for high efficiency of Na_2CO_3. Radicals then react with NH_3 which is injected to flue gas in SNCR process

$$NH_3 + OH \rightarrow NH_2 + H_2O$$
$$NH_3 + H \rightarrow NH_2 + H_2$$
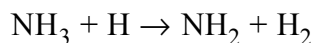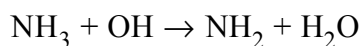
such that the efficiency of NH_3 as NO removing agent through the reaction

$$NH_2 + NO \rightarrow N_2 + H_2O$$
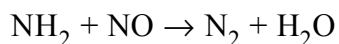
in the conventional AR process is significantly enhanced in presence of Na_2CO_3.

Our experiments indicate that other additives that have decomposition times similar to NaOH and produce active species that enhance production of OH and H radicals in flue gas should also be considered as potential NO control agents.

5. Completion of the Phase I research will include the following, as mentioned in the preceding sections. (a) Flow system experiments including ammonia and NO additives; (b) Translation of molecular electronic structure results into NASA-style thermochemical polynomials; and (c) Chemkin simulations with the expanded set of sodium species.

6.0 BENCH SCALE PROCESS OPTIMIZATION STUDIES

The Second Generation Advanced Reburning (SGAR) process includes different combinations of reburning, N-agent injection into the reburn zone, N-agent injection downstream of the reburn zone, and promoter injection. Bench scale tests were conducted at EER's Controlled Temperature Tower (CTT) to optimize each component of the technology individually and then to optimize overall performance of the combined process. Several nitrogen agents were tested. Sodium was used as the main promoter because its performance had been successfully demonstrated in previous tests. Specific test series included:

- Reburning alone
- Promoted AR-Lean
- Promoted AR-Rich
- Multiple injection advanced reburning

All tests were conducted in the CTT while firing natural gas at 20 kW (70,000 Btu/hr). The test facility and results of each test series are described in the following sections.

6.1 Controlled Temperature Tower

As shown in Figure 6.1, the CTT is a refractory lined, vertically down-fired combustion test facility designed to provide precise control of furnace temperature and gas composition. It consists of a variable swirl diffusion burner and a refractory furnace which is equipped with backfired heating channels. The furnace has an inside diameter of 8 inches. The backfired channels provide external heating to the refractory walls, allowing the rate of temperature decay to be controlled. Because of the relatively small size of the CTT, it is possible to use bottled gases (e.g. O_2, N_2, SO_2) to control furnace gas composition. In addition, characteristic mixing times in the CTT furnace are on the order of 100 ms, making it straightforward to separate zones and characterize individual processes.

Stack

Main Fuel and air
and NH3 doping

Port plugs with
injector access

Backfired
Heating
Channels

Flue Gas

Sampling
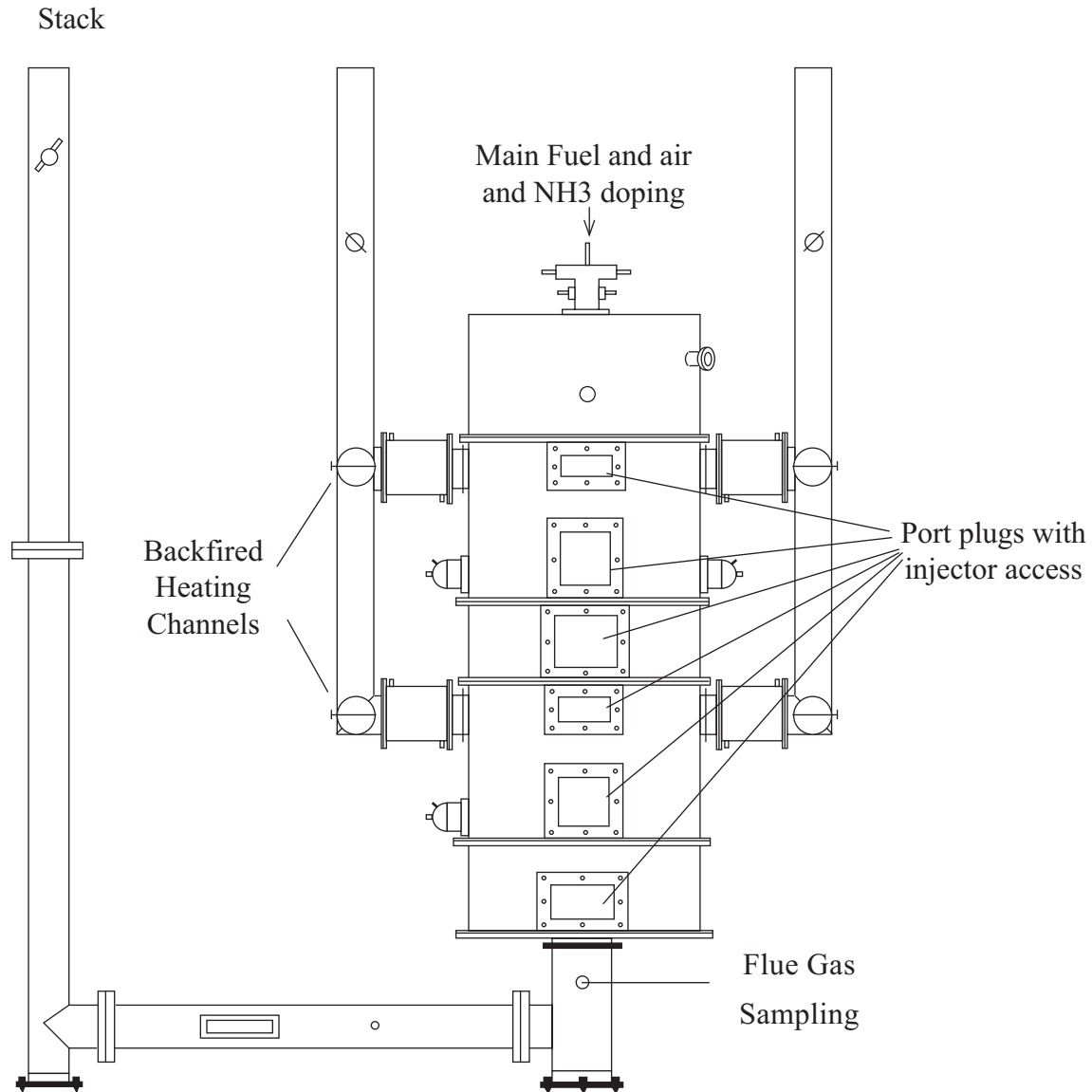
Figure 6.1 Controlled Temperature Tower (CTT).

Specific test equipment for the SGAR tests included injectors for the reburn fuel, N-agent/promoters, and overfire air. The reburn fuel and OFA were injected through radial injectors aligned upwards, i.e. countercurrent to the gas flow. The N-agents and promoters were injected through axial injectors aligned downwards. Delavan twin fluid nozzles were used for additive atomization, with bottled nitrogen as the atomization medium. Prior to the experiments, system temperature profiles were measured under various test configurations using a suction pyrometer. These profiles are presented in Figure 6.2.
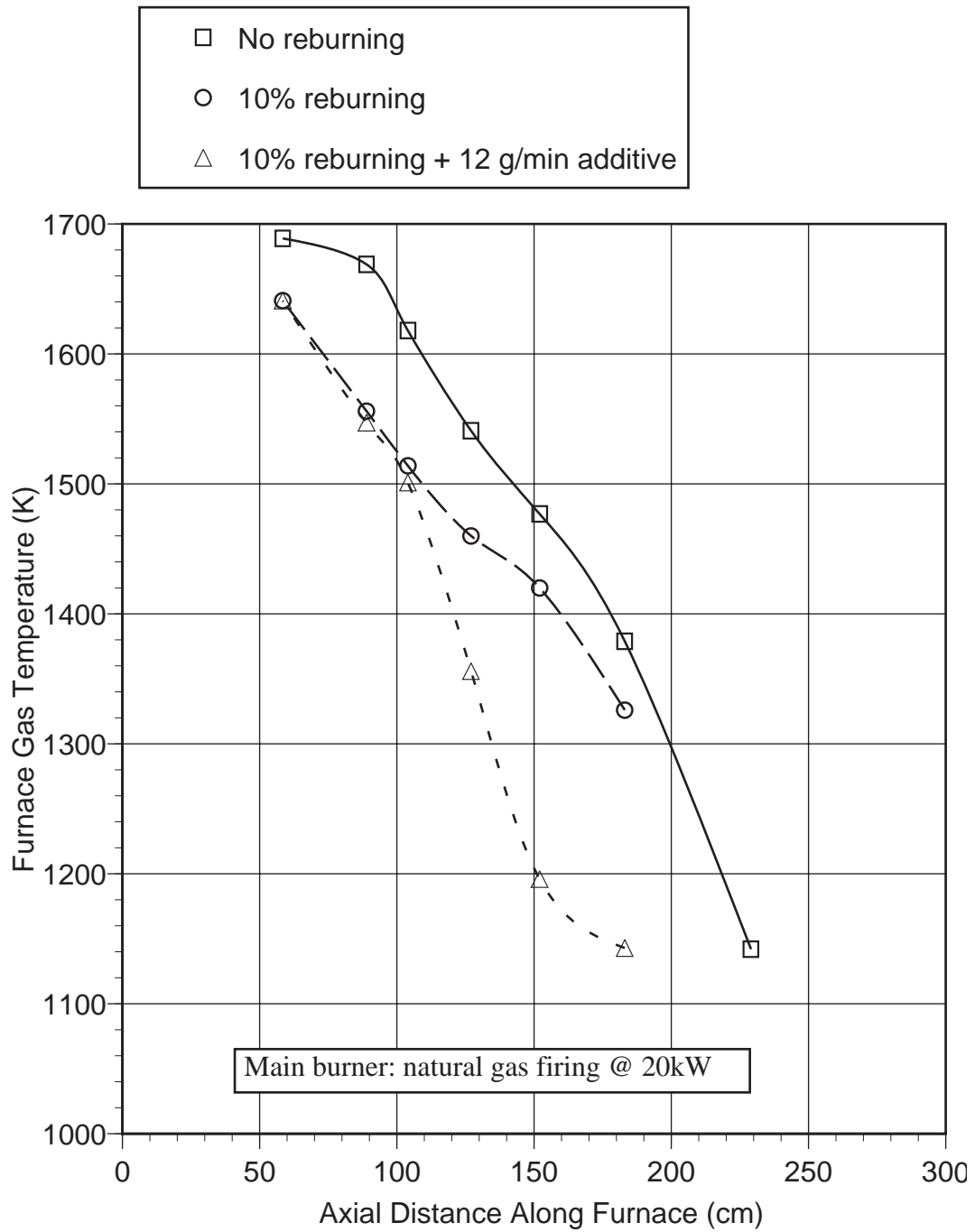
Figure 6.2 CTT temperature profiles.

Proper operation of system instrumentation was verified before the tests began, including thermocouples, pressure gauges, and the flue gas sample system. A continuous emissions monitoring system (CEMS) was used for on-line analysis of flue gas composition. The CEMS consisted of a heated sample line, sample conditioning system (to remove moisture and particulate), and gas analyzers. Species analyzed, detection principles, and detection limits were as follows:

- O_2: paramagnetism, 0.1%
- NO_x: chemiluminescence, 1 ppm
- CO: nondispersive infrared, 1 ppm
- CO_2: nondispersive infrared, 0.1%
- N_2O: nondispersive infrared, 1 ppm

Certified zero and span gases were used to calibrate the analyzers. A chart recorder was used to provide a hard copy of analyzer outputs.

6.2 Reburning Alone

The first series of tests was designed to define the nominal performance of gas reburning without additives. Test variables included reburn heat input (i.e. SR_2), reburn zone residence time, and reburn fuel transport medium (air or nitrogen). Baseline conditions were as follows:

- Reburn fuel injection temperature=1670 K
- SR_1=1.10, SR_3=1.15
- Overfire air injection temperature=1530 K
- Reburn zone residence time=350 msec
- NO_i=600 ppm as measured

Figure 6.3 shows the impact of varying reburn fuel heat input upon NO reduction. For both air and nitrogen transport, performance increased with increasing reburn heat input. Maximum NO reductions were 42% and 59% with air and nitrogen transport, respectively. On the basis of reburn heat input nitrogen transport gave greater NO reduction than air transport. However, this is primarily because nitrogen transport gives lower reburn zone stoichiometry than air. When compared on the basis of SR_2, results are nearly identical.

Main Fuel: Natural gas @ 20 kW
Reburn fuel: Natural gas
Reburn T=1670K
SR1=1.10
OFA T= 1530K
Reburn zone residence time = 0.35 sec
NOi=600 ppm as meas
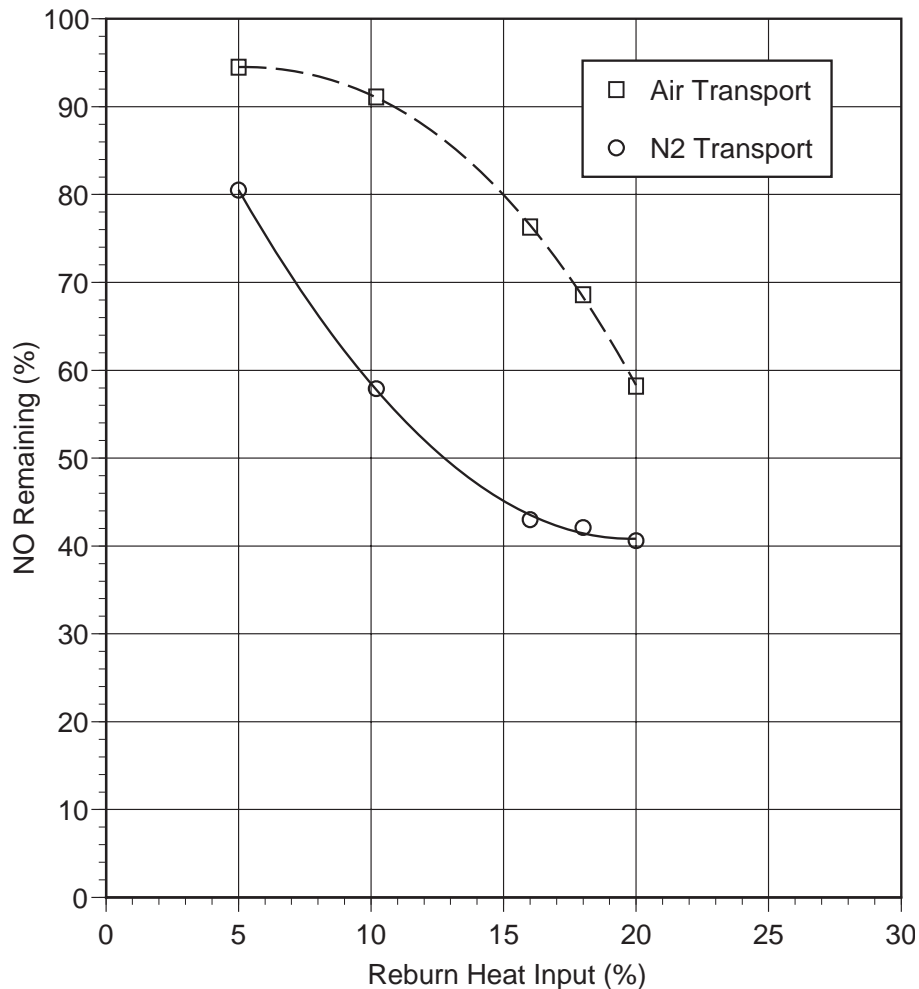
Figure 6.3 NO reduction vs. reburn heat input for CTT gas reburn: No additives or promoters.

Reburn zone residence time was varied by moving the OFA injector to different axial furnace positions. Reburn zone residence time was varied from 200 to 1600 msec at 10% reburn heat input. This corresponds to an overfire air injection temperature range of 1140 to 1590 K. As shown in Figure 6.4, with nitrogen transport NO control increased from 35 to 58% as reburn zone residence time increased from 200 to 1600 msec. With air transport NO control was not dependent upon residence time.

Main Fuel: Natural gas @ 20 kW
Reburn fuel: Natural gas
Reburn T=1670 K
SR1=1.10
10.2% Reburn
SR2 (air)=1.10, SR2(N2)=0.99
OFA T: varied
NOi=600 ppm as meas
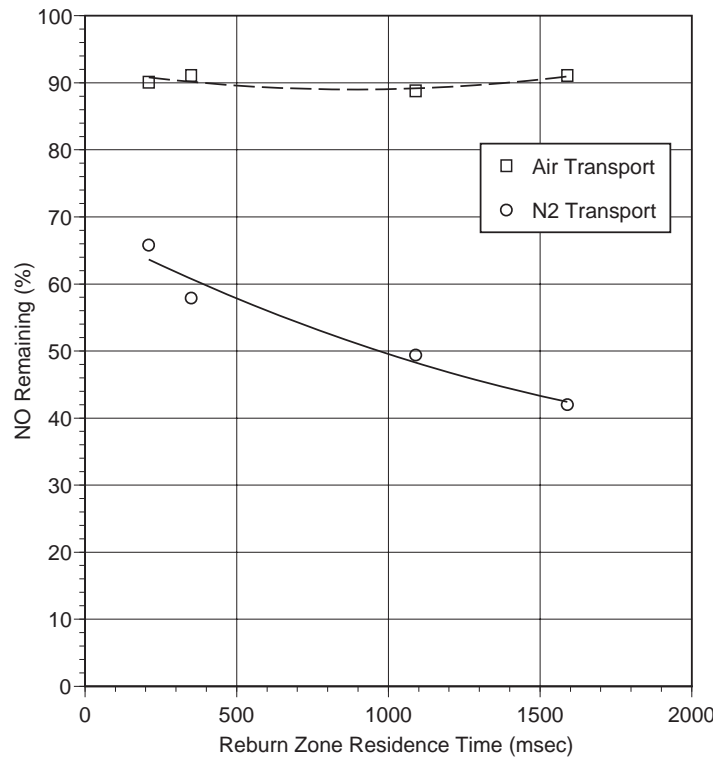
Figure 6.4 NO reduction vs. reburn zone residence time for gas reburn: No additives or promoters.

6.3 Promoted AR-Lean

In the AR-Lean tests, reburning was coupled with the injection of a single nitrogen agent, both with and without promoters. N-agent was injected with the overfire air. Reburn heat input was 10%. Figure 6.5 shows AR-Lean test results. The overfire air plus additive injection temperature was varied. This changed the reburn zone residence time, causing reburn performance to vary. Aqueous ammonia, urea, and ammonium sulfate were tested, each with and without 15 ppm of sodium carbonate promoter. The listed promoter concentration assumes complete conversion to the gas phase. Aqueous ammonia and urea performed somewhat better than ammonium sulfate. Sodium carbonate both expanded the optimum temperature window to the right (i.e. to higher temperatures) and increased maximum NO control. The highest NO reduction achieved was 87% with both promoted aqueous ammonia and promoted urea at an injection temperature of 1300 K.

Main Fuel: Natural gas @20 kW
10% Reburn @ 1670 K, N2 transport
Reburn zone res. time varies
SR1=1.10, SR2=0.99, SR3=1.15
NOi=600 ppm as meas, NSR=1.5
N agent added with OFA

Legend:
⊹ Reburn Alone
○ Reburn+NH4OH
△ Reburn+Urea
□ Reburn+(NH4)2SO4
● Reburn+NH4OH+15ppm Na2CO3
▲ Reburn+Urea+15ppm Na2CO3
■ Reburn+(NH4)2SO4+15ppm Na2CO3
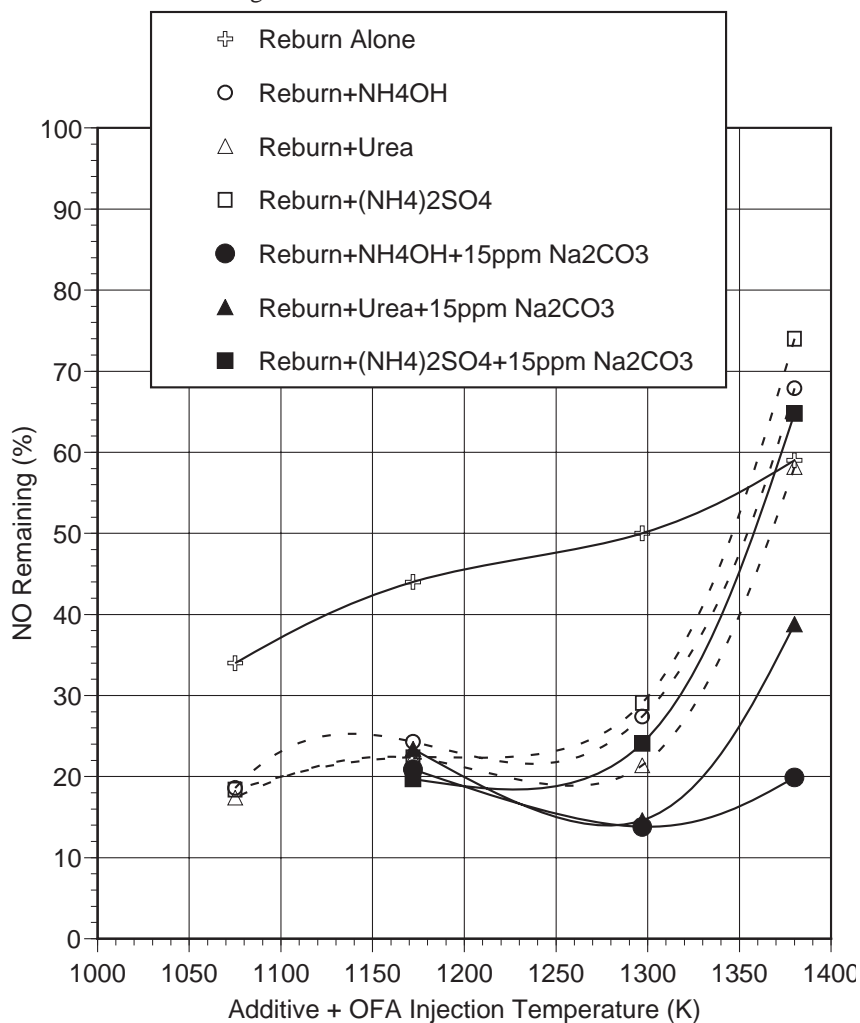
Figure 6.5 AR-Lean performance.

6.4 Promoted AR-Rich

In the AR-Rich tests aqueous ammonia and urea were injected into the fuel rich reburn zone. Overfire air was added at 1160 K. As shown in Figure 6.6, the impact of the promoter was pronounced for this test system. Sodium carbonate shifted the optimum temperature to the right and significantly widened the temperature window. Maximum NO reduction was 88%, obtained with both promoted aqueous ammonia and promoted urea at an injection temperature of 1470 K.

6-7

Figure 6.6 AR-Rich performance.

A series of screening tests was then conducted with different sodium promoter compounds. The promoters were injected along with aqueous ammonia into the reburn zone at 1460 K. Six different sodium compounds were characterized including Na_2CO_3, $NaHCO_3$, trona (a mineral product consisting of Na_2CO_3 and $NaHCO_3$), NaCl, $NaNO_3$, and NaOH. As shown in Figure 6.7, reburning alone provided 47% NO control, which was increased to 57% by the addition of ammonia. All six sodium compounds significantly enhanced performance, although NaCl and $NaNO_3$ were somewhat less effective than the other four. Na_2CO_3 is effective, non-toxic, readily soluble in water, and is the least expensive compound on a unit-sodium basis, and thus was selected as the primary promoter compound for subsequent tests.

The chart contains the following text box:

Main Fuel: Natural gas @ 20 kW
10% Reburn @ 1670 K, N2 transport
OFA@1300 K
Reburn zone res. time=0.50 sec
SR1=1.10, SR2=0.99, SR3=1.15
NOi=600 ppm as meas
NSR=1.5
Promoter conc.= 30 ppm
Additive Injection Temp=1460 K

Y-axis: NO Remaining (%), ranging from 0 to 100

X-axis categories: Reburn Only, Reb+NH4OH, +Na2CO3, +NaHCO3, + Trona, +NaCl, +NaNO3, +NaOH
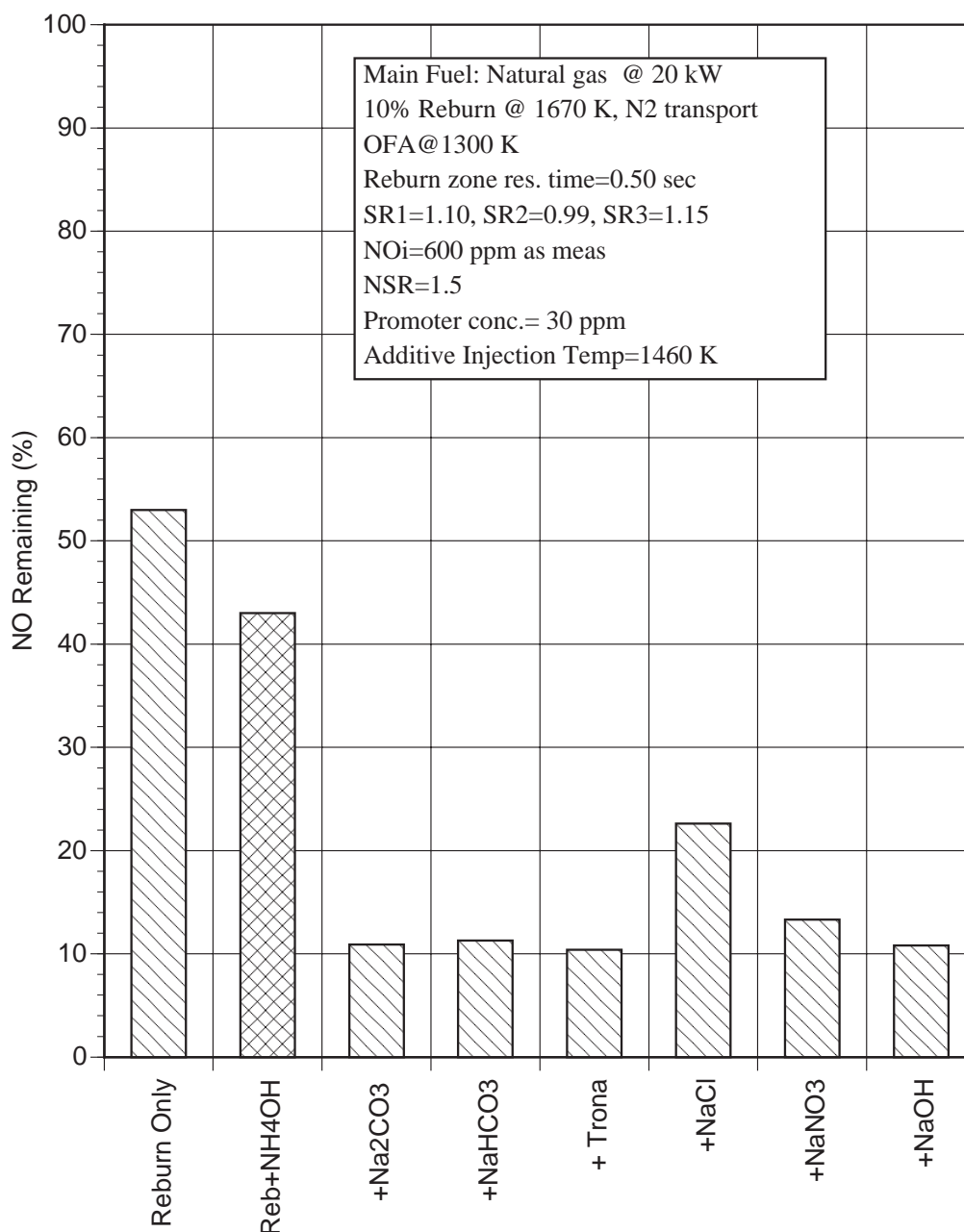
Figure 6.7 Alternative promoter screening test results.

Parametric studies were then conducted to evaluate the impact of three process variables: sodium concentration, initial NO concentration, and N-agent to NO stoichiometric ratio. Sodium concentration was varied during injection of aqueous ammonia and urea into the fuel rich zone with 10% reburning. As shown in Figure 6.8, NO control increased as sodium concentration increased from 0 to 30 ppm, and then levelled off as sodium concentration was further increased to over 100 ppm. Even 10 ppm Na (i.e. 5 ppm Na_2CO_3) reduced the remaining NO fraction by 21 percentage points, from 42 to 21%.

Main Fuel: Natural gas @ 20 kW
10% Reburn @ 1670 K, N2 transport
Reburn zone res. time=0.72 sec
OFA added at 1160 K
SR1=1.10, SR2=0.99, SR3=1.15
NOi=600 ppm as meas
NSRi=1.5
Additive Injection Temp=1380 K
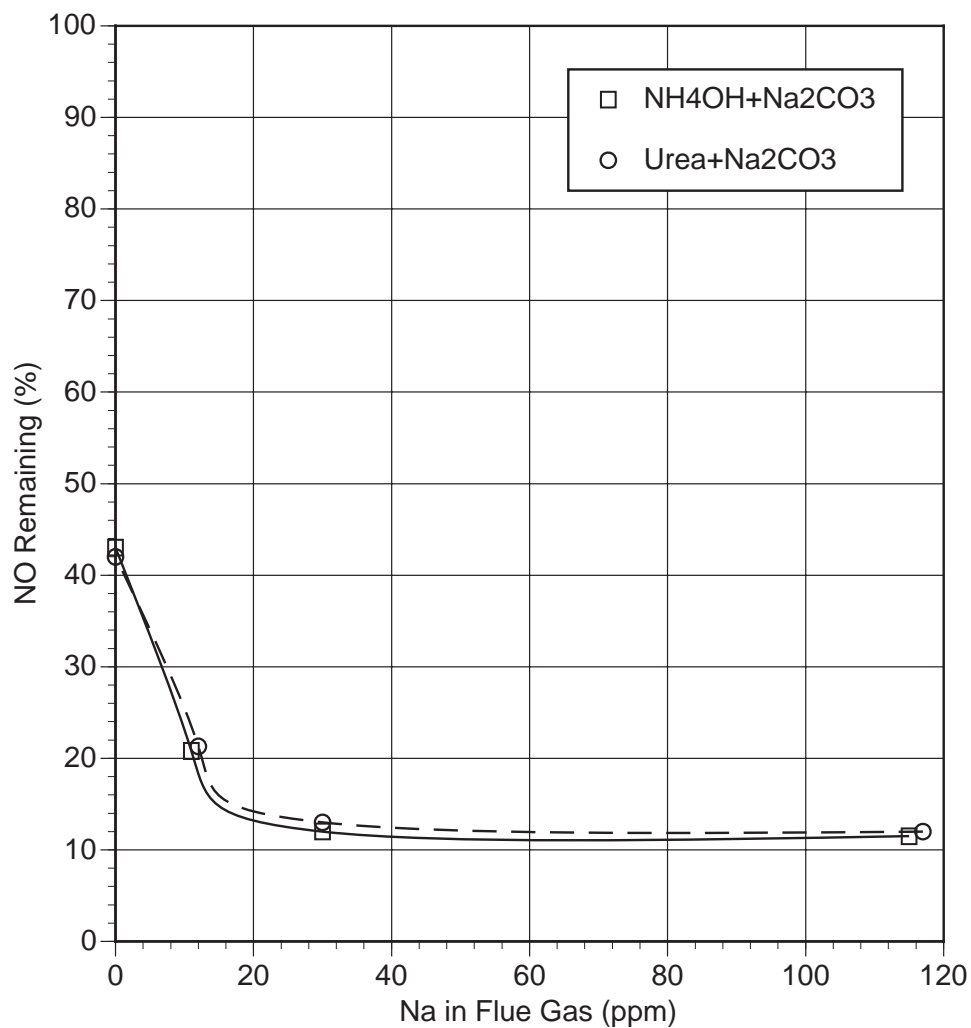
Figure 6.8 NO control vs. Na promoter concentration.

Initial NO concentration was varied from 150 to 950 ppm during tests with reburn alone and reburn plus injection of aqueous ammonia and sodium carbonate. As shown in Figure 6.9, NO reduction increased with increasing NO_i. For reburn plus injection of aqueous ammonia and sodium carbonate over 90% NO control was obtained at NO_i=950 ppm.

Main Fuel: Natural gas @ 20 kW
10% Reburn @ 1670 K
OFA @ 1300 K
Additive @ 1460 K
SR1=1.10, SR2=0.99, SR3=1.15
NSR=1.5
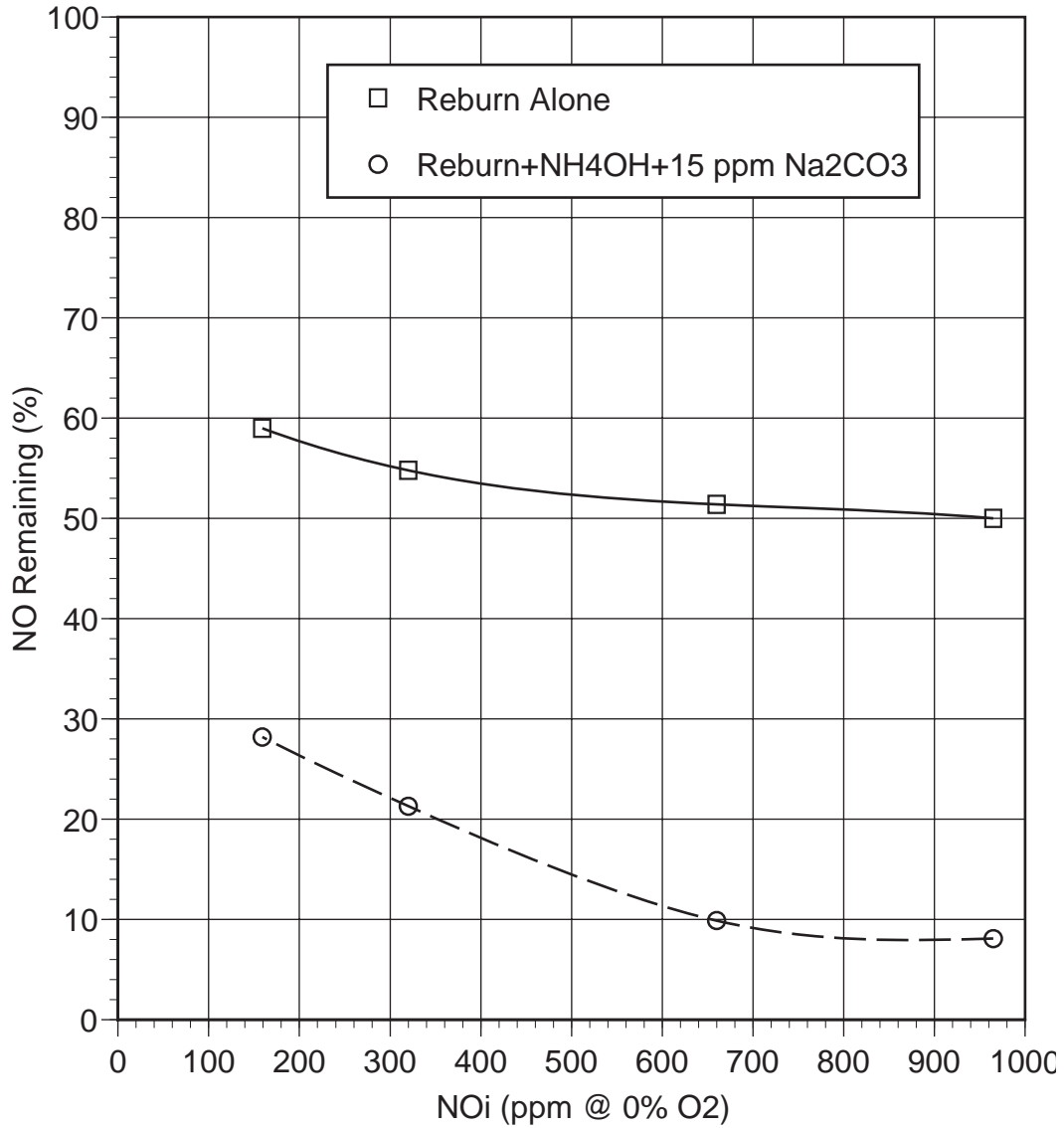
Figure 6.9 NO reduction vs. NO_i for rich side injection of $NH_4OH + Na_2CO_3$.

Nitrogen agent to NO_i stoichiometric ratio (NSR) was then varied from 0 to 2.0. As shown in Figure 6.10, NO reduction increased with increasing NSR. NO reduction was 93% at NSR=2.0.

Main Fuel: Natural gas @ 20 kW
10% Reburn @ 1670 K
OFA @ 1300 K
Additive @ 1460 K
SR1=1.10, SR2=0.99, SR3=1.15
NOi=600 ppm as meas
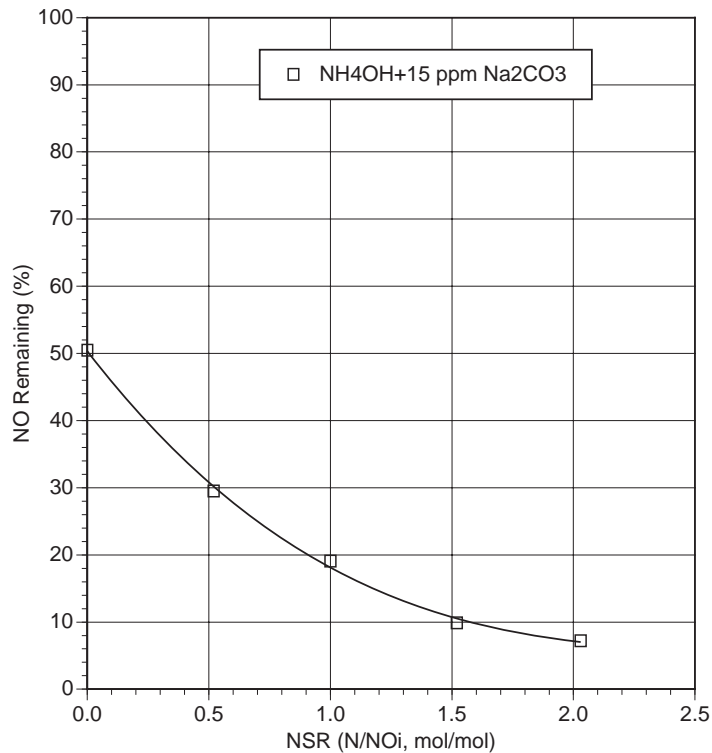
Figure 6.10 NO reduction vs. NSR for rich side injection of $NH_4OH + Na_2CO_3$.

6.5 Multiple Injection AR (MIAR)

In the MIAR process N-agents and promoters are injected both in the reburn zone and with the overfire air. CTT tests were conducted in which various combinations of rich and lean side additives were injected. Figure 6.11 shows MIAR results obtained with promoter added to the fuel rich zone. A maximum of 50% NO control was obtained by reburning alone. AR-Rich provided up to 67% NO control. Reburning plus both rich and lean side injection of aqueous ammonia with no promoter gave a maximum of 86% NO control. The best performance was obtained with reburning with rich side injection of N-agent plus promoter and lean side injection of N-agent alone. This system reduced NO emissions by over 90%. Reburning with rich side N-agent injection and lean side N-agent plus promoter injection also gave up to 90% NO control. Moreover, these systems were largely insensitive to injection temperature, with approximately 90% NO control obtained over the entire test range of 1380 to 1590 K.

Main Fuel: Natural gas @ 20 kW
10% Reburn @ 1670 K, OFA @ 1300 K
SR1=1.10, SR2=0.99, SR3=1.15
NOi=600 ppm as meas
First N-agent added in fuel rich zone: NSR=1.5
Second N-agent added w/OFA: NSR=1.5
Na_2CO_3 conc. in flue gas=15 ppm

△ Reburn Alone

○ Reburn+rich side NH4OH

□ Reburn+rich side (NH4OH+Na2CO3)

● Reburn+rich side NH4OH+lean side NH4OH

■ Reburn+rich side(NH4OH+Na2CO3)+lean side NH4OH
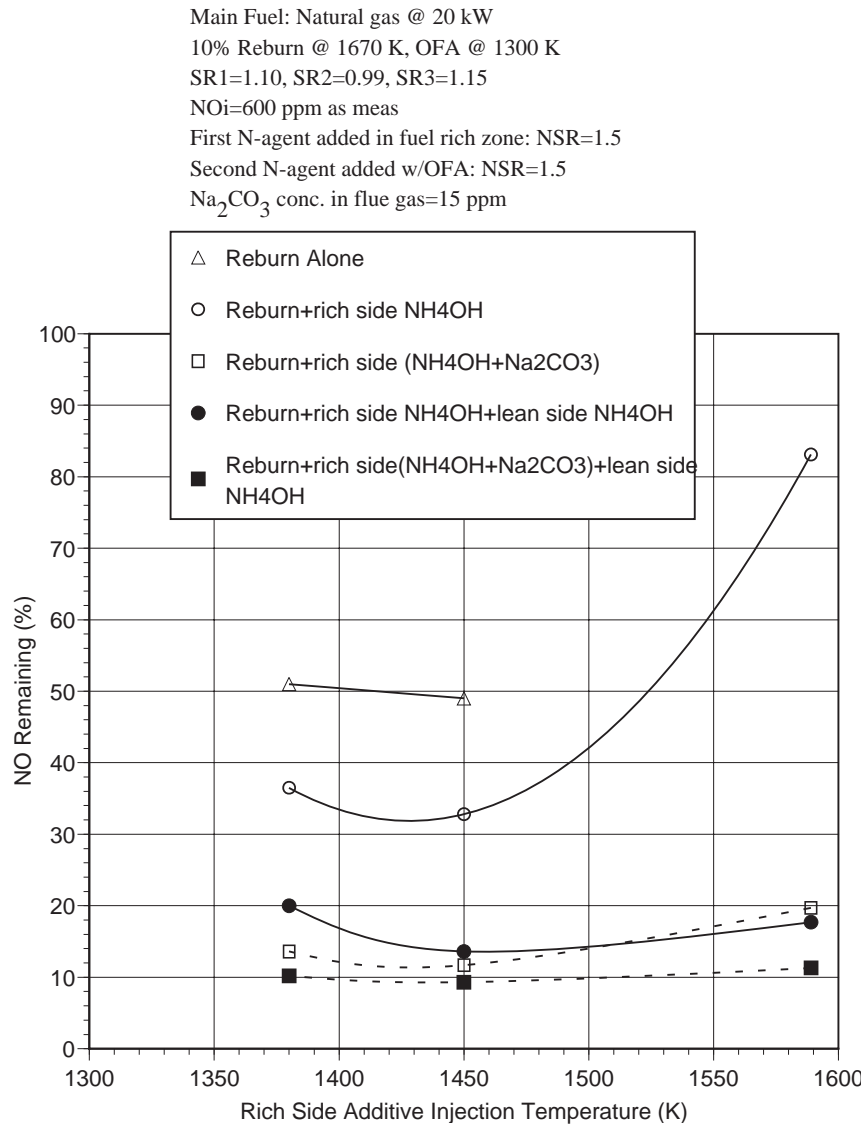
Figure 6.11 MIAR: NO reduction vs. additive injection temperature for reburn with both rich and lean side additives.

6.6 Bench Scale Combustion Tests: Conclusions

Under the closely-controlled process conditions obtained at the 20 kW combustion test facility, the following results were obtained:

1. Reburning alone achieved 50-60% NO reduction with SR_2=0.99-0.90 and high OFA injection temperature.

6-13

2. Promoted AR-Lean provided up to 86% NO reduction at 10% reburning heat input and 15 ppm Na_2CO_3 in the flue gas.

3. Promoted AR-Rich provided up to 88% NO reduction at 10% reburning heat input and 15 ppm Na_2CO_3 in the flue gas.

4. MIAR provided up to 91% NO removal, which is expected to increase at larger scale since the injectors will not affect the temperature profile.

7.0 PILOT SCALE DEVELOPMENT TESTS

Pilot scale tests were performed to build upon the bench scale results in a test facility more closely simulating the combustion conditions found in a full scale boiler. The test facility was first configured to match the residence time-temperature profile of a typical boiler, and then SGAR performance tests were conducted with both natural gas and coal as primary fuels. A series of sampling test runs was also performed to determine if the SGAR technologies caused concentrations of any byproduct species to increase.

7.1 Preparation of Pilot Scale Combustion Facility

The pilot scale test work was conducted in EER's Boiler Simulation Facility (BSF), which has a full load firing capacity of 300 kW (1 MMBtu/hr). The BSF is designed to provide an accurate subscale simulation of the flue gas temperatures and composition found in a full scale boiler. Prior to the tests the BSF was configured to provide access for all required reburn, additive, and overfire air injectors.

7.1.1 Boiler Simulator Facility

A schematic of the BSF is shown in Figure 7.1. The furnace is designed with a high degree of flexibility to produce combustion conditions typical of full scale utility boilers. The BSF consists of a burner, vertically down–fired radiant furnace, horizontal convective pass, and baghouse. A variable swirl diffusion burner with an axial fuel injector is used to simulate the approximate temperature and gas composition of a commercial burner in a full scale boiler. Primary air is injected axially, while the secondary air stream is injected radially through the swirl vanes to provide controlled fuel/air mixing. The swirl number can be controlled by adjusting the angle of the swirl vanes. Numerous ports located along the axis of the facility allow supplementary equipment such as reburn injectors, additive injectors, overfire air injectors, and sampling probes to be placed in the furnace.
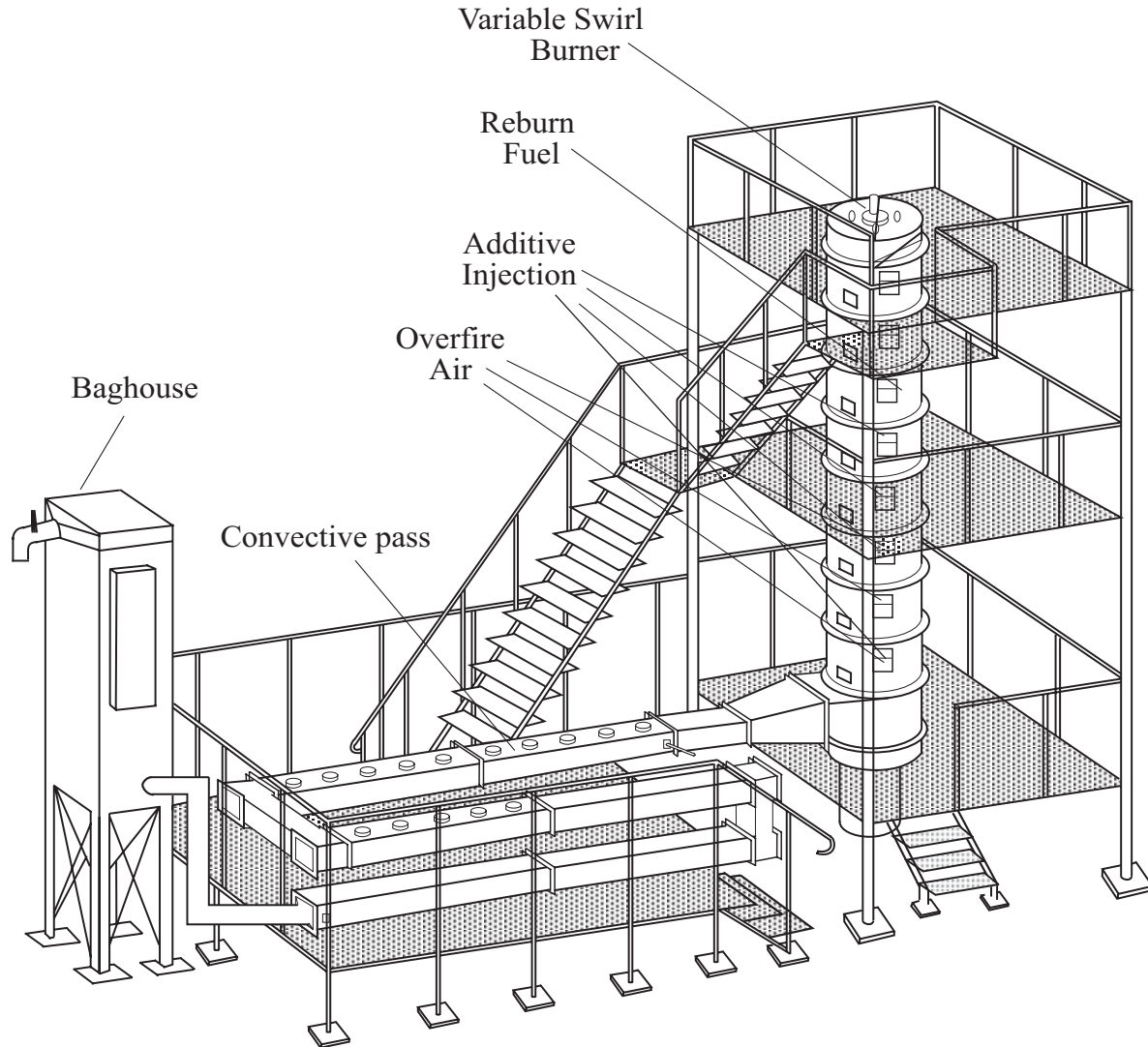
Figure 7.1 Boiler Simulator Facility (BSF).

The cylindrical furnace section is constructed of eight modular refractory lined sections with an inside diameter of 22 inches. The convective pass is also refractory lined, and contains air cooled tube bundles to simulate the superheater and reheater sections of a utility boiler. Heat extraction in the radiant furnace and convective pass can be controlled such that the residence time-temperature profile matches that of a typical full scale boiler. A suction pyrometer is used to measure furnace temperatures. Figure 7.2 shows the BSF temperature profile during natural gas firing with 10% reburning. Furnace temperatures are similar during coal firing.
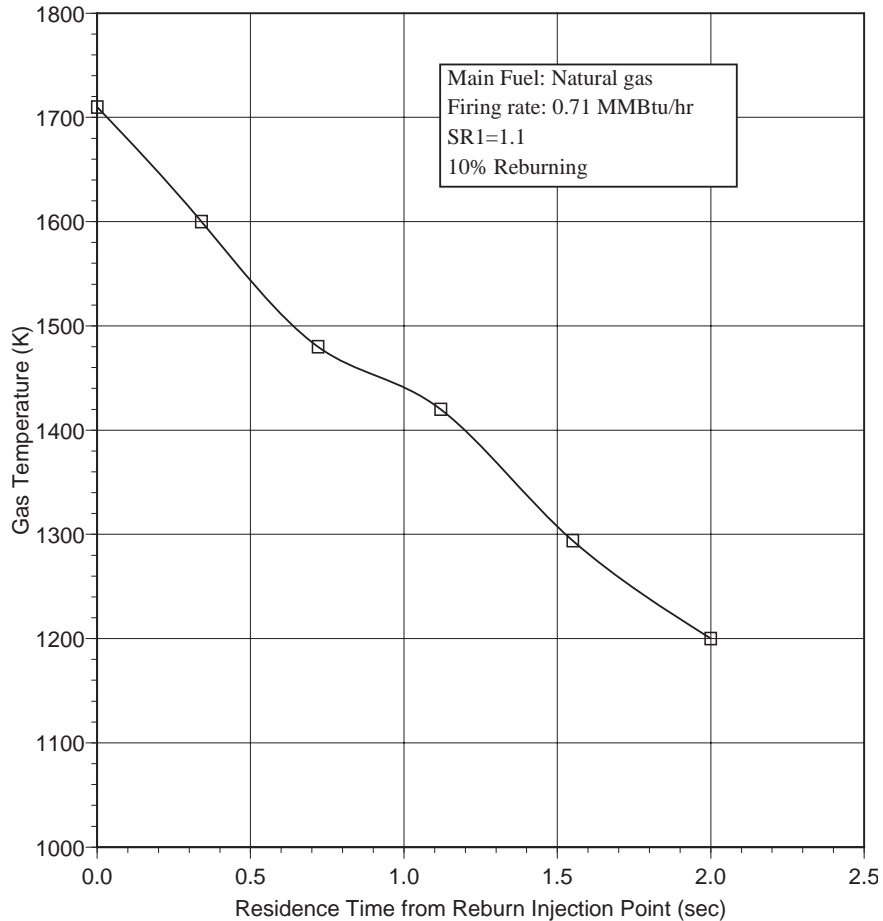
Figure 7.2 BSF temperature profile during 10% reburning.

Test fuels included natural gas and pulverized coal. Municipal natural gas was used, and was delivered by means of line pressure. Two test coals were employed, including a low sulfur bituminous Utah coal and a high sulfur bituminous Illinois coal. Each coal was pulverized such that 70% passed through a 200 mesh screen. Coal was metered using a twin screw feeder and was pneumatically transported to the burner.

7.1.2 Reburning and Additive Injection Systems

Natural gas was used as the reburn fuel. The reburn injector was elbow-shaped, and was installed along the centerline of the furnace, aligned in the direction of gas flow. A gaseous transport medium was added along with the reburn natural gas to provide sufficient momentum for good mixing with the furnace gas. Both air and bottled nitrogen were tested as transport media. Overfire air was injected through an elbow-shaped injector to burn out combustibles generated in the reburn zone. The OFA injection temperature was varied as required by the test plan.

Nitrogen agents and sodium promoters were injected as aqueous solutions. Twin fluid atomizers made by Delavan Corp. were used, employing both air and nitrogen as transport media. The additives were injected into the reburn zone and/or with the OFA. In the latter case, the OFA itself was used as the atomization medium.

7.1.3 Sampling and Analysis Methods

A continuous emissions monitoring system (CEMS) was used for on-line flue gas analysis. CEMS equipment and analyzers were identical to those for the bench scale tests, as described in Section 6.1. Manual method sampling was also performed for the following byproduct species:

- NH_3 and HCN: EPA Draft Method 206 with ion chromatography analysis
- SO_3: controlled condensation
- Fly ash mass loading, size distribution, PM10, and PM2.5: EPA Method 5 and cascade impactors
- Carbon in ash: Extractive ash sampling with induction furnace analysis

7.2 Pilot Scale Combustion Tests with Natural Gas Firing

In the initial pilot scale tests, natural gas was used as the main and reburning fuel. The initial NO concentration, 600 ppm, was established by addition of ammonia to primary natural gas. The reburning fuel (10% of total heat input) provided slightly fuel-rich conditions in the reburn zone with $SR_2=0.99$. Processes characterized included promoted AR-Lean, promoted AR-Rich, hybrid AR-Lean/SNCR, hybrid AR-Rich/SNCR, and MIAR.

7.2.1 Promoted AR-Lean

AR-Lean includes the addition of reburning fuel followed by injection of OFA along with an N-agent. The N-agent can be injected with or without promoter which is dissolved in the aqueous N-agent solution. In all tests, the amount of N-agent corresponded to NSR=1.5.

Figures 7.3 and 7.4 demonstrate the performance of the AR-Lean process for injection of urea and aqueous ammonia, respectively. Reburning alone gave about 50% NO reduction, and depended slightly on the OFA injection location. At OFA injection temperatures of 1140 and 1530 K, NO was reduced by 52 and 47%, respectively. Injection of urea with OFA provided 53-82% NO reduction depending on the injection temperature. The performance of ammonia was slightly lower, i.e. 45-

81%. At an injection location of 1330 K, urea gave 78% NO reduction, while ammonia only 70%. The results with ammonia injection are qualitatively consistent with modeling (Section 8) taking into account the fact that ammonia appears in the gas mixture with a short delay time that is necessary for evaporation of the solution. Addition of sodium carbonate to the N-agent greatly improved NO reduction. Performance was about equal for ammonia and urea, in the range of 54-94% with optimum performance obtained between 1200 and 1370 K. These data are in agreement with the CTT results, although slightly higher NO reduction (by about 2-5 percentage points) was obtained in the BSF. As in the CTT tests, there is almost no difference in NO reduction between injection of 30 and 50 ppm Na.
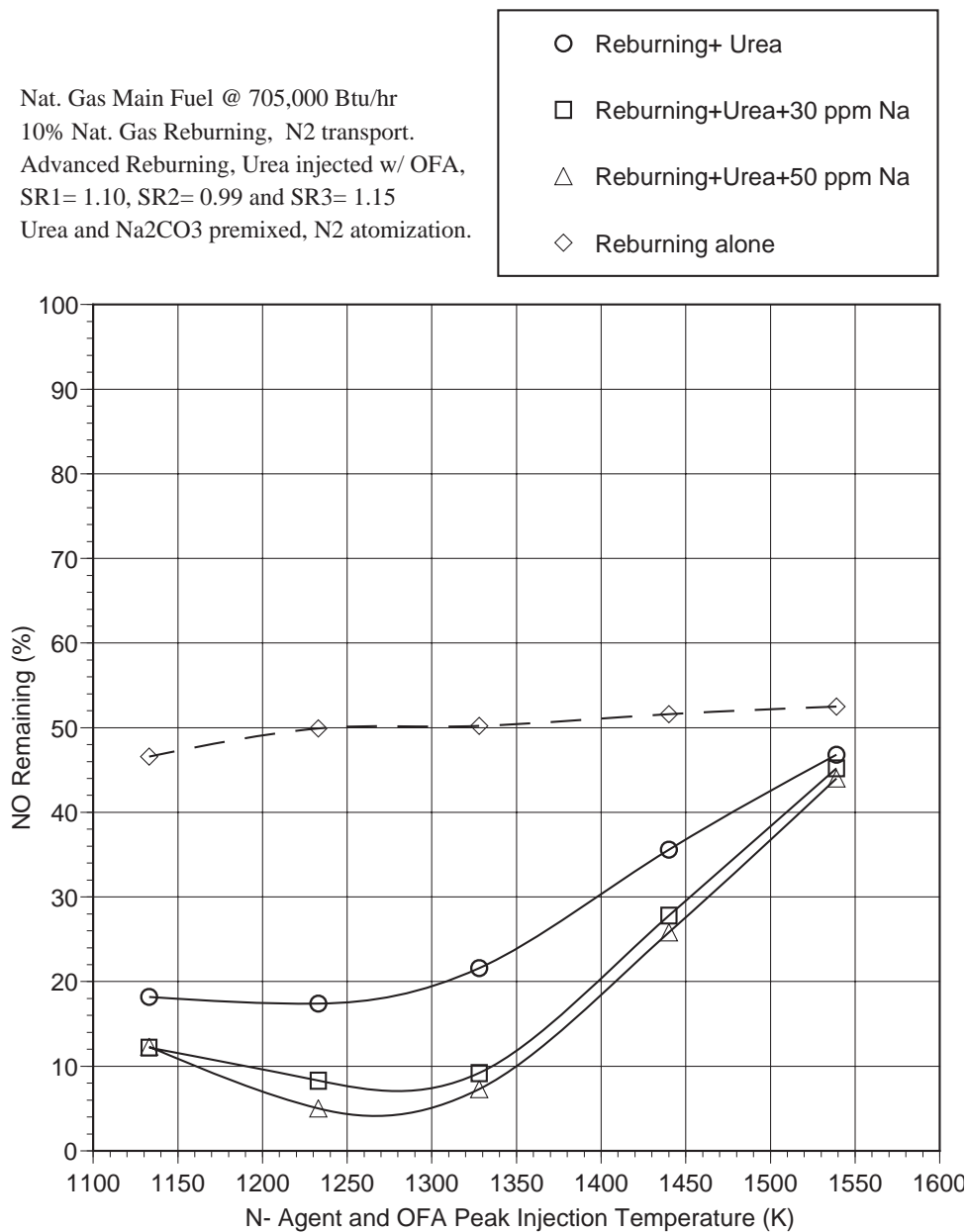
Figure 7.3 AR-Lean with aqueous urea/sodium injection.

Figure 7.4 AR-Lean with aqueous ammonia/sodium injection.

Interestingly, the presence of small sodium amounts (30-50 ppm) affected CO emissions at low OFA injection temperatures. Without sodium, CO emissions were 20-60 ppm when OFA and N-agent were injected at 1230 K, and 100-120 ppm at 1130 K. In the presence of sodium, CO emissions were 60-100 ppm at 1230 K, and 120-320 ppm at 1130 K. At OFA injection temperatures higher than 1230 K, CO emissions were 20-30 ppm even in the presence of sodium. Thus, the optimum OFA/N-agent injection temperature is about 1260-1370 K. At these temperatures, NO can be reduced by 89-94% without increasing CO emissions.

7.2.2 Promoted AR-Rich

The AR-Rich process includes injection of reburning fuel, injection of N-agent into the reburning zone, and injection of OFA. The N-agent can be injected with or without promoter which is, as in AR-Lean, dissolved in an aqueous solution of the N-agent. In all tests the amount of N-agent corresponded to NSR=1.5.

The performance of AR-Rich greatly depends on the OFA injection temperature. Figures 7.5 and 7.6 show experimental results obtained with injection of urea and aqueous ammonia, respectively, for OFA injection at 1180 K. Each reagent provided 70-77% NO reduction, depending on injection temperature. However, addition of sodium carbonate at 30-50 ppm Na significantly improved NO reduction, up to 94-95%. Again, the reduction of NO in the BSF was a few percentage points better than that in the bench scale CTT.

Nat. Gas Main Fuel @ 705,000 Btu/hr
10% Nat. Gas Reburning, N2 transport.
Advanced Reburn, Urea injected in reburn zone
SR1= 1.10, SR2= 0.99 and SR3= 1.15
Urea & Na2CO3 premixed, N2 atomization.

○ Reburning+Urea
□ Reburning+Urea+30 ppm Na
△ Reburning+Urea+50 ppm Na
◆ Reburning alone
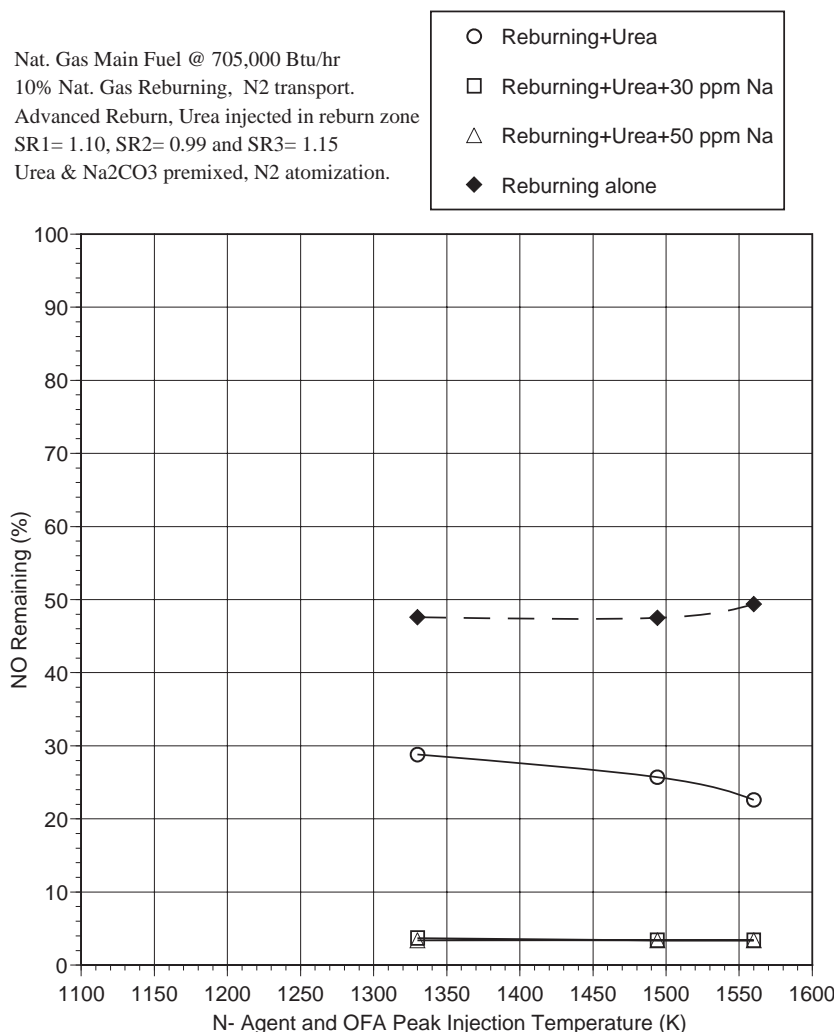
Figure 7.5 AR-Rich with urea/sodium injection. OFA is injected at 1180 K.
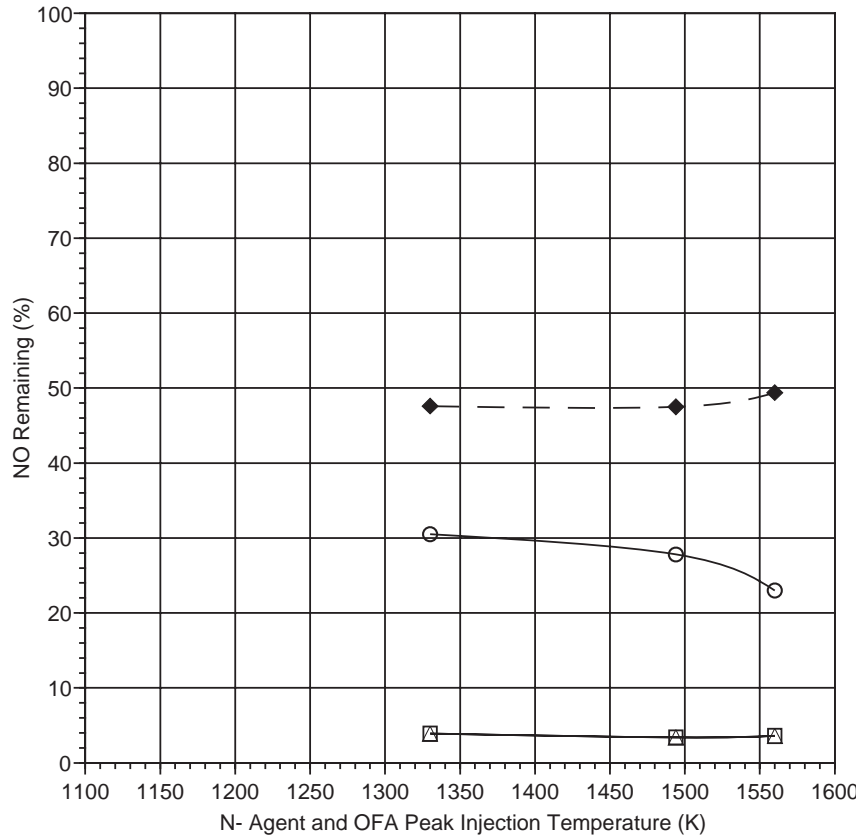
Figure 7.6 AR-Rich with ammonia/sodium injection. OFA is injected at 1180 K.

Surprisingly, injection of 30-50 ppm sodium resulted in much higher CO emissions (at low OFA injection temperatures) than in the AR-Lean process. Without sodium, CO emissions were within 10-25 ppm, but injection of sodium caused greater than 2500 ppm CO emissions. This effect (higher CO emissions after injection of sodium under fuel rich conditions) was noticed earlier in the CTT tests, but measurement accuracy was considered to be questionable. In the BSF tests, CO measurements were carefully checked and repeated. High CO emissions show that in the presence of sodium the process of CO oxidation is inhibited. This inhibition effect is stronger under fuel rich conditions. A possible explanation of this effect is the existence of the chain reaction involving sodium compounds, H atoms and OH radicals:

$$NaOH + H \rightarrow Na + H_2O \tag{7.1}$$

$$Na + OH + M \rightarrow NaOH + M \tag{7.2}$$

Sodium hydroxide, NaOH, can be formed via thermal decomposition of sodium carbonate followed by the reaction of sodium oxide with water vapor that is available in flue gas:

$$Na_2CO_3 = Na_2O + CO_2 \tag{7.3}$$
$$Na_2O + H_2O = 2\ NaOH \tag{7.4}$$

Then, NaOH reacts with H atoms via reaction (7.1) to form Na atoms and H_2O molecules. The Na atoms can then recombine with OH radicals to return NaOH (7.2). The total reaction (7.1)+(7.2) is just H and OH recombination into water:

Total (7.1)+(7.2): $$H + OH + M \rightarrow H_2O + M \tag{7.5}$$
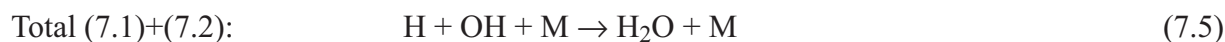
Thus, under certain conditions, the total amount of H and OH radicals can be reduced, due to the presence of sodium compounds. As a result, CO can escape oxidation, since the main reaction of CO oxidation is the interaction with hydroxyl radicals:

$$CO + OH \rightarrow CO_2 + H \tag{7.6}$$

Under fuel rich conditions, the total amount of radicals is typically lower than under fuel lean conditions. Therefore, this mechanism of radicals suppression can be more important under fuel rich conditions. The experimental effort at the University of Texas (Section 5) and the modeling study (Section 8) were conducted to model and better understand the reactions of Na in flue gas. A preliminary reaction mechanism with Na reactions was selected and is presented in Section 8.

Similar to AR-Lean, increasing the OFA temperature during AR-Rich can decrease CO emissions in the presence of sodium. AR-Rich tests were conducted with two higher OFA temperatures: 1380 and 1510 K. Figures 7.7 and 7.8 present the results. Injection of 20 g/min water in the reburning zone did not change NO reduction. When urea was added, 60-70% NO reduction was achieved. Sodium promoted the reaction up to 80-90% NO reduction, i.e. 10-20% NO remaining. CO emissions were also found to decrease to near baseline levels at these high OFA temperatures.

Main Fuel: Nat. gas @ 705,000 Btu/hr
10% Reburn @ 1710 K, N2 transport
SR1 = 1.10, SR2 = 0.99, SR3 = 1.15
NOi = 600 ppm as measured
OFA Temperature = 1380 K
Na2CO3 Concentration = 15 ppm
NSR = 1.5

☐ Reburn+20 g /min water

○ Reburn+20 g /min Soln. w/Urea

△ Reburn+20 g /min Soln. w/Urea & Na2CO3
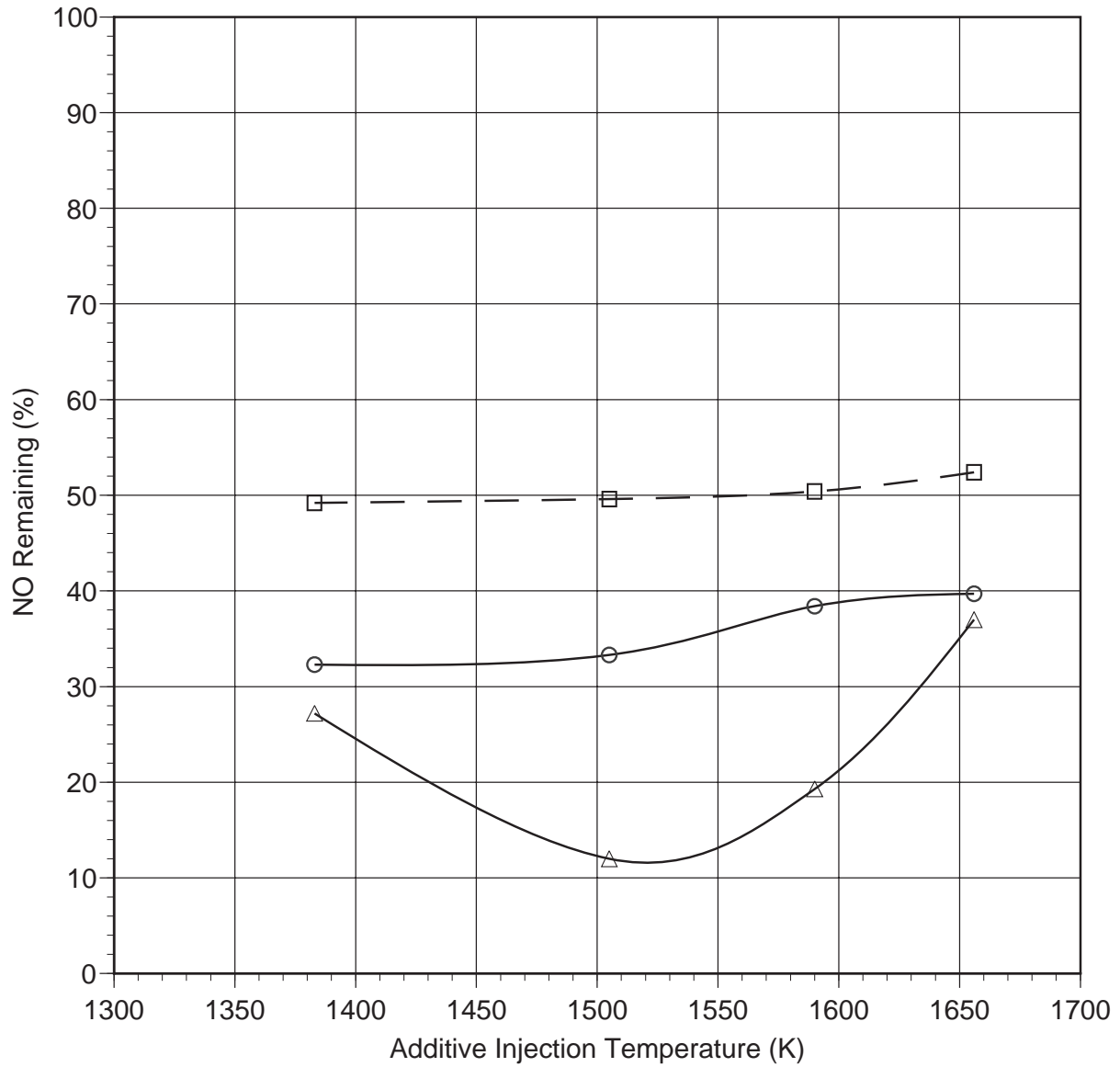
Figure 7.7 AR-Rich with urea/sodium injection. OFA is injected at 1380 K.

Main Fuel: Nat. gas @ 705,000 Btu/hr
10% Reburn @ 1710 K, N2 transport
SR1 = 1.10, SR2 = 0.99, SR3 = 1.15
NOi = 600 ppm as measured
OFA Temperature = 1380 K
Na2CO3 Concentration = 15 ppm
NSR = 1.5

CO below 20 ppm for all tests

□	Reburn+20 g /min water
○	Reburn+20 g /min Soln. w/Urea
△	Reburn+20 g /min Soln. w/Urea & Na2CO3
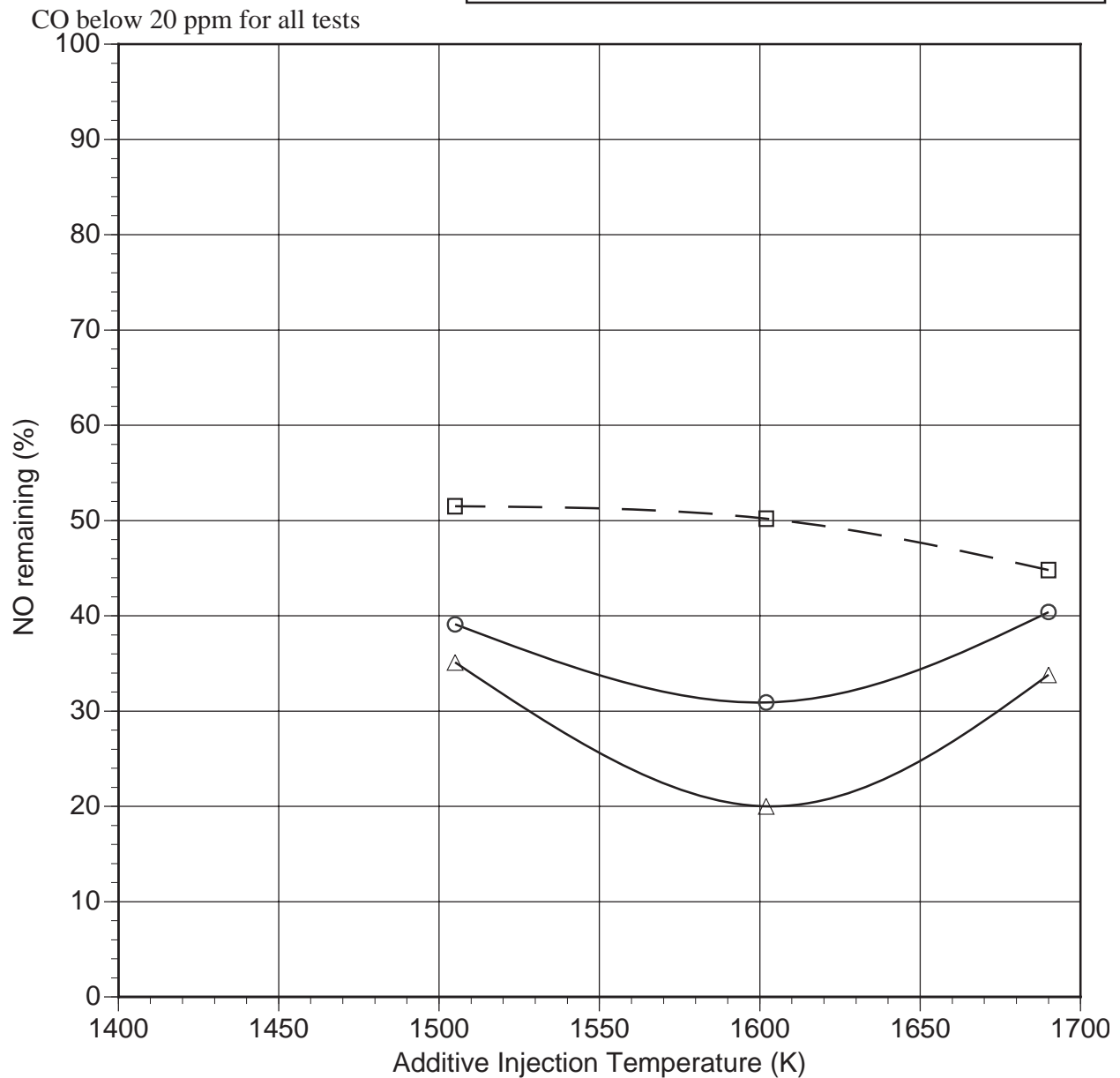
Figure 7.8 AR-Rich with urea/sodium injection. OFA is injected at 1510 K.

Figure 7.9 demonstrates the impact of sodium concentration on NO reduction for AR-Rich. In these tests, urea and sodium were injected at 1520 K and OFA at 1320 K. Increasing Na concentration

from 0 to 55 ppm resulted in improvement of NO reduction from 76 to 90%. However, the CO emissions increased from 20 ppm at Na=0 to 65 ppm at Na=22 ppm and to 500 ppm at Na=55 ppm. Thus, injection of sodium with a N-agent in the reburn zone requires a temperature of OFA injection higher than 1320 K to prevent CO formation. This result demonstrates the importance of sodium chemistry in NO control via reburning.

Main Fuel: Natural gas @ 705,000 Btu/hr
10% Reburn with N2 Transport
OFA at 1320 K
Urea and Na2CO3 injection at 1520 K
SR1 = 1.10, SR2 = 0.99, SR3 = 1.15
NOi = 600 ppm as measured
NSR = 1.5
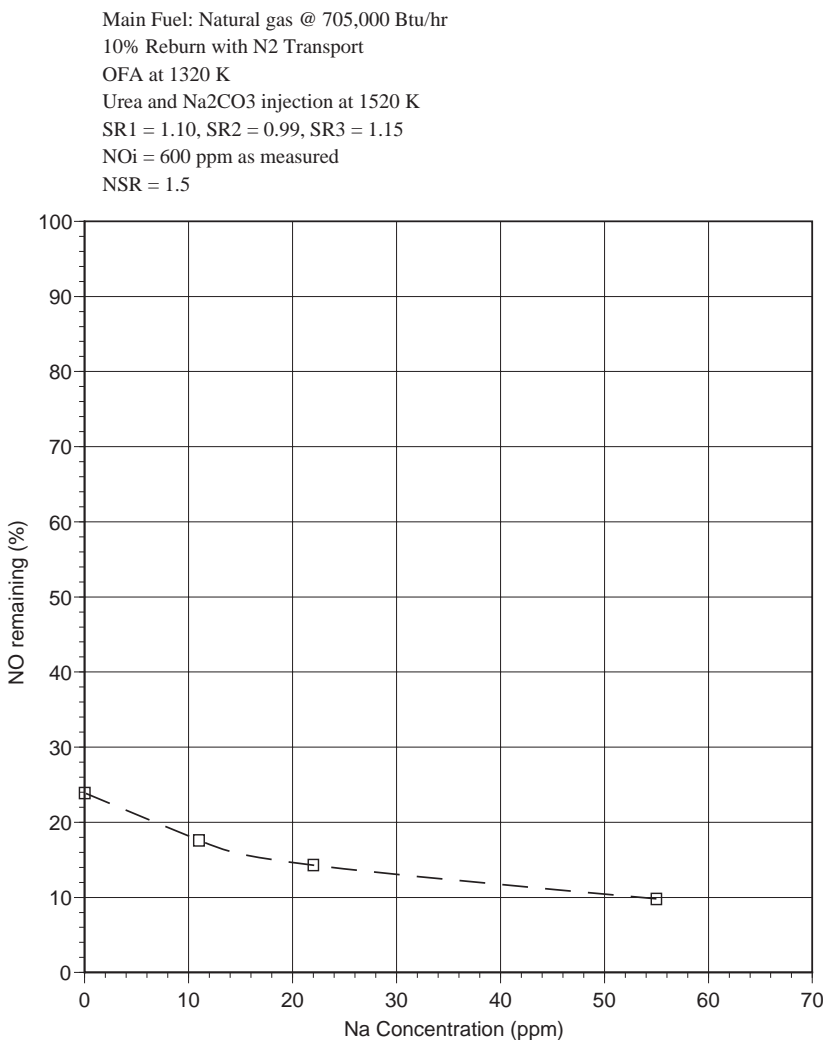
Figure 7.9 Effect of sodium on NO reduction in AR-Rich.

7.2.3 Hybrid AR-Lean/SNCR

Combined AR-Lean/SNCR tests were then conducted at the BSF. In these tests, the reburning fuel was injected at 1640 K and N-agent (aqueous ammonia or urea) was added with the OFA at 1370 K. Then, a second N-agent was injected under fuel lean conditions at 1160 K. Concentration of each N-agent corresponded to NSR=1.5. NO reduction was measured with and without addition of sodium

carbonate to each N-agent. The concentration of sodium was 100 ppm for each sodium carbonate addition. Figure 7.10 presents the results for the urea tests. Performance with urea was somewhat greater than that with ammonia.

Primary Fuel: Nat. gas @ 705,000 Btu/hr
10.2% Natural Gas reburning
SR1=1.10. SR2= 0.99, SR3= 1.15
Location #1 is at 1370 K w/OFA, NSR=1.5
Location #2 is at 1160 K, NSR=1.5
Na2CO3 Promoter, 100 ppm Na
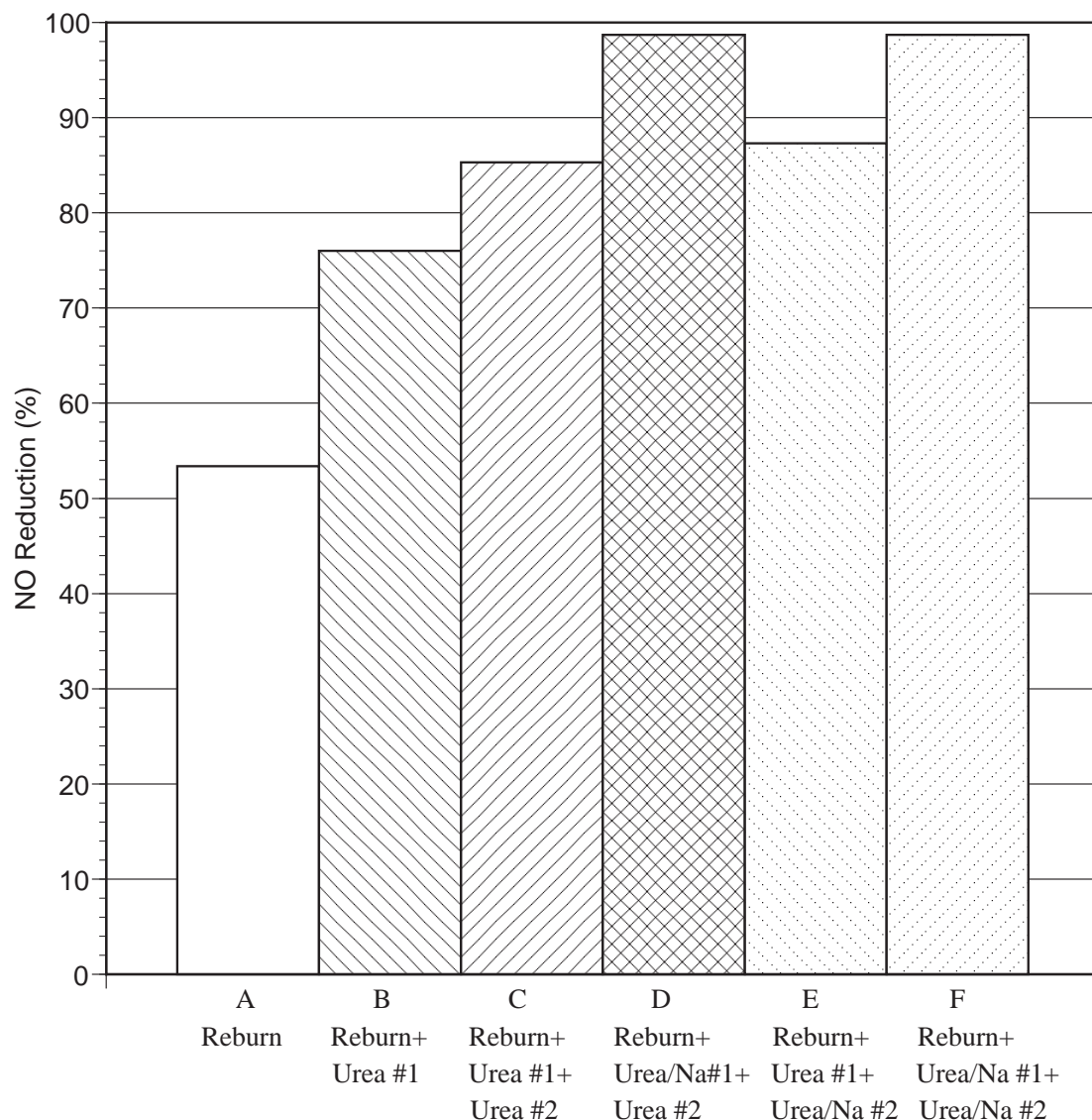
Figure 7.10 NO reduction during natural gas firing by combined AR-Lean/SNCR with urea injection at two locations.

Reburning alone (bar A) gave 53% NO reduction. Injection of urea with OFA, i.e. AR-Lean resulted in 76% NO removal, bar B. Injection of a second N-agent increased the NO_x control to 85%, bar C. The best result was achieved when sodium was injected with the first N-agent, bar D, for which NO removal increased from 85 to above 98%. Addition of sodium to the second N-agent was not effective, (see bars E and F). There is almost no difference in NO reduction for bars C and E, as well as for bars D and F. This would appear to imply that it is necessary to add the promoter with the high temperature N-agent for optimum performance.

7.2.4 MIAR

MIAR tests were conducted with natural gas as both the main and reburn fuels. N-agents and promoters were injected at rich and lean side locations. Rich and lean side additive injection temperatures and SR_2 were varied. In all tests urea was used as the N-agent and Na_2CO_3 was used as the promoter.

Tests were performed at SR_2 values of 0.99 (10% reburning) and 0.90 (18% reburning). In the first test series, rich side additive injection temperature was varied from 1370 to 1530 K, and lean side additives were injected along with the OFA at 1310 K. Figure 7.11 shows NO reduction as a function of rich side additive injection temperature at $SR_2 = 0.99$. The systems were fairly insensitive to temperature. Reburning alone gave 49% NO reduction. Reburning plus rich and lean side N-agents with no promoters gave 77 - 82% NO reduction. Addition of sodium promoter to the lean side additive improved NO reduction by about 4 percentage points at each temperature. When sodium promoter was added to the rich side N-agent, NO reduction increased to 95 - 97%. Addition of sodium to both N-agents also gave 95 - 97% NO reduction. These results indicate that for natural gas firing sodium is most effective when added to the rich side additive.

BSF, Firing Rate: 705,000 Btu/Hr
Main Fuel: Nat.Gas, 10% Nat.Gas Reburn
SR1=1.10, SR2=0.99 and SR3=1.15
NOi=600 ppm @0%O2
Rich side urea + Na2CO3 injection temperature varied
Lean side urea + Na2CO3 injected w/OFA at 1310 K
30 ppm Na

● Reburning
✖ Reburning +Rich N-agent+Lean N-agent
△ Reburning +Rich N-agent+Lean N-agent w/Na
□ Reburning +Rich N-agent w/Na+Lean N-agent
○ Reburning +Rich N-agent w/Na+Lean N-agent w/Na

Figure 7.11 Effect of rich side additive injection temperature upon MIAR performance during natural gas firing at $SR_2 = 0.99$.

The promoters also demonstrated the ability to control N_2O emissions. When N-agents were injected without promoters, N_2O ranged from 80 ppm at 1370 K to 39 ppm at 1530 K. When sodium promoters were added with either N-agent, N_2O fell to near zero.

Figure 7.12 shows NO reduction as a function of rich side additive injection temperature at $SR_2 = 0.90$. Reburn alone provided 72% NO control. The N-agents provided limited additional NO control, and in some cases actually caused NO to increase. Sodium promoted addition improved performance, with the strongest effects seen when promoter was added in the rich zone. Maximum NO control was 90% at a rich side additive injection temperature of 1370 K. N_2O ranged from 13 to 32 ppm with N-agents but no promoter, and decreased to near zero when sodium was added.

7-15

BSF, Firing Rate: 705,000 Btu/Hr
Main Fuel: Nat.Gas, 18% Nat.Gas Reburn
SR1=1.10, SR2=0.90 and SR3=1.15
NOi=600 ppm @0%O2
Rich side urea + Na2CO3 injection temperature varied
Lean side urea + Na2CO3 injected w/OFA at 1310 K
30 ppm Na

●	Reburning
✖	Reburning +Rich N-agent+Lean N-agent
△	Reburning +Rich N-agent+Lean N-agent w/Na
□	Reburning +Rich N-agent w/Na+Lean N-agent
○	Reburning +Rich N-agent w/Na+Lean N-agent w/Na

Figure 7.12 Effect of rich side additive injection temperature upon MIAR performance during natural gas firing at $SR_2 = 0.90$.

The test results indicate that optimum MIAR performance is obtained at $SR_2 = 0.99$ (10% reburning). This relatively low reburn heat input has several operational advantages. Specifically, the near-stoichiometric conditions serves to minimize high temperature boiler corrosion problems, and the low reburn heat input minimizes changes in boiler heat distribution and corresponding decreases in thermal efficiency.

7.3 Pilot Scale Combustion Tests with Coal Firing

Pilot scale tests were then conducted with coal as the primary fuel and natural gas as the reburning fuel. Both low sulfur Utah coal and high sulfur Illinois coal were tested. The initial NO concentration was 800-1000 ppm. Processes characterized included promoted AR-Lean, promoted AR-Rich, hybrid AR-Lean/SNCR, and MIAR. A series of byproduct sampling runs was also conducted while firing coal.

7.3.1 Promoted AR-Lean

In the first AR-Lean tests, low sulfur Utah coal was used as the main fuel and natural gas as the reburning fuel. Reburn fuel (10%) was injected at 1640 K, providing a reburn zone stoichiometry of 0.99. Aqueous urea and sodium carbonate were injected along with the OFA at varying temperatures. Figure 7.13 demonstrates that 55-60% NO reduction was achieved by 10% reburning alone. Performance strongly depended on the urea/OFA injection temperature. Injection of urea with the OFA had virtually no effect at high injection temperatures of 1480-1590 K. Under these conditions, emissions of CO were about 40 ppm without Na and 60 ppm in the presence of Na. At urea/OFA injection temperatures lower than 1480 K, NO is substantially reduced, by up to 90%. However, higher CO emissions were measured, i.e. 40-60 and 80-100 ppm CO in the absence and presence of sodium, respectively. The concentration of Na was varied from 0 to 200 ppm, equivalent to 0 to 100 ppm Na_2CO_3 in the flue gas. The effect of sodium on NO reduction was noticeable, 2-8 percentage points, but not as great as in the natural gas firing tests.

Utah Coal main fuel, 705,000 Btu/hr
10% Nat. Gas Reburning, N2 transport.
SR1= 1.10, SR2= 0.99 and SR3= 1.15
Urea or Urea/Na2CO3 injected with OFA
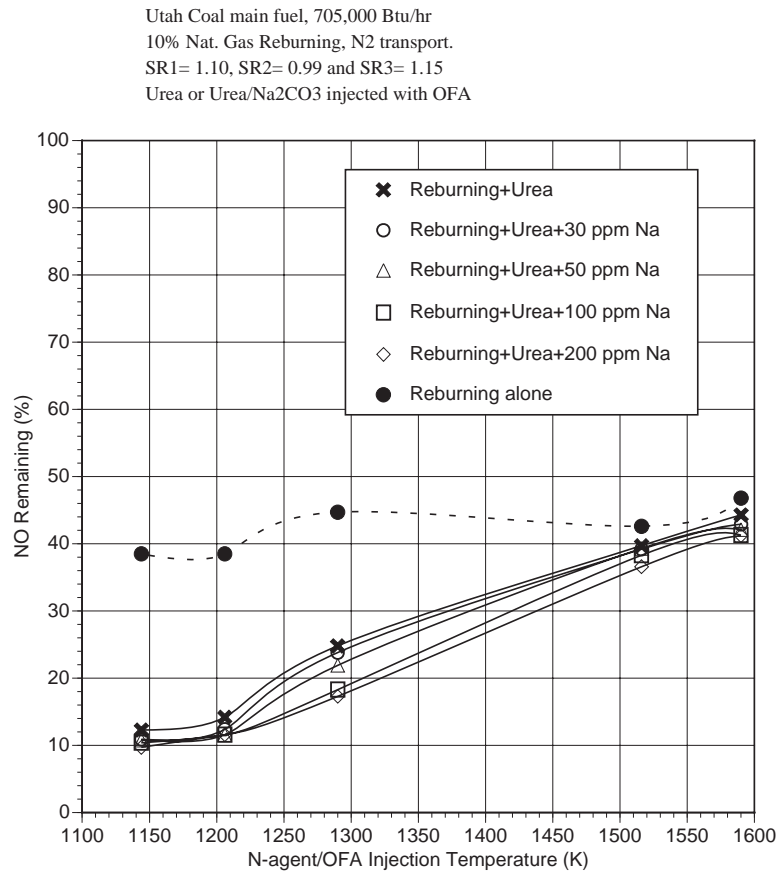
Figure 7.13 NO reduction by AR-Lean during coal firing.

Tests were then conducted with high sulfur Illinois coal as the primary fuel. Figure 7.14 shows NO reduction as a function of the N-agent/OFA injection temperature. Reburning alone gave 48% NO reduction. For both the promoted and unpromoted cases, optimum performance was obtained at 1310 K. Maximum NO reduction was 78% with no promoter and 84% with 150 ppm of Na. Sodium exhibited a greater promotional effect at the lower injection temperatures. Performance was slightly lower than that obtained with Utah coal, possibly because the higher SO_2 concentration generated by the Illinois coal partially deactivated the sodium promoter.

Firing Rate: 705,000 Btu/Hr
Main Fuel : Illinois Coal
9% Nat.Gas Reburn
SR1=1.10, SR2=0.99, SR3=1.15
NO level: 1000 ppm @0%O2 dry
Additive co-injected with OFA, NSR=1.5
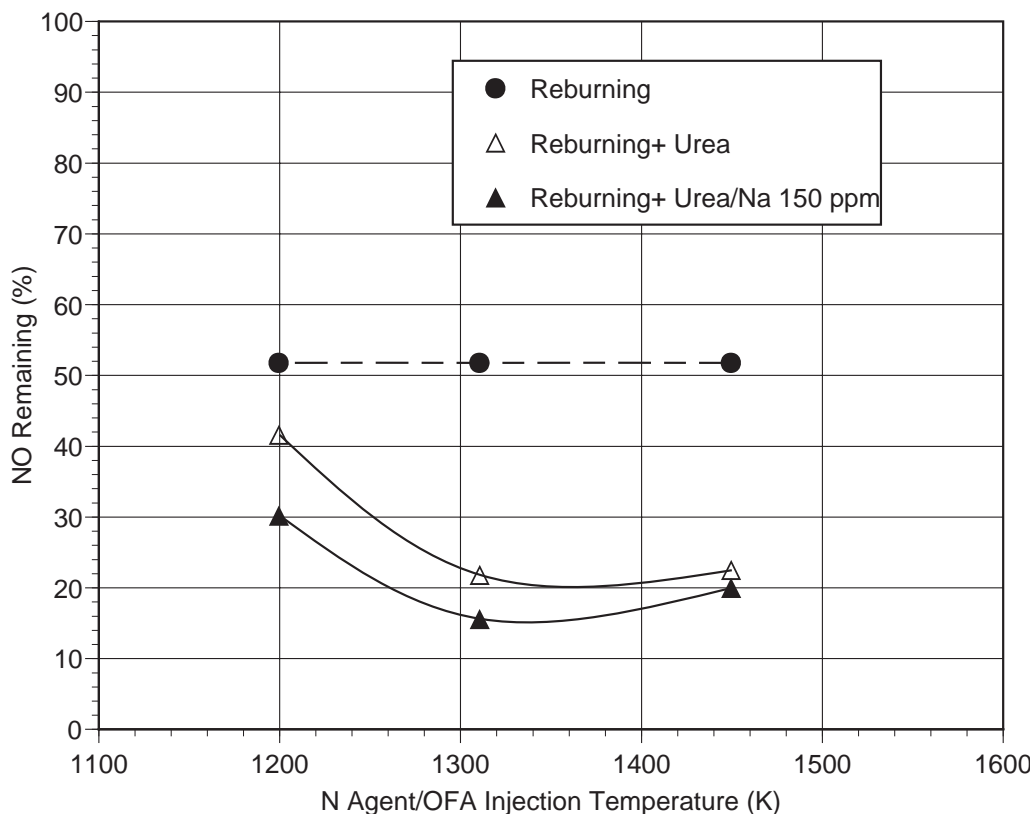
Figure 7.14 AR-Lean tests: Effect of N-agent/OFA injection temperature upon performance.

7.3.2 Promoted AR-Rich

Similar to natural gas firing, the performance of AR-Rich during coal firing depends strongly on the OFA injection temperature. Figures 7.15 and 7.16 demonstrate experimental results for injection

of OFA at 1170 and 1300 K, respectively. Utah coal was the main fuel. Urea (NSR=1.5) and different amounts of sodium (0-200 ppm) were injected at varying temperatures. Lower OFA injection temperature was found to provide better NO reduction. Reburning followed by urea injection in the reburn zone at different temperatures provided 78-88% NO control with OFA at 1170 K (Figure 7.13) and 70-77% NO control with OFA at 1300 K (Figure 7.15). With sodium addition, maximum NO reductions were 92% with OFA at 1170 K and 83% with OFA at 1300 K. The effect of sodium was less than for natural gas firing. A possible reason for this is interaction of sodium compounds with SO_2 and HCl in flue gas to form sodium sulfite, sodium sulfate or sodium chloride.

Utah Coal main fuel, 705,000 Btu/hr
10% Nat. Gas Reburning, N2 transport.
SR1= 1.10, SR2= 0.99 and SR3= 1.15
NOi=800 ppm as meas.
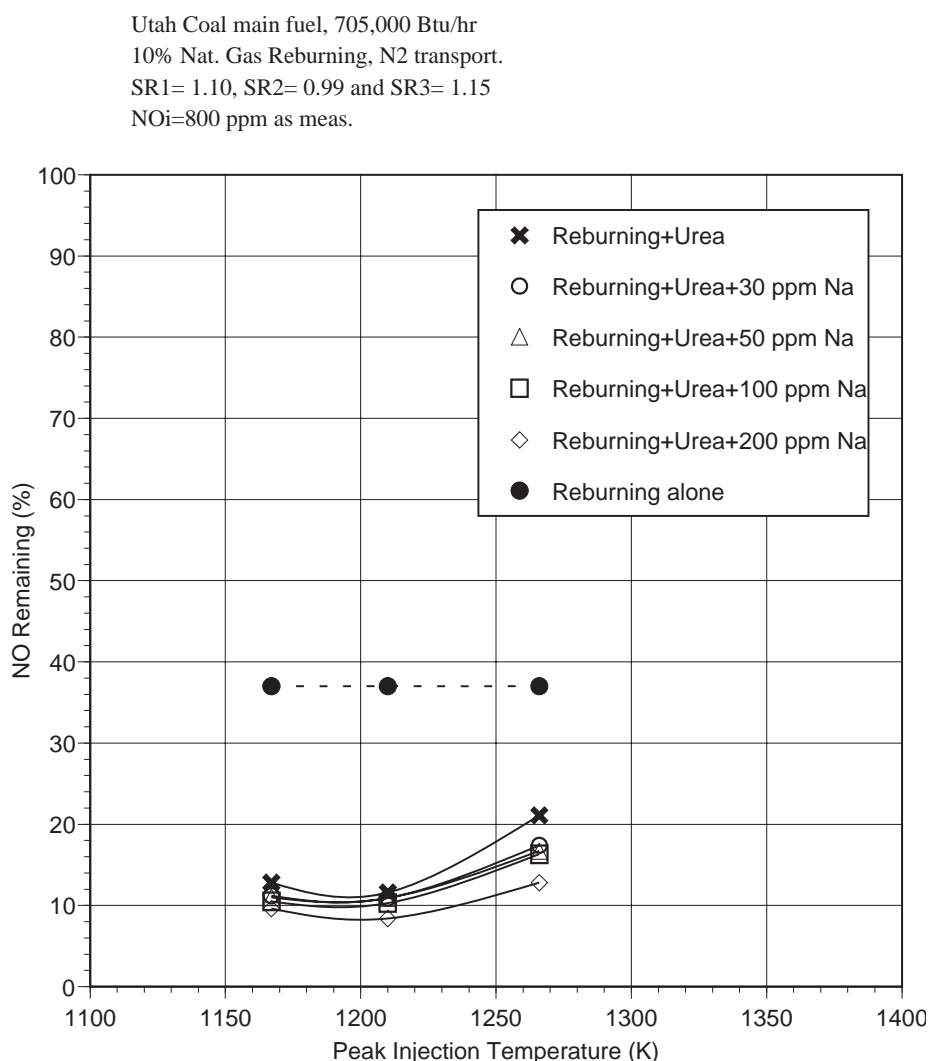
Figure 7.15 Effect of urea injection temperature and concentration of sodium on NO reduction in AR-Rich with coal firing. OFA injection temperature is 1170 K.

7-19

Utah Coal main fuel, 705,000 Btu/hr
10% Nat. Gas Reburning, N2 transport.
SR1= 1.10, SR2= 0.99 and SR3= 1.15
NOi=800 ppm as meas.
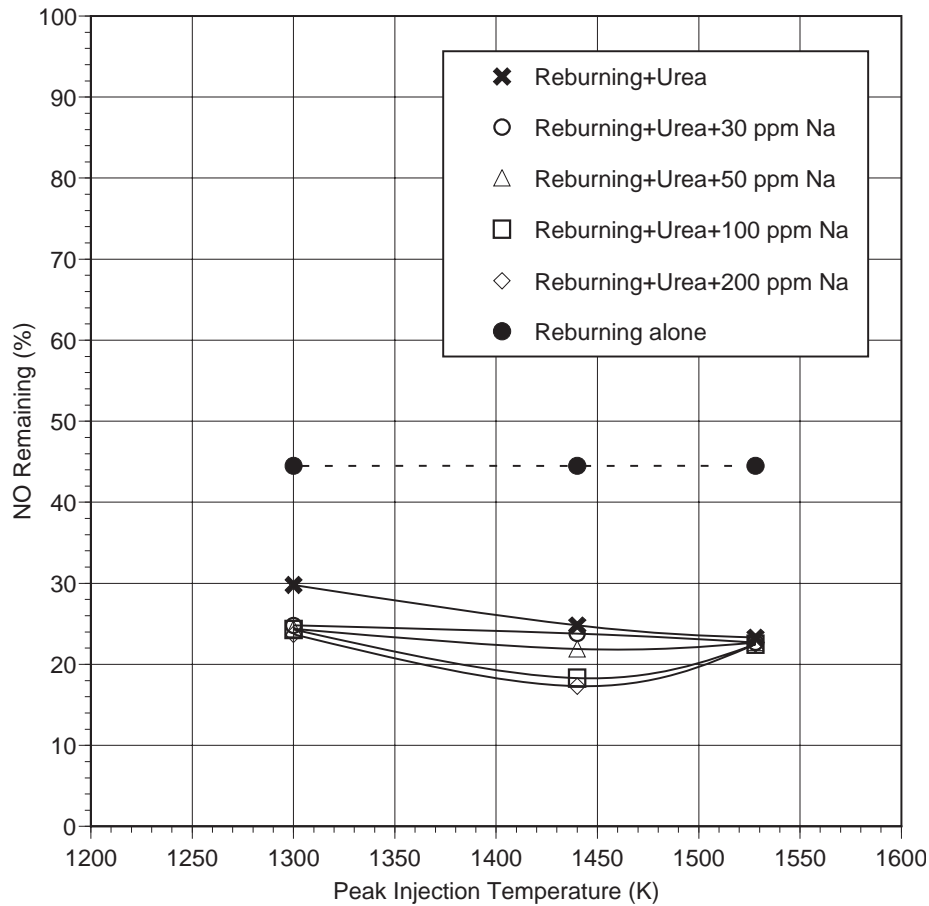
Figure 7.16 Effect of urea injection temperature and concentration of sodium on NO reduction in AR-Rich with coal firing. OFA injection temperature is 1300 K.

For injection of OFA at 1170 K, CO emissions were about 60 ppm without sodium and 100 ppm in the presence of sodium. Variation of the sodium concentration did not affect CO emissions. At an OFA injection temperature of 1300 K, CO emissions were about 40 and 60 ppm in the absence and in the presence of sodium, respectively.

AR-Rich tests were then conducted with high sulfur Illinois coal as the main fuel, with OFA added at 1310 K. Figure 7.17 shows NO reduction as a function of the N-agent injection temperature. Performance increased with decreasing injection temperature, with greatest NO reduction obtained at 1370 K. Maximum NO control was 86% with no promoter and 93% with 150 ppm sodium. The incremental benefit provided by the sodium promoter appeared to increase with decreasing temperature.

Firing Rate: 705,000 Btu/Hr
Main Fuel : Illinois Coal
9% Nat.Gas Reburn
SR1=1.10, SR2=0.99, SR3=1.15
NO level: 1000 ppm @0%O2 dry
OFA injected at 1310 K, NSR=1.5
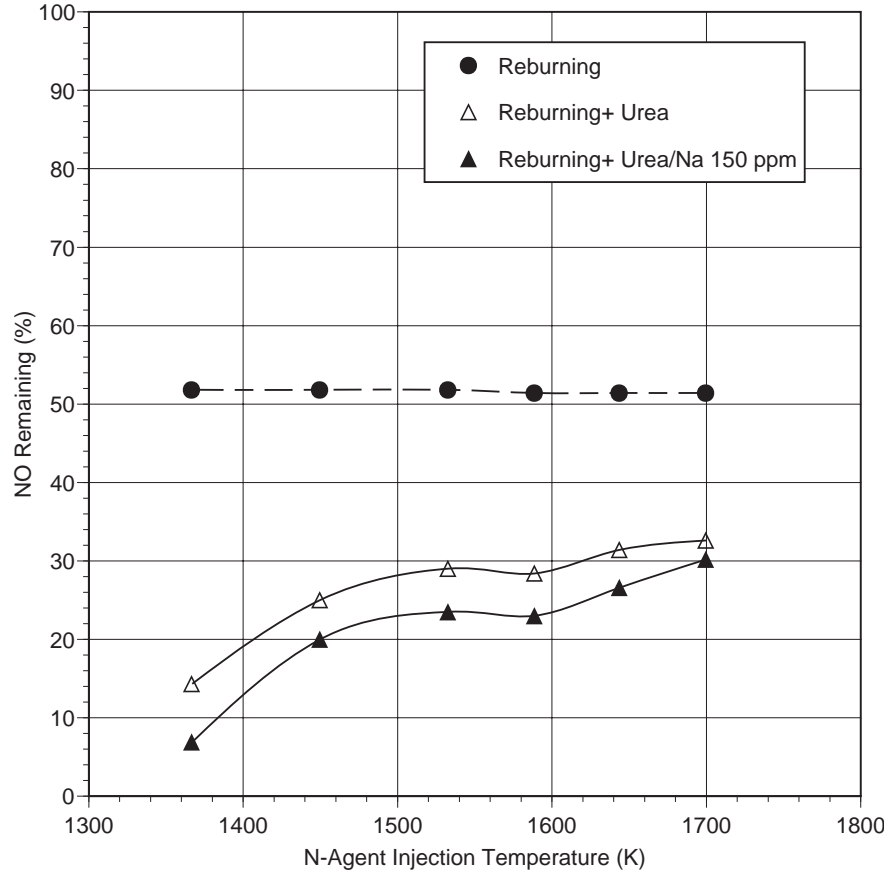
Figure 7.17 AR-Rich tests: Effect of N-agent injection temperature upon performance.

Illinois coal AR-Rich tests were then conducted in which the OFA injection temperature was varied, with the N-agent injection temperature held constant at 1530 K. This temperature is well above the optimum, but is of interest for boilers that have limited access at lower temperatures for liquid injectors. As shown in Figure 7.18, performance increased with decreasing OFA temperature. Sodium provided an incremental increase in NO reduction of about 6 percentage points at each temperature.

Firing Rate: 705,000 Btu/Hr
Main Fuel : Illinois Coal
9% Nat.Gas Reburn
SR1=1.10, SR2=0.99, SR3=1.15
NO level: 1000 ppm @0%O2 dry
Additive injected at 1530 K, NSR=1.5
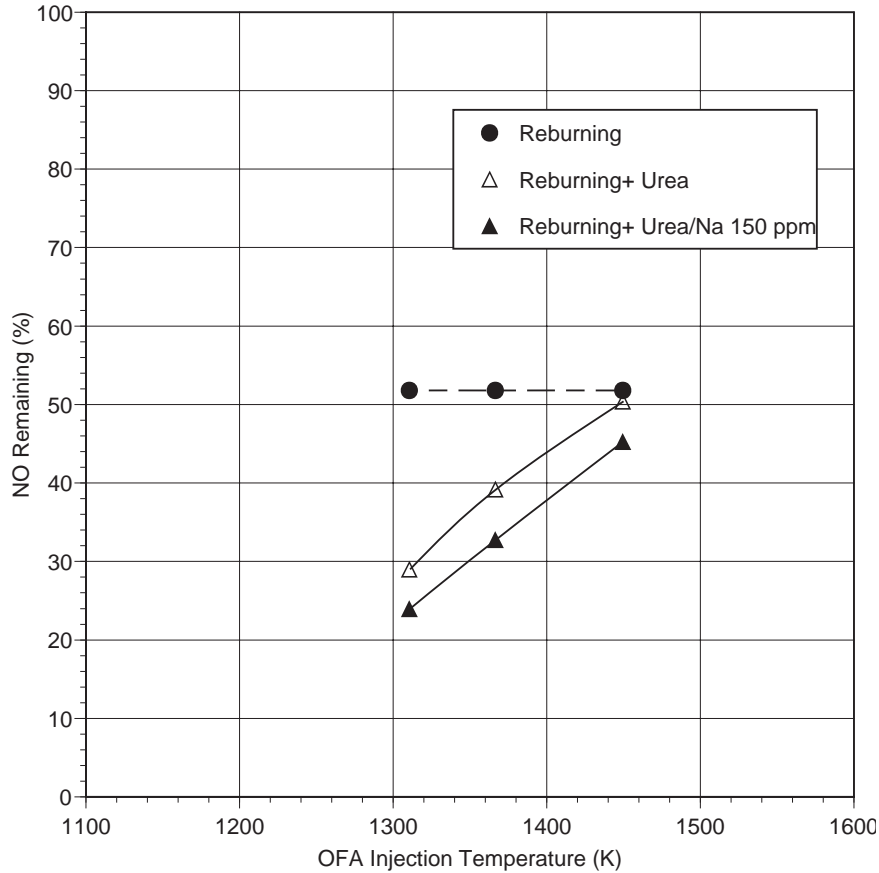
Figure 7.18 AR-Rich tests: Effect of OFA injection temperature upon performance.

Illinois coal AR-Rich tests were then conducted at high sodium concentrations to define the maximum achievable extent of NO reduction. Sodium promoter concentration was varied from 0 to 2000 ppm. Reburn zone SR was 0.99, additives were injected at 1450 K, and OFA was injected at 1370 K. As shown in Figure 7.19, NO reduction increased from 63% at 0 ppm sodium to 86% at 2000 ppm sodium. The main drawback of high sodium level is the potential for increased boiler fouling. A sodium concentration of 150 ppm was selected for most of the test work as a concentration providing significant promotion while being low enough to minimize fouling effects. As shown in Figure 7.19, this level of sodium addition can also provide a small degree of SO_2 control by reaction to form sodium sulfate.

Figure 7.19 AR-Rich tests: Effect of sodium promoter concentration upon performance.

7.3.3 Hybrid AR-Lean/SNCR

Combined AR-Lean/SNCR tests were conducted with Utah coal as the main fuel. The conditions were similar to those for the natural gas tests: reburning fuel was injected at 1640 K, ammonia or urea was added at 1370 K, and 100 ppm Na was injected with each N-agent. NO reduction was measured with and without sodium. The second N-agent was injected under fuel lean conditions at 1200 K, a slightly higher temperature than in the natural gas firing tests. Figure 7.20 shows results for urea injection. Similar results were obtained with urea and ammonia.

Primary Fuel: Utah coal @ 705,000 Btu/hr
10.2% Natural Gas reburning
SR1=1.10. SR2= 0.99, SR3= 1.15
Location #1 is at 1370 K w/OFA, NSR=1.5
Location #2 is at 1200 K, NSR=1.5
Na2CO3 Promoter, 100 ppm Na
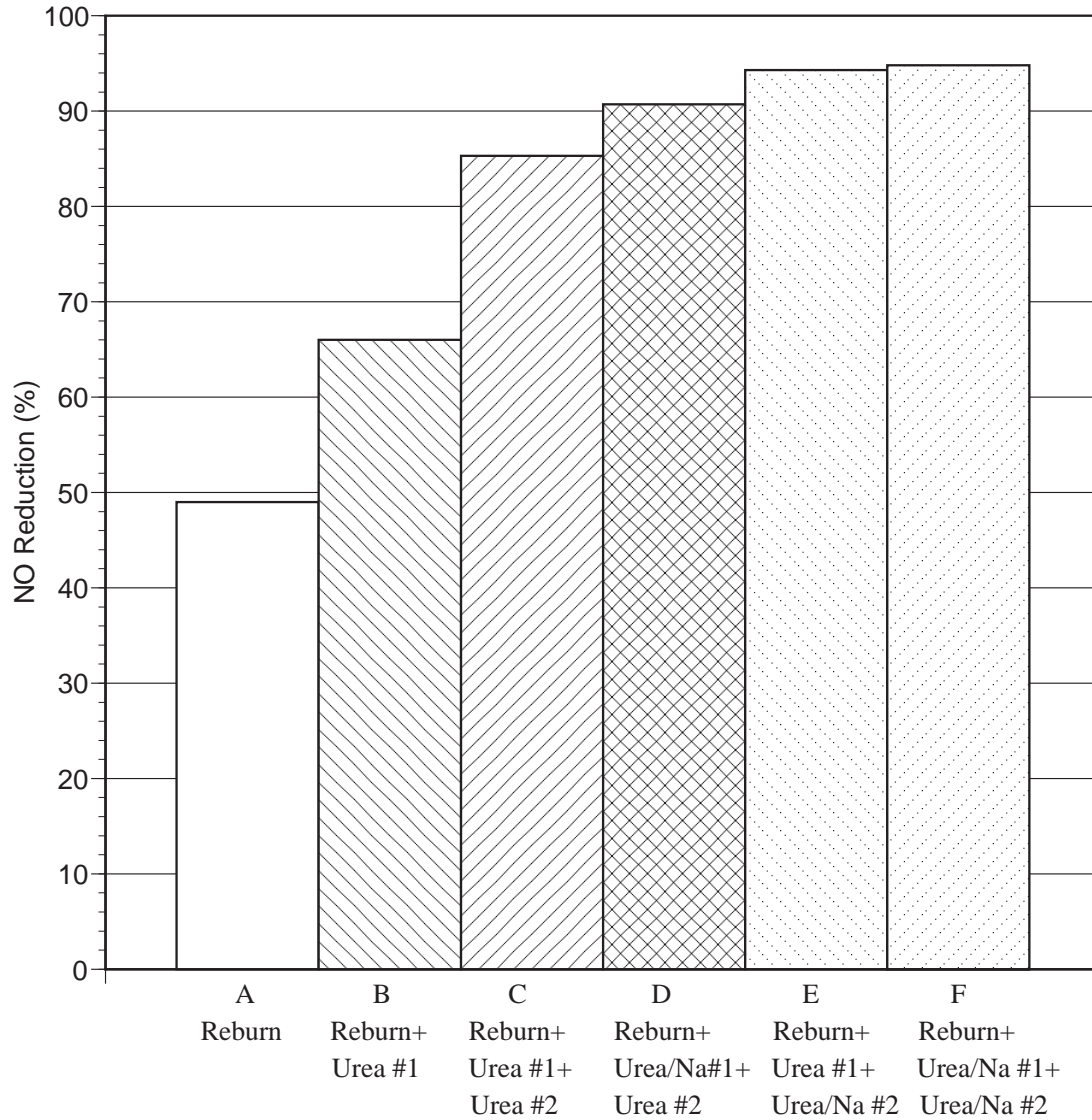
Figure 7.20 NO reduction during coal firing by combined AR-Lean/SNCR with urea injection at two locations.

It is of interest to compare the performance of the combined AR-Lean/SNCR process for natural gas and coal firing, as summarized in Table 7.1. Corresponding test conditions are shown in Figures 7.10 and 7.20 for gas and coal firing, respectively.

Table 7.1. Comparison of NO reduction (%) for hybrid AR-Lean/SNCR with gas and coal firing. Corresponding CO emissions in ppm are shown in parentheses.

Bar	Test Conditions	Natural Gas Firing		Coal Firing	
		Urea	Ammonia	Urea	Ammonia
A	10% Reburn @ 1640 K, OFA @ 1370 K	53(20)	53(20)	49(60)	49(60)
B	AR-Lean, OFA @ 1370 K	76(30)	58(30)	66(60)	62(60)
C	AR-Lean + SNCR	85(30)	73(30)	85(60)	84(60)
D	AR-Lean/Na + SNCR	98(190)	96(180)	91(60)	90(60)
E	AR-Lean + SNCR/Na	87(30)	78(30)	94(60)	93(60)
F	AR-Lean/Na + SNCR/Na	98(190)	96(180)	95(60)	94(60)

Reburning alone provided 53% NO reduction with natural gas firing and 49% NO reduction with coal firing. Mixed results were obtained for AR-Lean: 58-76% for natural gas and 62-66% for coal. AR-Lean + SNCR provided up to 85% NO reduction for both natural gas and coal firing. The best results for natural gas firing were achieved by addition of sodium to the first N-agent, 96-98% NO control. Under the same conditions, 90-91% NO was reduced in coal firing. Sodium can likely react with SO_2 and HCl in flue gas, and therefore the performance is not as great in the coal firing tests. Addition of sodium to the second N-agent can be considered as the best result for coal firing: 93-94% NO reduction. Surprisingly, the same arrangements with natural gas firing resulted in only 78-87% NO reduction. Coal flue gas includes vapors of some mineral compounds which can promote the reburning process, and therefore, the presence of the mineral matter in the reburn zone of coal combustion can improve NO reduction. Finally, addition of sodium to both N-agents shows that the second Na additive is not effective for natural gas firing, and the first Na additive has virtually no effect for coal firing.

Data on CO emissions are also presented in Table 7.1. The CO emissions increased in some tests with natural gas firing, but not with coal tests. Two important conclusions can be made based on these hybrid AR/SNCR tests:

1.   The hybrid AR-Lean/SNCR process is very effective for NO_x control and can achieve up to 95 and 98% NO reduction for coal and natural gas firing, respectively.
2.   Addition of sodium to the second N-agent is more effective for coal than for natural gas firing. The first Na additive is more effective for natural gas than for coal firing.

7.3.4 Hybrid AR-Rich/SNCR

A series of tests was conducted involving AR-Rich plus SNCR during Illinois coal combustion. The first N-agent was injected at 1590 K and OFA was added at 1530 K. The second N-agent was injected downstream of the reburn zone at temperatures ranging from 1230 to 1390 K. Four conditions were run, including no promoter, sodium addition to the first N-agent alone, sodium addition to the second N-agent alone, and sodium addition to both N-agents. As shown in Figure 7.21, performance increased with increasing second N-agent injection tempeature. Adding 150 ppm sodium to both N-agents increased NO reduction by 4 to 6 percentage points at each temperature. Maximum NO reductions, obtained at 1390 K, were 88% with no promoter and 93% with sodium added to both N-agents.

Firing Rate: 705,000 Btu/Hr
Main Fuel : Illinois Coal
9% Nat.Gas Reburn
SR1=1.10, SR2=0.99, SR3=1.15
NOi: 1000 ppm @0%O2 dry
First additive injected at 1590 K
OFA injected at 1530 K
NSR=1.5
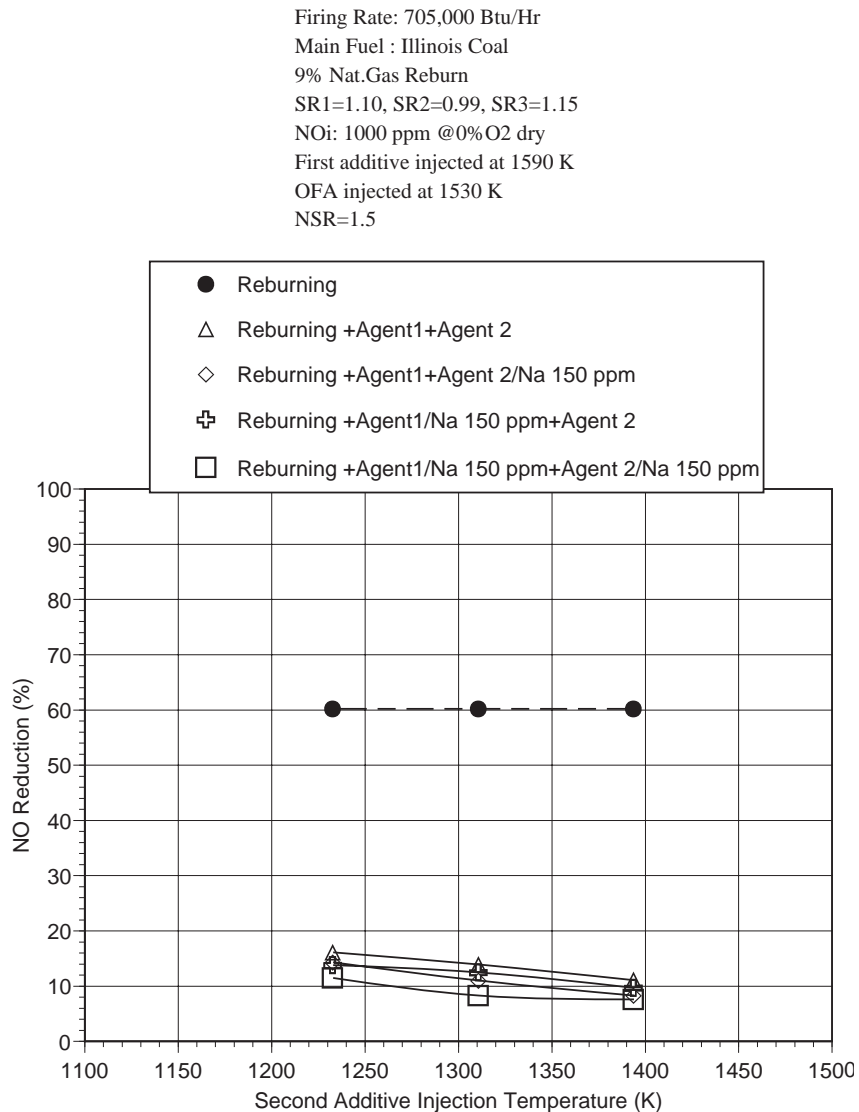
Figure 7.2.1 AR-Rich + SNCR tests: Effect of second additive injection temperture upon performance.

7.3.5 MIAR

Multiple injection advanced reburning (MIAR) components include reburning, AR-Rich, and AR-Lean (both with and without promoters). Test variables at the BSF included reburn heat input, AR-Rich injection temperature, AR-Lean injection temperature, and sodium promoter concentration. Illinois coal was used as the main fuel. Figure 7.22 shows NO reduction as a function of the AR-Rich injection temperature at reburn zone SR_2=0.90 (18% reburning heat input). OFA was injected at 1310 K. Reburning alone gave 74% NO reduction. Overall MIAR NO reduction was 80-82%, and was nearly constant as additive injection temperature was varied from 1370 to 1530 K. Addition of sodium promoter did not significantly impact performance. Because performance was relatively low at this SR_2, temperatures above 1530 K were not tested. Thus, the effectiveness of N-agents and promoters is low at $SR_2 = 0.90$.

Firing Rate: 705,000 Btu/Hr
Main Fuel : Illinois Coal
18% Nat.Gas Reburn
SR1=1.10, SR2=0.90, SR3=1.15
NOi: 1000 ppm @0%O2 dry
Second additive co-injected with OFA at 1310 K
NSR=1.5
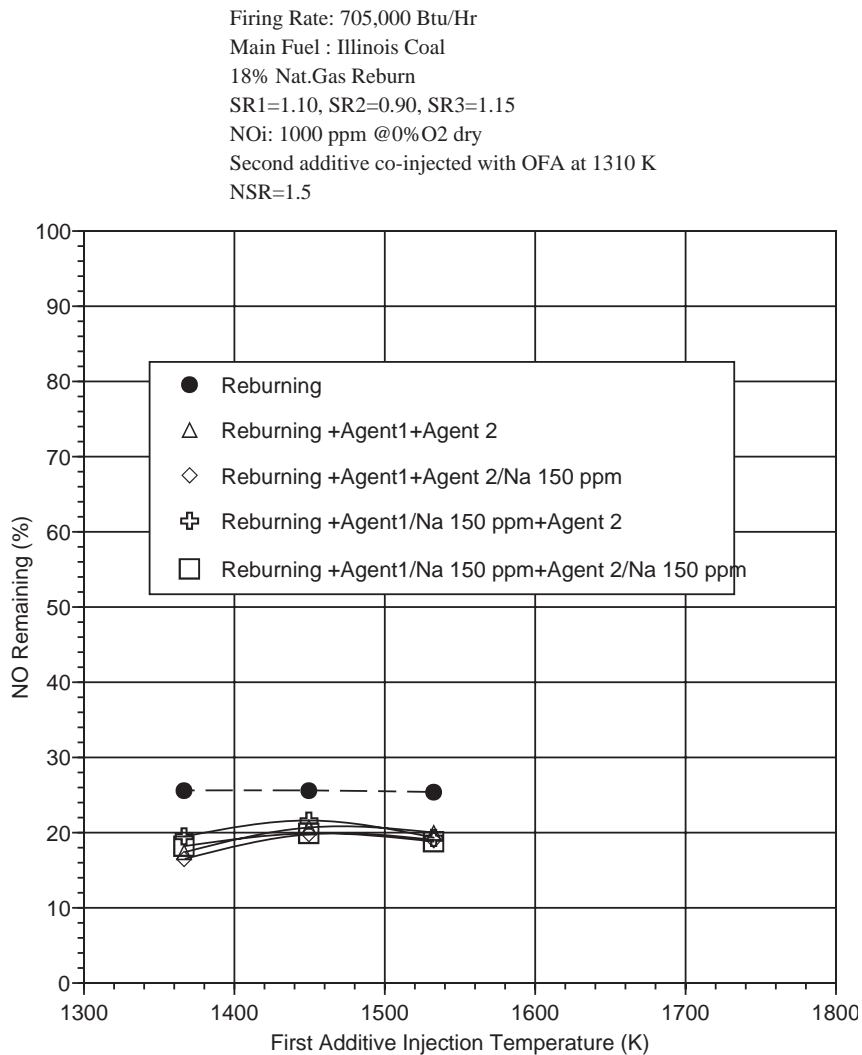
Figure 7.22 MIAR tests: Effect of first additive injection temperature upon performance at 18% reburning.

Similar tests were then conducted at $SR_2=0.99$ (9% reburning). Figure 7.23 shows performance as a function of AR-Rich additive injection temperature. Reburning alone gave 48% NO reduction. MIAR NO reduction increased with decreasing first additive injection temperature. Sodium promoter was added to each N-agent individually and to both agents. Adding promoter to both N-agents provided an incremental performance increase of about 5 percentage points at each temperature. Maximum NO reduction was 94%, obtained with promoter added to both N-agents at an AR-Rich injection temperature of 1370 K. It is also noteworthy that performance remained relatively good at high injection temperatures. NO reductions above 80% were obtained at injection temperatures below 1590 K. This insensitivity can provide greater flexibility for application to boilers with limited furnace access for injectors.

Firing Rate: 705,000 Btu/Hr
Main Fuel : Illinois Coal
9% Nat.Gas Reburn
SR1=1.10, SR2=0.99, SR3=1.15
NOi: 1000 ppm @0%O2 dry
Second additive co-injected with OFA at 1310 K
NSR=1.5
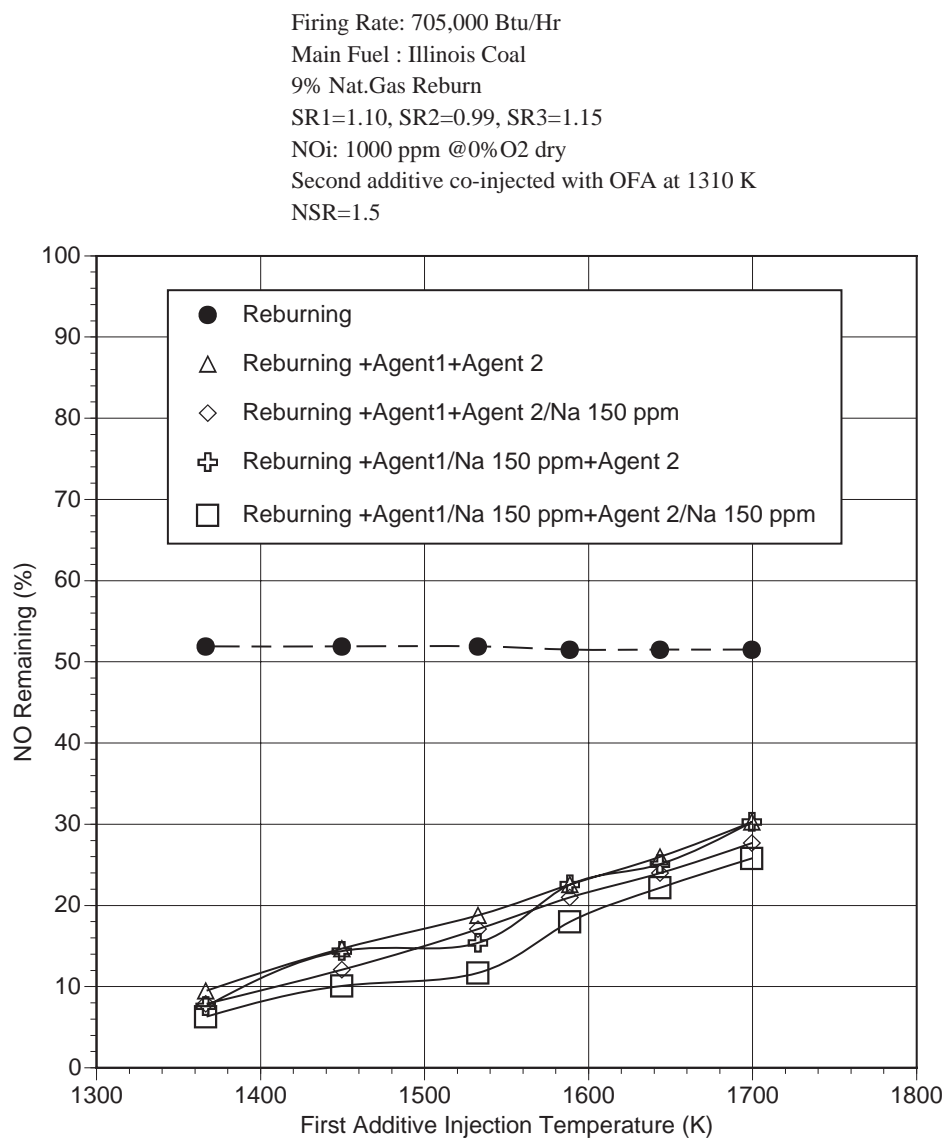
Figure 7.23 MIAR tests: Effect of first additive injection temperature upon performance at 9% reburning.

MIAR tests were then conducted in which the AR-Lean additive injection temperature was varied, with the AR-Rich temperature fixed at 1450 K. The AR-Lean additives were co-injected along with the OFA. Figure 7.24 shows results obtained at SR_2=0.90 (18% reburning heat input). Reburning alone gave 74% NO reduction. Overall MIAR NO reduction was 76-82%, and was nearly constant as additive injection temperature was varied from 1200 to 1370 K. Addition of sodium promoter to both N-agents increased NO reduction by 5 percentage points at 1200 K, but did not significantly impact performance at 1370 K. These tests confirmed that N-agents and Na promoters have relatively low effect at SR_2 = 0.90.

Firing Rate: 705,000 Btu/Hr
Main Fuel : Illinois Coal
18% Nat.Gas Reburn
SR1=1.10, SR2=0.90, SR3=1.15
NOi: 1000 ppm @0%O2 dry
First additive injected at 1450 K
Second additive co-injected with OFA
NSR=1.5
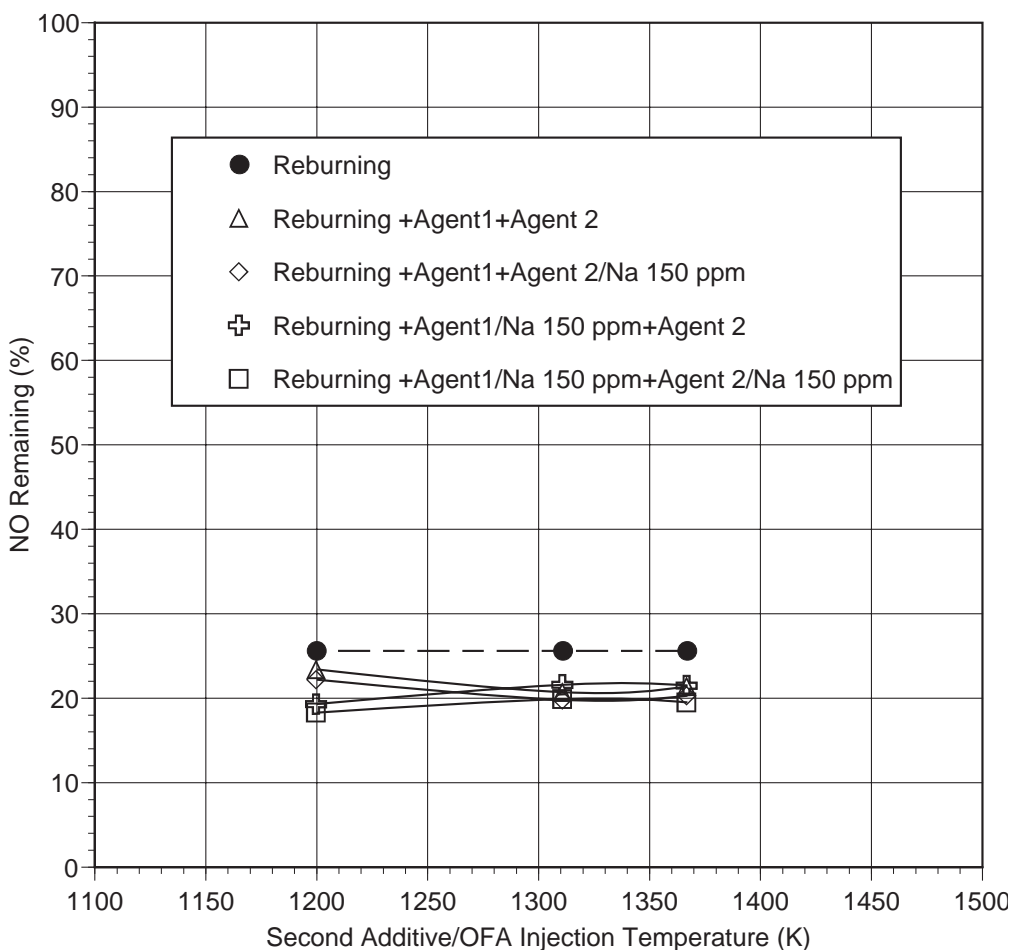
Figure 7.24 MIAR tests: Effect of second additive injection temperature upon performance at 18% reburning.

AR-Lean additive injection temperature was then varied at reburn zone SR=0.99 (9% reburning). As shown in Figure 7.25, reburning alone gave 48% NO reduction. With two N-agents with no promoters, a maximum of 86% NO reduction was obtained. The optimum temperature was 1310 K, and performance decreased as additive injection temperature increased to 1370 K. However, with 150 ppm sodium promoter added to the first N-agent, performance increased with increasing temperature. Highest NO reduction was 95%, obtained at an AR-Lean additive injection temperature of 1370 K. It is theorized that adding sodium with the first N-agent at higher temperatures makes it available to promote reduction of NO by the second N-agent.

Firing Rate: 705,000 Btu/Hr
Main Fuel : Illinois Coal
9% Nat.Gas Reburn
SR1=1.10, SR2=0.99, SR3=1.15
NOi: 1000 ppm @0%O2 dry
First additive injected at 1450 K
Second additive co-injected with OFA
NSR=1.5
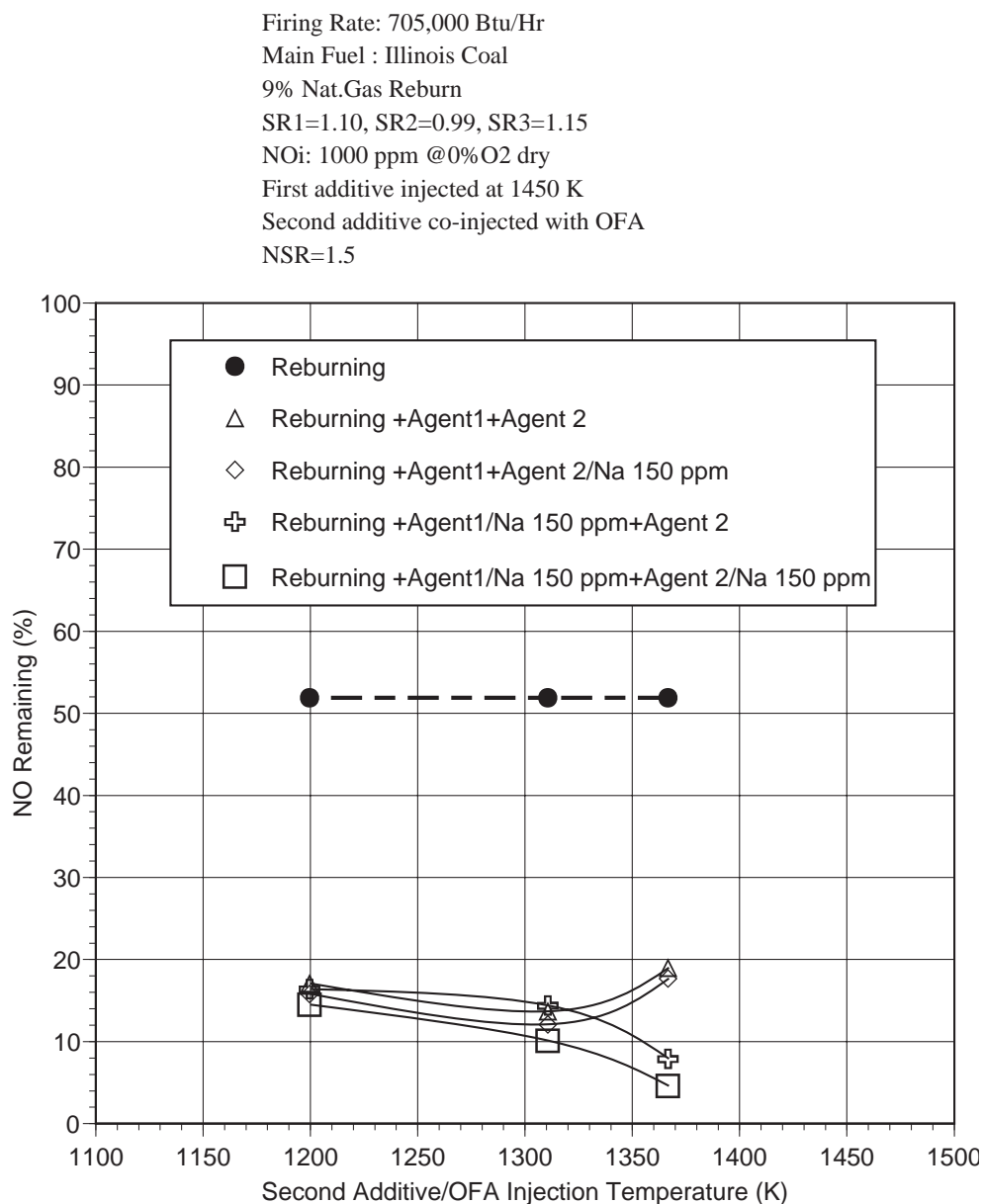
Figure 7.25 MIAR tests: Effect of second additive injection temperature upon performance at 9% reburning.

7.3.6 Byproduct Sampling Tests

While the AR technologies have shown the ability for effective NO_x control, another consideration is whether they generate any undesirable byproducts. Specifically, it was sought to determine whether the different variations of AR generate byproduct emissions greater than those of commercially accepted technologies such as SNCR and reburning. To answer this question, byproduct sampling tests were performed at the BSF. The following seven conditions were tested:

- Baseline coal firing
- SNCR
- Reburning
- AR-Rich
- AR-Lean
- Reburning plus SNCR
- MIAR

Test conditions, including reburn heat input, injection temperatures, promoter amounts and OFA temperatures, were selected as providing NOx control in the 80 - 90% range and also being achievable in a typical utility boiler. For each condition, sampling included:

- CO, SO_2, N_2O, and total hydrocarbons
- NH_3 and HCN
- SO_3
- Fly ash mass loading, size distribution, PM10, and PM2.5
- Carbon in ash

Test conditions and sampling data are summarized in Table 7.2. The byproducts were measured at conditions which were preliminarily optimized for NO_x control. Additional optimization tests on byproduct emissions is planned for Phase II. However, even without significant byproduct optimization efforts, the AR technologies do not generate more byproducts than reburning or SNCR. Results for each of the byproduct compounds tested are described below.

Table 7.2 Byproduct sampling conditions and results.

Baseline configuration: Illinois coal @ 0.71 MMBtu/hr   Test conditions: NSR=1.5
                                        NOi=1000 ppm as measured   N-agent: Urea
                                        SR1=1.10, SR3=1.15   Na promoter: Na2CO3

Parameter	Test Case						
	1. Baseline	2. SNCR	3. AR-Rich	4. MIAR	5. Reburn +SNCR	6. AR-Lean	7. Reburning
Test Conditions							
Reburn heat input (%)	None	None	10%	10%	10%	10%	20%
Rich side additive T (F)	None	None	2100	2000	None	None	None
Rich side Na (ppm)	None	None	150	150	None	None	None
OFA T (F)	None	None	1900	1900	2300	1900	2300
Lean side additive T (F)	None	1900	None	1900	1900	1900	None
Lean side Na (ppm)	None	None	None	0	None	150	None
Sampling Results							
CO (ppm @0% O2)	58	120	75	95	129	95	57
SO2 (ppm @0% O2)	3140	3011	3050	3012	3120	3045	3011
N2O (ppm @0% O2)	1	73	1	38	98	69	1
THC (ppm @0% O2)	2	2	2	2	2	2	2
NH3 (ppm @0% O2)	0.0	47.3	0.0	4.4	50.1	0.0	0.0
HCN (ppm @0% O2)	0.0	0.0	1.1	1.2	1.6	1.0	0.5
SO3 (ppm @0% O2)	2.0	0.8	1.3	1.1	1.7	2.8	1.2
Particulate loading (gr/dscf)	2.0	2.3	1.8	1.9	2.2	2.3	2.1
Fly ash MMD (microns)	8.1	8.7	10.8	10.1	8.2	8.6	8.5
PM10 (%)	54.4	52.1	49.2	49.8	55.4	53.0	53.5
(gr/dscf)	1.09	1.21	0.88	0.93	1.24	1.23	1.10
PM2.5 (%)	10.5	10.1	9.4	13.6	14.3	11.2	12.6
(gr/dscf)	0.21	0.23	0.17	0.25	0.32	0.26	0.26
Carbon in ash (%)	0.08	0.03	0.17	0.26	0.07	0.10	0.08

CEMS Emissions

A continuous emissions monitoring system (CEMS) was used to sample for CO, SO$_2$, N$_2$O, and total hydrocarbons. SO$_2$ concentrations were in the range of 3010 to 3140 ppm (@ 0% O$_2$) for each condition, and were not affected by the AR technologies. Total hydrocarbon emissions were 2 ppm for each test condition. Figure 7.26 summarizes CO and N$_2$O emissions for each of the seven test conditions. CO and N$_2$O generally increased during application of the NO$_x$ control technologies relative to baseline coal firing. The largest increases were associated with the low temperature N-agent injection technologies, i.e. SNCR and reburning + SNCR. For SNCR, CO increased from 58 to 120 ppm, and N$_2$O increased from 1 to 73 ppm. OFA was injected at 1310 K. Thus AR-Lean, AR-Rich, and MIAR generate lower concentrations of CO and N$_2$O than does SNCR under similar conditions. It is believed that CO and N$_2$O concentrations could be further reduced by injecting OFA at a higher temperature.

Main Fuel: Illinois Coal @ 705,000 Btu/hr
SR1=1.10, SR3=1.15
NOi=1000 ppm as measured
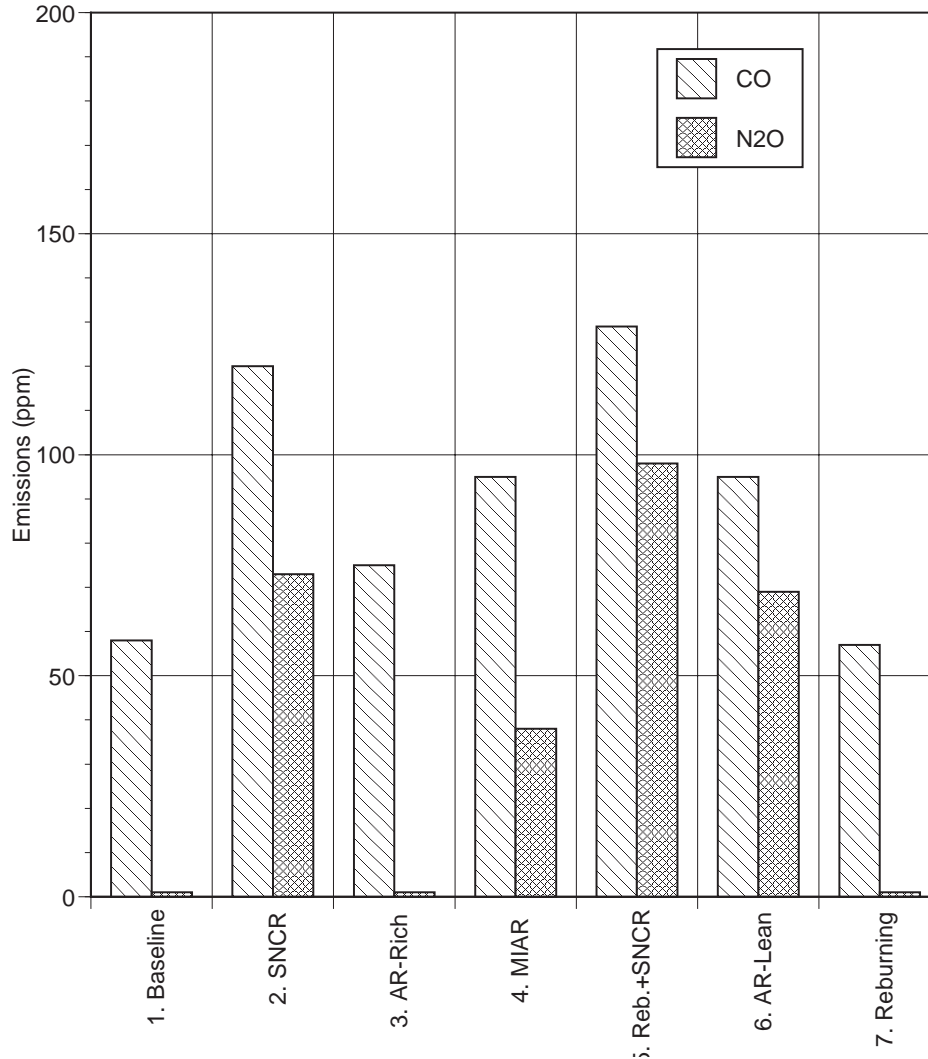
Figure 7.26 CO and N_2O emissions for AR technologies.

NH$_3$ and HCN Emissions

NH$_3$ and HCN emissions were measured by EPA Draft Method 206, using ion chromatography analysis. Results are shown in Figure 7.27. NH$_3$ emissions were fairly high (>40 ppm) for the two SNCR conditions, but were below 5 ppm for all other conditions (including MIAR). HCN emissions were below 2 ppm for baseline coal and all AR test conditions. Thus AR-Lean, AR-Rich, and MIAR generate significantly lower NH$_3$ emissions than does SNCR under similar conditions. These results would appear to indicate that as long as the N-agent(s) are added with or upstream of the OFA, NH$_3$ and HCN emissions can be minimized. For the SNCR cases, it is believed that a higher reagent injection temperature would reduce NH$_3$ emissions.

Main Fuel: Illinois Coal @ 705,000 Btu/hr
SR1=1.10, SR3=1.15
NOi=1000 ppm as measured
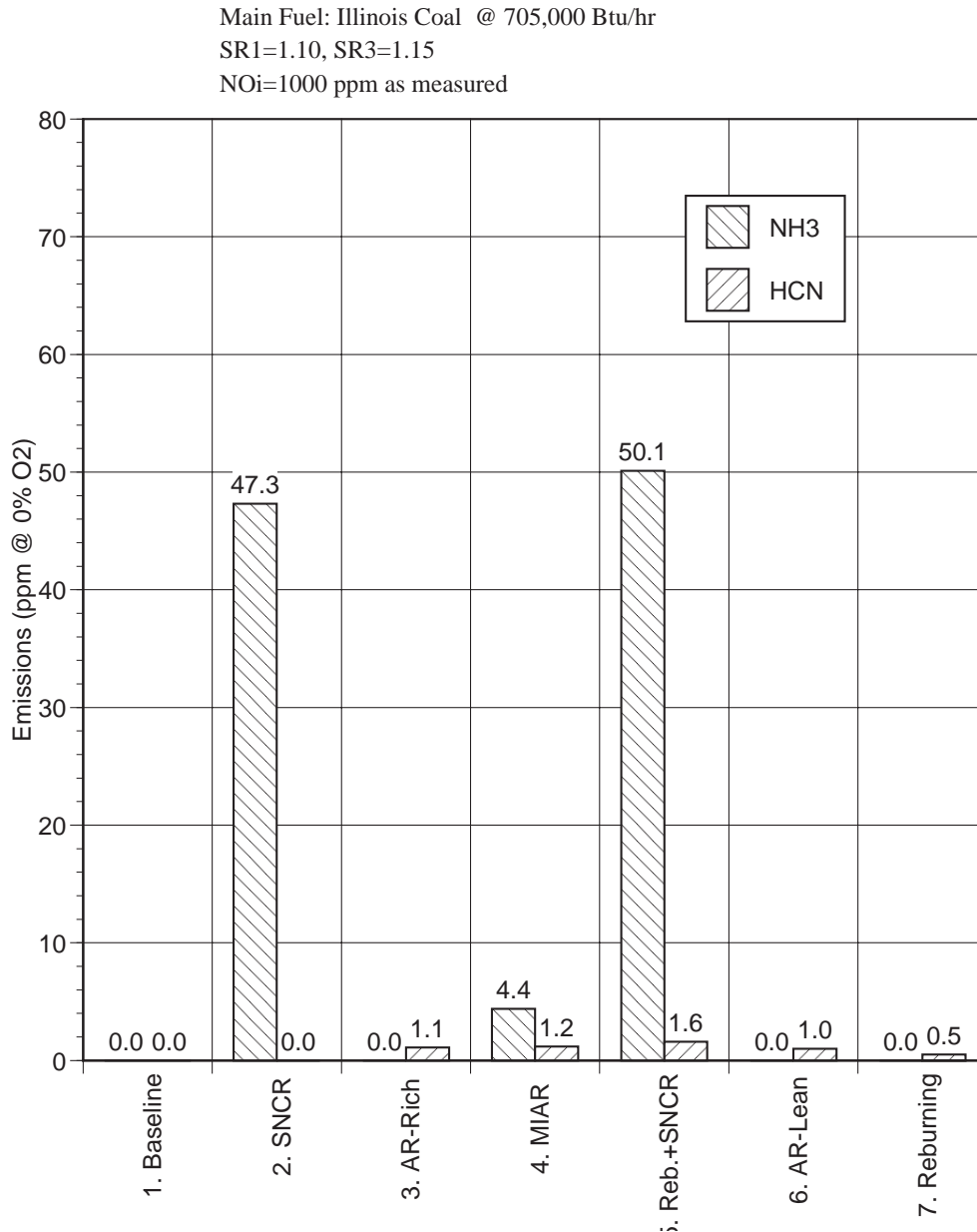
Figure 7.27 NH$_3$ and HCN emissions for AR technologies.

SO$_3$ Emissions

SO$_3$ emissions can impact electrostatic precipitator performance and, if present in high concentrations, cause boiler corrosion problems. SO$_3$ emissions were measured using the controlled condensation method, as detailed in the EPA's "Process Measurement Procedures - Sulfuric Acid Emissions" (1977). The sample probe was operated at a temperature of 590 K. Figure 7.28 shows SO$_3$ test results. The SO$_3$ concentration for baseline coal firing was about 2 ppm. For each of the NO$_x$ control technologies, SO$_3$ remained below 3 ppm. It is concluded that none of the technologies cause a significant increase in SO$_3$ emissions.

Figure 7.28 SO$_3$ emissions for AR technologies.

Particulate Size Distribution

Fly ash particle size can affect dust control equipment efficiency as well as causing respirability and health considerations. Particulate size distribution was measured using a cascade impactor. Figure 7.29 shows fly ash distributions for each of the seven test conditions. Fly ash mass mean diameter was between 8 and 11 microns for each condition. The AR technologies did not appear to significantly alter overall size distribution.
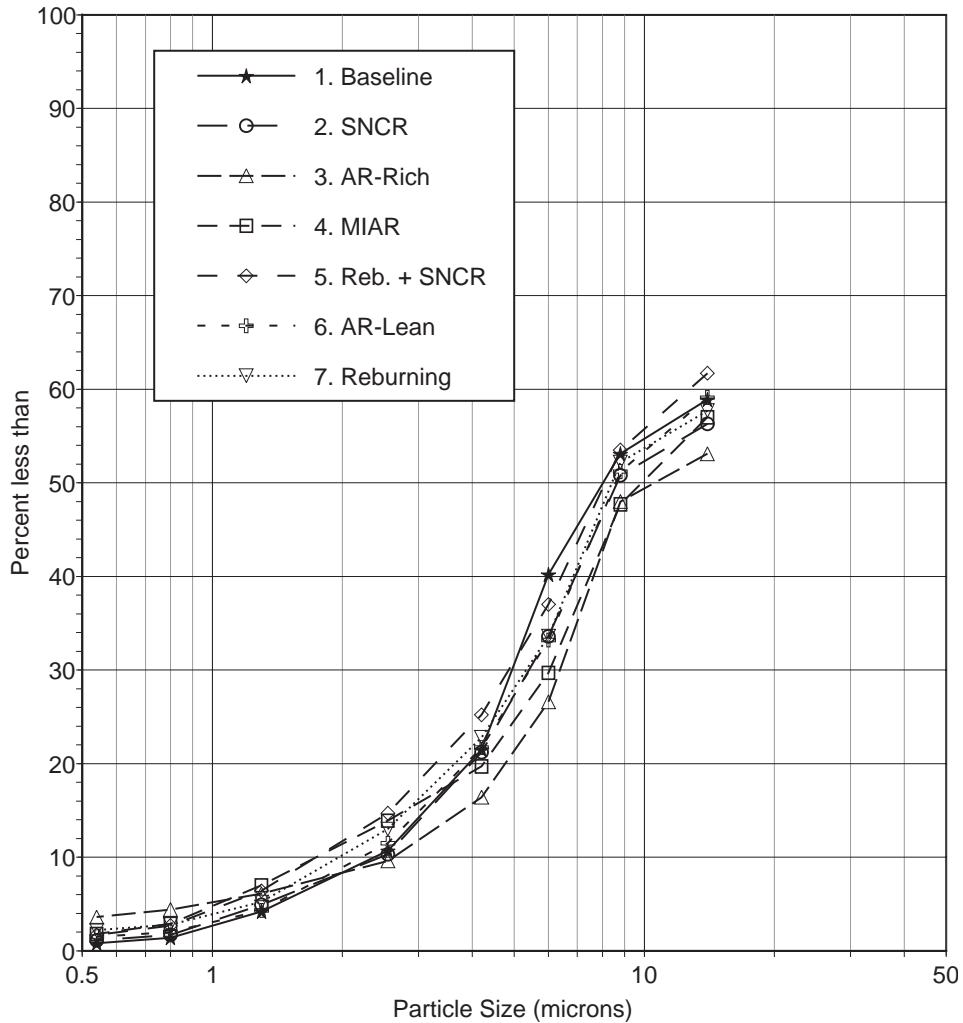
Figure 7.29 Fly ash size distribution.

Particulate Loading, PM10, and PM2.5

PM10 and PM2.5 are defined as the fraction of fly ash material of diameter less than 10 and 2.5 microns, respectively. EPA Method 5 and cascade impactors were used to determine total particle loading, PM10, and PM2.5. Results are shown in Figure 7.30. Total particulate loading was 2.0 gr/dscf for baseline coal firing, and ranged from 1.8 to 2.3 gr/dscf for the different NO$_x$ control technologies. PM10 was about 1.1 gr/dscf for baseline coal firing, and ranged from 0.9 to 1.2 gr/dscf for the different technologies. PM2.5 was about 0.21 gr/dscf for baseline coal firing, and ranged from 0.17 to 0.32 gr/dscf for the different technologies. These results would appear to indicate that the AR NO$_x$ control technologies do not significantly impact particulate loading, PM10, or PM2.5.

Main Fuel: Illinois Coal @ 705,000 Btu/hr
SR1=1.10, SR3=1.15
NOi=1000 ppm as measured
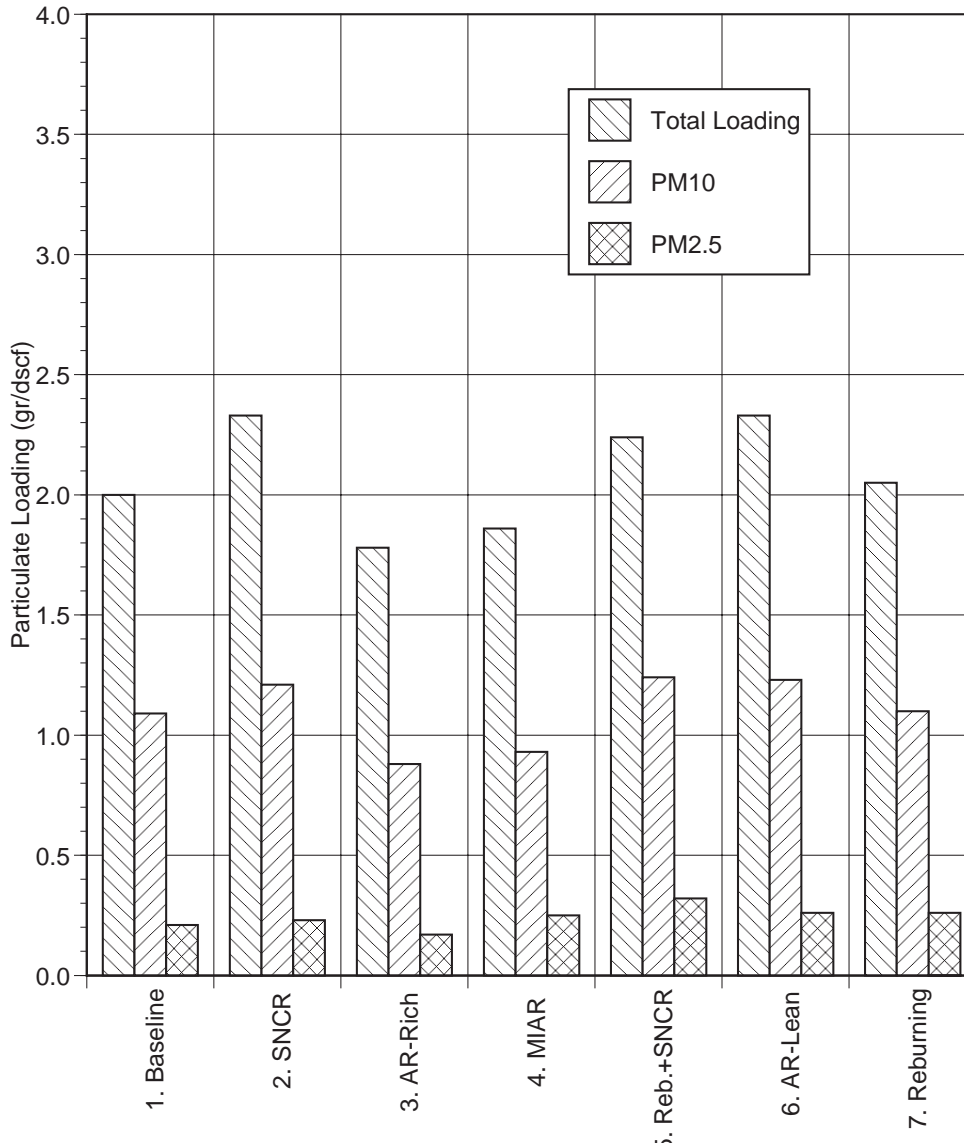
7.30 Fly ash total loading, PM 10, and PM 2.5.

Carbon in Ash

Poor carbon burnout can adversely impact boiler thermal performance, along with the commercial
value of collected fly ash. Fly ash is generally salable to the construction industry if it contains less
than 5% carbon. Ash samples were collected from the BSF convective pass using a volumetric
sampler and were analyzed for carbon in an induction furnace. Figure 7.31 shows carbon in ash
results. For all conditions, carbon in ash was well below 1%. Thus it is concluded, based on these
tests, that the AR technologies do not significantly decrease carbon burnout.

Main Fuel: Illinois Coal @ 705,000 Btu/hr
SR1=1.10, SR3=1.15
NOi=1000 ppm as measured
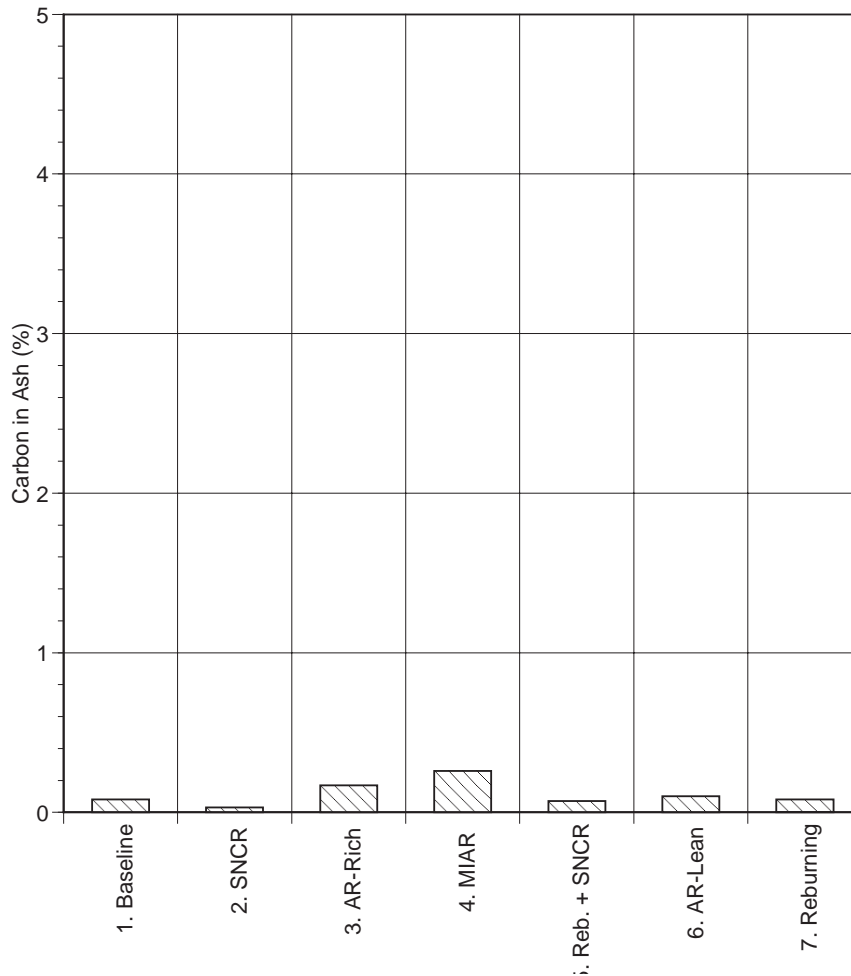
Figure 7.31 Carbon in ash results.

7.4 Pilot Scale Combustion Tests: Conclusions

In summary, the parametric tests showed that the AR technologies are able to provide effective NO_x control for a high-sulfur coal fired combustor. Three technologies were originally envisioned for development: AR-Lean, AR-Rich, and MIAR. Along with these, three additional technologies were identified during the course of the testing: Reburning plus SNCR, AR-Lean plus SNCR, and AR-Rich plus SNCR, where SNCR performance can be enhanced by addition of promoters.

Sodium was found to significantly promote performance more effectively during gas firing than coal firing. A possible reason for this is interaction of sodium compounds with fly ash, as well as reaction with SO_2 or HCl to form sodium sulfite, sodium sulfate or sodium chloride. Nevertheless,

even for high sulfur coal sodium was found to significantly improve performance when added at 150 ppm, which is a manageable level for most utility boilers.

Maximum NO reductions achieved by the promoted AR technologies during gas and coal firing were as follows:

		Gas firing	Coal firing
•	AR-Lean:	95%	90%
•	AR-Rich:	96%	93%
•	AR-Lean + SNCR:	98%	94%
•	AR-Rich + SNCR:	97%	93%
•	MIAR:	98%	95%

These technolgies have different optimum reburn heat input levels and furnace temperature requirements. For full scale application, an optimum technology can be selected on a boiler specific basis depending on furnace temperature profile and regions of injector access.

In terms of byproduct emissions, in some cases CO was observed to increase when sodium was added. This may be due to chain reactions involving sodium compounds, H atoms and OH radicals which allow CO to escape oxidation. However, it was found that CO could be controlled by increasing the OFA injection temperature. Emissions of N_2O and NH_3 showed the potential to increase under low-temperature SNCR conditons. Adding the second N-agent at higher temperature was found to minimize these emissions.

In summary, the promoted AR technologies demonstrated the ability to readily achieve NO reductions of 95+% during gas firing and 90+% during coal firing. Byproduct emissions were found to be manageable. Additional test work could be performed to further optimize variables such as N-agent stoichiometric ratio and additive-furnace gas mixing requirements, as well as to provide scale-up data for utility boiler application.

8.0 MECHANISM DEVELOPMENT AND KINETIC MODELING

The objective of this task is to develop a kinetic analytical model of the Advanced Reburning technologies. A high temperature reaction mechanism has been developed for use in this model, based on a standard natural gas combustion model (GRI-Mech) combined with nitrogen chemistry as well as reactions of sodium, sulfur, and chlorine. The chemical kinetic model has been implemented using chemical kinetics codes CHEMKIN-II and SENKIN, developed at Sandia National Laboratories, and EER's One Dimensional Flame (ODF) code. The experimentally validated model is used as a tool to investigate the process analytically.

The chemical kinetic model has been applied to an expirimentally feasible range of conditions, with appropriate variations in controllable conditions including initial species concentrations, temperature, and residence time. Rate constants fo the reactions in the mechanism have not been varied, and the model does not describe quantitatively the experimental data. However, the predicted exit concentrations do provide qualitative insight into expected performance trends. The predicted species histories also provide insight into internal details of the process which are not readily measured. In addition, sensitivity analysis has been applied to selected cases to identify the relative importance of specific reactions in the process as modeled. The mechanism development and modeling has extended the understanding of AR and provides a tool for future development and implementation of the process.

8.1 Mechanism Development

A high temperature kinetic mechanism has been developed and tested to model the AR systems process. This mechanism includes reactions of C-H-O species applicable to both rich and lean combustion chemistry. It also includes N-containing species reactions reflective of variations in stoichiometry (reburning), and the effect of additives (N-agents and/or promoters) on the species pool. To model the effect of promotion, the most important reactions of Na-containing compounds have been analyzed and incorporated. In addition, reactions of S- and Cl-containing compounds have been included to assist in future modeling of AR processes applied to coal combustion.

The resulting mechanism, which has been used in modeling, is presented in Appendix 1. The reaction numbers assigned there are used througout this section for reference. Reversible rate data also requires thermodynamic properties for the participating species. To complete the description of the model mechanism, the thermodynamic database is presented in Appendix 2.

8.1.1 GRI-Mech

GRI-Mech (Bowman et al., 1995, and Frenklach, et. al., 1994) was selected for the basic C-H-ON mechanism as it represents the current industry standard in natural gas combustion chemistry. The mechanism includes the elementary chemical reactions, the rate coefficients and parameters describing the thermodynamic properties of the included species. The basic combustion mechanism has been validated extensively against available experimental data, listed in the cited references.

The most current version as of the initiation of the modeling task is version 2.11, which contains 276 reactions with 49 species containing C, H, O, N, as well as Ar as a third body species. These are presented in Appendix 1 as reactions 1-278 (two duplicate reactions being added for compatibility with the kinetics software). Version 2.11 is an extension of the earlier Version 1.2, which was optimized specifically for accurate prediction of C, H, O combustions, in particular natural gas flames and ignition, with nitrogen included only as inert N_2. The nitrogen chemistry introduced in versions 2.11 is optimized specifically for natural gas flames and reburning. GRIMech by itself has not yet been optimized for other NO_x control technologies. The authors also caution that the agreement with nitrogen chemistry and reburning data is not as close as for C-HO chemistry, and therefore is subject to further development. Nevertheless, this mechanism represents the state of the art in these aspects of nitrogen chemistry, representing a significant improvement over previously published mechanisms such as Miller and Bowman (1989).

Due to these limitations in the current GRI-Mech, additional nitrogen reactions must be incorporated to obtain a mechanism capable of predicting AR processes which extend beyond conventional reburning, such as the SNCR chemistry inherent in N-agent addition.

8.1.2 SNCR Reactions

The analysis of available kinetic information resulted in preliminary selection of two reaction mechanisms for modeling the chemical behavior in the C-H-O-N system. Both mechanisms are based on GRI-Mech, with SNCR reactions added from other sources. The selection process is described in further detail in Zamansky and Maly (1996a).

Two variants of the C-H-O-N mechanism, denoted here as A and B, were considered. Mechanism A includes all GRI-Mech Version 2.11 reactions and reactions selected from the SNCR scheme suggested by Bowman, 1996. Mechanism B consists of the C-H-O system of GRI-Mech-1.2, N-chemistry reactions proposed by Glarborg et al., 1993, and reactions of CH_i radicals with nitrogenous

species ("C-N chemistry") selected from GRI-Mech Version 2.11. Either scheme could be considered to be state of the art for C-H-O-N chemistry modeling.

The two selected mechanisms include the complete GRI-Mech Version 1.2, which was verified by its authors against multiple C-H-O experimental data from various sources. The N-chemistry from GRI-Mech-2.11 and the Glarborg's N-mechanism were also verified against experimental data on reburning. However, because both mechanisms were broadened to include SNCR submechanisms, they required verification associated with the SNCR nitrogen chemistry. Calculations were performed based on available experimental data for the Thermal DeNOx process. Two sets of experiments were selected for comparison with modeling:

1. Laboratory-scale data presented by Lyon and Hardy, 1986. Conditions: flow system tests, variation of reactor temperature, residence time 0.1 s. Mixture composition: 225 ppm NO - 450 ppm NH_3 - balance He.

2. EER's recent pilot-scale experimental data. Conditions: BSF natural gas combustion tests, variation of NH_3 injection temperature, quenching rate 167 K/s. Flue gas composition: 200 ppm NO - 300 ppm NH_3 - 3.8% O_2 (dry measure) - 8% CO_2 - 15% H_2O - balance N_2.

The CHEMKIN-II kinetic program developed at the Sandia National Laboratories (Kee et al., 1991) was used for modeling. Figure 8.1.1 demonstrates comparison of the experimental results and modeling by the use of the mechanisms A and B. Although both mechanisms show some difference from the experimental data and there is a shift in temperature, they both qualitatively model the temperature window of the Thermal DeNOx process. The differences can be explained by the values of rate constants, by errors in experimental temperature measurements, and by influence of mixing effects on NO removal. Calculations with both mechanisms were performed without any adjustments in rate constants taking into account an actual BSF temperature profile. Both models qualitatively described the most substantial feature of the SNCR process: the temperature window of NO reduction. However, this validation also shows that differences in quantitative comparison of modeling and AR experiments are to be expected.

Since both mechanisms show about the same performance in modeling experimental data, it is difficult to prefer one of them. Mechanism A was selected for further calculations since it includes less constituent parts (sub-mechanisms) and all of them were suggested by the same group of authors. The SNCR reactions which are added to GRI-Mech 2.11 are included in Appendix A as reactions 279-312.
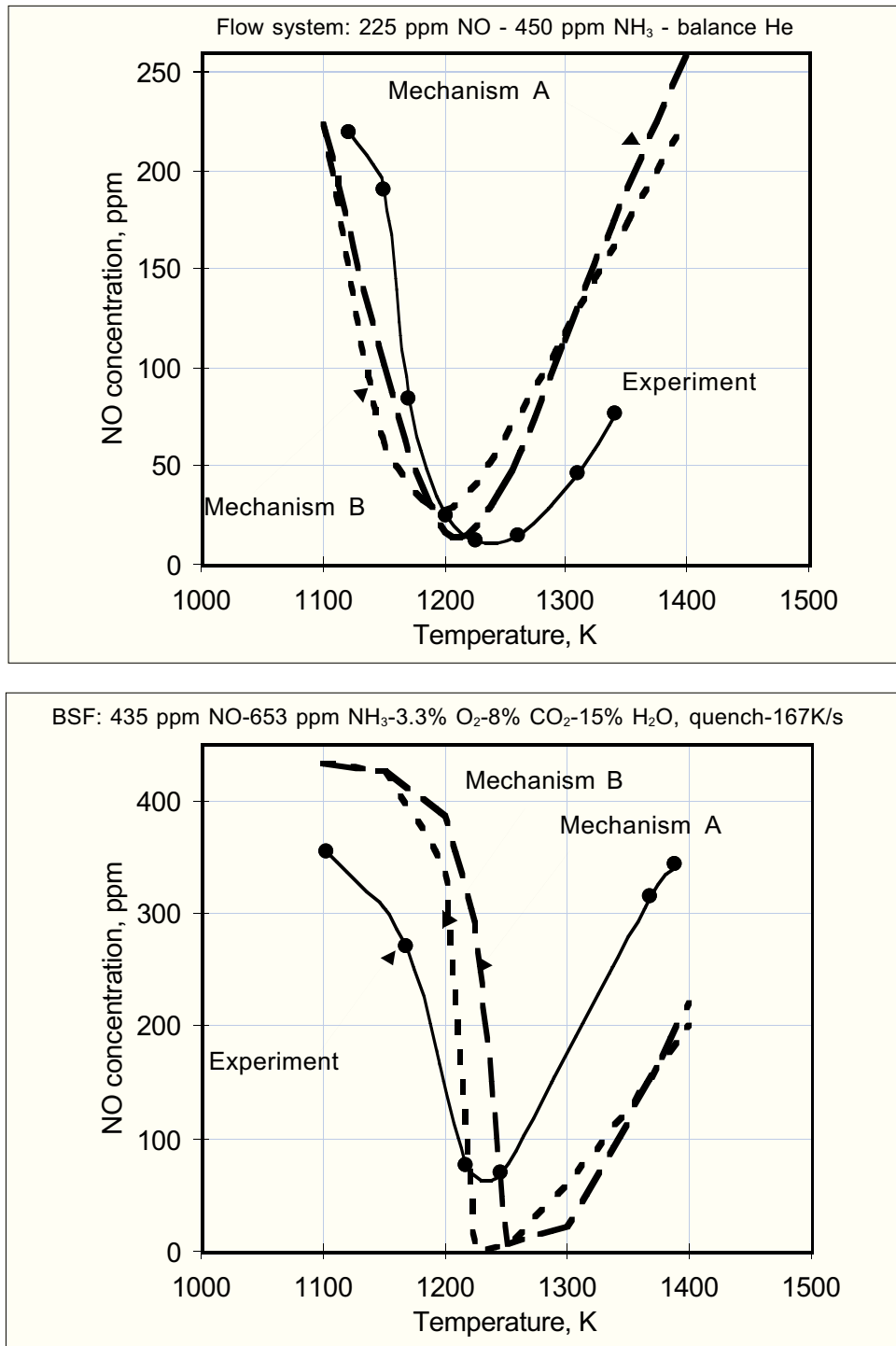
Figure 8.1.1. Comparison of experimental data and modeling with mechanisms A and B for the Thermal DeNOx process.

8.1.3 Reactions of Sodium

Experimental data demonstrate that the addition of sodium compounds, such as sodium carbonate and sodium hydroxide, can increase reburning efficiency. However, the high temperature chemistry of sodium compounds is not well understood. Only a few rate constants have been measured directly, and kinetic information on many reactions is absent. However, estimates are available for several other rate constants.

Sodium carbonate was used as a promoter in most CTT and BSF experiments. It was also shown that sodium hydroxide has about the same efficiency as sodium carbonate. When sodium carbonate is injected into flue gas, it decomposes into oxides. The mechanism of Na_2CO_3 thermal decomposition and the corresponding rate constants are the subject of an experimental task at the University of Texas, as documented in Section 5.

Most likely, sodium carbonate dissociates at high temperatures to different oxides. The oxides react with water molecules which are available in flue gas to form sodium hydroxide. The specific reactions considered here (numbered corresponding to Appendix 1), based on the University of Texas study, are:

$$Na_2CO_3 \rightarrow Na_2O + CO_2 \tag{317}$$

$$Na_2O + CO_2 \rightarrow Na_2CO_3 \tag{318}$$

$$Na_2O + CO_2 \iff 2\ NaOH \tag{319}$$

The conversion from Na_2CO_3 to NaOH is rapid, and it is most likely the reason for the equal promotion efficiency of Na_2CO_3 and NaOH.

Since the modeling effort was conducted in parallel with the University of Texas experimental effort, it was necessary to develop the modeling mechanism based on preliminary estimates of the reaction rates. For this reason, the rate constant used in modeling for Reaction 319 may not exactly match those reported for the experimental task (Section 5). For this reaction, rate expression used in modeling was 1.00E13 exp(+35390/RT), rather than the later experimental result of 9.18E12 exp(-3120/RT), which is now recommended. However, both versions of the rate constants predict rapid initial conversion of Na_2CO_3 to NaOH for example. The estimated rate constants in the model mechanism result in a characteristic decay time of 3 ms at 1400 K, while the University of Texas

rate constants predict less than 1 ms. In either case, the rates are sufficiently fast that the difference is not considered to be serious.

The additional 23 reactions (320 through 342) of sodium compounds with C-H-O-N species consider the reactions of NaOH and its decomposition products. The source for rate constants and expected behavior of some of the reactions follows:

- Reaction 320 is the most important for removing N_2O from flue gas. The rate constants for reaction 320 are from Plane, 1992, but several measurements of the rate constant agree rather well with each other (Mallard et al., 1994).

- Reactions 321-324 are important steps of NaO interaction with H_2O, O, NO and H_2. Rate constant of these reactions have been measured; Reactions 321 and 324 rates are from Ager and Howard (1987), Reaction 322 from Plan and Husain (1986), and Reaction 323 from Ager et al. (1989).

- Reaction 325 represents oxidation of Na atoms by molecular oxygen. The rate constant of this reaction was measured several times and the most reliable value (Plane and Rajasekhar, 1989) was selected. Reaction 326 can be important for N_2O removal under fuel rich conditions. If the reaction proceeds as written to form Na atoms, they will react with N_2O via reaction 320. If reaction 320 is faster in reverse direction, it will be not effective.

- Reaction 327 is probably important for defining the processes of radicals formation and removal. Indeed, if the recombination reaction 327 of sodium atoms and hydroxyl radicals is fast enough, the efficiency of the promoter will be low. Measurements by Jensen and Jones, 1982 were accepted as rate constants for reactions 327 and 328.

- Other reactions of sodium, 329-341, were recently estimated by Perry and Miller, 1996.

- Reaction 342 represents a process of sodium-ammonia interaction. It was observed in experiments that sodium promoters are effective mainly in the presence of N-agents. However, no kinetic data on sodium-ammonia interaction was found in the literature. The rate constant was estimated to be close to the collision frequency.

To complete these mechanism enhancements, the thermodynamic database was updated to include the thermodynamic data for the sodium compounds. The value of the $Na-O_2$ bond energy was

selected to be $D_o = 37.2$ kcal/mol as was determined theoretically by Partridge et al., 1992 and recommended by Perry and Miller, 1996.

Additional sodium reactions include interactions with sulfur-containing species (reactions 343 through 346) and chlorine-containing species (374 through 350).

8.1.4 Reactions of Sulfur and Chlorine

It has been found that sodium promoters are less effective in flue gas from coal combustion flue gas compared to that from natural gas. Coal includes sulfur and chlorine compounds which can react with sodium, decreasing its efficiency. The submechanisms for reactions of S- and Cl- compounds with Na-O-H species have been added to the mechanism for future modeling of the effect of sulfur and chlorine compounds on reburning efficiency and to understand the chemistry of sodium promotion under different conditions. All selected reactions are presented in Appendix 1 as reactions 312-316 and 343-355.

Rate constants for SO_2/SO_3 reactions, 312-316, were taken from the literature review by Atkinson et al., 1992 and direct measurements by Armitage and Cullis, 1971 (for reaction 312) and Smith et al., 1982 (for reaction 316). Though many kinetic measurements of these reactions were reported in the literature, most of them were performed at relatively low temperatures, mainly below 400 K. Therefore, there is a significant uncertainty in high temperature kinetic data for SO_2/SO_3 interaction.

Reactions 343-346 represent interaction of sodium and sulfur compounds. Reaction 343 was suggested by Fenimore, 1973; the rate constant for this reaction was estimated to be $k = 10^{13} \exp(-17700/T)$ cm^3/mol·s where the activation energy is equal to the reaction endothermicity. A single rate constant measurement for reaction 344 was reported by Shi and Marshall, 1991. Rate constants for reactions 345 and 346 were assumed to be close to that measurement.

During the combustion process, most chlorinated compounds are converted into HCl. Therefore, to model the effect of chlorine on reburning efficiency and Na promotion, it is logical to perform modeling using the initial concentration of HCl in flue gas corresponding the amount of chlorine in coal. For this reason, chlorine reactions have been added which address the reactions of HCl and its products.

Nine reactions of chlorine were included in the mechanism. The first four, 347-350, represent the reactions of sodium compounds (Na, NaO, NaO_2, and NaOH) with HCl. All these reactions are

fast, and available experimental measurements of the rate constants were selected (Silver et al., 1984; Husain and Marshall, 1986; DeMore et al., 1987; and Silver and Kolb et al., 1986, respectively). Five other chlorine reactions, 351-355, include the well known steps of Cl_2-H_2 interaction. Their rate constants were taken from kinetic tables by Baulch et al., 1981.

The thermodynamic database was updated to include data for the sulfur and chlorine containingcompounds. Thermodynamic data for $NaSO_2$ were calculated by using the Na-SO_2 bond energy $D_o = 47.1$ kcal/mol defined by Steinberg and Schofield, 1990. This value corresponds to the heat of formation of $NaSO_2$, $\Delta H_{f,0} = -92$ kcal/mol.

Thermodynamic analysis. To verify which species are important to include in the sulfur and chlorine mechanisms, an analysis of equilibrium flue gas compositions was performed. This predicts the species concentrations if the thermodynamic state of the gas (*e.g.*, temperature, pressure) were held uniform indefinitely. Although actual conditions are far from invariant, the analysis is still useful. Species participating in reactions which are fast relative to the rate of change in temperature (e.g. natural gas combustion) may establish a partial equilibrium in the mixture, and thermodynamic analysis can indicate the relative amounts to expect. Furthermore, products which are favored thermodynamically are important to include in the reaction mechanism so that all likely products are considered.

The calculations were performed using the latest version of the NASA Chemical Equilibrium program, CET93 (McBride et al., 1994). To ensure that all potentially important species are considered, the completeness of the code's species database (which identifies species to consider and their thermodynamic properties) is crucial. The standard CET93 database includes over 1000 compounds mostly from the JANAF tables, including combustion products as well as alkali metals. EER has extended this by adding data from other sources, including the Barin (1989) tables and current research at Lawrence Livermore National Laboratories (Ebbinghaus, 1993). Several metals and radionuclides are thus incorporated, as well as their oxides, hydroxides, oxyhydroxides, chlorides, metal-sulfur compounds, and other species. A list of sodium compounds included in the updated CET93 thermodynamic database, and sample properties, is presented in Appendix 3.

CET93 was used to predict concentrations of sodium compounds in the reburning and overfire air zones at various conditions, including different temperatures, stoichiometries, quantities of sodium, and the presence of sulfur and chlorine. Equilibrium was calculated for each composition for a range of temperatures from 1100 to 1900 K. Zamansky et al. (1997a) provides further details of the calculations.

For stoichiometric ratios ranging from 0.9 to 1.25, with 10 ppm Na in the mixture, the most favored sodium species are NaOH and Na, with all other sodium species at less than 0.1 ppm. The same species dominate with 50 ppm Na at an SR of 0.99. The major species as a function of temperature are shown in Figure 8.1.2(a) for 10 ppm Na and SR=0.99. When 2000 ppm SO_2 is included in this mixture, the presence of sulfur does not result in formation of significant amounts of sodium sulfate over the temperature range considered, as shown in Figure 8.1.2(b). However, Na_2SO_4 increases as temperature is reduced and could be significant in modeling the interaction between sodium and sulfur. If 50 ppm Cl_2 is included instead of sulfur, sodium chloride becomes the most stable sodium compound, as shown in Figure 8.1.2(c). It must be cautioned, however, that thermodynamic data for gaseous sodium salts are not considered reliable, and so these results should not be considered conclusive without future validation. Nevertheless, these results establish NaOH, Na, Na_2SO_4 and NaCl as potentially important species in a C-H-O-N-Na-S-Cl mechanism. Appropriately, reactions involving these species have been included in the current mechanism.

8.1.5 Mechanism Development: Summary

The mechanism developed based on the above considerations consists of 355 reactions and 66 species. It has been developed based on the best existing data for mechanisms and individual reactions as of the time of its development. The core of the mechanism is based on the industry standard for natural gas combustion and reburning, GRI-Mech 2.11. The mechanism was then extended to include reactions for the prediction of N-agent chemistry.

The resulting C-H-O-N mechanism was further extended to include Na compounds in order to model processes involving sodium carbonate or sodium hydroxide promoters. The sodium reactions were developed in parallel with the experimental effort at the University of Texas.

The addition of sulfur and chlorine reactions enable predictions of the behavior of promoted AR in coal combustion. Thermodynamic analysis shows that the most significant species for interaction of S and Cl with with Na have been included. The rates for reactions involving S and Cl species were estimated based on published data, and have not yet been tested against experimental results.

8.2 Modeling with Instantaneous Mixing Times

Initial modeling focused on the chemistry of individual AR processes after premixing the combustion gases with the reactant stream being introduced. This approximation represents instantaneous mixing of the reactants, thus removing the details of the physical mixing process from the model. Once
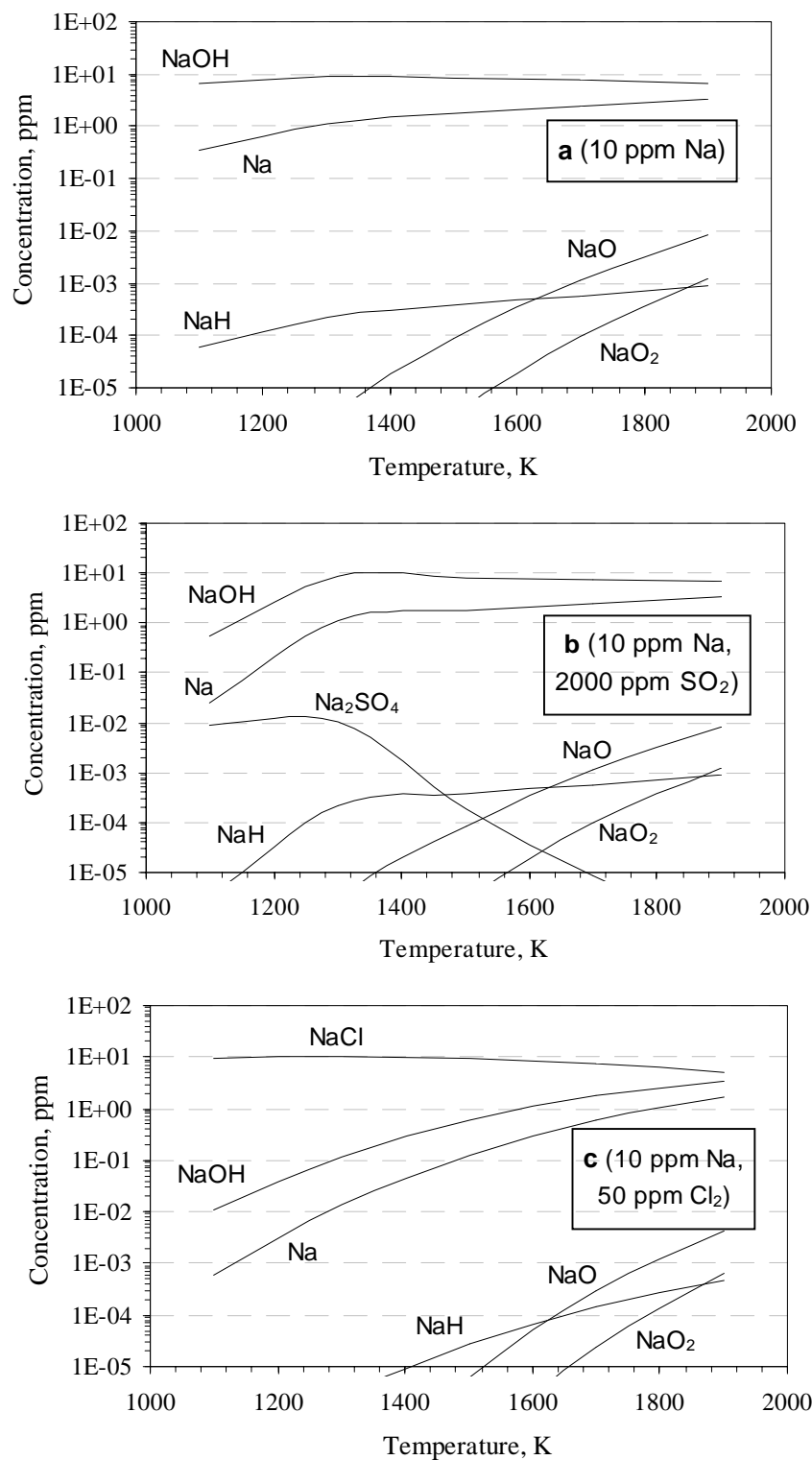
Figure 8.1.2. Effect of sulfur and chlorine on equilibrium concentrations of sodium species in flue gas.

premixed, the reactions proceed along a one-dimensional (plug flow) reactor, which again allows the reactions to proceed in time without any fluid dynamic effects. Thus, this approach focuses on the chemistry of the process.

Individual AR injection processes include reburning, N-agent injection in the reburning zone (ARRich) or with OFA (AR-Lean), addition of promoters with the N-agent, and OFA addition. Each injection involves different parameters which affect its performance. One of these parameters is the location of injection, characterized either by time from the point of reburn fuel or OFA injection, or by temperature at the point of injection. Another is the amount of added reactants, characterized by concentration, stoichiometric ratio following addition (for fuel or air addition), or NSR (for N-agent addition).

In these modeling studies, the reburning fuel is CH_4, the N-agent is NH_3, and the promoter is Na_2CO_3. In all cases the pressure is held constant at 1 atm. The temperature profile was specified at a constant quench rate of 300 K/s, reflective of the actual reburning zone environment in the BSF.

The CHEMKIN-II kinetic program developed at the Sandia National Laboratories (Kee et al., 1991) was used for most instantaneous modeling. CHEMKIN-II is used to predict the kinetic curves of major components in the reaction zone (concentration vs. time) for comparison with experimental data. However, the kinetic curves do not provide information about the importance of specific elementary reactions with respect to increasing or decreasing concentrations of certain components. The next step, sensitivity analysis, was done to obtain this information. Sensitivity analysis is a procedure to quantitatively determine the dependence of the model solution on the elementary reaction rate constants. It provides insight about how important certain reactions are to the model's predictions. The sensitivity analysis was performed with the use of the SENKIN code developed by Sandia National Laboratory (Lutz et al., 1987). SENKIN is a FORTRAN computer program for predicting the species and temperature histories and for calculating the first order sensitivity coefficients of each species with respect to the elementary reaction rate parameters.

In addition to species mole fraction histories (kinetic curves) which are also available from Chemkin-II, Senkin provides information about contribution and sensitivity factors. Contribution factors for a selected species show the effect of elementary reactions with participation of the species on its concentration. Sensitivity factors for a selected species show the effect of each elementary reaction in the mechanism on the concentration of the species.

The chief difference between these two parameters is that contribution factors show the direct influence of specific reactions on a given species. Sensitivity factors show indirect influences hidden in the complex reaction mechanism, to show how a change in the rate for a given reaction would affect the production or removal of a given species. Both measures are important. While contribution factors show the reactions directly involved in formation and destruction, often groups of reactions work rapidly and in opposition to each other, masking the net influence of another reaction which is driving them. Sodium promotion, in which injected sodium species significantly affect NO but have very little direct interaction with it, is an example of a process where sensitivity analysis is particularly useful. By ranking reactions with respect to these factors, the most important direct and indirect influences on a given species can be determined, along the length of the reactor.

The contribution factor $c_{i,k}$ is defined as the contribution of reaction i to the net production rate of species k at a given instant, and may be calculated as:

$$c_{i,k} = v_{k,i} \, q_i$$

$v_{k,i}$ is the net stoichiometric coefficient of species k in reaction i (the number of molecules of species k on the right side of the reaction minus the number of molecules on the left side, the net number of molecules of k produced as the reaction proceeds to the right). q_i is the rate of progress variable, calculated as:

$$q_i = k_{f,i} \prod_k [x_k]^{v'_{k,i}} - k_{r,i} \prod_k [x_k]^{v''_{k,i}}$$

where $k_{f,i}$ is the forward rate constant and $k_{r,i}$ is the reverse rate constant for reaction i, $v'_{k,i}$ and $v''_{k,i}$ are the stoichiometric coefficients of species k on the left and right hand side of reaction i, respectively, and x_k is the mole fraction of species k. Note that $v_{k,i} = v''_{k,i} - v'_{k,i}$.

The sensitivity of species k to reaction i is defined as

$$(dx_k / dA_i) (A_i / x_{k,max})$$

where A_i is the frequency factor from the Arrhenius rate expression for reaction i, and $x_{k,max}$ is the maximum value of x_k over all points in time which are processed by Senkin. (In other words, the normalizing value of $x_{k,max}$ is somewhat dependent on the timestep resolution of the Senkin calculation if the species undergoes a very rapid transient).

The histories of concentration, contribution factors, and sensitivities provide information useful for understanding chemistry of the processes under investigation. This is a valuable tool in optimizing NO removal while ensuring that other emissions such as NH_3 remain low.

8.2.1 Modeling of the Basic Reburning Process

Stoichiometric ratio SR_1 in the primary zone was kept at $SR_1=1.1$ for all calculations. This SR_1 corresponds to methane combustion with the following mixture composition:

8.72% CH_4 - 19.18% O_2 - balance N_2

If the combustion process in the primary zone is complete, it generates about 8% CO_2 and 15% H_2O. At the same time, 1.74% O_2 is left which is available for oxidation of the reburning fuel. Therefore, the premixed reactants for reburning can be described as:

[CH_4] - 1.74% O_2 - 600 ppm NO - 8% CO_2 - 15% H_2O - balance N_2,

where [CH_4] is the molar percent of reburning fuel. For example, [CH_4] is 1.94% for reburning zone stoichiometry $SR_2=0.90$, 1.37% for $SR_2=0.95$, and 0.967% for $SR_2=0.99$.

An initial NO concentration NO_i = 600 ppm was used for calculations. Figures 8.2.1-8.2.3 demonstrate concentration profiles of main species in the reburning zone at an injection temperature T_1 = 1700 K and SR_2 equals 0.99, 0.95, and 0.90, respectively. Comparison of these graphs shows that CH_4 is rapidly converted to CO and H_2. Only at $SR_2=0.90$, about 300 ppm CH_4 is present in the mixture. At $SR_2=0.99$ and 0.95, the amount of CH_4 is lower than 1 ppm.

At $SR_2 = 0.99$ (Figure 8.2.1), NO concentration drops during a very short period of time from 600 ppm to about 540 ppm and then, slowly decreases to 502 ppm. Concentrations of NH_3 and HCN are lower than 1 ppm, though some O_2 is still present.

At $SR_2 = 0.95$ (Figure 8.2.2), oxygen disappears within 0.05 s, and NH_3 concentration slowly increases. NO again rapidly drops to about 430 ppm and decay slowly to 330 ppm. Total Fixed Nitrogen (mole fraction of N in species other than N_2, approximated by $NO+NH_3+HCN$) is a measure of the total unreacted nitrogen in the mixture. In this case, TFN concentration is 332 ppm by 0.5 s.
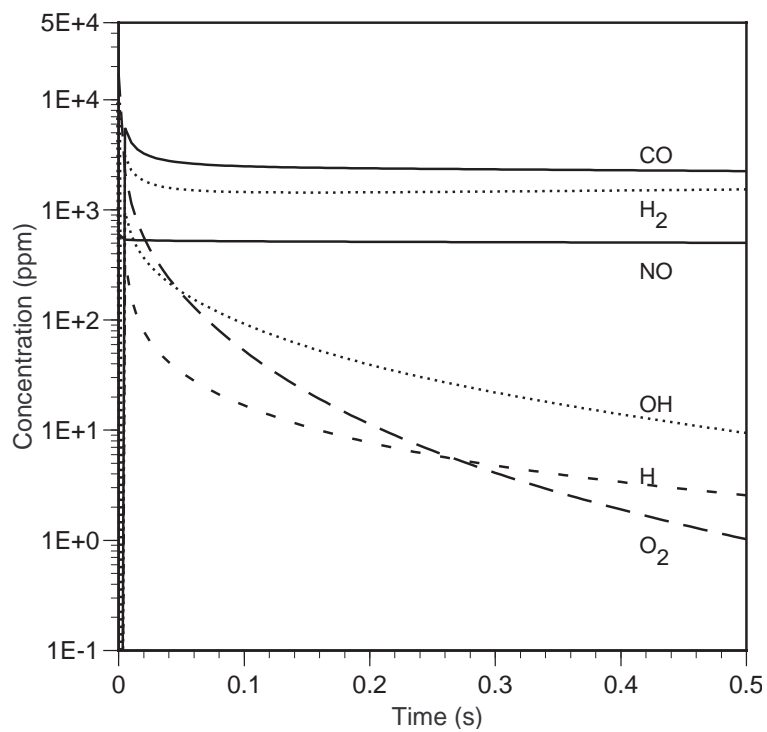
Figure 8.2.1. Kinetic curves of the main species in the reburning zone at $SR_2 = 0.99$ and injection temperature $T_1 = 1700$ K.
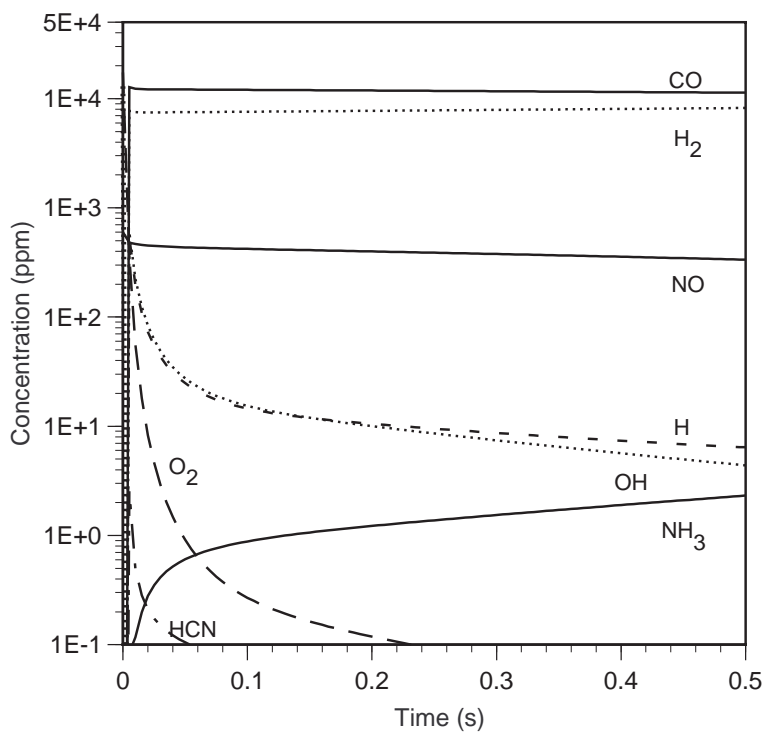
Figure 8.2.2. Kinetic curves of the main species in the reburning zone at $SR_2 = 0.95$ and injection temperature $T_1 = 1700$ K.
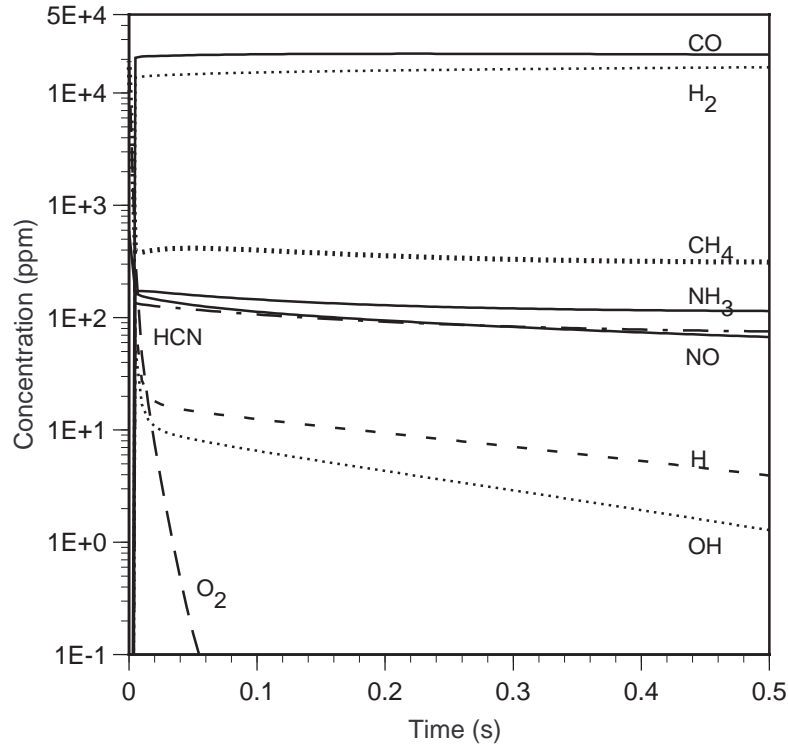
Figure 8.2.3. Kinetic curves of the main species in the reburning zone at $SR_2 = 0.90$ and injection temperature $T_1 = 1700$ K.

At $SR_2 = 0.90$ (Figure 8.2.3), NO rapidly and more efficiently decreases from 600 to 160 ppm, and then slowly to 67 ppm. However, in this case, the mixture contains 75 ppm HCN and 115 ppm NH_3 at t = 0.5 s. Hence, TFN equals 257 ppm.

Chemistry at Short Time Scales. The results show that there are two steps of NO reduction in the reburning process: the first very fast step and the second slow step. The cause of these fast and slow decreases in NO concentration is of primary interest for understanding the reburning phenomenon. To clarify the main processes in the fast NO reduction zone, calculations were carried out over a reaction time interval of 5 msec for $SR_2 = 0.99$ and 0.90. Figures 8.2.4 and 8.2.5 represent the results.

Figure 8.2.4 demonstrates kinetic curves in the reburning zone at $SR_2 = 0.99$, $T_1 = 1700$ K, and t = 5 ms. The NO concentration has a little minimum at about 2 ms. This minimum is explained by reactions of NO with C-containing radicals: CH_3, CH_2, HCCO, $CH_2(S)$, CH, and C. The radicals are formed from CH_3 which, in turn, is formed from CH_4. The radicals participate also in recombination reactions with each other and in reactions with oxygen and other species. As a result of these processes, concentrations of the radicals increase within 2 ms, and then, since all CH_4 is
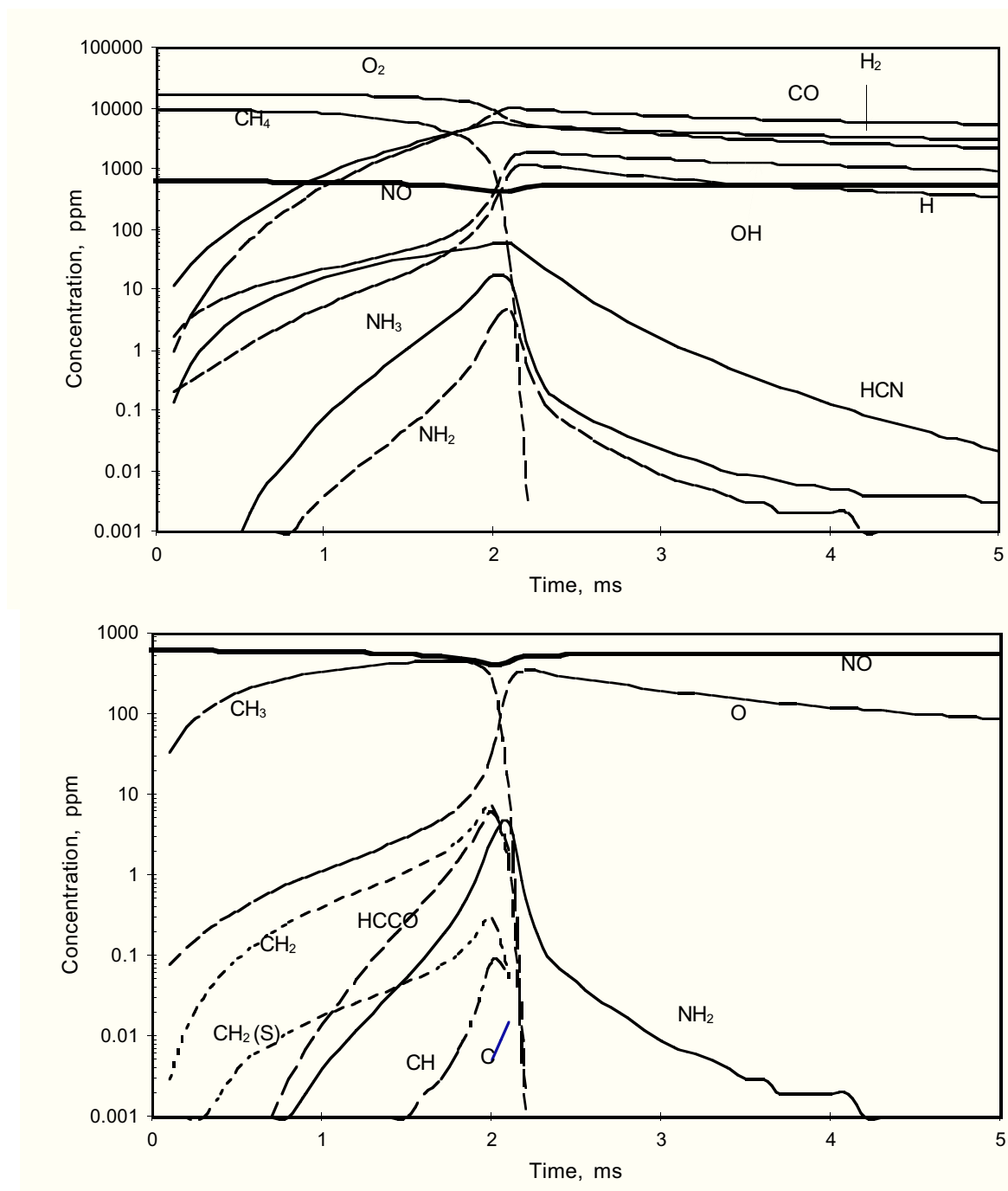
Figure 8.2.4. Kinetic curves in the reburning zone at $SR_2 = 0.99$, $T_1 = 1700$ K, and t = 5 ms.

consumed and there is no more feed, the concentration of C-radicals reduces, due to recombination and oxidation, by several orders of magnitude. Concentrations of HCN and NH_3 rise simultaneously with C-radicals because HCN and NH_3 are the main molecules formed due to reactions of the radicals with NO. At about 2 ms, both HCN and NH_3 are oxidized by existing oxygen into NO. Therefore, the NO concentration slightly increases. It is of interest to note that concentrations of

CH$_2$ and HCCO reach 8-9 ppm, though CH concentration does not exceed 0.1 ppm. Main reactions of NO removal can be compared by considering their rates at the maximum point of radical concentrations. Table 8.2.1 presents the NO reactions with C-radicals and their rates in arbitrary units at 2 ms.

This comparison shows that HCCO radicals, followed by CH$_2$ radicals, are the most important species depleting NO concentration. Thus, the reactions of HCCO and CH$_2$ radicals are dominant pathways (in the scope of the assumed mechanism) for NO consumption during the initial fast NO removal after reburn fuel injection under the conditions examined.

Table 8.2.1. Comparison of NO reaction rates with C-radicals at $SR_2 = 0.99$, $T_1 = 1700K$ and $t = 2$ ms.

C-radical	Reaction	Rate, arb. units	Total rate, a. u.	Rank
C	$C + NO = CN + O$	1	2.6	6
	$= CO + N$	1.6		
CH	$CH + NO = HCN + O$	25	51	4
	$= H + NCO$	10		
	$= N + HCO$	16		
CH$_2$	$CH_2 + NO = H + HNCO$	560	900	2
	$= OH + HCN$	140		
	$= H + HCNO$	200		
CH$_2$(S)	$CH_2(S) + NO = H + HNCO$	14	22.6	5
	$= OH + HCN$	3.6		
	$= H + HCNO$	5		
CH$_3$	$CH_3 + NO = HCN + H_2O$	71	76.6	3
	$= H_2CN + OH$	5.6		
HCCO	$HCCO + NO = HCNO + CO$	1860	1860	1

Figure 8.2.5 shows kinetic curves in the reburning zone within first 5 ms at $SR_2 = 0.90$ and $T_1 = 1700$ K. NO concentration decreases from 600 to 165 ppm, and this is explained by reactions of NO with the same C-containing radicals. Concentrations of the radicals also have a maximum, in this case at about 3 ms, but they are removed not so rapidly since CH$_4$ concentration is much higher, and the source of the radicals (CH$_4$ and CH$_3$) still exists within 5 ms. Concentrations of HCN and NH$_3$ again rise simultaneously with C-radicals, but, in this case, HCN and NH$_3$ are almost not oxidized since O$_2$ concentration drops rapidly (only 1 ppm O$_2$ exists in the mixture in 30 ms).
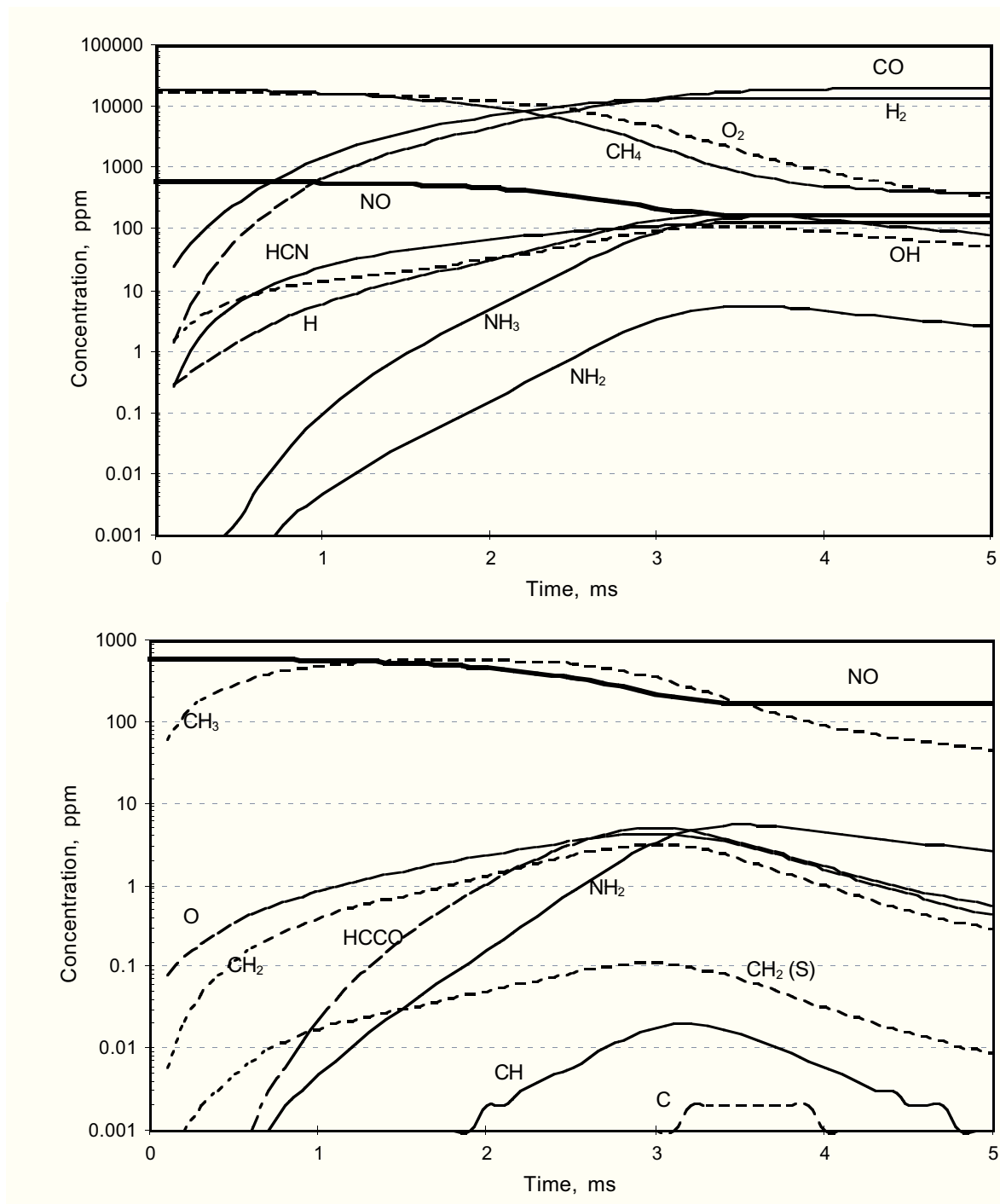
Figure 8.2.5. Kinetic curves in the reburning zone at $SR_2 = 0.90$, $T_1 = 1700$ K, and t = 5 ms.

Analysis of reaction rates for the NO reactions with C-radicals at $SR_2 = 0.90$ has been performed at the maximum point of radical concentrations (3 ms). The same conclusion can be made as for $SR_2 = 0.99$: the primary NO-removing radicals in decreasing order of importance is HCCO, CH_2, CH_3, CH, $CH_2(S)$, and C.

Dependence on Reburn Zone Stoichiometry. Figure 8.2.6 compares modeling and experimental data on concentrations of NO, NH_3, HCN, and TFN in the reburning zone (t = 0.5 s) at $T_1 = 1700$ K for different reburn fuel concentrations (various SR_2). The main difference between the experimental and modeling data sets is observed at low SR_2 where modeling predicts higher NH_3 concentration, but experiment demonstrates higher HCN level.

However, at $SR_2 = 0.90$-0.99, experimental and modeling concentrations are close to each other. It worth noting that experimental data can, of course, be affected by the rate of mixing. For this reason, mixing rates will be introduced as a variable in Section 8.3. However, Figure 8.2.6 demonstrates the current level of confidence in kinetic mechanisms developed for modeling of reburning. Even for the simplified treatment of mixing, the model can predict major reaction trends and can help to find prospective conditions of NO removal, for verification by experiment.

Dependence on Reburn Fuel Injection Temperature. Figure 8.2.7 compares performance of the reburning process at different temperatures for $SR_2 = 0.99$, 0.95, and 0.90. Under conditions close to stoichiometry, $SR_2 = 0.99$, concentrations of NH_3 and HCN in the reburning zone are less than 1 ppm, and all TFN is in the form of NO. TFN concentration in the reburning zone is decreased by 20-30%, and it is smaller at lower temperatures where C-radicals exist longer. Since they do not disappear too fast, more C-radicals are available for the reactions with NO. For instance, as shown in Figure 8.2.4, the first, fast reburning stage proceeds within 5 ms at T = 1700 K, mainly within 2 ms. At 1500 K, C-radicals do not disappear so fast, and the first stage proceeds longer, within about 20 ms. As a result, NO concentration drops in this fast stage from 600 to 535 ppm at 1700 K, but at 1500 K the process is more efficient: NO decreases from 600 to 450 ppm.

At $SR_2 = 0.95$ (Figure 8.2.7), only small amounts of NH_3 and HCN are formed at about 1500 K, and most of TFN exists in the form of NO. TFN concentration again lower at low temperatures, and it is within 40-65% TFN reduction range. At $T_1 = 1500$ K, the fast reburning stage proceeds in about 30-40 ms, much slower than at 1700 K (5 ms). The slower reactions of C-radicals cause more efficient first reburning stage: NO concentration decreases from 600 to 475 ppm and from 600 to 300 ppm at 1700 and 1500 K, respectively.

At higher reburn fuel injection rate (Figure 8.2.7, $SR_2 = 0.90$) most of NO is converted to NH_3 and HCN. Efficiency of TFN removal is 20-55%, and, in the contrary to the previous cases, TFN removal is more efficient at higher temperatures. Explanation of this effect is straightforward. At $SR_2 = 0.90$, the efficiency of NO removal continues to increase, as seen in Figure 8.2.7, and NO level is smaller at low temperatures. However, concentrations of NH_3 and HCN are much higher
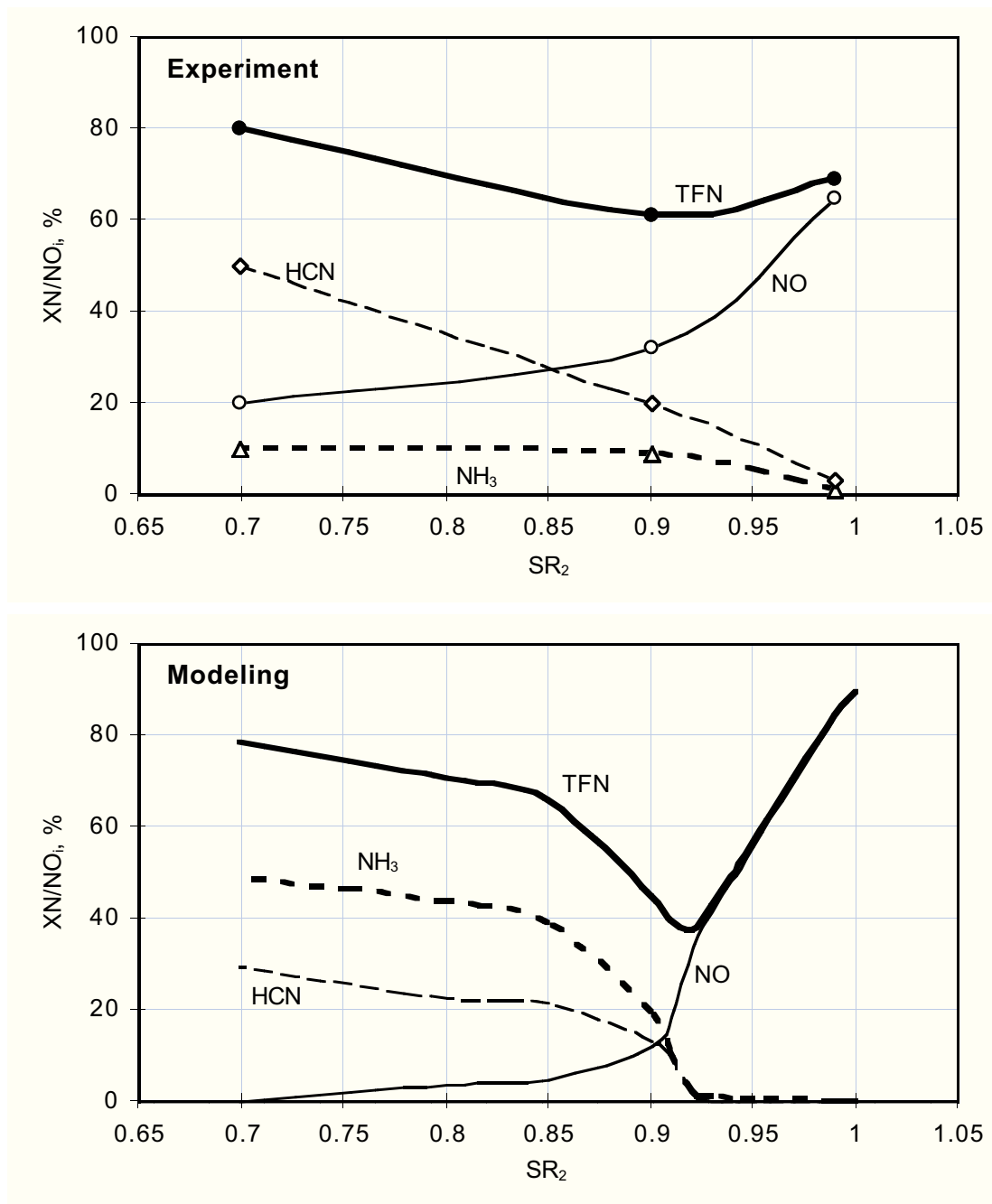
Figure 8.2.6. Modeling and experimental data on concentrations of NO, NH_3, HCN, and TFN in the reburning zone (t = 0.5 s) at T_1 = 1700 K for different concentrations of reburning fuel, SR_2.
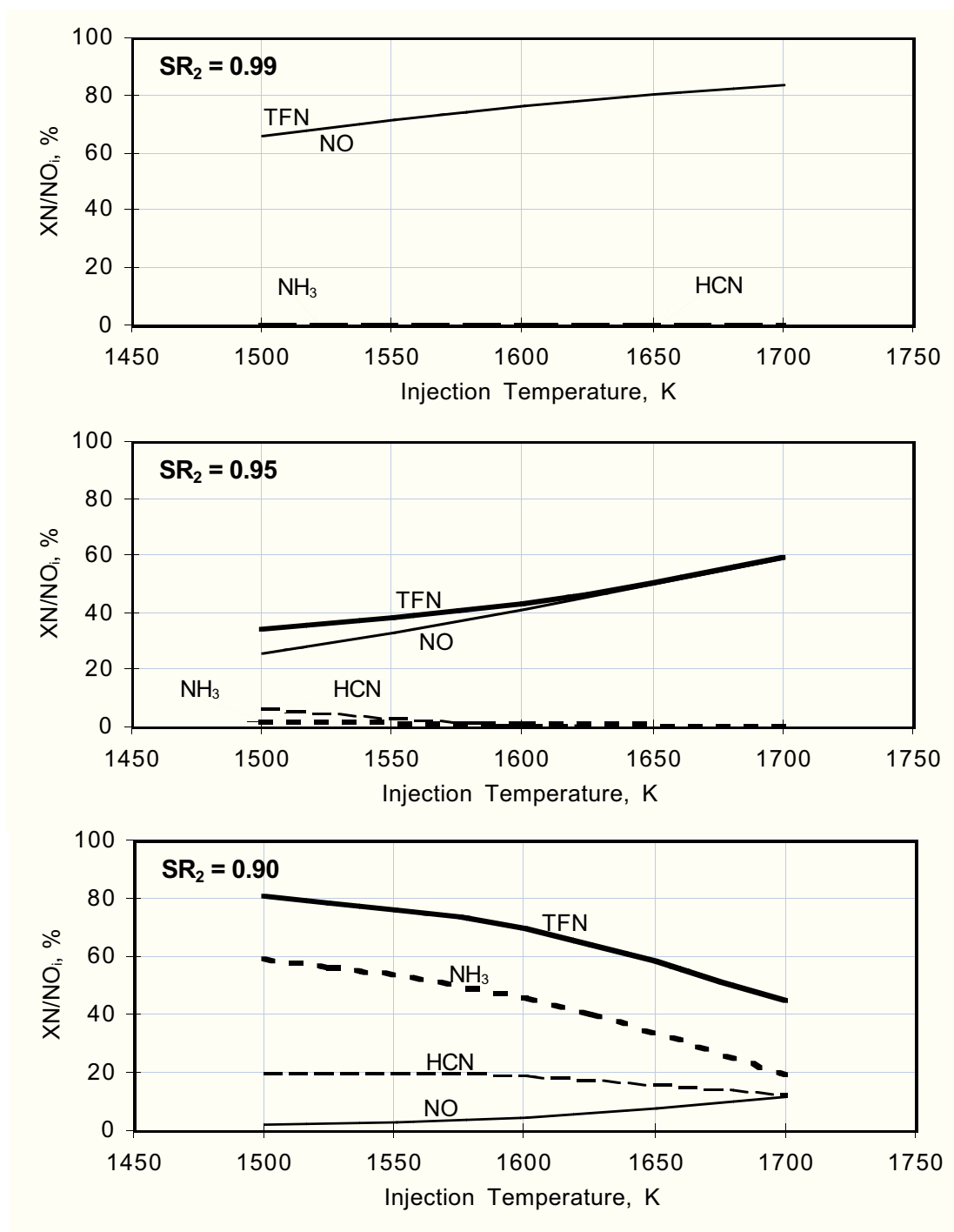
Figure 8.2.7. Modeling data on concentrations of NO, NH_3, HCN, and TFN in the reburning zone ($t = 0.5$ s) at $T_1 = 1500$-1700 K for different concentrations of reburning fuel, SR_2.

than NO, and they decrease at higher temperatures since they react faster. Therefore, TFN decreases at T = 1700 K.

Thus, modeling shows that at higher reburn fuel mass flow rates (SR_2 at about 0.90), higher temperatures results in higher efficiency of TFN removal. At lower injection rates ($SR_2 = 0.950.99$), reburning efficiency is higher at lower temperatures.

Sensitivity Analysis at $SR_2=0.99$. Sensitivity analysis was performed for reburn fuel injection at 1700 K, for $SR_2=0.99$ and 0.90, to better understand the important reactions for these conditions. The following is a summary of the reburn zone analysis. A more detailed analysis appears in Zamansky et al. (1997a). Results for $SR_2=0.99$ will be addressed first, followed by those for $SR_2=0.90$.

The kinetic curves for $SR_2=0.99$ are presented in Figure 8.2.1. As previously discussed, there are two regions of NO reduction: the initial fast decrease (from 600 to 540 ppm) which lasts for a very short period of time (about 2-3 ms), followed by a slow decrease (to 502 ppm). Figures 8.2.8 and 8.2.9 present reactions which contribute to NO reduction during the fast and slow NO reduction regions, respectively. (In these and other plots which follow, some curve labels overlap near the y-axis. Note that the reactions of interest are those with large positive or negative contribution or sensitivity factors; it is not important to read values close to the axis.) The most important steps of NO reduction in the fast region (Figure 8.2.8) are reactions (273) and (248):

$$HCCO + NO = HCNO + CO \qquad\qquad (273)$$
$$CH_2 + NO = H + HNCO \qquad\qquad (248)$$

Simultaneously, some HNO and NO_2 are formed which can contribute to both NO formation

$$H + NO + M = HNO + M \qquad\qquad (-211)$$
$$HNO + H = H_2 + NO \qquad\qquad (213)$$
$$HNO + OH = NO + H_2O \qquad\qquad (214)$$
$$NO_2 + H = NO + OH \qquad\qquad (188)$$

and NO reduction via reaction (211) and (186):

$$NO + O + M = NO_2 + M \qquad\qquad (186)$$

Figure 8.2.8. NO contribution factors at $SR_2 = 0.99$ in the fast NO decrease region.

273	HCCO+NO<=>HCNO+CO	249	CH2+NO<=>OH+HCN
248	CH2+NO<=>H+HNCO	179	N+OH<=>NO+H
211	H+NO+M<=>HNO+M	254	CH3+NO<=>HCN+H2O
213	HNO+H<=>H2+NO	185	HO2+NO<=>NO2+OH
214	HNO+OH<=>NO+H2O	250	CH2+NO<=>H+HCNO
188	NO2+H<=>NO+OH	198	NH+NO<=>N2O+H
186	NO+O+M<=>NO2+M	245	CH+NO<=>HCN+O
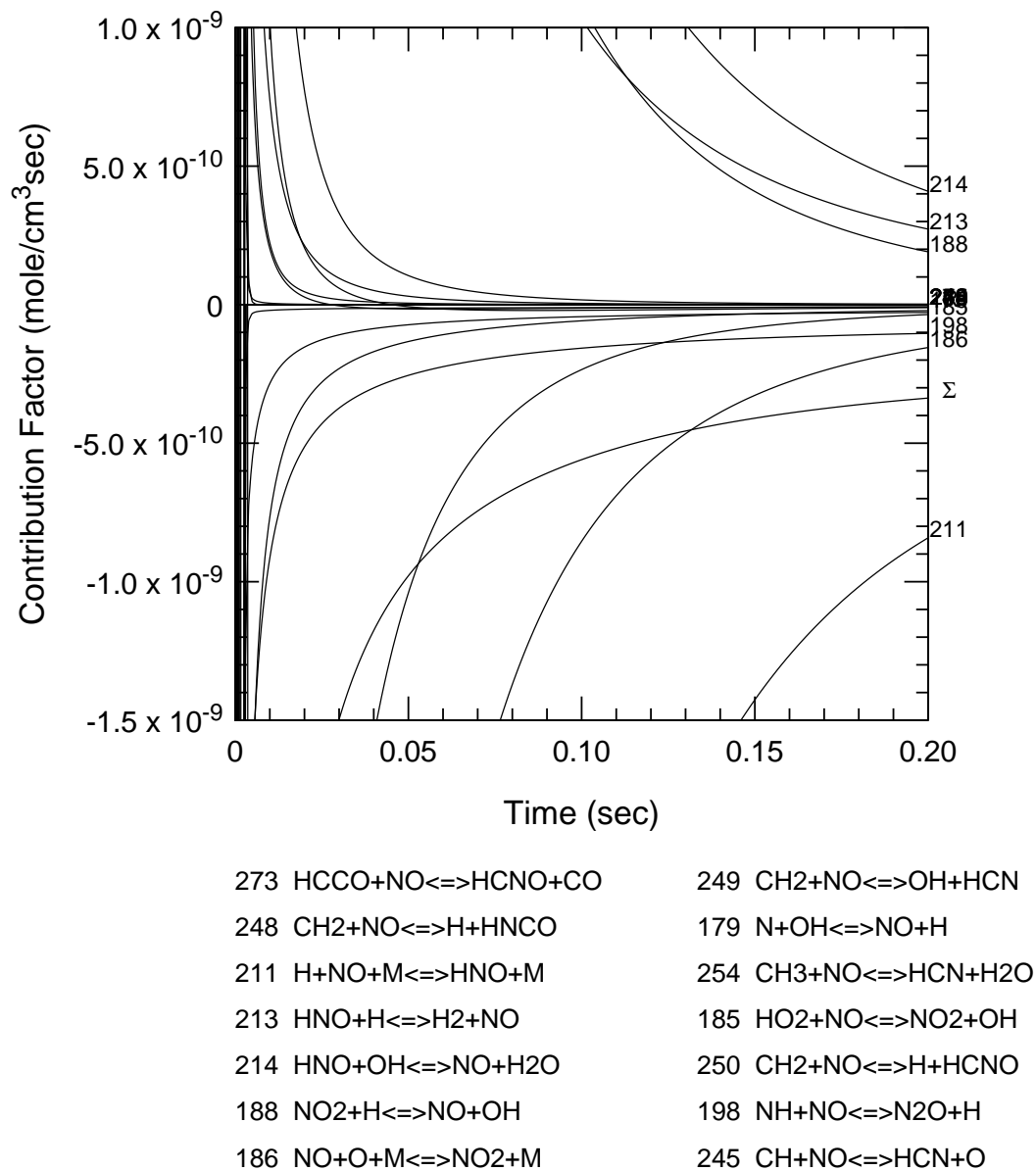
Figure 8.2.9 NO contribution factors at $SR_2 = 0.99$ in the slow NO decrease region.

273 HCCO+NO<=>HCNO+CO	249 CH2+NO<=>OH+HCN
248 CH2+NO<=>H+HNCO	179 N+OH<=>NO+H
211 H+NO+M<=>HNO+M	254 CH3+NO<=>HCN+H2O
213 HNO+H<=>H2+NO	185 HO2+NO<=>NO2+OH
214 HNO+OH<=>NO+H2O	250 CH2+NO<=>H+HCNO
188 NO2+H<=>NO+OH	198 NH+NO<=>N2O+H
186 NO+O+M<=>NO2+M	245 CH+NO<=>HCN+O

Reactions (211) and (186) are mainly responsible for the slow NO decrease as shown in Figure 8.2.9. The NO decrease is slow since these reactions compete with NO formation via (188), (213), and (214).

Figures 8.2.10 and 8.2.11 show sensitivity coefficients for NO formation and reduction in the reburning zone with $SR_2=0.99$ in the fast and slow NO reduction regions, respectively. Figure 8.2.10 clearly demonstrates that the chain branching steps

$$H + O_2 = O + OH \tag{38}$$
$$CH_3 + O_2 = O + CH_3O \tag{155}$$
$$2\,CH_3 = H + C_2H_5 \tag{159}$$

are responsible for the boost of radicals. In these reactions, each H atom and CH_3 radical forms several active species. Reaction (159) is also a chain branching step since C_2H_5 instantly decomposes into C_2H_4 and H. The increased radical pool generates carbon-containing radicals (HCCO and CH_2) which reduce NO via reactions (273) and (248).

Figure 8.2.11 shows that two reactions

$$N + NO = N_2 + O \tag{177}$$
$$\text{and} \quad NH + NO = N_2O + H \tag{198}$$

primarily contribute to NO removal in the slow region. Reaction (177) competes with reaction

$$N + OH = NO + H \tag{179}$$

Interestingly, the major chain branching step, reaction (38), behaves differently in the fast and slow reduction regions. In the fast region, this reaction supports formation of the radical pool and increases concentrations of carbon-containing radicals, such as HCCO, CH_2, etc. As a result, the radicals react with NO, and its concentration decreases. At a certain point, concentrations of carbon-containing radicals decrease since all methane is oxidized, and NO removal becomes slow. However, in this slow region, concentrations of N and NH are relatively high, and reactions (177) and (198) are responsible for NO reduction. The decrease of NO concentration is slow since reaction (38) results in an increase of the OH level that causes acceleration of NO formation via (179).

0.5

10
53
153
84

99
179
0

177
135

Sensitivity

-0.5
159
155

-1.0
38

0   0.05   0.10   0.15   0.20

Time (sec)
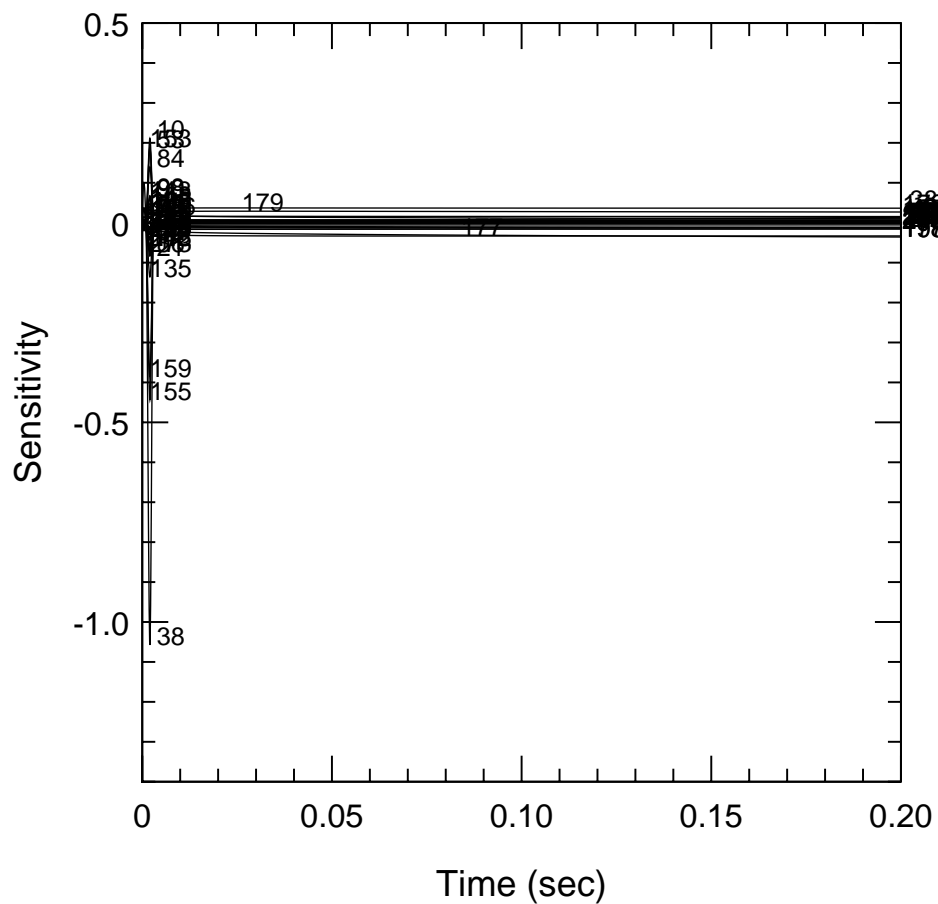
38 H+O2<=>O+OH	135 CH2+O2<=>OH+HCO
155 CH3+O2<=>O+CH3O	21 O+C2H2<=>H+HCCO
159 2CH3<=>H+C2H5	273 HCCO+NO<=>HCNO+CO
10 O+CH3<=>H+CH2O	86 2OH<=>O+H2O
153 CH2(S)+CO2<=>CO+CH2O	98 OH+CH4<=>CH3+H2O
53 H+CH4<=>CH3+H2	11 O+CH4<=>OH+CH3
84 OH+H2<=>H+H2O	99 OH+CO<=>H+CO2

Figure 8.2.10. NO sensitivity coefficients at SR_2=0.99 in the fast NO decrease region. Graph shows imporant reactions at early reaction times. Sensitivities for long reaction times (over lapping here) are shown in Figure 8.2.11.
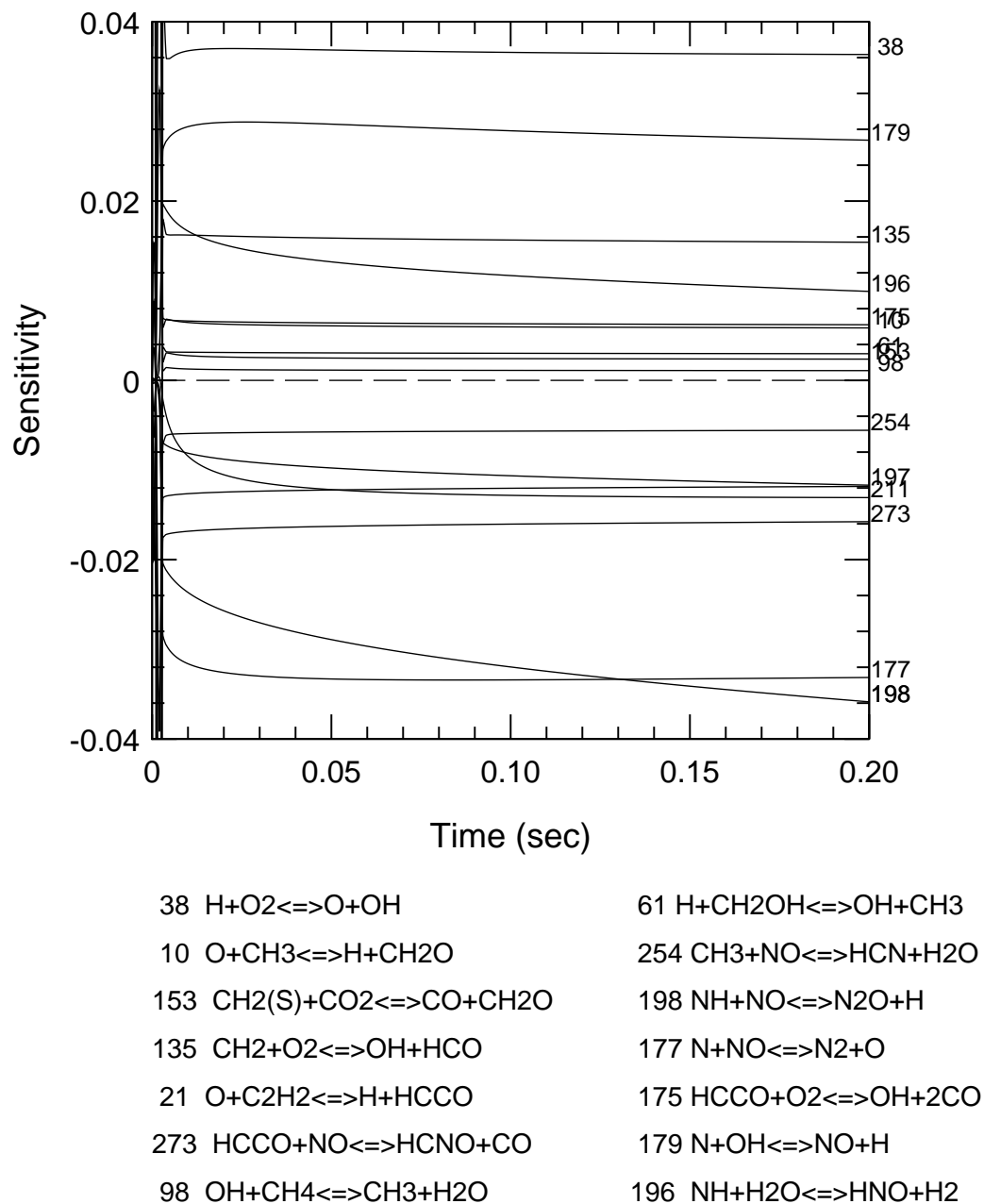
Figure 8.2.11. NO sensitivity coefficients at SR_2=0.99 in the slow NO decrease region.

38 H+O2<=>O+OH

61 H+CH2OH<=>OH+CH3

10 O+CH3<=>H+CH2O

254 CH3+NO<=>HCN+H2O

153 CH2(S)+CO2<=>CO+CH2O

198 NH+NO<=>N2O+H

135 CH2+O2<=>OH+HCO

177 N+NO<=>N2+O

21 O+C2H2<=>H+HCCO

175 HCCO+O2<=>OH+2CO

273 HCCO+NO<=>HCNO+CO

179 N+OH<=>NO+H

98 OH+CH4<=>CH3+H2O

196 NH+H2O<=>HNO+H2

Sensitivity Analysis at SR$_2$=0.90. The kinetic curves for SR$_2$=0.90 are presented in Figure 8.2.3. In this case, the NO concentration decreases from 600 to 160 ppm, and then slowly to 67 ppm. At t=0.5 s, the mixture contains 75 ppm HCN and 115 ppm NH$_3$. Methane is even more rapidly converted to CO and H$_2$. Again there are two steps of NO reduction: the fast short and slow long regions.

Figures 8.2.12 and 8.2.13 show NO contribution coefficients for the fast and slow NO reduction regions, respectively, at SR$_2$=0.90. The same as at SR$_2$=0.99, the most important step of NO reduction in the fast region (Figure 8.2.12) is reaction (273). Reactions (248) and:

$$CH_3 + NO = HCN + H_2O \hspace{4cm} (254)$$

are less important, and some NO is formed from HNO via (-211).

At longer reaction times (Figure 8.2.13), reaction (281) is of primary importance for NO reduction
$$NH_2 + NO = N_2 + H_2O \hspace{4cm} (281)$$

followed by reactions (254) and (273). In this region, the NO is also formed from HNO (-211).

Sensitivity coefficients in the reburning zone at SR$_2$=0.90 in the fast NO reduction regions shows that chain branching reactions (38), (155), and (159) are primarily responsible for increasing the radical pool and initially reducing NO, the same as for SR$_2$=0.99.

In the slow region (Figure 8.2.14), there are many elementary processes which affect the NO concentration. The main NO reducing reactions include interaction of NO with NH$_2$ and HCCO radicals, via (281) and (273), and reaction (281) becomes increasingly important at longer times. Reaction

$$NH_2 + H = NH + H_2 \hspace{4cm} (201)$$
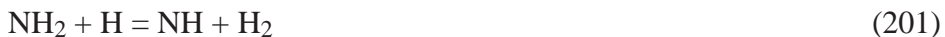
decreases the NH$_2$ concentration and consequently contributes to increasing NO.

Contribution and sensitivity factors have also been calculated at SR$_2$=0.90 for NH$_3$, HCN, and HNO. Contribution factors are dominated by transients occuring in about the first 10 ms. Reverse reactions

Figure 8.2.12. NO contribution factors at $SR_2 = 0.90$ in the fast NO decrease region.

273 HCCO+NO<=>HCNO+CO   250 CH2+NO<=>H+HCNO

211 H+NO+M<=>HNO+M   249 CH2+NO<=>OH+HCN

254 CH3+NO<=>HCN+H2O   281 NH2+NO<=>N2+H2O

248 CH2+NO<=>H+HNCO   198 NH+NO<=>N2O+H

188 NO2+H<=>NO+OH   214 HNO+OH<=>NO+H2O

213 HNO+H<=>H2+NO   R Remainder

185 HO2+NO<=>NO2+OH   Σ Summation
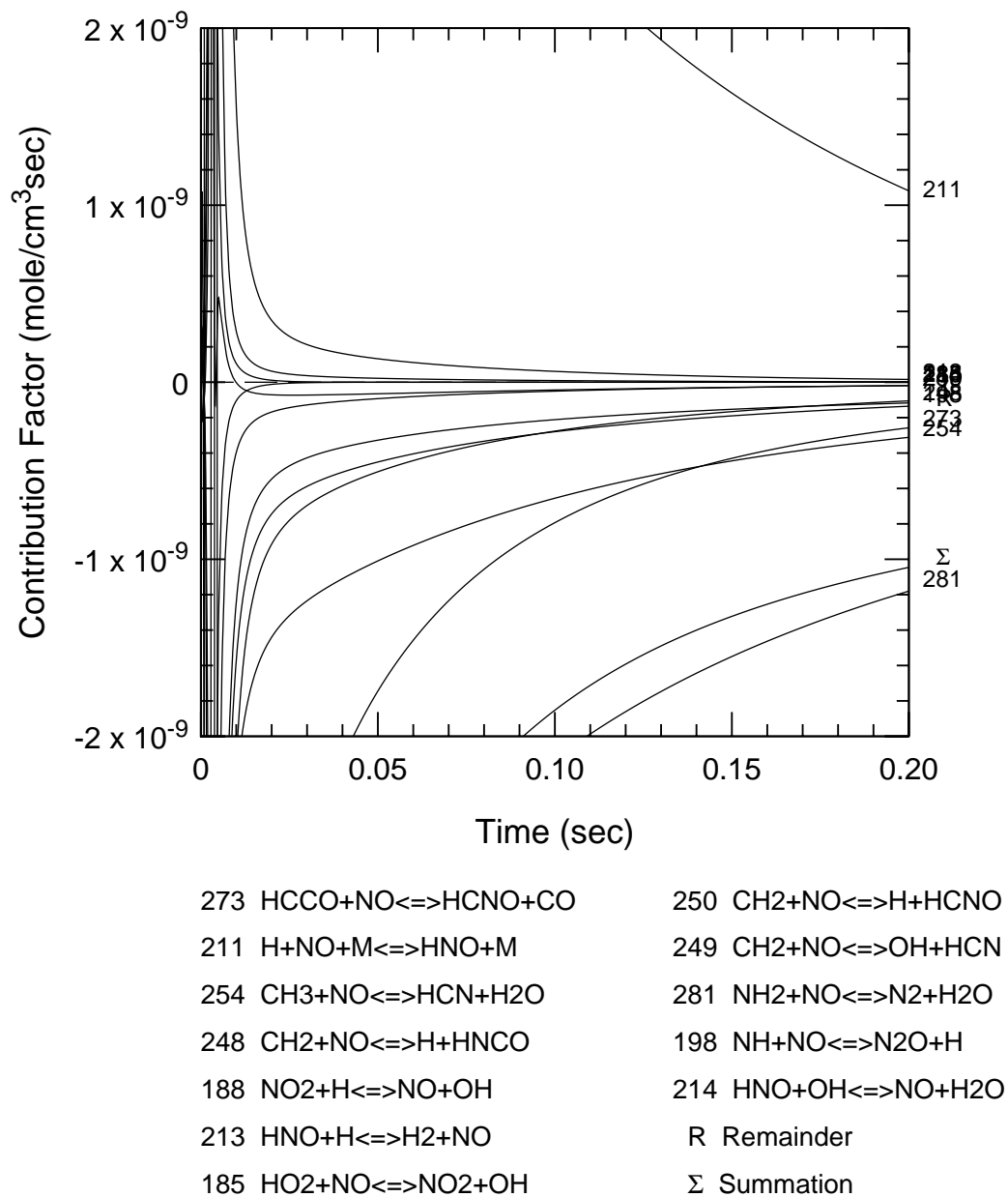
Figure 8.2.13. NO contribution factors at $SR_2 = 0.90$ in the slow NO decrease region.

273 HCCO+NO<=>HCNO+CO	250 CH2+NO<=>H+HCNO
211 H+NO+M<=>HNO+M	249 CH2+NO<=>OH+HCN
254 CH3+NO<=>HCN+H2O	281 NH2+NO<=>N2+H2O
248 CH2+NO<=>H+HNCO	198 NH+NO<=>N2O+H
188 NO2+H<=>NO+OH	214 HNO+OH<=>NO+H2O
213 HNO+H<=>H2+NO	R Remainder
185 HO2+NO<=>NO2+OH	Σ Summation
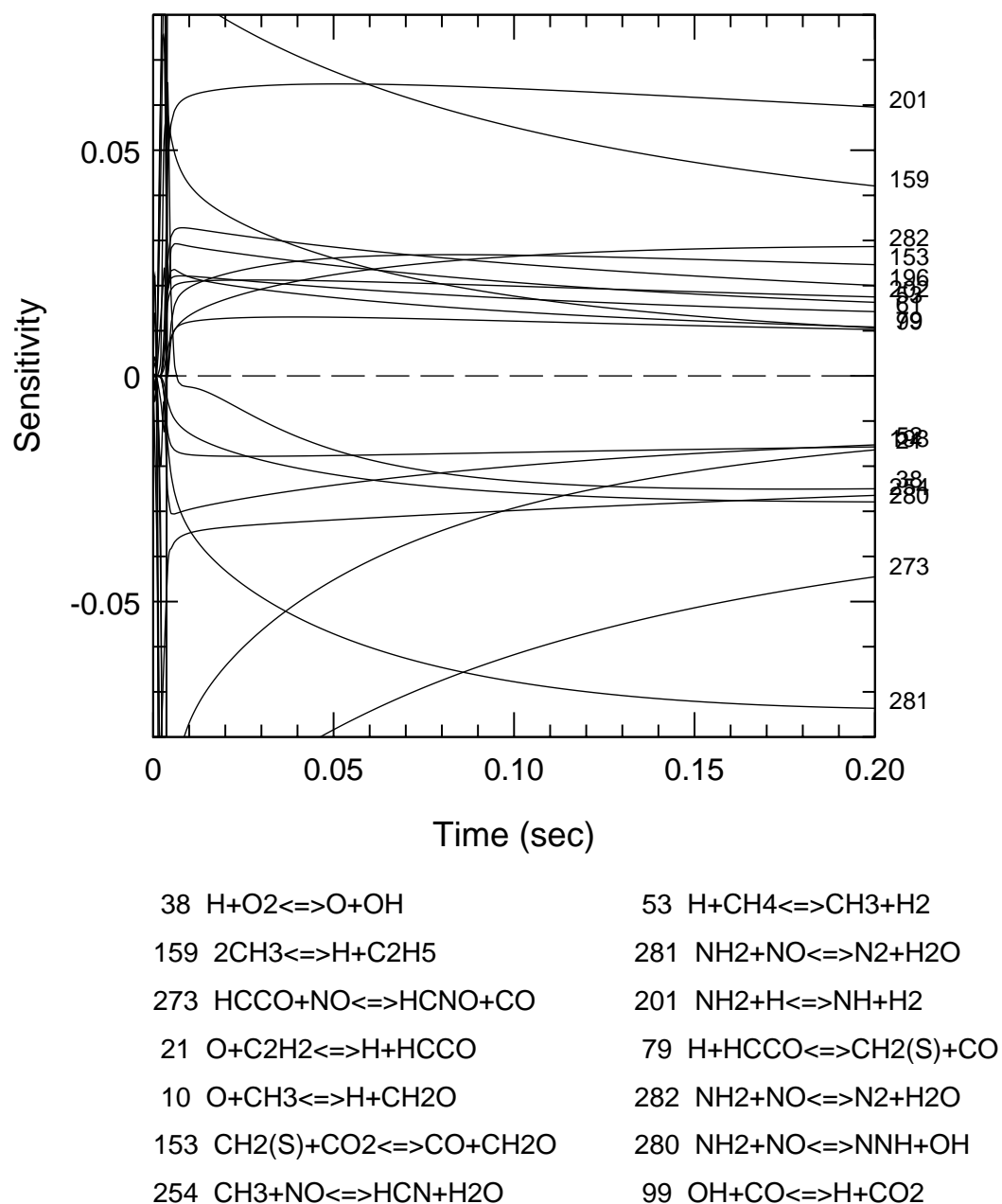
Figure 8.2.14. NO sensitivity coefficients at $SR_2=0.90$ in the slow NO decrease region.

38 H+O2<=>O+OH

159 2CH3<=>H+C2H5

273 HCCO+NO<=>HCNO+CO

21 O+C2H2<=>H+HCCO

10 O+CH3<=>H+CH2O

153 CH2(S)+CO2<=>CO+CH2O

254 CH3+NO<=>HCN+H2O

53 H+CH4<=>CH3+H2

281 NH2+NO<=>N2+H2O

201 NH2+H<=>NH+H2

79 H+HCCO<=>CH2(S)+CO

282 NH2+NO<=>N2+H2O

280 NH2+NO<=>NNH+OH

99 OH+CO<=>H+CO2

$$NH_3 + OH = NH_2 + H_2O \qquad\qquad (-277) \qquad \text{and}$$

$$NH_3 + H = NH_2 + H_2 \qquad\qquad (-276)$$

are important contributors to NH_3 formation. HCN is mainly formed via (254) and

$$HCNO + H = OH + HCN \qquad\qquad (270)$$

HNO radicals are important intermediate species in the fast reaction region. They are rapidly formed from NH

$$NH + H_2O = HNO + H_2 \qquad\qquad (196)$$

and decompose via reaction (211).

Sensitivity analysis for NH_3 at SR=0.90 show an initial fast transient where the same chain branching steps (38, 155, 159) which influence NO also result in a higher NH_2 level and a faster rate of NH_3 formation via reverse reactions (-276) and (-277). In the slow region, NH_3 removal is enhanced by reactions (159), (281), and

$$NH_2 + H = NH + H_2 \qquad\qquad (201).$$

The HCN concentration is initially increased due to reactions (254) and (38), and then reduced mainly due to reaction

$$HCN + OH = HOCN + H \qquad\qquad (233)$$

8.2.2 Injection of Ammonia into the Reburning Zone (AR-Rich)

When fuel is added into the reburning zone, the oxygen disappears very fast in the reaction with the fuel to form CO and H_2. If N-agents (ammonia, urea, etc.) are injected into the reburning zone, they form NH_i radicals (NH_2, NH, N) which are active in NO removal reactions. The NH_i radicals can react either with O_2 into NO or with NO into N_2. The NO reduction process is effective if the NH_i precursors (N-agents) appear in the gas mixture when concentration of oxygen has been significantly depleted by the reburning fuel, thus preventing oxidation of Nagents into NO. Calculated characteristic times for O_2 disappearance after reburn fuel injection are less than 0.01 s at 1700 K

and about 0.1 s at 1450 K. The delay time between reburn fuel injection and the formation of NH_i species should be close to these times for effective NO reduction.

Results of calculations which demonstrate the effect of the delayed ammonia injection on NO reduction by CH_4 reburning are presented in Figure 8.2.15. The first graph shows concentrations of NO, NH_3, HCN, and TFN after 0.5 s as a function of SR_2 for injection of 600 ppm NH_3 without delay, i.e. co-injection with the reburning fuel. At $SR_2 = 0.90$, ammonia co-injection causes a decrease in TFN from 1200 ppm (600 ppm NO and 600 ppm NH_3) to 327 ppm. At $SR_2 = 0.90$, the concentration of the reburning fuel is high, and its reaction with the oxygen forms a large radical pool. The radicals initiate a rapid reaction between NH_3 and NO, and the TFN concentration is depleted. This reaction requires a small amount of oxygen to support the radical pool, and this amount is available in the mixture during the first rapid reaction stage. The concentration of ammonia decreases slowly at $SR_2 = 0.90$ since most of the oxygen reacts with the high concentration of CH_4. Some CH_4 (about 400 ppm) remains unreacted in the reburning zone. At $SR_2 = 0.99$, all NH_3 and CH_4 are instantly oxidized since the concentration of O_2 is the same, but the $[CH_4]$ level is much lower. In this oxidation process, ammonia forms some additional NO, and this NO cannot be decreased in the reaction with ammonia since it is no longer present in the mixture. Therefore, TFN $= NO = 742$ ppm, i.e. the NO concentration increases.

The picture is completely different if ammonia is injected with a 0.1 s delay time, as shown in the second graph in Figure 8.2.15. In this case, at $SR_2 = 0.90$, ammonia is injected when the O_2 concentration is already very low (about 0.01 ppm). Concentration of NO is reduced in the first rapid reburning stage within the delay time of 0.1 s and it decreases further utilizing some ammonia. However, in 0.5 s the NH_3 concentration is still high, about 420 ppm, and it does not react rapidly with NO since there is no oxygen to feed the radical pool. At $SR_2 = 0.99$, NH_3 is injected when the O_2 concentration is about 50 ppm (see Figure 8.2.1) and the OH concentration is still high. Therefore, in the presence of this oxygen level, NH_3 and NO are capable of reacting with each other, and TFN concentration efficiently decreases. Thus, at the right conditions, delayed ammonia injection can result in more effective NO removal. These conditions require the presence of both reagents and some oxygen, and so is most effective under near-stoichiometric conditions.

Parametric Dependencies. The effect of the delayed ammonia injection depends on many factors, including the value of SR_2, the delay time, ammonia concentration, oxygen concentration, etc. Figure 8.2.16 presents concentrations of fuel-N species in the reburning zone at $SR_2 = 0.99$ as a function of ammonia injection delay time. If ammonia is injected along with the reburning fuel, it rapidly disappears in the reaction with the high amount of oxygen and causes some NO formation.
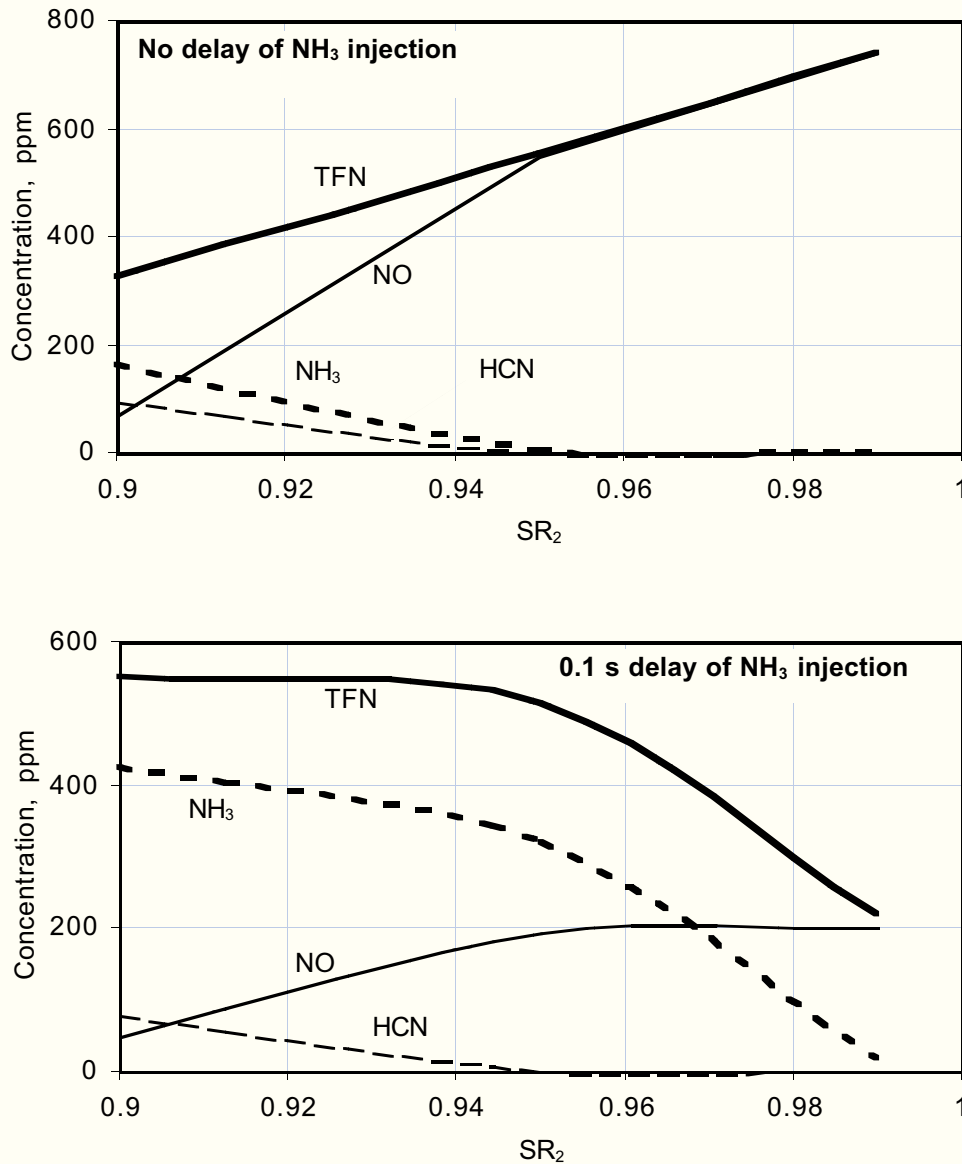
Figure 8.2.15. Effect of ammonia co-injection with the reburning fuel and 0.1 s delayed NH_3 injection on fuel-N species in the reburning zone. $[NH_3] = 600$ ppm, $NO_i = 600$ ppm, $T_1 = 1700$ K.

As previously discussed, the initial stage of reburning is fast and forms high concentrations of radicals. Therefore, injection of ammonia with a short delay time results in NH_3-O_2 interaction in the presence of the radicals and small amounts of oxygen. This interaction efficiently reduces concentrations of NO and TFN. If ammonia is injected with a longer delay time, NH_3 and NO interact with lower radical (and O_2) concentrations, and so the efficiency of NO and TFN removal is lower.
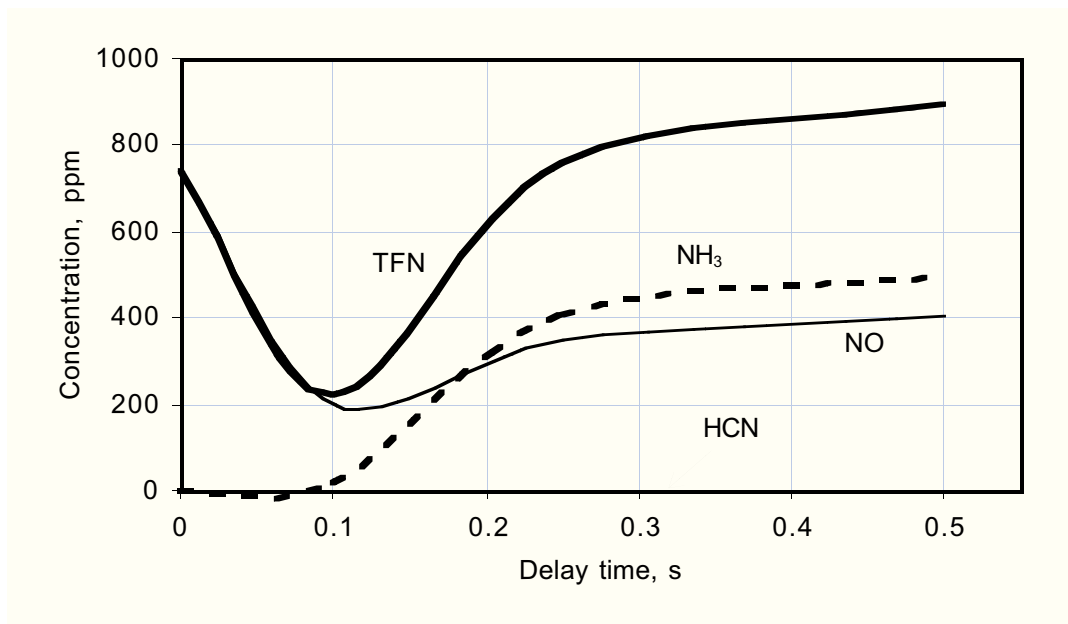
Figure 8.2.16. Effect of the delay time of NH_3 injection into the reburning zone at $SR_2 = 0.99$. Other conditions are the same as in Figure 8.2.15.

Figure 8.2.17 shows the dependence of NO and TFN on the quantity of NH_3 injected with a 0.1 s delay time at $SR_2 = 0.99$. As injected $[NH_3]$ increases, the resulting NO concentration decreases, but the residual $[NH_3]$ increases. The TFN concentration has a minimum which approximately corresponds to equimolecular amounts of NO and NH_3 in the gas mixture (NSR = 1.0 - 1.3).
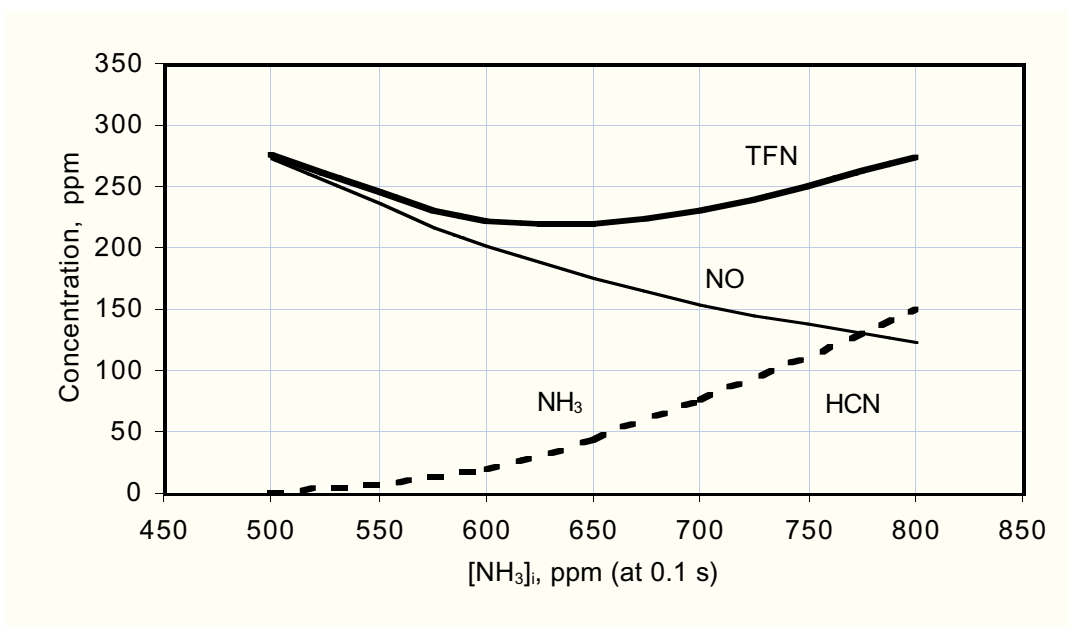
Figure 8.2.17. Effect of the NH_3 concentration injected into the reburning zone at $SR_2 = 0.99$ and 0.1 s delay time. Other conditions are the same as in Figure 8.2.15.

Although the concentrations in the reburn zone are presented here, post-burnout concentrations remain consistent with this observation. Zamansky (1996b) includes further discussion and comparison of the concentration histories for different ammonia injection scenarios.

Sensitivity Analysis. Figure 8.2.18 shows kinetic curves of major components for injection of 800 ppm ammonia with the reburning fuel at $SR_2=0.99$ and $T_1=1700$ K. The predictions are similar to those for reburning without ammonia injection (Figure 8.2.1) except that NO concentration jumps from 600 to about 900 ppm and then slowly decreases to 800 ppm. Thus, part of the ammonia is converted to molecular nitrogen and another part to NO. Figure 8.2.19 presents NO contribution factors for the first 10 ms at these conditions. Reaction (211) is primarily responsible for the NO decrease, but the NO is formed via reaction (213) and to lesser extent via (214) and (188). Sensitivity analysis shows that as for reburning without N-agent (Figure 8.2.11), reaction (38) accelerates NO formation by increasing the radical pool. Reactions of NH_i radicals with NO ((198), (281), and (177)) decrease the NO level. The most notable difference from conventional reburning is the increased importance of reaction 281, which involves NH_2, compared to those involving NH and N.

Figure 8.2.20 shows the concentration curves for the same conditions as in Figure 8.2.18, but with the 800 ppm NH_3 injected with a 0.1 s delay after the reburning fuel. This delay dramatically changed the NO concentration as well as concentrations of other species. NO was reduced to slightly above 100 ppm and about 150 ppm NH_3 is present in the mixture at t=0.5 s. Significant amounts of HNCO and O_2 are present at t=0.5 s. Figure 8.2.21 shows the main reactions contributing to NO formation and reduction in the first 0.10 s under these conditions. Reactions (281) and (282) represent one elementary step which was formally written as two reactions in the mechanism. The code calculated the sum of these reactions which result in NO reduction. Another important NO reducing step is the reaction

$$NH_2 + NO = NNH + OH \hspace{4cm} (280)$$

NO formation is largely via reaction (-211). Figure 8.2.22 presents NO sensitivity coefficients which also demonstrate the importance of the sum (281+282). Interestingly, this reaction reduces NO at early reaction stages (t<0.03 s), then increases the NO concentration at about 0.04-0.16 s, and finally reduces NO again. The reason for this "strange" behavior is that reaction (280) includes the same reagents, NH_2 and NO, and it is a single process which is mainly responsible for NO reduction under these conditions. Indeed, though reaction (281+282) forms molecular nitrogen from NO, it removes the NH_2 radical from the reaction media thus decreasing the radical pool.

48 N2	5 OH
6 H2O	2 H
16 CO2	36 NO
4 O2	34 NH3
14 CH4	3 O
15 CO	41 HCN
1 H2	46 HNCO
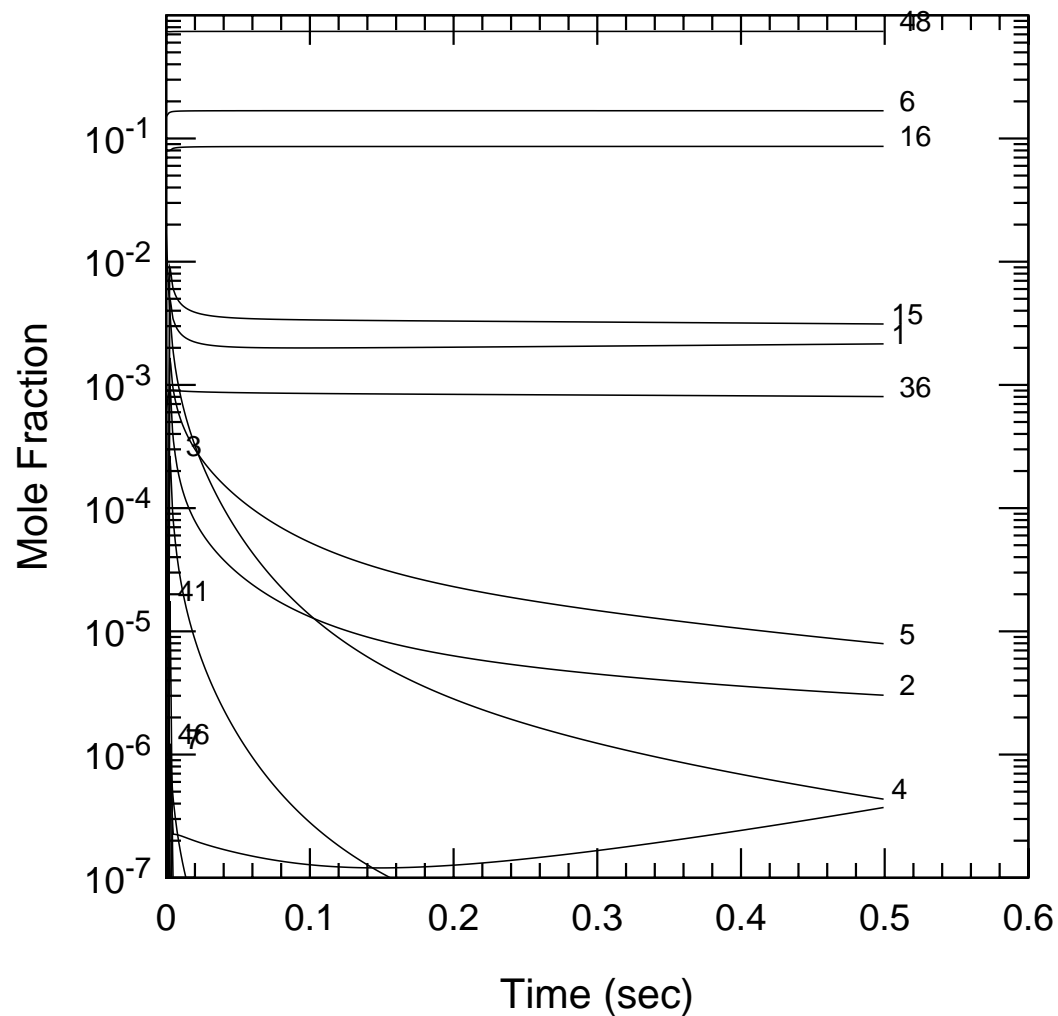
Figure 8.2.18. Kinetic curves of species in the reburning zone at $SR_2 = 0.99$ for injection of 800 ppm ammonia along with the reburning fuel at 1700 K.

Figure 8.2.19. NO contribution factors for conditions of Figure 8.2.18.
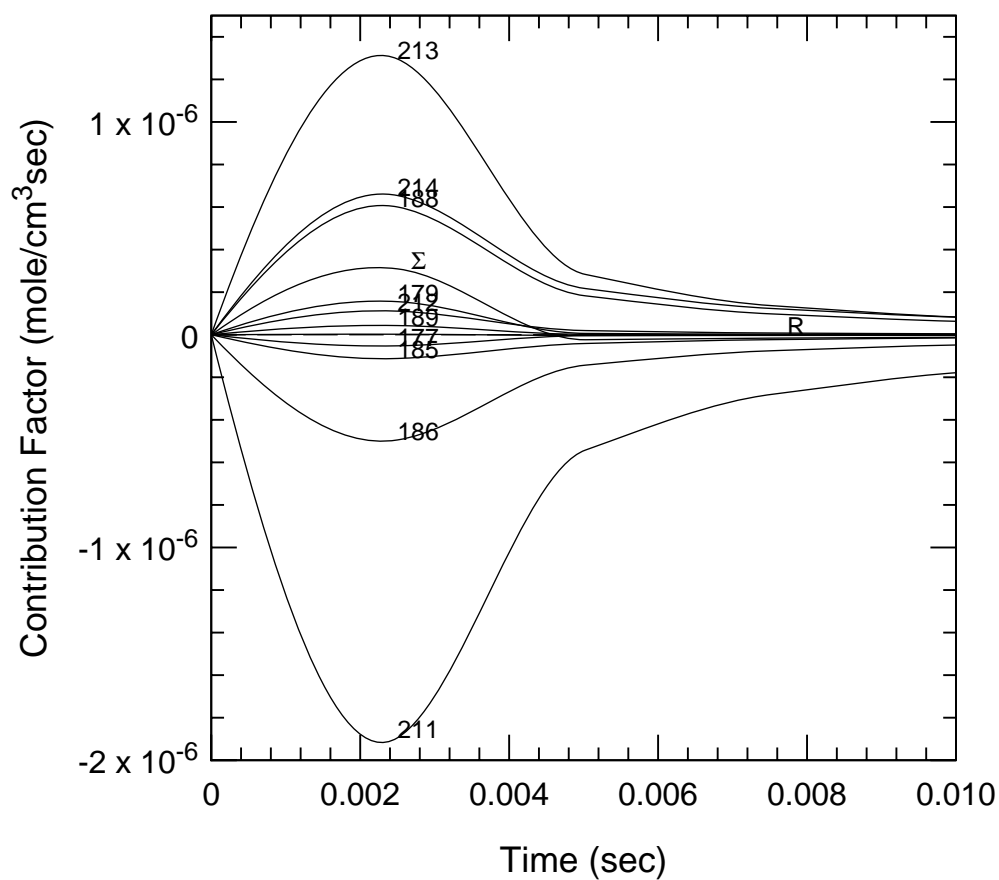
211 H+NO+M<=>HNO+M   212 HNO+O<=>NO+OH

213 HNO+H<=>H2+NO   177 N+NO<=>N2+O

214 HNO+OH<=>NO+H2O   189 NH+O<=>NO+H

188 NO2+H<=>NO+OH   R   Remainder

186 NO+O+M<=>NO2+M   Σ Summation

179 N+OH<=>NO+H

185 HO2+NO<=>NO2+OH
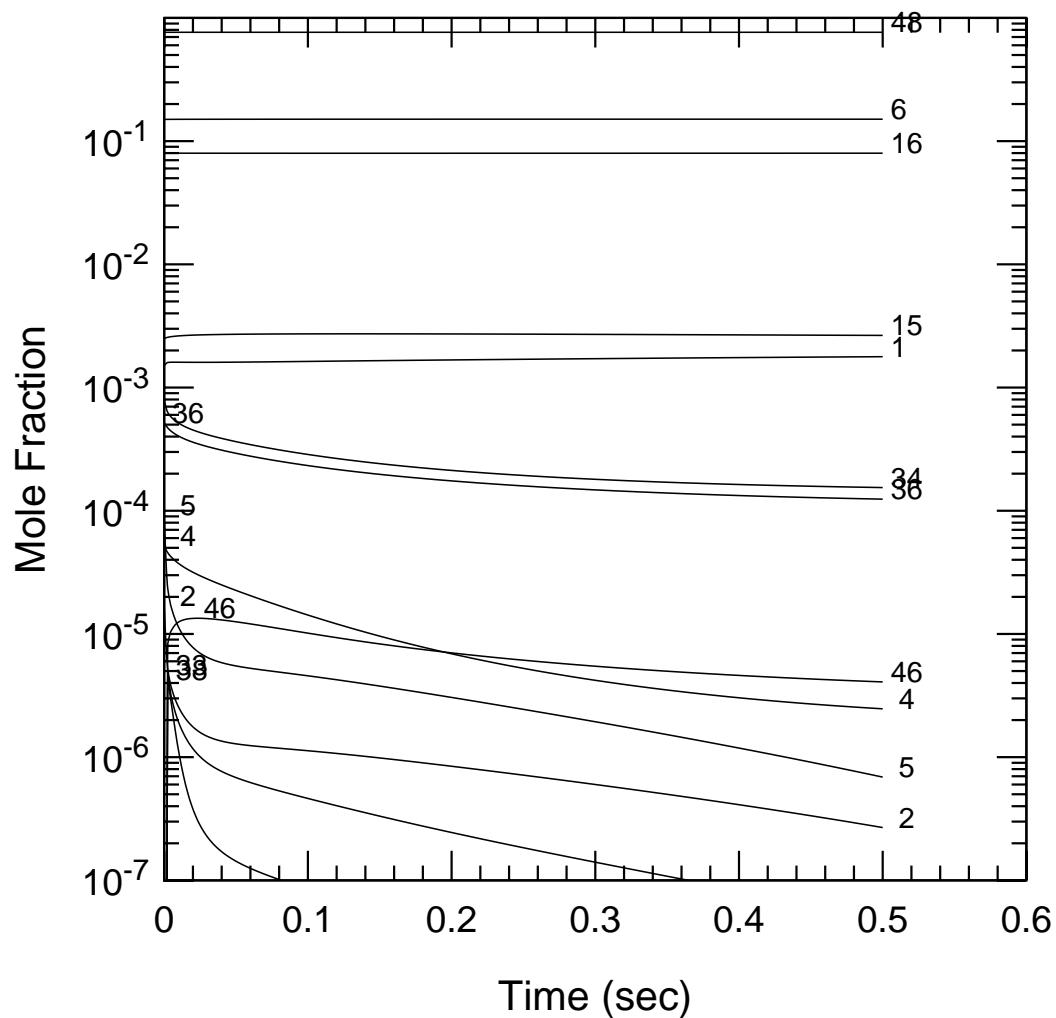
Figure 8.2.20. Kinetic curves of species in the reburning zone at $SR_2 = 0.99$ for injection of 800 ppm ammonia with a 0.1 s delay after the reburning fuel injected at 1700 K.

Figure 8.2.21. NO contribution factors for conditions of Figure 8.2.20.

Figure 8.2.22. NO sensitivity coefficients for conditions of Figure 8.2.20.
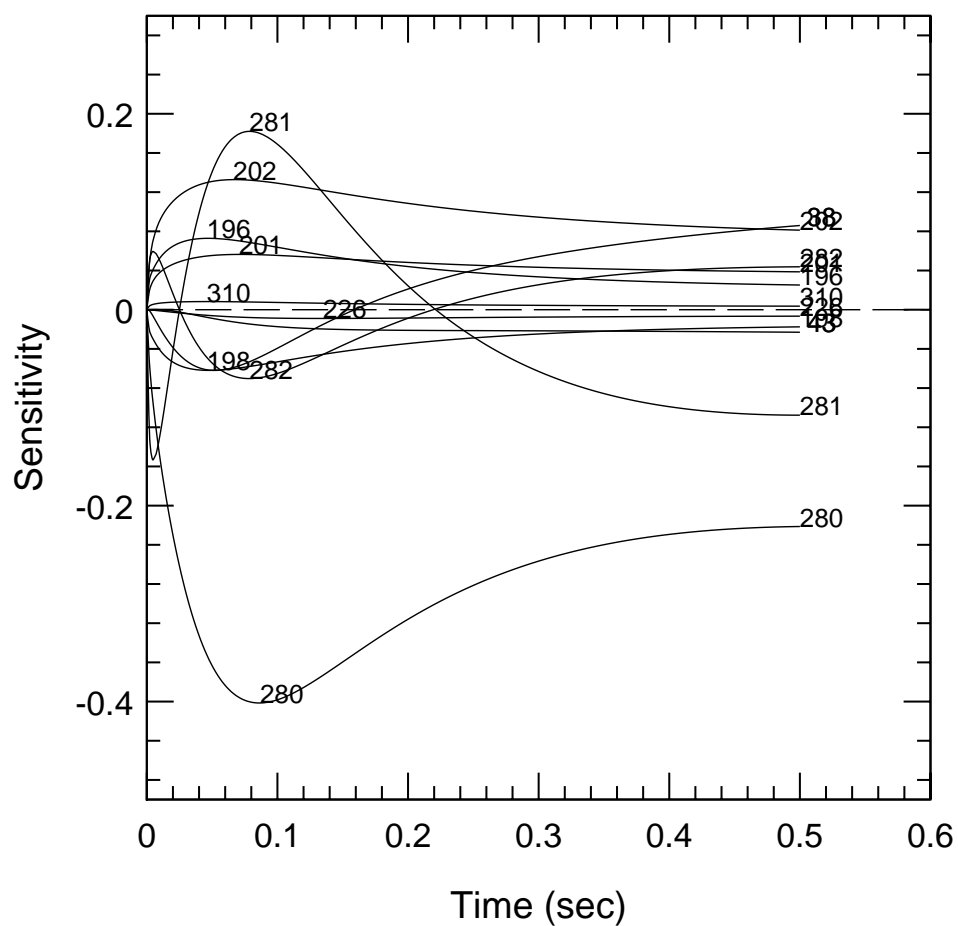
280 NH2+NO<=>NNH+OH   201 NH2+H<=>NH+H2

281 NH2+NO<=>N2+H2O   43 H+OH+M<=>H2O+M

202 NH2+OH<=>NH+H2O   226 NCO+M<=>N+CO+M

 38 H+O2<=>O+OH   310 2NH2<=>NH+NH3

196 NH+H2O<=>HNO+H2

282 NH2+NO<=>N2+H2O

198 NH+NO<=>N2O+H

Reaction (280) also removes NO and one NH_2 radical, but it forms NNH radical which is unstable and decomposes with returning active species (H atoms) via reactions

$$NNH = N_2 + H \tag{203}$$
$$NNH + M = N_2 + H + M \tag{204}.$$

8.2.3 Promotion of the NO-NH$_3$ Interaction in the Reburning Zone

Consideration of the kinetic curves of the reburning process (Figures 8.2.1 to 8.2.3) demonstrates that after the initial fast reaction stage, concentrations of main components in the reburning zone (CO, H_2 and NO at $SR_2 = 0.99$-0.95 and CO, H_2, CH_4, HCN, NH_3, NO at $SR_2 = 0.90$) remain almost constant, and, simultaneously, concentrations of radicals (OH and H) and O_2 decrease. The goal of modeling is to find conditions under which NO and TFN concentrations will further decrease in the reburning zone. As previously discussed, delayed injection of ammonia can reduce NO and TFN concentrations under certain conditions. The effectiveness of the NO-NH$_3$ interaction in the reburning zone can be further improved in the presence of promoters. The influence of different promoter species on NO/TFN removal is analyzed in the following. The initial analysis focuses on the effect of boosting the concentration of specific species upon NO. In some cases (e.g. radicals) direct injection of the species is not intended. Rather, the goal is to find target species whose increase is beneficial; the next step is to find injectable species which will have the desired effect.

The analysis focuses on the later part of the reburning zone in which NO reduction is relatively slow. Parameters affecting the NO/TFN level are varied to find optimum conditions of NO/TFN removal. These parameters include the stoichiometric ratio in the reburning zone (SR_2); reburn fuel injection temperature (T_1); concentrations of ammonia, oxygen, radicals, and other compounds capable of promoting the NO-NH$_3$ interaction. It is clear that the influence of ammonia is different at various values of SR_2. Variation of process parameters was performed for $SR_2 = 0.99$ and 0.90 at a constant temperature gradient of 300 K/s. For all conditions, concentrations are shown at a reaction time of 1 s, for injection with 0.1 s delay after reburn fuel injection. This injection point is after the fast reaction stage, at which point all CH_4 was consumed, and concentrations of CO, H_2 and NO stabilized on a certain level. The composition at $SR_2 = 0.99$ and at the NH$_3$/promoter injection point (mixture I) is:

500 ppm NO - 0.16% H_2 - 0.23% CO - 8% CO_2 - 15% H_2O - balance N_2.

The effect of ammonia addition alone to mixture I is shown in Figure 8.2.23. Without NH_3 injection (the upper graph), NO is slightly reduced at lower temperatures. Injections of 500 and 800 ppm NH_3 cause an increase in TFN at lower temperatures and significant NO/TFN reduction at higher temperatures.

Performance of candidate promoter species was modeled by co-injection with ammonia in different amounts into mixture I at 1600 K. Figure 8.2.24 compares effect of different additives: O_2, OH, H, O, O_2+OH, and O_2+H_2O_2. Different promoters show different degrees of TFN removal, some with a clear optimum.

Carbon-containing compounds can also provide radicals which promote the NO-NH_3 interaction in the reburning zone. Effect of different potential promoters on concentrations of NO, NH_3 and TFN is shown in Figure 8.2.25. This graph compares the effect of 500 ppm NH_3 injection into mixture I at 1600 K with co-injection of 100 ppm promoter: oxygen, methanol, methane, ethylene or ethane. Of the hydrocarbons considered, only ethane results in much TFN reduction beyond the original NO level. This screening of hydrocarbon promoters does not reveal a significant performance benefit.

Of the promoters considered in figures 8.2.24 and 8.2.25, the best performance is shown for O_2 injection. Oxygen participates in formation of different radicals via reactions with CO, H_2 and NH_3, shows better or about the same performance as the other additives tested. The next section will discuss the effect of oxygen in some additional detail.

All promotive additives presented so far were co-injected with ammonia and appeared instantly in the gas phase. However, under real conditions, the promoter species may be formed in the mixture with a certain rate constant. As has been proven by Zamansky and Borisov, 1992, the rate of promoter formation may be optimum, i.e. formation of promoters with a certain optimum rate constant results in maximum promotion effect. It was assumed for modeling that a hypothetic promoter X dissociates with formation of radicals or oxygen in the gas mixture. The following reaction was added to the mechanism:

$$X + M => OH + H + M \quad \text{or}$$
$$X + M => O_2 + M.$$
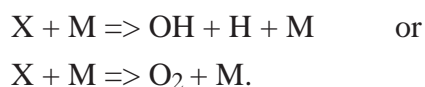
These equations simulate fast interaction of the hypothetic promoter X with water molecules or other species in flue gas with formation of OH, H, and O_2. The initial concentration of X was
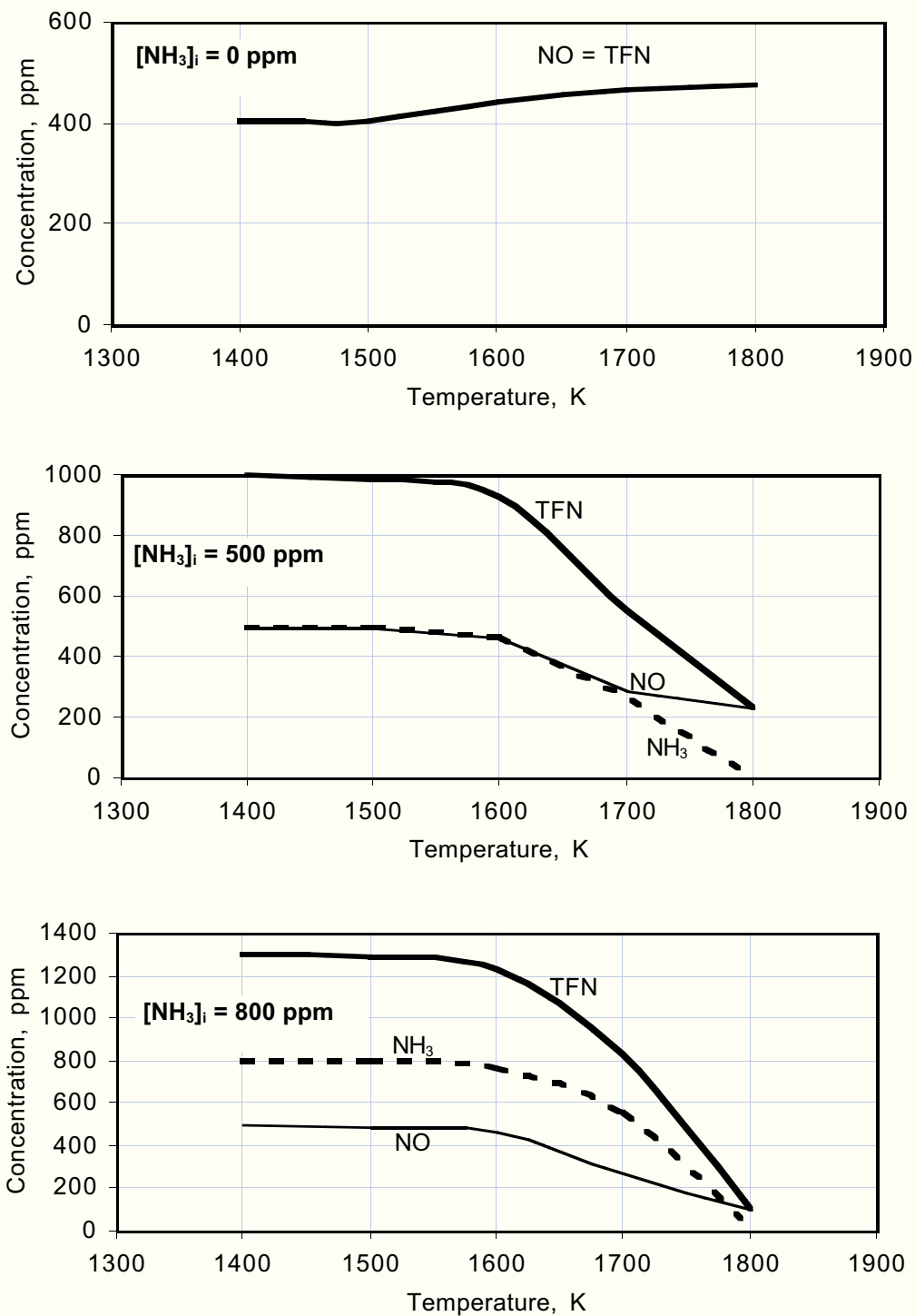
Figure 8.2.23. Effect of NH_3 injection temperature and NH_3 concentration in mixture I on NO/ TFN reduction.
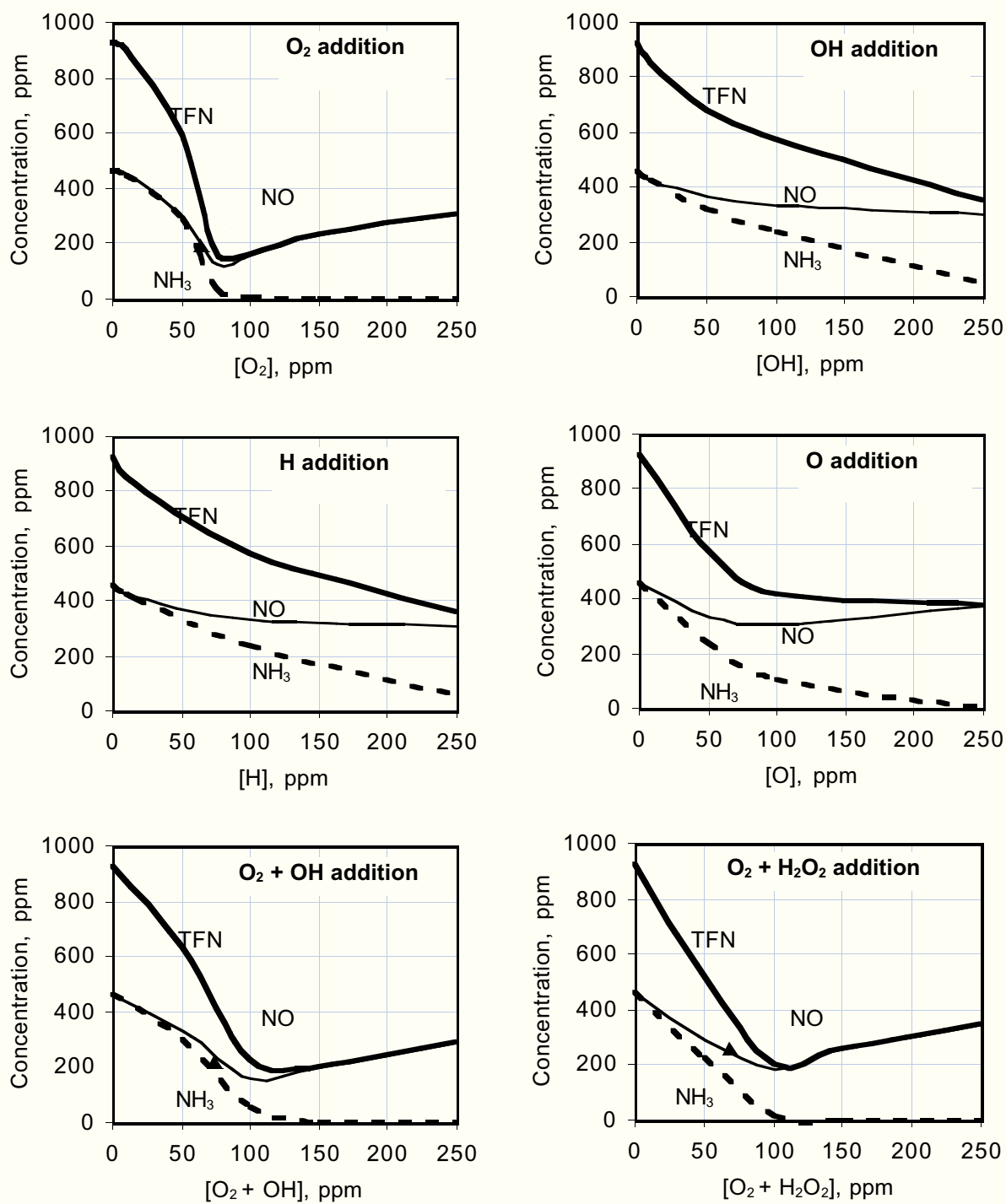
Figure 8.2.24. Effect of radicals co-injection with 500 ppm NH$_3$ into mixture I, T$_2$ = 1600 K.
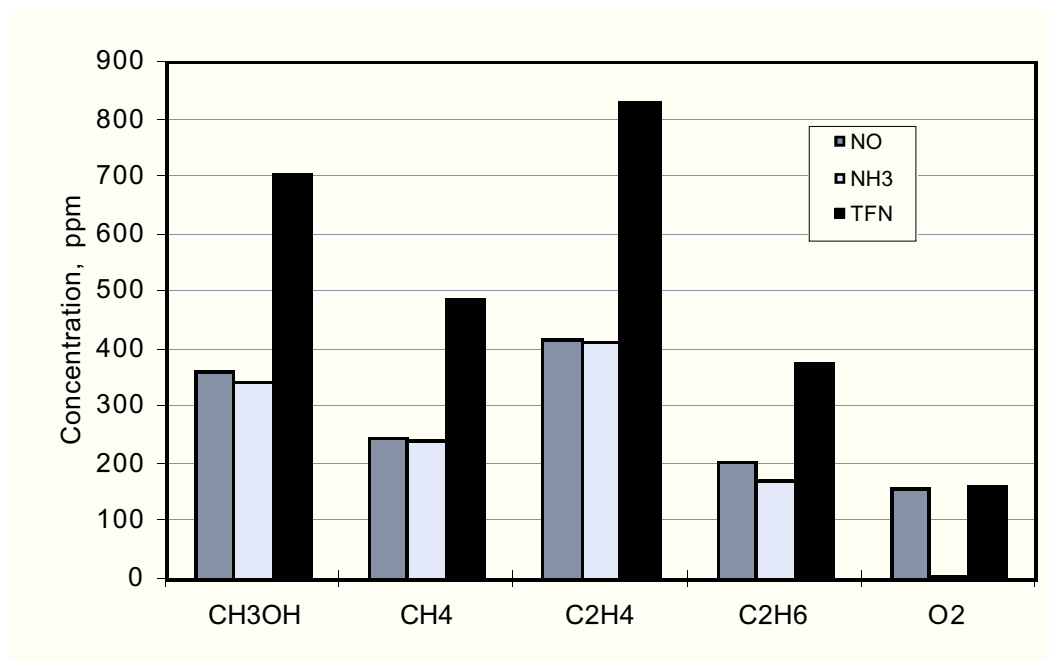
Figure 8.2.25. Comparison of the promotion effect of different compounds. The promoter (100 ppm) is co-injected with 500 ppm NH_3 into mixture I at $T_1 = 1600$ K and $SR_2 = 0.99$.

assumed to be 50 ppm in modeling. The rate constant for X decomposition was selected in the Arrhenius form

$$k = A \cdot \exp(-20,000/T) \text{ cm}^3/\text{mol·s}$$

where the predexponential factor A was varied in the range from 10^9 to 10^{13}. These values of the rate constant provided formation of radicals and O_2 with characteristic times between approximately 0.1 and 100 s.

Figure 8.2.26 compares the results of modeling NO, NH_3 and TFN concentrations at different values of the factor A (i.e. depending on the rate of active species formation in the mixture) for three different cases: formation of OH+H radicals, formation of O_2, and formation of the OH/H radicals with co-injection of NH_3 and 75 ppm O_2. In a wide range of the promoter decomposition rate, NO and TFN concentrations are substantially lower than their values without promoter. In all cases, an optimum rate constant exists which results in minimum TFN concentration. The optimum factor A is in the range logA = 10.5-12.0. Oxygen formation and co-injection present the most attractive cases because the TFN minimum is lower.

8-46
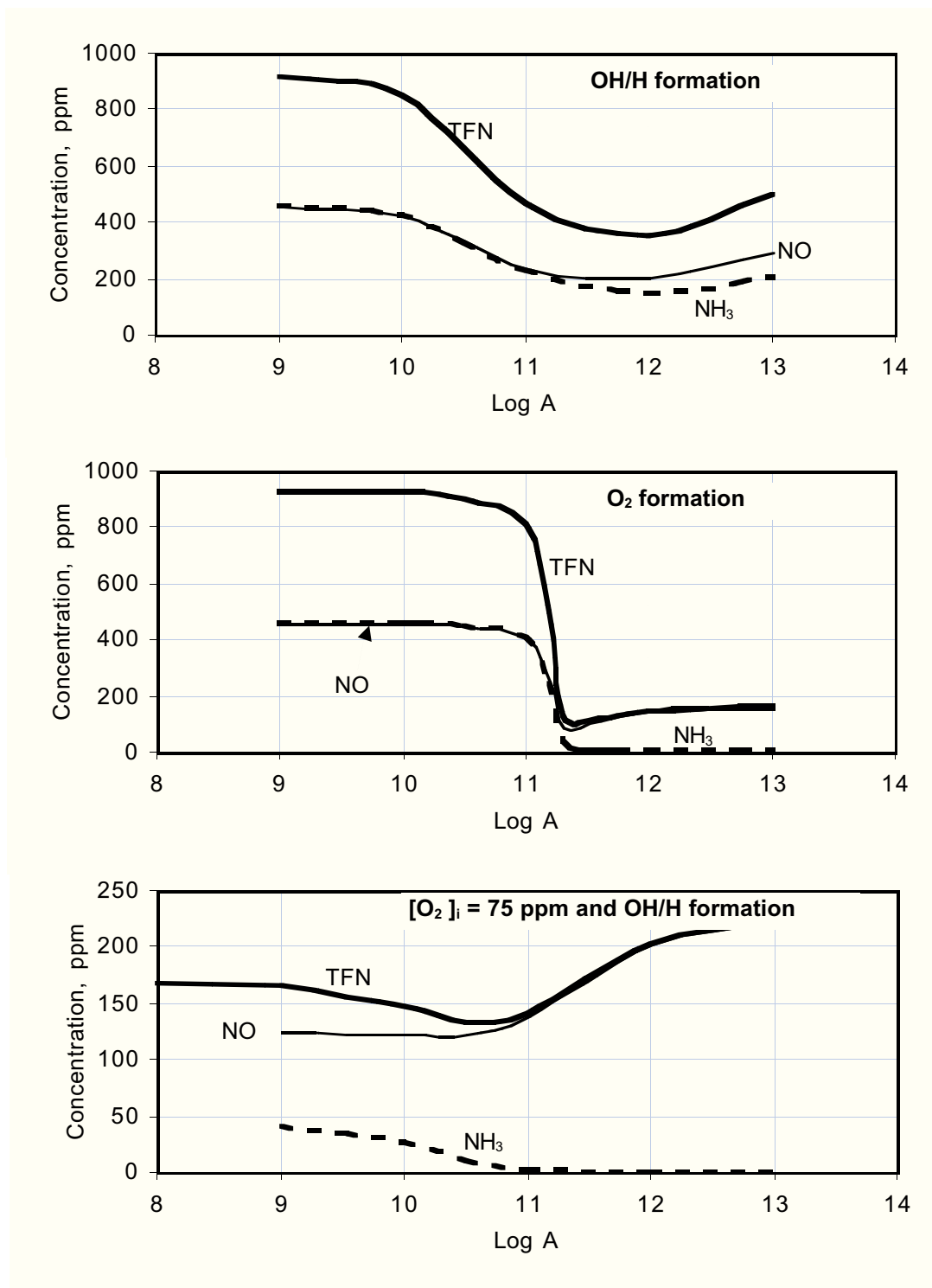
Figure 8.2.26. Modeling of the promotion effect at different predexponential factors A. The promoter appears with different rate constants in mixture I + 500 ppm NH_3 at $T_1 = 1600$ K.

8.2.4 Effect of Different Factors on the NO-NH$_3$ Interaction in the Reburn Zone

Effect of Oxygen. Performance of ammonia in the reburning zone greatly depends on the level of oxygen. If the oxygen concentration is high, NH$_3$ is partially converted to NO. If oxygen concentration is low, active radicals are not formed in oxidation processes. Thus, a maximum performance of NO/TFN removal should correspond to a certain optimum O$_2$ concentration. When sufficient O$_2$ is available, CO and H$_2$ react with O$_2$ via chain branching reactions producing radicals, which in turn participate in reactions with ammonia to form NH$_2$ followed by the reaction of NH$_2$ and NO.

To determine the optimum O$_2$ concentration, calculations were performed with injection of 500 ppm NH$_3$ with various amounts of oxygen into mixture I, as shown in Figure 8.2.27. The optimum O$_2$ amounts, and the resulting TFN removal performance, increase as injection temperature decreases. O$_2$ promotion provides a means for promoting the NH$_3$-NO interaction at lower temperatures in the reburning zone, where it would normally not be effective due to low oxygen and radical concentrations.

At lower temperatures, there is a certain threshold level of oxygen below which NO does not react with NH$_3$. This threshold depends on temperature, CO/H$_2$ concentrations, and initial NO and NH$_3$ concentrations. At [O$_2$] above the optimum, the efficiency of NO removal decreases slowly. At sufficiently high O$_2$ concentrations the NO level will actually increase.

Effect of CO and H$_2$. NO reduction efficiency is controlled by active radicals formed in CO and H$_2$ interaction with oxygen. Therefore, concentrations of CO and H$_2$ are important factors affecting NO-NH$_3$ interaction. The amounts of CO and H$_2$ in the mixture depend on composition of the main and reburning fuels and on the stoichiometric ratios, SR$_1$ and SR$_2$. For the current modeling study, with natural gas as both the primary and reburning fuel, the dependence is only on SR$_2$. Variations in SR$_2$ for 500 ppm NH$_3$ injection into Mixture I at 1300-1500 K, accompanied by the optimum level of O$_2$, show that there is an optimum SR$_2$ in the neighborhood of 0.99 to 1.0 (depending on injection temperature) for TFN reduction. Both CO and H$_2$ generate radicals in the oxidation process and help to reduce NO. The relative importance of each compound depends on conditions: temperature and concentrations of main components. For example, CO is more efficient than H$_2$ in reducing NO concentration at 1500 K, but H$_2$ has higher efficiency at 1300 K. Thus, modeling predicts that at the low temperature end of the reburning zone, NO/TFN removal is more efficient at lower temperatures with an optimum CO/H$_2$ level in the mixture as well as oxygen.
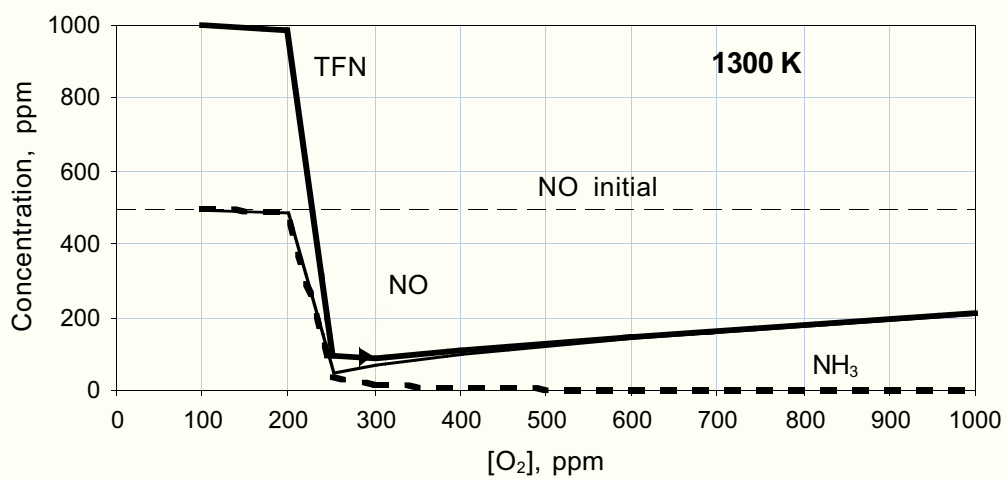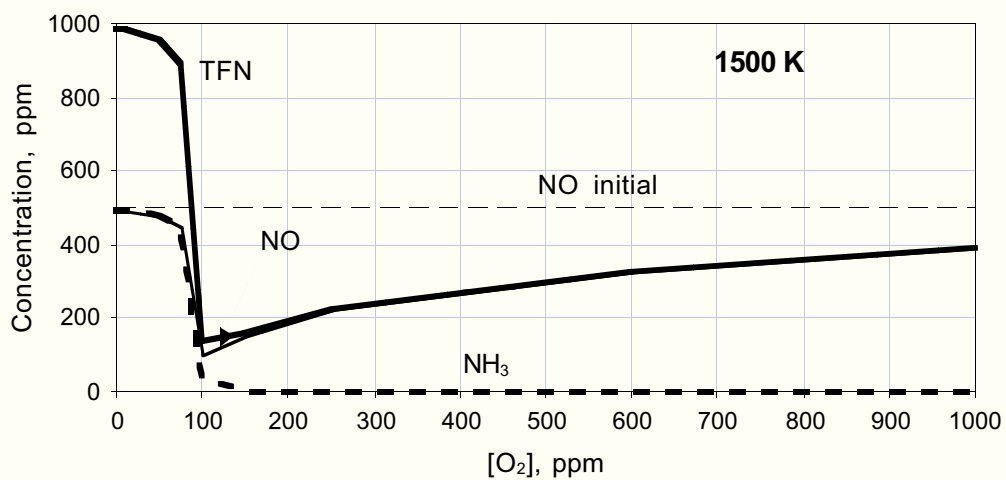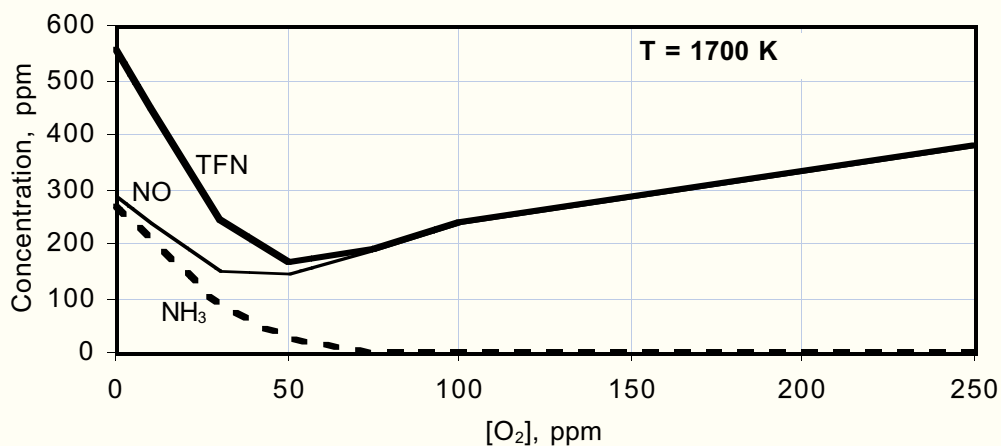
Figure 8.2.27. Effect of O₂ co-injection with 500 ppm NH₃ into mixture I at different injection temperatures.

Effect of Initial NO. Modeling suggests that injection of ammonia and oxygen into the reburning zone is less efficient at lower initial NO concentrations. This has been confirmed by modeling with 200 ppm NO and 200 ppm NH_3 in the reburning zone at $SR_2 = 0.99$ and $T_2 = 1300\text{-}1000$ K. Comparing performance with previous results at 500 ppm, a substantial decrease was noted in both the NO removal efficiency (from 80% to 50%) and in the range of effective O_2 concentrations. It was also found that a decrease in the injection temperature is capable of widening the O_2 window, but the NO removal efficiency is about the same.

8.2.5 Injection of Ammonia into the Burnout Zone (AR-Lean)

Modeling suggests that injection of OFA at different values of SR_2, SR_3, and temperature results in a final NO concentration which is near the TFN level in the mixture before OFA injection. Only at relatively high values of SR_2 (about 0.9) and at low OFA injection temperatures (about 1250 K), a small decrease of final NO concentration was observed (about 15%) compared with the TFN concentration upstream of OFA injection.

If ammonia is injected along with OFA in the reburning zone at $SR_2 = 0.99$, the NO reduction process is not effective at injection temperatures above 1100 K. Figure 8.2.28 (Curve 1) demonstrates the effect of OFA injection at different locations with co-injection of ammonia at $NSR_2 = 1.0$ on the final NO concentration. The initial NO concentration (100%, i.e. 350-500 ppm depending on the residence time in the reburning zone) increases when OFA is injected at 1120 K or higher. At these temperatures, some ammonia reacts with NO, but some is converted to NO, resulting in a final NO concentration (NO_f) higher than the initial NO concentration at the point of OFA injection. The concentration of NH_3 decreases to less than 1 ppm after the OFA/NH_3 injection. In the temperature range of 950-1050 K, the NO concentration is decreased, but this range is too low for OFA injection since all CO from the reburning zone remains unreacted.

Curve 1 represents the conditions of NO removal via the Thermal DeNOx process in the presence of high concentrations of CO and H_2. It is well known (for instance, Lyon and Hardy, 1986) that the presence of CO and/or H_2 shifts the temperature window of NO removal by the SNCR process to lower temperatures. In order to avoid that shift, ammonia can be injected into flue gas with a short delay after injection of the OFA or in the aqueous form to allow some time for evaporation of the water. In this case, the OFA rapidly reacts with CO and H_2, and the NH_3 appears in the gas mixture when all CO and H_2 are already oxidized. Modeling shows that a delay time of about 0.1 s is enough for complete CO and H_2 removal. The results of calculations are shown in Figure 8.2.28,
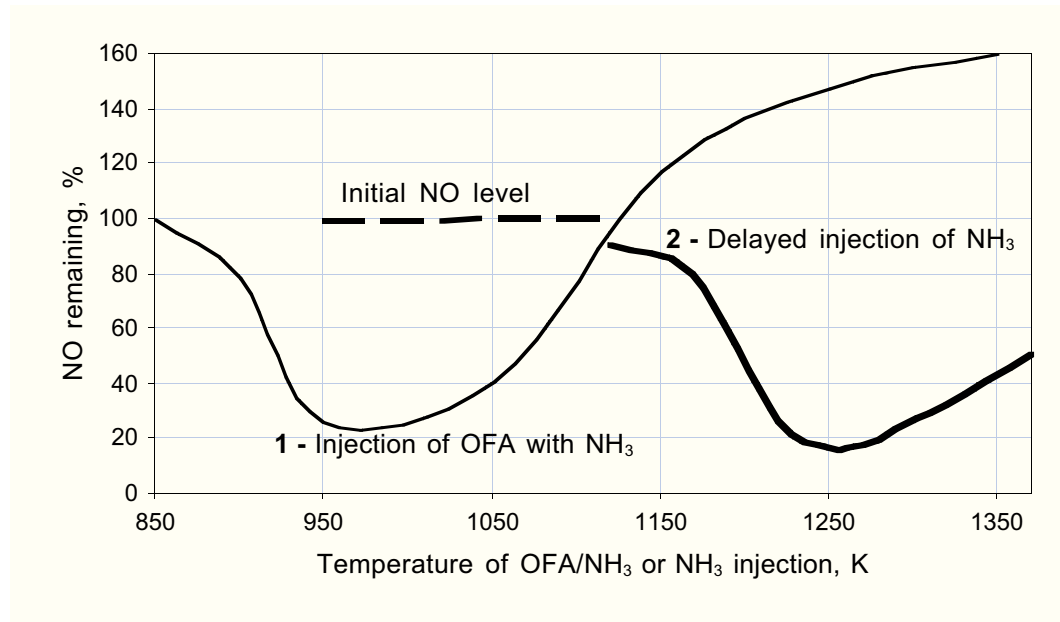
Figure 8.2.28. Effect OFA co-injection with NH_3 on the final NO concentration. NSR = 1.0.

Curve 2 which represents the effect of NH_3 injection temperature (NH_3 is injected with a 0.1 s delay time after the OFA) on NO concentrations. Under these conditions, the ammonia reacts with NO in the presence of oxygen and in the absence of CO and H_2, and the optimum temperature for NH_3 injection is about 1200 K, which is typical for the Thermal DeNOx process.

If the reburning fuel is injected with $SR_2 = 0.90$ at $T_1 = 1700$ K, modeling shows that the concentration of ammonia in the reburning zone is higher than the NO concentration. For example, at $T_3 = 1400$ K, concentrations of fuel-N species are: 71 ppm HCN, 50 ppm NO, and 113 ppm NH_3. Injection of OFA converts all fuel-N species to NO. Therefore, co-injection of gaseous ammonia with OFA does not make sense for these conditions either. Variation of the O_2 concentration in OFA does not change the final NO level.

8.2.6 Modeling with Instantaneous Mixing Times: Summary

The performance of individual AR processes has been considered using a time-dependent chemistry calculation, putting aside the influence of finite-rate mixing effects. Some of the most important points are summarized here.

Reburning zone chemistry has been examined over the range of stoichiometric ratios from 0.90 to 0.99. It has been shown that there is a short, fast initial reduction in NO followed by slower reduction over the remainder of the reburning zone. This effect is linked to the disappearance of oxygen and radicals, and highlights an opportunity for introduction of species which can reestablish optimum concentrations for NO removal.

Injection of N-agents is effective at reducing NO when temperatures and concentrations of oxygen and other radicals are conducive. Conditions are more favorable at reburn SRs close to stoichiometric. Mixing of the N-agent with flue gas must occur in a window downstream of reburn fuel injection to encounter the correct environment for effective NO reduction. This delay may be achieved by locating injectors downstream of fuel injectors, or by use of aqueous N-agent solutions with associated evaporation delays.

Introduction of promoter species along with the N-agent may enhance its performance by making the reactant mixture more favorable to NO reduction by NH_3 and associated species. Injection of ammonia with small amounts of oxygen upstream of the OFA improves NO reduction. The efficiency of NO removal depends mainly on SR_2 and concentrations of oxygen, CO/H_2, and NO. The optimal oxygen concentration depends on the injection temperature. The efficiency is lower at lower NO initial concentrations. Radical species also exhibit a promotion effect, calling for the injection of species which provide them in the proper amounts and at the proper rates.

Injection of OFA into the fuel-rich reburning zone converts all fuel-nitrogen species into NO as long as the temperature of OFA injection is adequately high.

Co-injection of ammonia with the OFA significantly shifts the temperature window of the Thermal DeNOx process to lower temperatures because of the CO and H_2 present. To avoid this shift, ammonia should be injected after a short delay time relatively to the OFA location. This delay can be provided by evaporation of aqueous ammonia or urea co-injected with OFA.

8.3 Evaluation of Mixing Effects

8.3.1 Approach

The modeling discussed above treated the AR process as a one-dimensional plug flow reactor with instantanous mixing at each injection point. This approach simplifies the analysis by focusing on chemistry, but puts aside the effect of finite rate mixing. The results demonstrated qualitative trends

but did not quantitatively reproduce experimental data. Indeed, quantitative predictions are challenging even in the most sophisticated (and computationally demanding) three dimensional model coupling chemistry and fluid dynamic effects, as ongoing research continues to develop understanding of chemical reaction mechanisms and turbulent mixing. However, the basic one dimensional model which has already proven useful may be incrementally improved by incorporating a simplified treatment of finite-rate mixing of an injected stream into the main flow.

The tool chosen for this study is a one dimensional chemical kinetics code developed at EER. This program is known as "ODF," for "One Dimensional Flame," although the code is applicable to any gas phase system. ODF contains the same basic capabilities as Chemkin, including the evaluation of pressure-dependent and reversible Arrhenius rate expressions, and the specification of time-dependent profiles of temperature and pressure. Most importantly for the current study, the solution algorithm has been formulated to allow for the introduction of an arbitrary profile of mass injection along the length of the reactor.

ODF has been applied to basic and advanced reburning scenarios. The reburning system is treated as a plug flow reactor, beginning with the introduction of reburning fuel into primary combustion products at 1700 K. The reacting flow is cooled at a uniform rate of -300 K/s. Overfire air and (for AR) gaseous ammonia are introduced at different locations along this temperature ramp, and the reactions continue until the system reaches a temperature of about 600 K, at which point the reaction rates may be considered negligible.

The primary mixture is at a stoichiometric ratio of about 1.1, with initial (wet) concentrations of 600 ppm NO, 1.74% O_2, 8% CO_2, 15% H_2O, after mixing with methane which is the reburn fuel. The two reburning stoichiometries are nominally 0.90 (1.94% CH_4), and 0.99 (0.967% CH_4). The OFA is added for a final stoichiometry of 1.15. Unless otherwise noted, OFA injection is at 1300 K, based on previous modeling suggesting that this is a good temperature for effective NO reduction as well as burnout of other fixed nitrogen species and incomplete combustion products. Some cases were also run with OFA introduced at 1200 K or 1400 K for comparison.

In each AR case presented here, the ammonia addition was adjusted to NSR=1.0, matching the concentration of added NH_3 to the concentration of NO at the start of N-agent injection. Because NO varied with injection location, the quantity of added ammonia varied. Additional calculations with a uniform quantities of ammonia, with NSRs greater than equal to 1.0, is discussed in Zamansky et al. (1997a and 1997b).

To evaluate the effect of mixing time, three mixing scenarios were applied to each basic or advanced reburning condition modeled: instantaneous mixing, 30 ms mixing, and 300 ms mixing. The same mixing time was applied to all external streams (reburn fuel, N-agent, and OFA), and mixing over 30 or 300 ms was applied at a uniform rate of mass addition. The instantaneous mixing case is the limiting case corresponding to the approach in earlier Chemkin modeling. 30 ms mixing may be considered fast, corresponding to bench and small pilot scale systems such as EER's combustion facilities CTT and BSF. 300 ms mixing is more typical of large pilot-scale systems such as EER's Tower Furnace (10 MMBTU/hr) and full-scale industrial combustion systems.

8.3.2 Effect of Mixing Times on Basic Reburning

The kinetic behavior of the model during and after reburning fuel addition was examined closely to determine the effects of finite mixing time on kinetic behavior in the reburning zone. Figures 8.3.1 through 8.3.4 show the concentrations of important species as a function of time from the start of the reburning fuel injection, for nominal reburning stoichiometries of 0.99 and 0.90, and for the finite rate mixing scenarios (30 ms, and 300 ms mixing). In addition to the individual species concentrations, there is also a curve for TFN (total fixed nitrogen), which in these four figures includes not only NO, NH_3, and HCN, but all sources of N-atom except N_2.

The case with instantaneous mixing was also run, and results correspond to those already presented in Figures 8.2.1 (for SR_2=0.99) and 8.2.3 (for SR_2=0.90). Comparison with the figures generated by Chemkin shows that the same trends are predicted. This serves to validate the ODF model setup against the equivalent modeling previously done in Chemkin. However, note that Figures 8.2.1 and 8.2.3 cover a different range of time and concentration than the other plots presented here.

As mixing time is increased to 30 ms (Figure 8.3.1) and to 300 ms (Figure 8.3.2) for a nominal reburn stoichiometry of 0.99, the behavior in the mixing zone is modified by the slower rate of fuel addition and the accompanying slower rate of stoichiometry change. At 30 ms, distributed mixing of the reburn fuel results in a spike in CH_4 concentration along with other species, which persists on about the same time scale as the mass addition interval. Also present but less obvious are increases in the concentrations of other species including O_2, OH, and H for a couple of hundred milliseconds following the end of reburn fuel injection. These species are then more available for the reactions involved in reburning and so NO reduction is more effective as mixing time is increased. In Figure 8.3.2, the 0.3 injection interval is now more obvious and reflects a more dramatic impact on all species concentrations. Several species, including O_2, HCN and NH_3 persist in higher quantities throughout the reburning zone. The net effect is a decrease in NO.
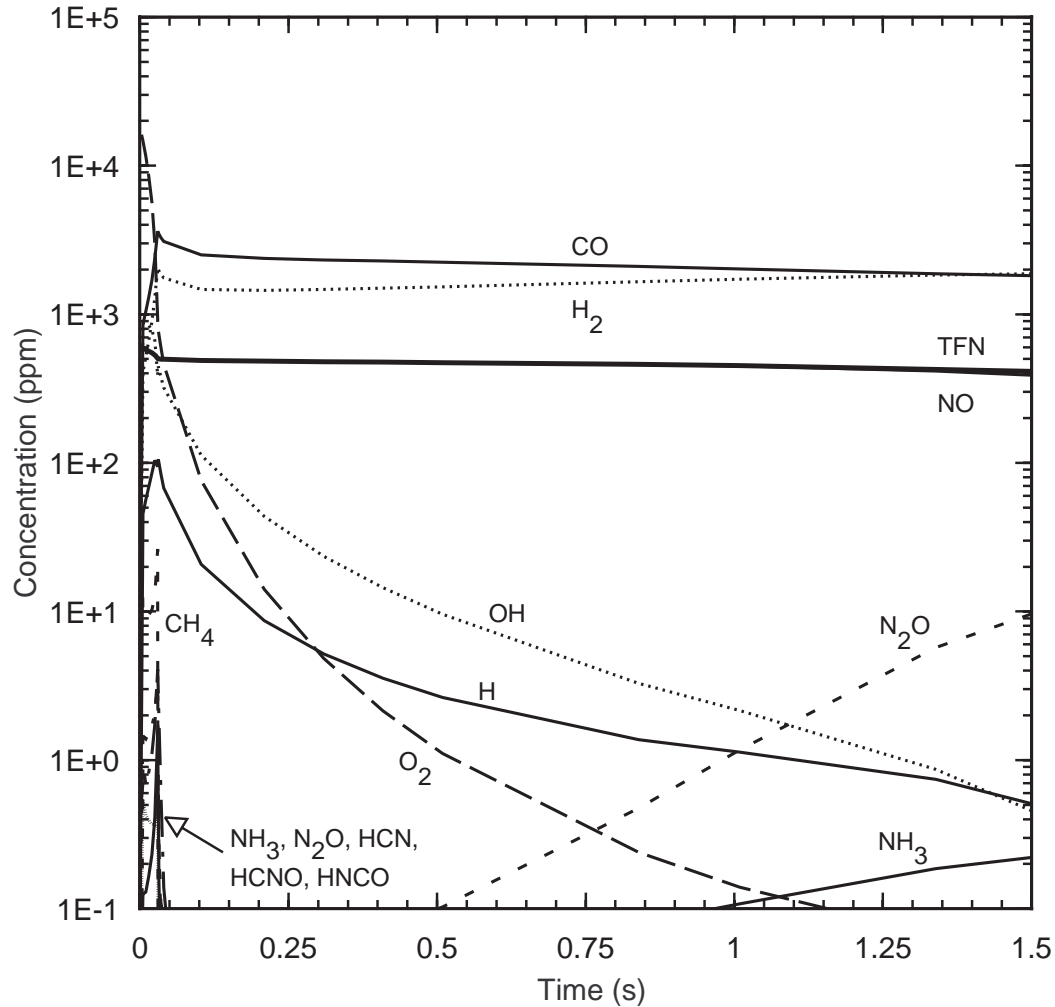
Figure 8.3.1. Kinetic curves of important species in the reburning zone at $SR_2 = 0.99$ and with mixing of the reburning fuel over an interval of 30 ms.

The same trends are found for a nominal reburn stoichiometry of 0.90 as mixing is varied from instantaneous (Figure 8.2.3) to 30 ms (Figure 8.3.3) to 300 ms (Figure 8.3.4). The impact on the kinetic curve for NO is similar but more obvious than at $SR_2=0.99$ since the magnitude of NO reduction due to reburn fuel addition alone is more pronounced at the more fuel rich condition. Even at 30 ms mixing time, O_2 persists for a longer time. It is interesting to note that most of the decrease in NO is on roughly the same time scale as the decrease in O_2 in all cases. The result is a clear improvement in NO reduction as mixing time is increased.

8.3.3 Effect of Mixing Times on AR-Rich

The AR-Rich cases were run with either co-injection of ammonia with reburn fuel ("no delay") or with the start of ammonia injection delayed by a specified time after the beginning of reburn fuel
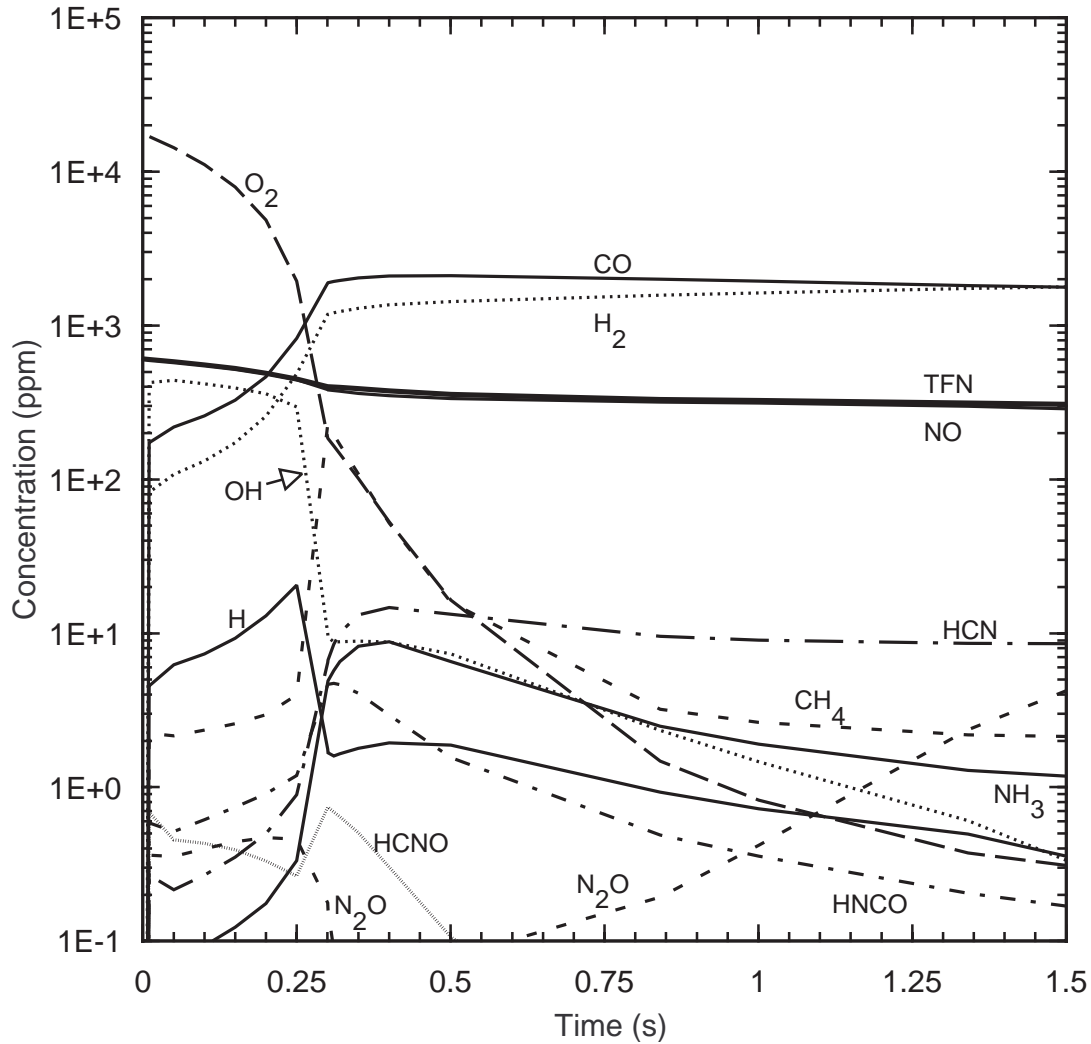
Figure 8.3.2. Kinetic curves of important species in the reburning zone at $SR_2 = 0.99$ and with mixing of the reburning fuel over an interval of 300 ms.

injection. Since the same mixing time is used for every stream in this simulation, some cases with short delay times (e.g. 0.1 s) and long mixing times (e.g. 0.3 s) included an overlap between the end of reburn fuel mixing and the beginning of ammonia mixing.

In all of the basic reburning and AR-Rich cases presented here, OFA was injected at 1300 K. However, some cases were run at 1200 K and 1400 K which verified earlier modeling conclusions that 1300 K gives better overall results in terms of NO reduction and destruction of other nitrogen containing species.

Figure 8.3.5 shows the NO reduction for basic reburning and AR-Rich at a nominal reburning zone stoichiometry of 0.99. Co-injecting ammonia with the reburn fuel increases the final NO compared
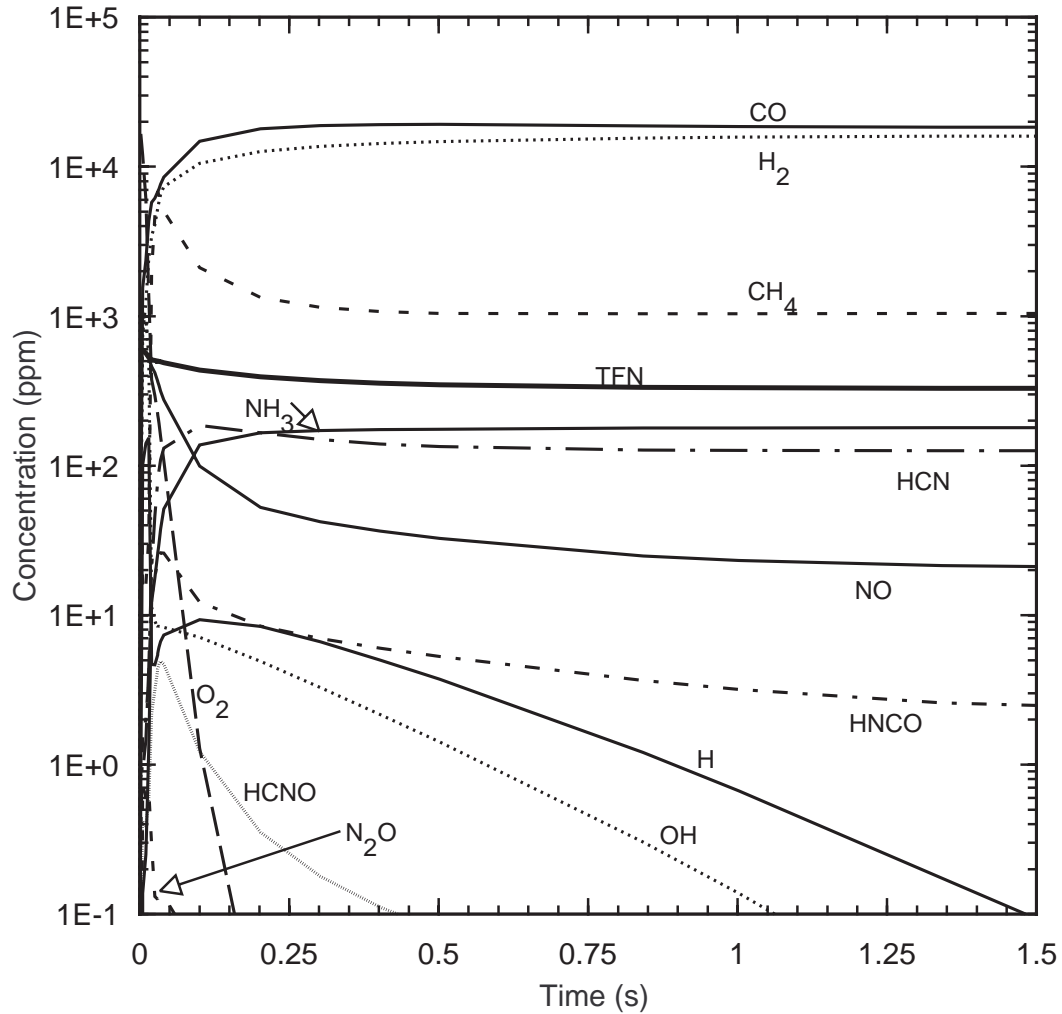
Figure 8.3.3. Kinetic curves of important species in the reburning zone at $SR_2 = 0.99$ and with mixing of the reburning fuel over an interval of 30 ms.

to basic reburning, but a delay of 0.1 s causes the final NO to decrease substantially. An additional condition with a longer delay time (0.833 s) returns to the higher final NO concentrations. These results show that there is clearly an optimum delay time for ammonia injection, in the neighborhood of 0.1 s. This optimum delay time effect is shown in Figure 8.2.16; note that the results there are before burnout, for which TFN is the best indicator of postburnout NO. At 0.1 s delay time, shorter mixing times actually yield slightly better results than longer mixing times, but the difference is small. These results also make it clear that there is a distinction between delay of the start of injection and the duration of mixing, underscoring the importance of both parameters in this system.
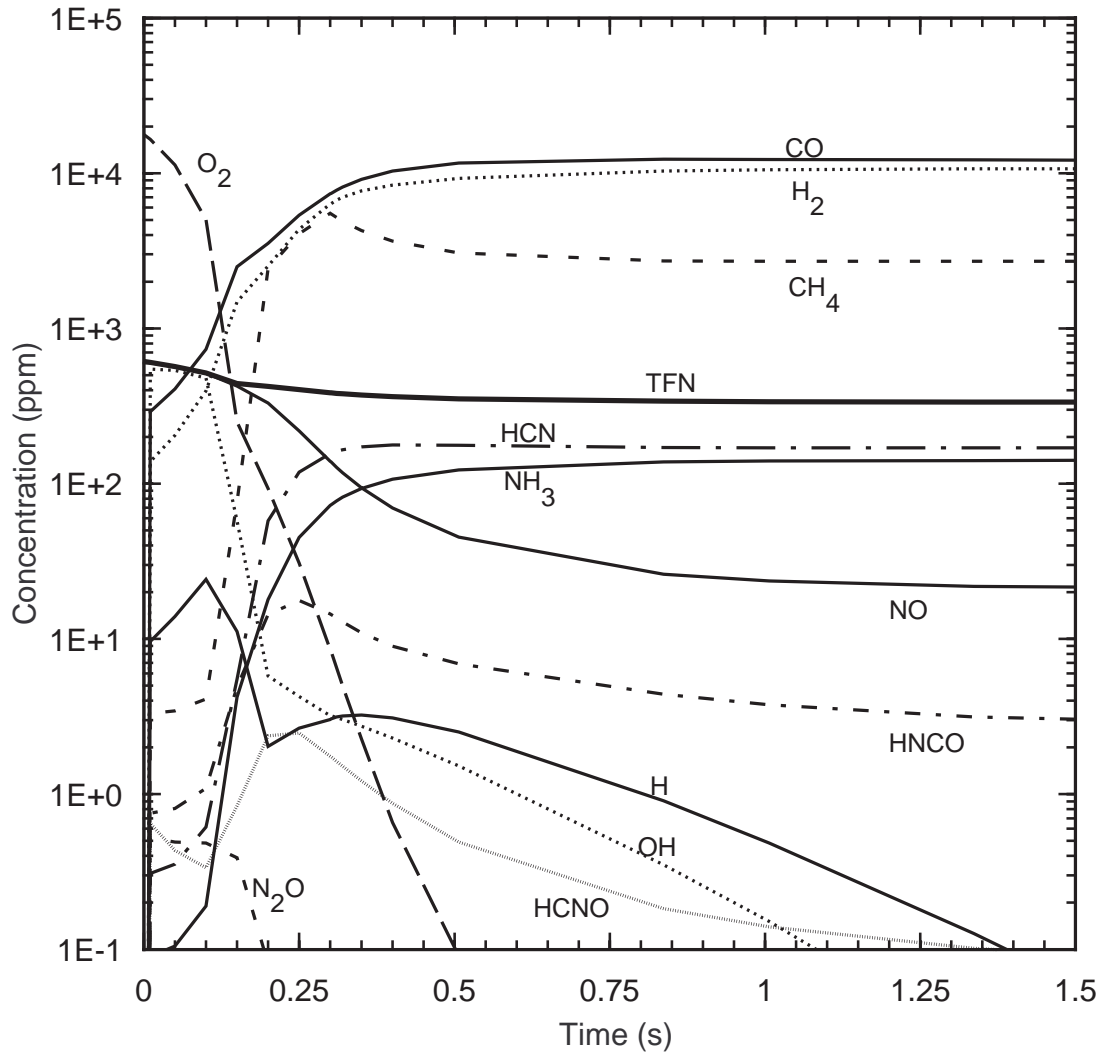
Figure 8.3.4. Kinetic curves of important species in the reburning zone at $SR_2 = 0.99$ and with mixing of the reburning fuel over an interval of 300 ms.

8.3.4 Effect of Mixing Times on AR-Lean

Further modeling addressed the injection of ammonia into the burnout zone (AR-Lean), either coinjected with the OFA or introduced with a short delay time (0.1 s). All cases were run for a nominal reburning zone stoichiometry of 0.99 only as this is the condition of greatest interest for AR. The location of OFA addition was varied between 1200, 1300, and 1400 K. The same three mixing scenarios (instantaneous, 30 ms, and 300 ms) were applied to each condition.

Figure 8.3.6 shows the NO reduction as a function of mixing time for OFA injection at 1300 and 1400 K when ammonia is co-injected. As mixing time increases, NO decreases at both temperatures. For the temperature range considered, NO reduction is better at 1300 K for short mixing times, but
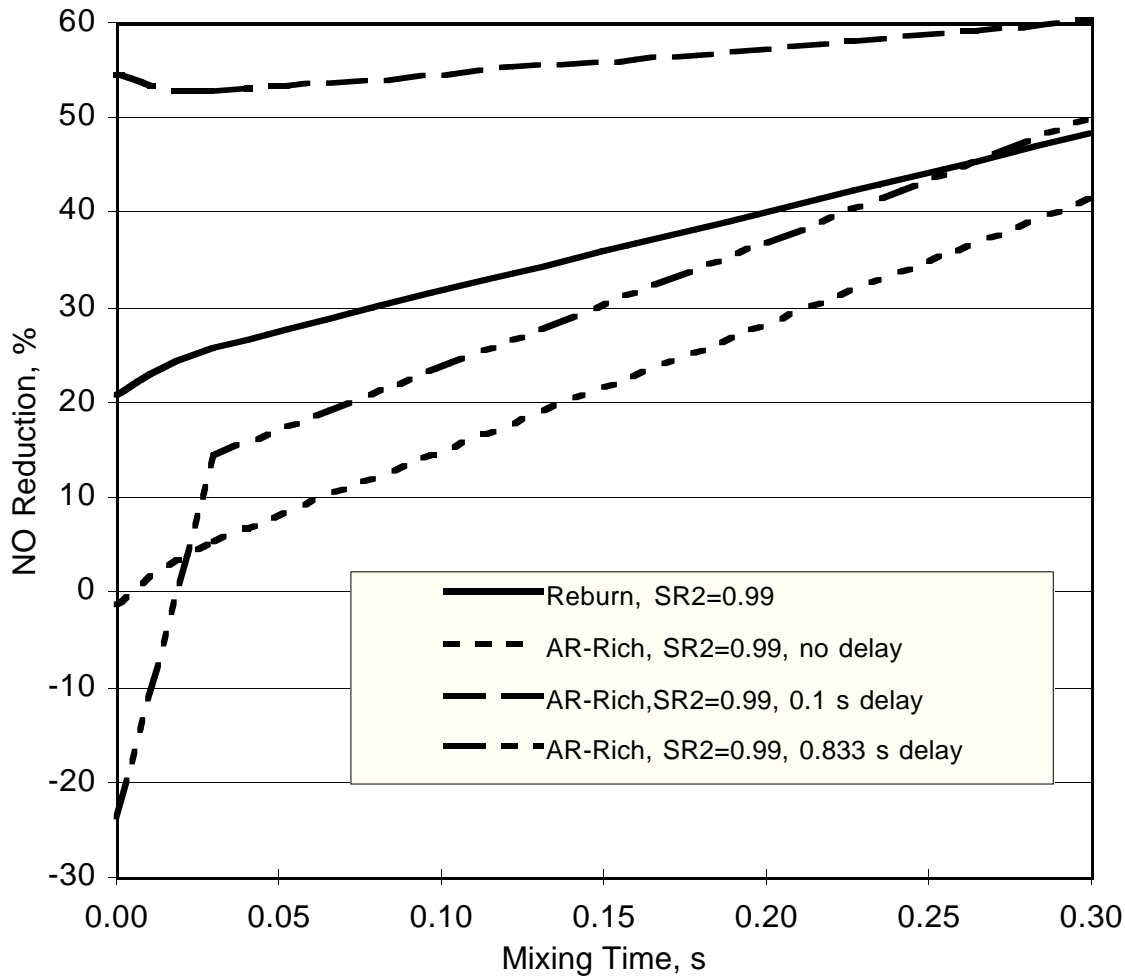
Figure 8.3.5. AR-Rich NO emissions, for $SR_2 = 0.99$ and NH_3 added at NSR = 1.

for longer (300 ms) mixing, 1400 K is preferable as it provides good NO reduction with a minimum of other fixed nitrogen species.

Figure 8.3.7 shows the corresponding cases when ammonia injection is delayed by 0.1 s after the beginning of OFA injection. Longer mixing time leads to lower NO in most cases, but there is less difference in NO between instantaneous mixing and 30 ms mixing in this case. This implies that the kinetics is less sensitive to mixing time for the introduction of ammonia at lean conditions, than for ammonia when introduced at initially rich conditions.

Figure 8.3.7 shows that final NO is lower for 1300 K than for 1400 K at all mixing times. However, at 300 ms mixing times, 1300 K OFA injection also results in significant TFN in addition to NO, about 69 ppm NH_3). Therefore, 1300 K injection gives the best performance for fast mixing conditions, and 1400 K is better for slower mixing conditions due to the lower TFN.
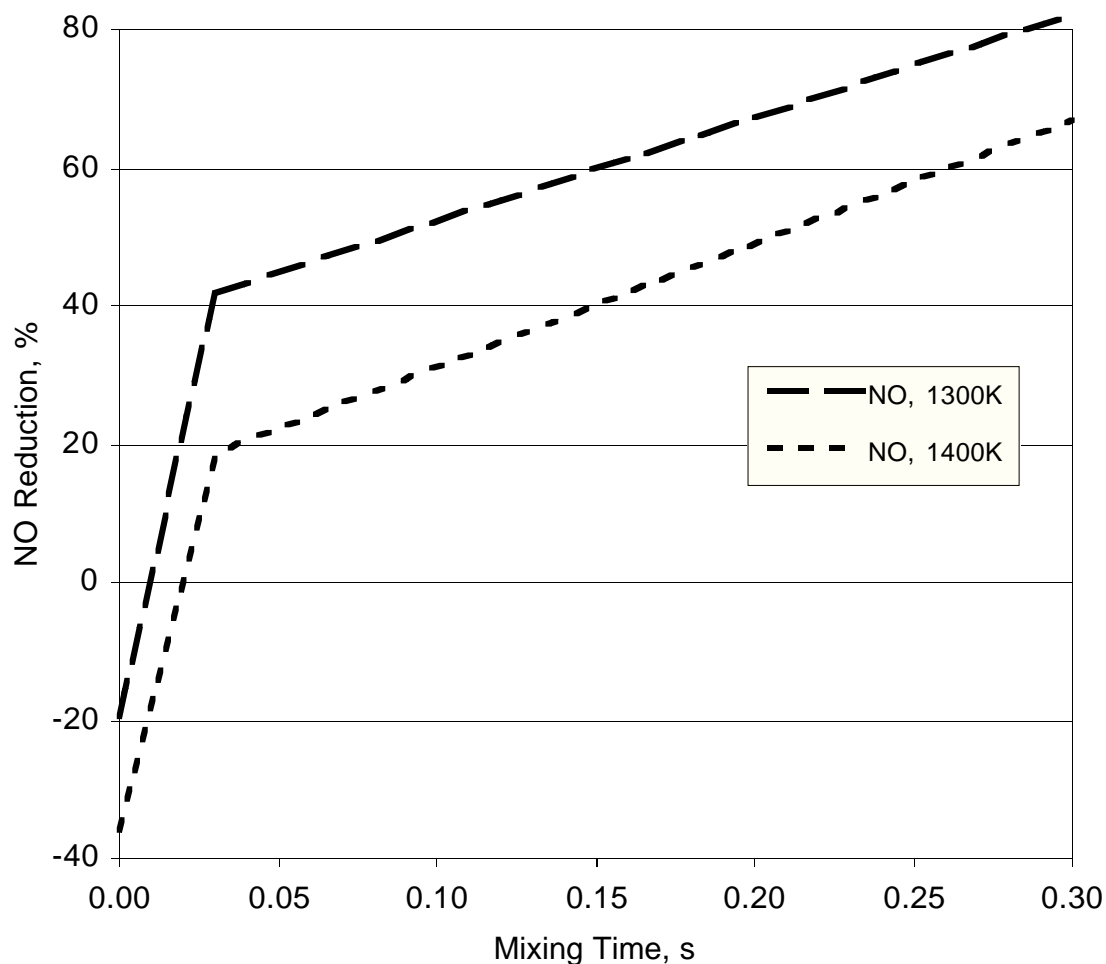
Figure 8.3.6. AR-Lean NO emissions, for $SR_2 = 0.99$ and NH_3 added at the same time as overfire air, at NSR = 1.

8.3.5 Mixing Studies: Summary

These studies demonstrate that the rate of mixing of injected streams may have a significant impact on basic or advanced reburning performance. A simplified one-dimensional chemical reactor model is significantly amplified in its scope of prediction by incorporating a simple mass injection model.

In the design of AR systems, the predicted impacts of mixing time may provide guidance in selecting injection nozzles for a given installation. In an experimental study such as this one, however, the most important issue is the prediction of trends which guide in the interpretation of experimental results from reduced scale furnaces, to anticipate the results to be expected for fullscale implementation.
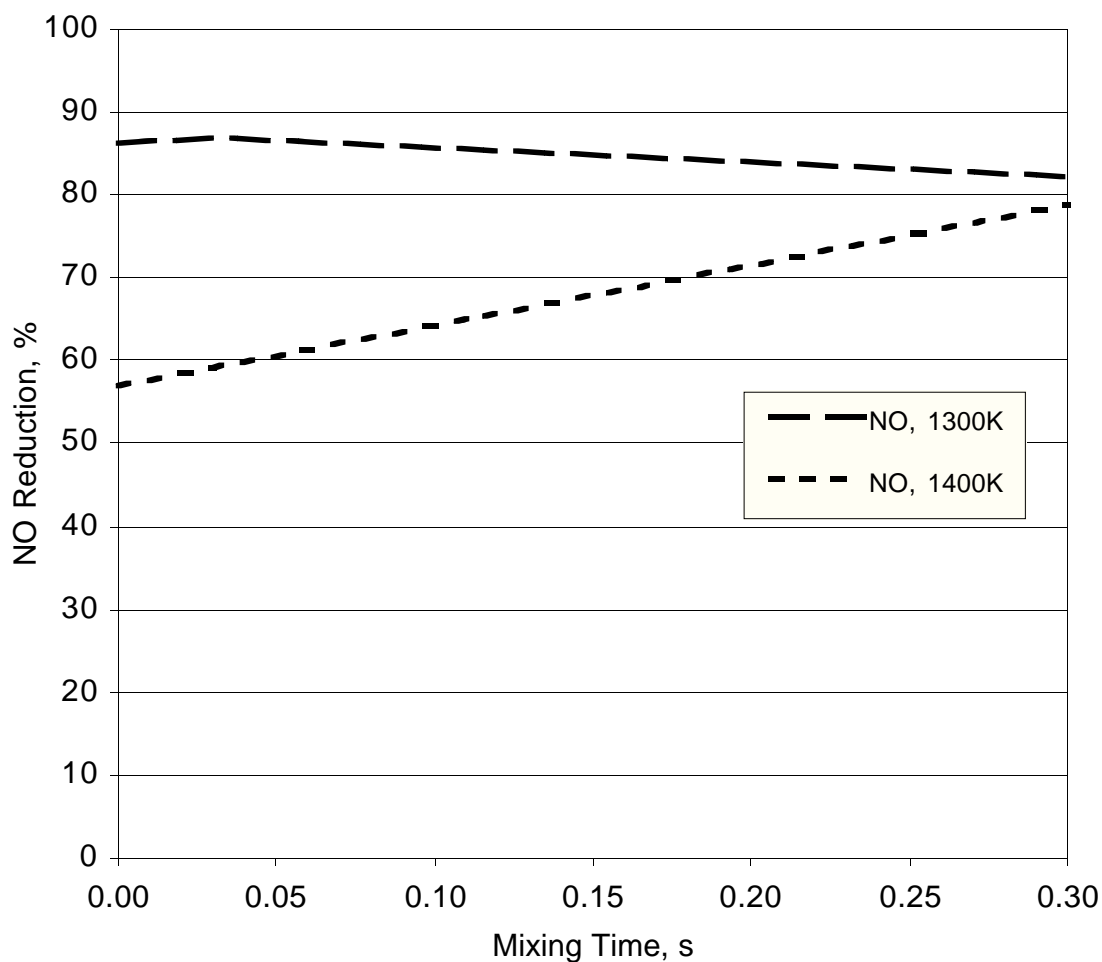
Figure 8.3.7. AR-Lean NO emissions, for $SR_2 = 0.99$ and NH_3 added 0.1 s after burnout air at NSR = 1.

For the basic and advanced reburning conditions considered here, four major parameters were varied: the reburn zone stoichiometry, the OFA injection temperature, the location of ammonia injection, and the mixing time. In general, good results were obtained with longer mixing times and with about 0.1 s delay in ammonia injection for both AR-Rich and AR-Lean systems. Very long delays in ammonia injection led to poor performance.

8.4 Effect of Sodium

Of immediate interest is gas-fired AR with sodium promotion. As discussed in Section 8.1.3, the kinetic mechanism has been extended to include reactions of sodium so that this process may be examined.

8.4.1 Effect of Sodium Promotion in AR-Rich

Effect of Mixing Time. The cases considered here for AR-Rich conditions are based on the reactor model with finite-rate mixing, described in Section 8.3 above. The first results examine the effect of mixing time, similarly to Section 8.3.2.

As before, the stoichiometric ratios are nominally 1.10 in the primary zone, 0.99 in the reburn zone, and 1.15 in the burnout zone. Reburn fuel is injected at 1700 K, after which the gas cools at a constant rate of 300 K/s. N-agent and sodium promoter, if any, are co-injected at 0.1 s after the beginning of reburn fuel injection (this condition was selected for initial screening as it showed promise in the earlier AR-Rich studies). When included, the sodium promoter is 50 ppm of Na_2CO_3.

Figures 8.4.1 through 8.4.3 show the kinetic curves for the AR-Rich reburning zone with and without promotion, for NSR=1.0. The curves start at the point at which the injection of reburn fuel begins (1700 K), and continues for 1.0 s of reactor time (to a temperature of 1400 K).

Figure 8.4.1 shows the kinetic curves with and without sodium promoter, respectively, for the reactor with instantaneous mixing. The discontinuity at 0.1 s is due to the sudden premixing of the additives at that location. For these conditions, there is little net impact of sodium promotion. The greatest change is that O_2 disappears more rapidly in the presence of the promoter. Correspondingly, the radicals H and OH also decrease more quickly for the case with sodium. The net impact is that the final concentrations of NO and NH_3 are actually somewhat lower in the case without promoter. However, the differences are relatively small.

Figure 8.4.2 shows the corresponding behavior for 30 ms mixing. The kinetic curves are similar to those for instantaneous mixing, again with promotion causing a more rapid decline in O_2, OH, and H. With the distributed mixing, however, the sudden change in concentrations at the addition points is smoothed over the mixing time. 30 ms is relatively fast in terms of the overall reaction time, but at the given conditions the chemical reactions are faster. Therefore, the distributed mixing does change the shape of the curves and affect the downstream composition. In this case the net effect of the sodium promoter is a slight decrease in the NO concentrations near the end of the zone shown.

Figure 8.4.3 shows the kinetic curves for 300 ms mixing, with and without promoter. Here the mixing is distributed over such a long time that the chemistry is definitely affected. The long mixing times result in slow progression though a range of stoichiometries and local NSR's as the reburn fuel, N-agent, and overfire air are slowly introduced. Since the mixing time is longer than the delay

50 ppm Na$_2$CO$_3$ added with NH$_3$

NH$_3$ added without sodium
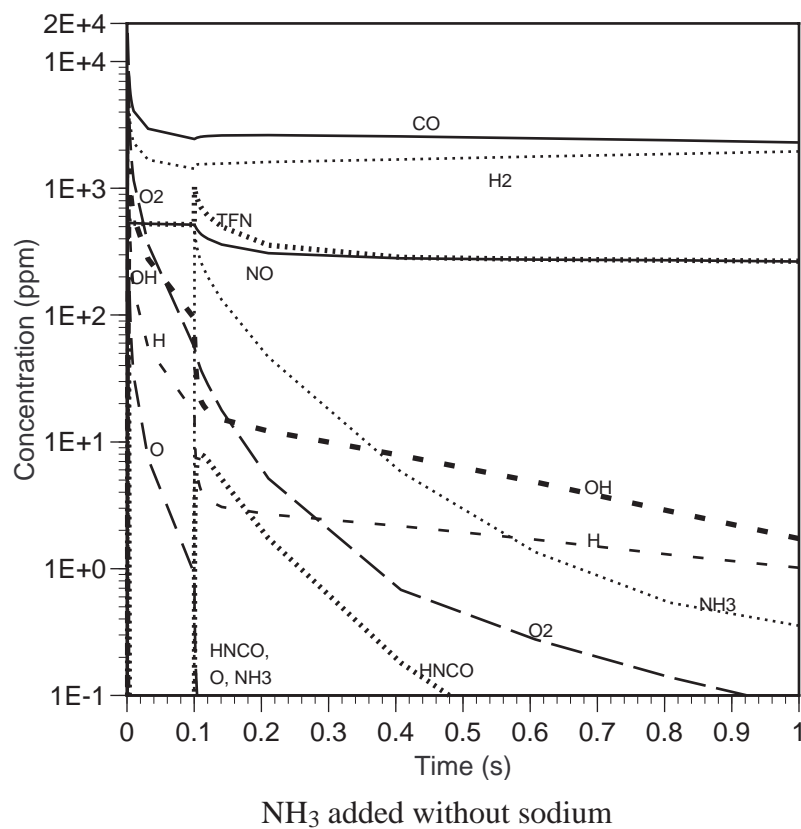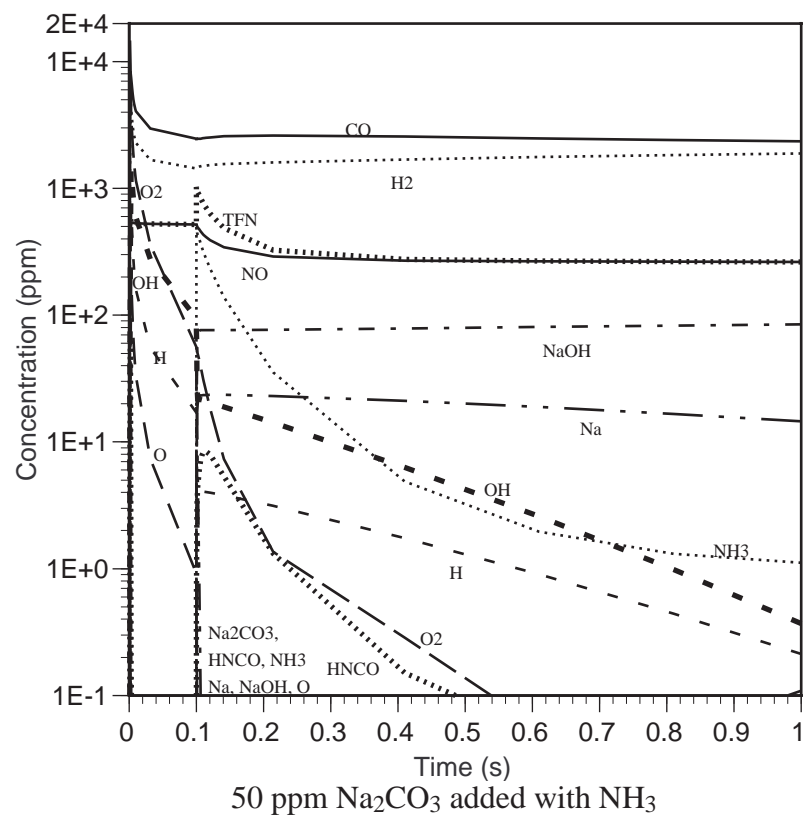
Figure 8.4.1. AR-Rich kinetic curves with instantaneous mixing, from the point of reburn fuel injection with NH$_3$ (NSR = 1) injected after 0.1 s.

50 ppm Na$_2$CO$_3$ added with NH$_3$

NH$_3$ added without sodium
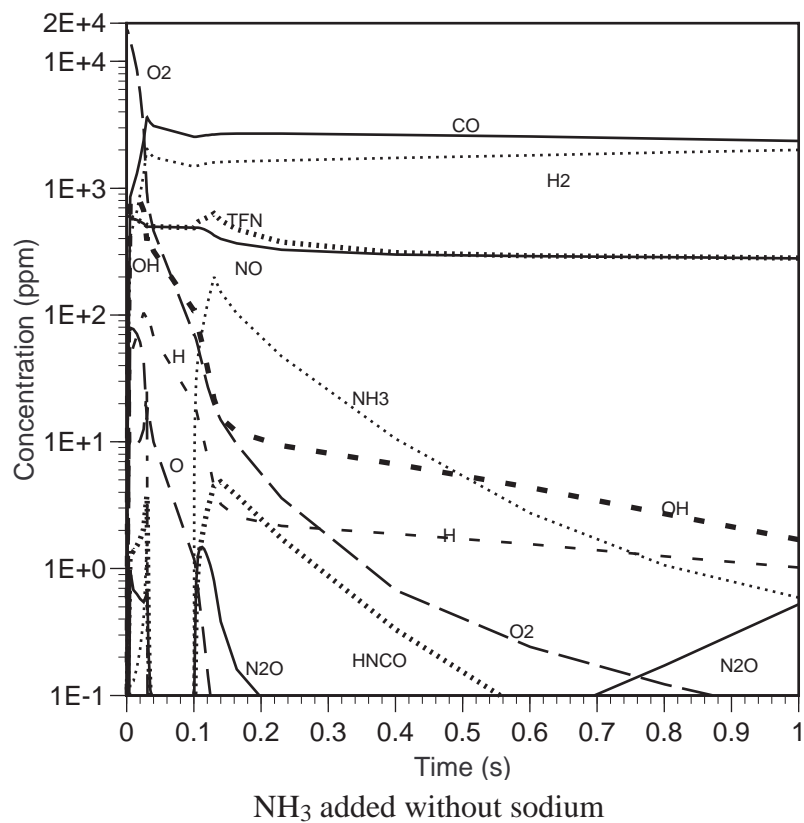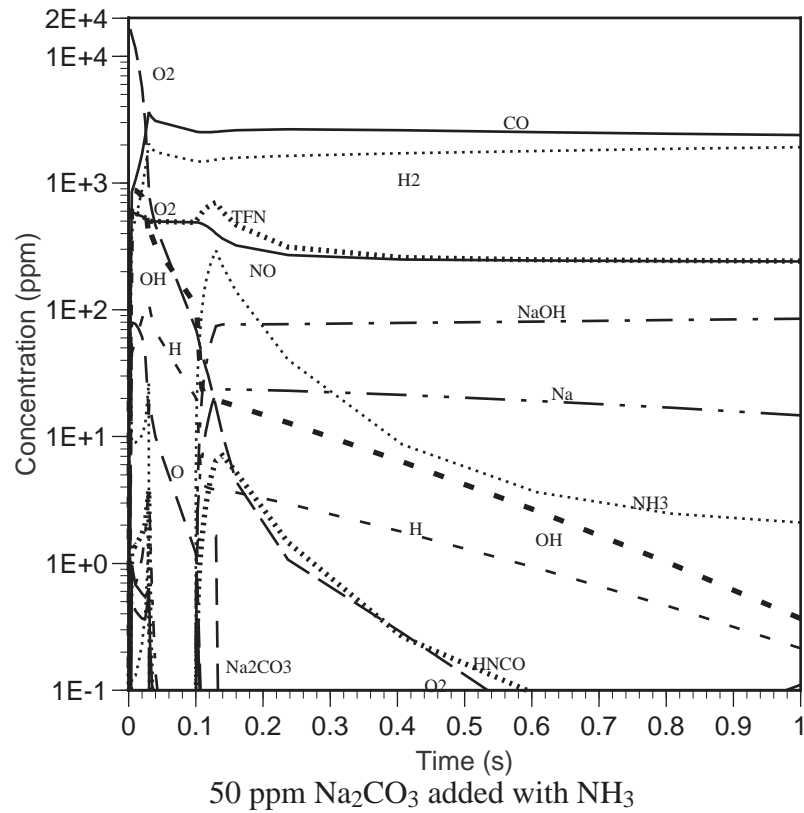
Figure 8.4.2. AR-Rich kinetic curves with 30 ms mixing, from the point of reburn fuel injection with NH$_3$ (NSR = 1) injected after 0.1 s.
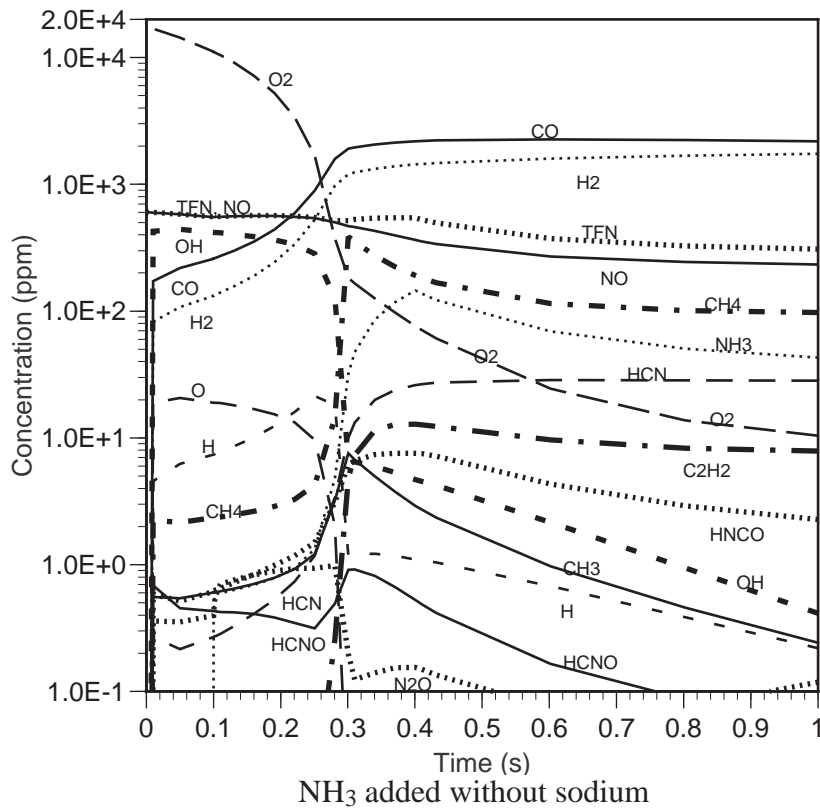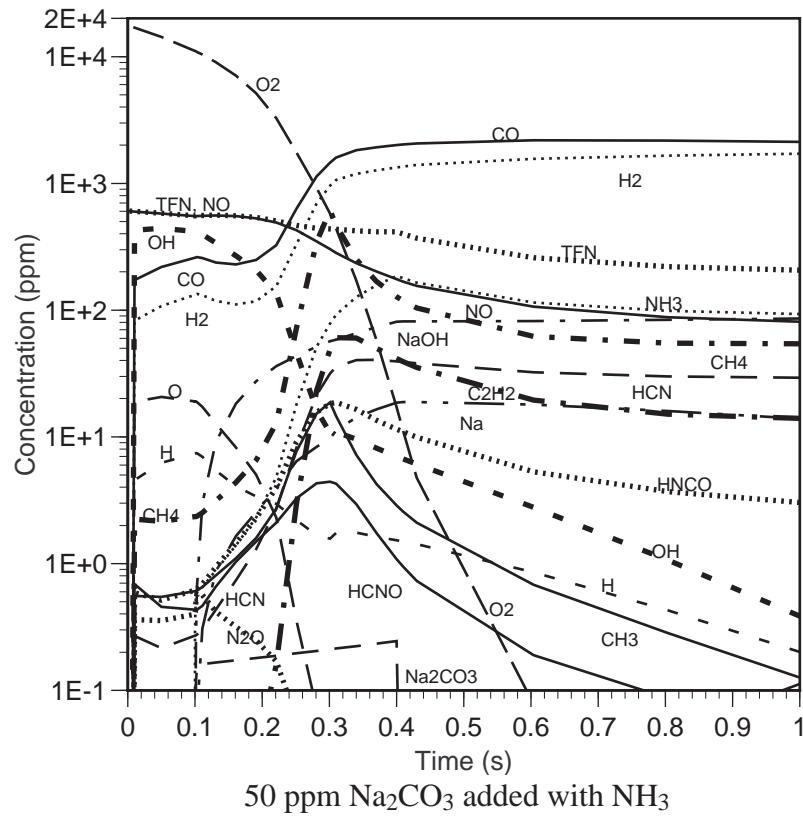
Figure 8.4.3. AR-Rich kinetic curves with 300 ms mixing, from the point of reburn fuel injection with NH_3 (NSR = 1) injected after 0.1 s.

8-65

between reburn fuel and N-agent addition, these two mixing zones actually overlap. At 0.3 s, the supply of reburn fuel is out and the pool of radicals and unburned fuel that it helps to sustain now begins to disappear, changing the direction of the kinetic curves at that point. With sodium promotion, even this transition is spread out, suggesting that in this case the sodium promoter helps to sustain the radical pool and has a definite beneficial effect on NO and TFN emissions.

The net impact of promotion is illustrated in Figure 8.4.4, which shows the concentration of NO and TFN in the reburn zone at 1300 K (1.33 s after the start of reburn fuel injection), with and without sodium promotion. At instantaneous mixing, the promoter has a very slight negative effect on emissions. However, for mixing times as short as 30 ms, promotion begins to show a beneficial effect. For longer mixing times representative of industrial installations, the effect is quite pronounced. Longer mixing times also show very large TFN concentrations aside from NO, but it should be remembered that this is before burnout.

As discussed before, the quantity of N-agent can have a significant impact on system performance. To illustrate this, Figure 8.4.5 shows the results of AR-Rich calculations with the same conditions as for Figure 8.4.4, except that the injected N-agent is 800 ppm in all cases. This guarantees an NSR greater than 1 since the initial NO is 600 ppm. The actual NSR is approximately 1.5 based on NO at the point of injection. As would be expected, the NO concentration decreases as more N-agent is added, but note that the effect is non-linear. For instant mixing, the adverse effect of the sodium promoter within the reburning zone increases, but systems with finite mixing times still perform better with sodium promotion. The differences in the effect of promotion at different mixing times reflect the difference in kinetic behavior with mixing time, as illustrated in Figures 8.4.1 through 8.4.3. These changes in characteristic behavior are due to the effect of distributing mass addition, and at long mixing times the shift in temperature due to gas cooling also has an impact. Figures 8.4.4 and 8.4.5 demonstrate the potential improvement in NO and TFN reduction due to the inclusion of a promoter at finite mixing times characteristic of real combustion systems.

Effect of Delay Time. To better understand the temperature dependence of promoted AR-Rich, variations were run varying the delay time with a fixed mixing time of 30 ms and NSR=1.0. Cases were run with NH_3 only, with NH_3+50 ppm Na_2CO_3, with 50 ppm Na_2CO_3 only, and with no additives (basic reburning). The delay time was varied from 0 s (co-injection with the reburning fuel) to 1 s.
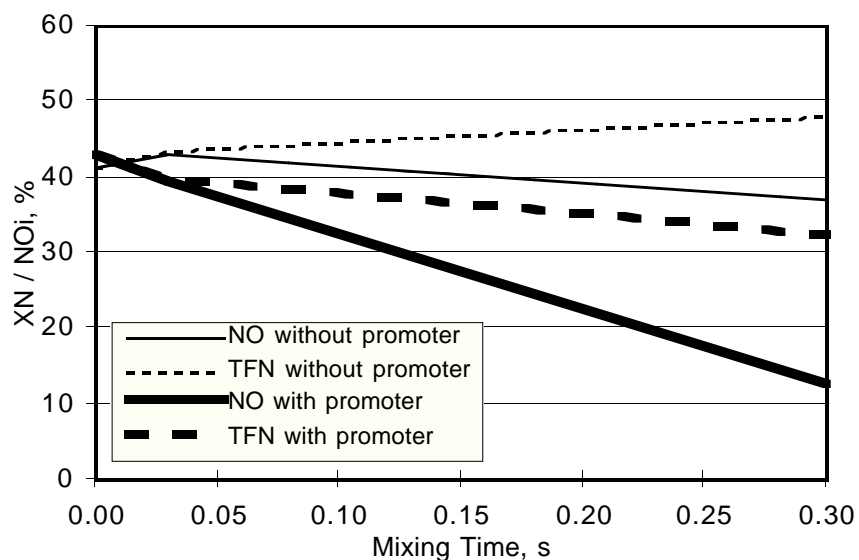
Figure 8.4.4. NO and total fuel nitrogen before burnout for AR-Rich vs. mixing time. NH_3 added at NSR = 1.0 with and without 50 ppm Na_2CO_3 promoter.
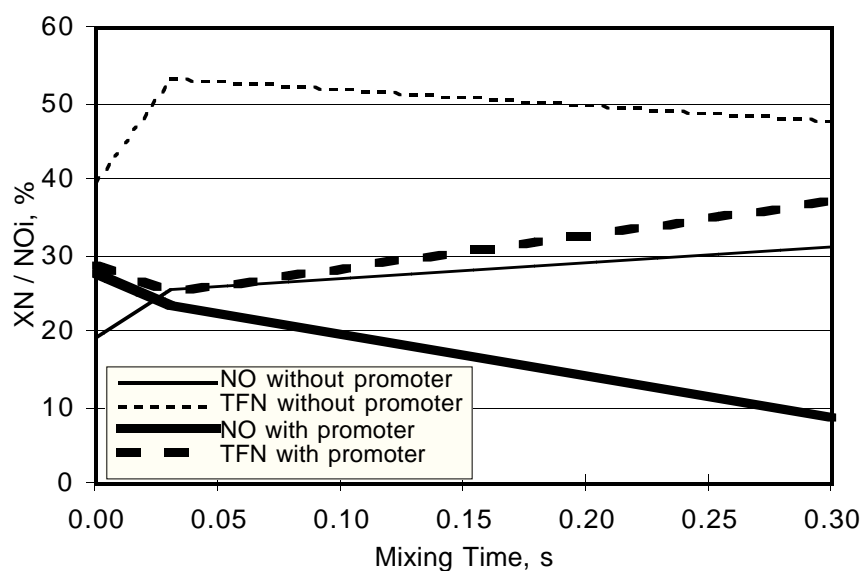
Figure 8.4.5. NO and total fuel nitrogen before burnout for AR-Rich vs. mixing time. 800 ppm NH_3 added (NSR approximtely 1.5), with and without 50 ppm Na_2CO_3 promoter.

Figure 8.4.6 and 8.4.7 respectively show the NO and TFN concentration just before the addition of OFA at 1300 K. TFN includes all nitrogen-containing species except N_2, weighted by the number of N-atoms. From these curves there is an obvious difference due to the addition of promoter along with NH_3, considerably broadening the interval over which high levels of NO_x reduction are achieved. Figure 8.4.8 shows the final concentration of NO after OFA addition and completion of burnout, at 600 K. There is very little TFN other than NO at this point, so a TFN plot would appear the same. Comparing with Figure 8.4.6, it is seen that NO has improved for the case with N-agent and promoter added, particularly at late delay times. However, there is relatively less improvement due to burnout for the case in which N-agent is added without promoter.

Figure 8.4.8 indicates a very broad optimum for delayed addition of $NH_3+Na_2CO_3$. The optimum delay time for NO reduction is at about 0.4 s. However, the maximum effect of Na addition (that is, the greatest difference between Reburn+NH_3 and Reburn+NH_3+Na_2CO_3 results) is at somewhat higher delay times. To better understand the role of sodium promotion at a condition where the effect is maximized, the cases with delay times of 0.5 s were selected for further analysis. The kinetic curves for 0.5 s delay, with and without Na promoter, are shown in Figure 8.4.9.

Results at 0.5 s delay (shown in Figure 8.4.8), compared with those at 0.1 s delay (shown in Figure 8.4.2) provide a picture of the effect of sodium under conditions where it has a significant impact (at 0.5 s) versus conditions where the impact is minor (0.1 s), consistent with results in Figures 8.4.6 through 8.4.8. At 0.5 s, Figure 8.4.8 shows that the NH_3 concentration stays high in the AR-Rich zone, compared with it's fairly rapid decline at 0.1s. This may be attributed to the reduced temperature at which the NH_3 is added. Without promoter present, the radical populations at 0.5 s are also very low, and so NH_3 and NO coexist without reacting. The addition of promoter at these conditions increases the radical population, allowing NH_3 to react with NO while the radicals persist in adequate concentrations.

Table 8.4.1 provides a summary of the parameters and results of the promoted and unpromoted AR-Rich cases at 0.1 s and 0.5 s delay time. These conditions have been labeled as Cases 1 through 4, and are analyzed for further insight into the chemical basis for the differences between them. Table 8.4.1, in conjunction with Figures 8.4.2 and 8.4.9 with the corresponding kinetic curves, shows an important correlation between TFN species (NO and NH_3) and radicals (OH an H). All cases have similar NO concentrations just prior to N-agent injection.
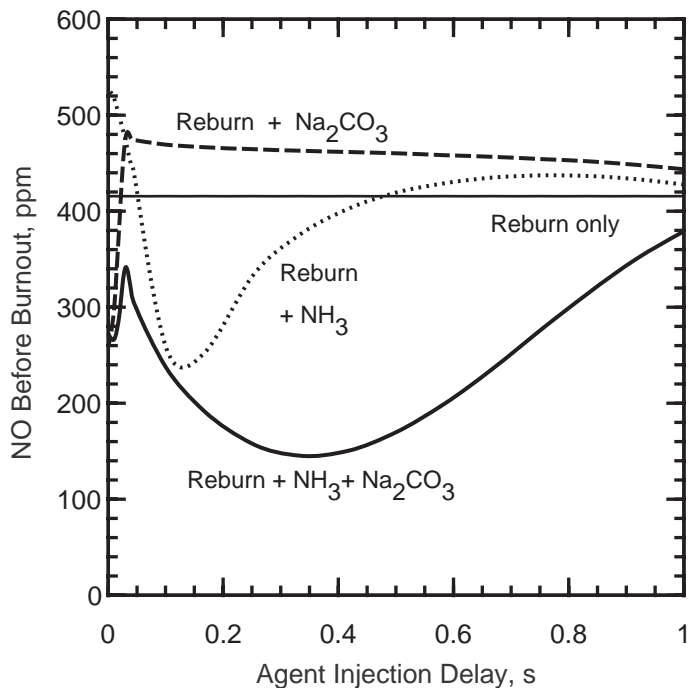
Figure 8.4.6. NO concentration prior to start of overfire air injection at 1300 K, as a function of N-agent/promoter injection delay time.
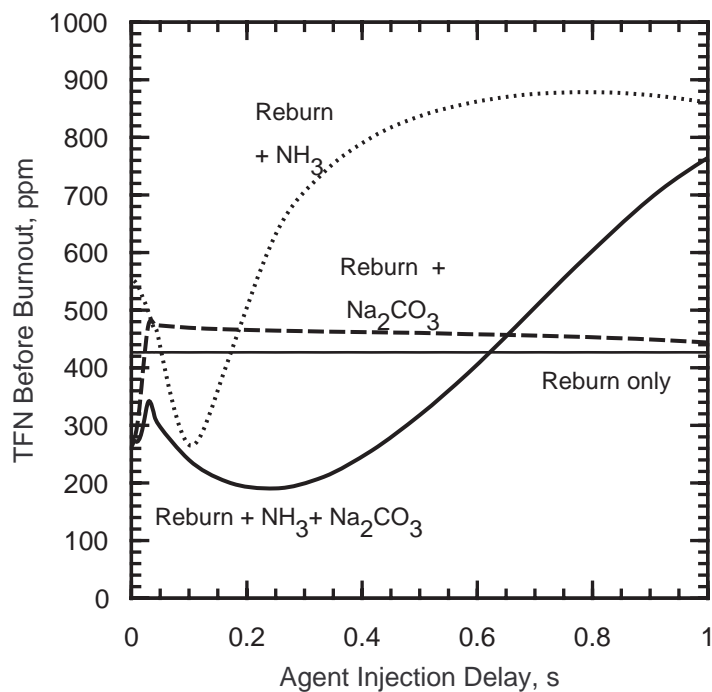
Figure 8.4.7. TFN concentration prior to start of overfire air injection at 1300 K, as a function of N-agent/promoter injection delay time.
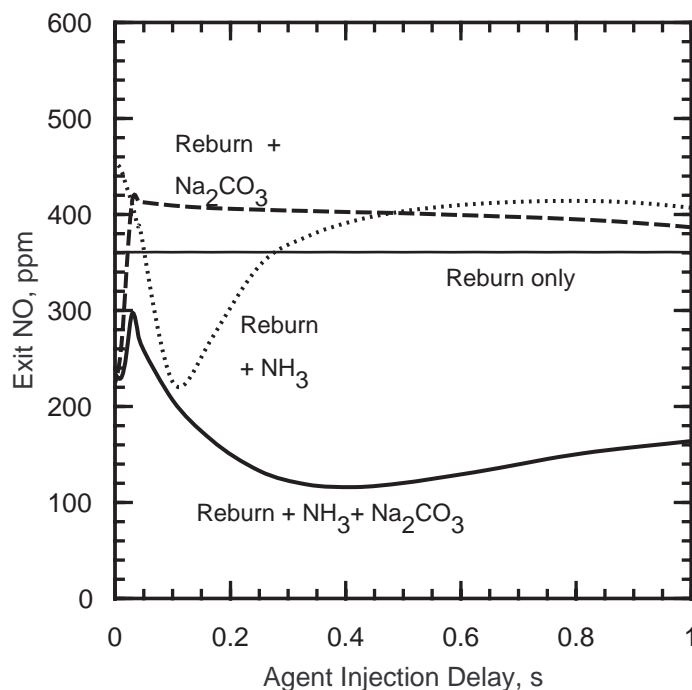
Figure 8.4.8. Final NO concentration at 600 K, as a function of N-agent/promoter injection delay time.

Cases 1 and 2 represent a delay of 0.1 s between the injection of reburn fuel and N-agent, with and without sodium added to the NH_3. For these cases, the OH and H concentrations are relatively high before injection, and are still several ppm at 0.1 s after N-agent injection, but have dropped an order of magnitude from the pre-injection values and are rapidly declining. NH_3, which is added in the same amount as NO at the point of injection (so that NSR=1.0), is also rapidly declining. As a result, these species are only available to react with NO over a limited time, and by 0.1 s after the start of injection most of the ultimate NO reduction is achieved. The remaining rich zone residence time is not as effectively utilized because the necessary reactants are not available in the proper quantities.

The presence of sodium (Case 1) appears to enhance this trend somewhat, compared to the same conditions without sodium (Case 2). After 0.1 s, somewhat higher concentrations of OH, H and NH_3 are present for Case 1 than at the same point in Case 2, and NO reduction is more effective in this interval. As shown in Figure 8.4.2, in the remainder of the rich zone OH and H decline more rapidly and NH_3 less rapidly with sodium than without. However, sodium is unable to provide any

8-70

Table 8.4.1. Results of AR-Rich at Different Delay Times.

Case	1	2	3	4
Injection Conditions				
Delay time (s)	0.1	0.1	0.5	0.5
Temperature (K)	1670	1670	1550	1550
Na_2CO_3 added (ppm)	50	0	50	0
Concentrations (ppm)				
Just Before NH_3 added				
NO	490.	490.	473.	473.
OH	111.4	111.4	9.7	9.7
H	20.3	20.3	2.6	2.6
0.1 s after start of NH_3 Addition				
NO	284.	342.	309.	429.
NH_3	59.	52.	287.	423.
OH	15.	11.	2.8	0.06
H	3.2	2.4	0.9	0.02
Before OFA added				
NO	243.	274.	168.	420.
NH_3	1.3	0.3	140.2	413.8
After burnout				
NO	210.	237.	121.	403.
NH_3	<0.001	<0.001	0.02	<0.001

Notes: Delay time is defined as time from start of Reburn Fuel injection
to the start of NH_3 injection
For all cases, mixing time is 30 ms for all injected streams, and SR2 = 0.99.
NSR = 1.0 based on NO concentration at point of NH_3 injection.
Na_2CO_3, when added, is always premixed with the added NH_3.
Temperature profile is -300 K/s from start of reburn fuel addition at 1700 K.
Initial (primary zone) NO before reburn fuel injection is 606 ppm for all cases.
OFA is added at 1300 K in all cases.

beneficial effect without a sufficient amount of NH3. The resulting NO reduction in the last part of the reburning zone (after 0.1 s) is less with sodium than without. The net effect of sodium promotion in this case, however, is a modest improvement of 30 ppm in NO removal, by increasing NO destruction rates at earlier times, where the reaction is most effective.

These results imply that at the high temperature conditions of Case 1, that increasing the quantity of NH3 added would beneficial, particularly in the presence of sodium. The more N-agent present in

50 ppm Na$_2$CO$_3$ added with NH$_3$

NH$_3$ added without sodium
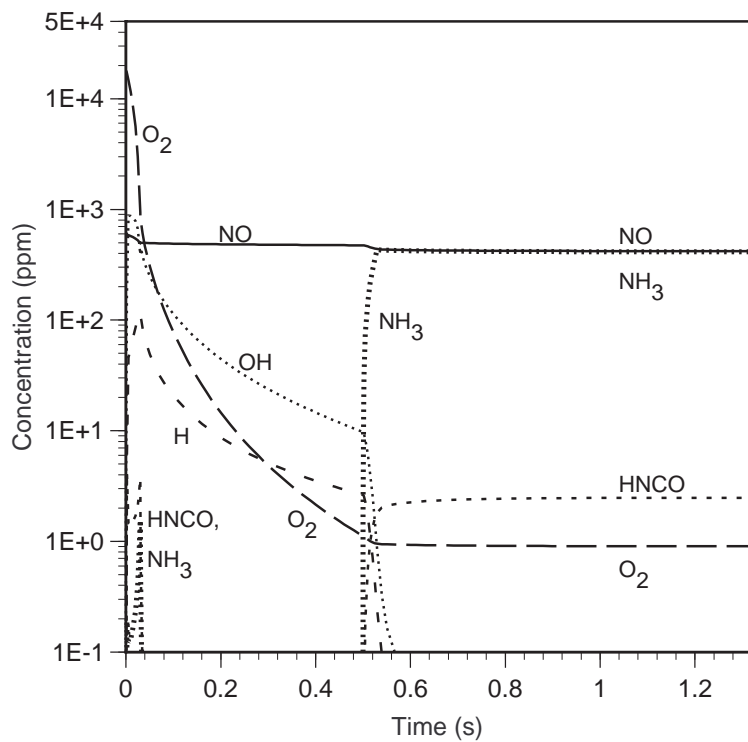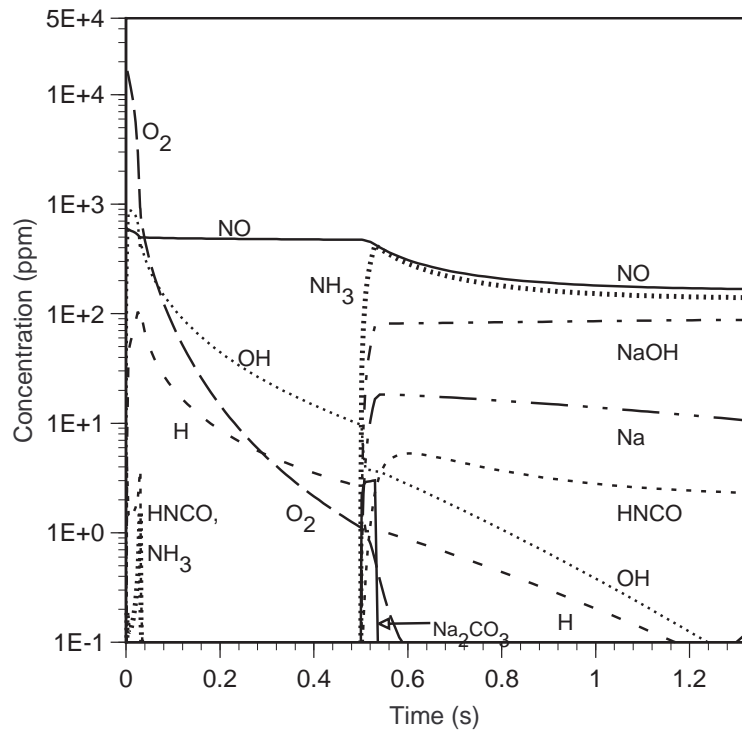
Figure 8.4.9. AR-Rich kinetic curves with 30 ms mixing from the point of reburn fuel injection with NH$_3$ (NSR = 1) injected after 0.5 s.

the initial, fast-reaction interval, the more NO reduction may be expected. Further, under these conditions, particularly with sodium added, NH_3 is effectively destroyed in the last part of the reburning zone, so that little ammonia slip would be expected even at higher NSR's. This approach provides a means of improving AR-Rich performance at higher injection temperatures. Comparison of Figures 8.4.4 and 8.4.5 supports this hypothesis and also indicates that it is true over a wide range of mixing times as well.

Cases 3 and 4 represent a delay of 0.5 s between the injection of reburn fuel and N-agent, with and without sodium added to the NH_3. In these cases, the OH and H concentrations are not as high before injection as in Cases 1 and 2. In Case 3, in which sodium is included, OH and H have decreased after 0.1 s, but not as quickly as in Cases 1 and 2, and are still present in quantities on the order of 1 ppm. After 0.1 s in the presence of sodium, NH_3 has not declined as much as in Case 1. NO also declines somewhat less in the first 0.1 s, but continues to decline over the remainder of the rich zone and achieves a lower final concentration (168 ppm) than for Case 1 (243 ppm). The TFN at the end of the rich zone for Case 3 is high because NH_3 is still present in substantial quantities. However, this TFN is effectively burned out when OFA is added at 1300 K, as indicated by Figures 8.4.7 and 8.4.8.

In Case 4, OH and H decrease to very low concentrations (0.06 and 0.02 ppm) in the first 0.1 s from the start of NH_3 injection, while NO and NH_3 have declined only by about 50 ppm. In the remainder of the rich zone, NO and NH_3 decline by only about another 10 ppm. Apparently the concentration of radicals was inadequate to sustain reactions of NO and NH_3 in the rich zone. Although burnout does reduce the high level of rich zone TFN, the final NO is still on the order of 400 ppm as shown in Figure 8.4.8.

These results show the importance of maintaining the proper concentrations of important reactants for effective NO reduction. High initial levels of NH_3 and radicals promote rapid initial reduction, but the NO reduction rate is not sustained if the NH_3 concentration declines too quickly, as in Cases 1 and 2. In Case 4, it is seen that a sustained high level of NH_3 is also ineffective if radicals are not sustained in sufficient quantities. Case 3 represents the most desirable situation: even though the initial radical levels are the same as for Case 4, in the presence of sodium the radicals are sustained

at those levels for a longer time. Even though the initial reaction rate is slower in Case 3 than Case 1, it is effective for a longer time and results in better overall performance.

The implication of these observations is that NO reduction is optimized by sustaining radical populations at the proper concentrations to maintain a steady rate of reaction of NO with NH_3 and its decomposition products. In these cases, sodium is only partially successful at short delay times/ higher temperatures, but is very successful at longer delay times/lower temperatures.

Sensitivity Analysis. The results shown so far strongly imply a correlation between radical concentrations and NO-NH_3 chemistry, but do not show what specific reactions are involved. Analysis of sensitivity and contribution factors, as discussed in Section 8.2, provides specific information about the relative importance of different reactions in the mechanism. This analysis has been performed for Cases 1 through 4 defined in Table 8.4.1, examining the rich zone from the end of NH_3/Na_2CO_3 injection to just before OFA injection at 1300 K.

Contribution factors for all four cases show the same predominant reactions involving NO as discussed earlier (see Figure 8.2.21). Reaction (280) and the combined Reaction (281+282) dominate NO removal:

$$NH_2 + NO \quad <=> \quad N_2 + H_2O \qquad\qquad\qquad (281+282)$$

$$NH_2 + NO \quad <=> \quad NNH + OH \qquad\qquad\qquad (280)$$
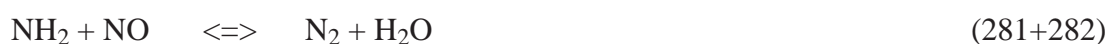
Opposing these, the reverse of Reaction (211) is the predominant source of NO formation during the fast reaction stage:

$$HNO + M \quad <=> \quad H + NO + M \qquad\qquad\qquad (-211)$$

At the lower temperatures corresponding to longer delay times (Cases 3 and 4), Reaction (-211) has smaller effect relative to Reactions (280-282) than at higher temperatures. This indicates that NO formation reactions, which compete with the NO removal process, are less effective at lower temperatures.

Sensitivity analysis for the four cases shows that Reactions (280-282) are also among the most important from a sensitivity perspective. The net effect of Reaction (281-282) generally dominates, with a net negative impact on NO (that is, an increase in the rates of reactions (281-282) increases the rate of NO reduction).

In Case 1, the sensitivity impact of Reactions (280-282) is opposed significantly, particularly after the initial fast NO reduction period, by Reaction (202):

$$NH_2 + OH \quad <=> \quad NH + H_2O \hspace{4cm} (202)$$

This reaction acts as a chain termination step because it converts NH_2 to NH, which is less reactive in NO reduction.

A review of sensitivity coefficients for several species in the mechanism, under conditions where sodium is added (Cases 1 and 3), indicate that Reaction (327) has the most significant effect among the reactions involving sodium, and that Reaction (326) is important as well. This combination of reactions is believed to be especially significant because of its impact on the radical pool:

$$NaOH + H \quad <=> \quad Na + H_2O \hspace{4cm} (326)$$

$$Na + OH + M \quad <=> \quad NaOH + M \hspace{3.5cm} (327)$$

The net effect of these two reactions acting together is $H + OH <=> H_2O$. If both reactions proceed forward, they are removing OH and H radicals, and if both proceed in reverse they contribute these radicals. While these reactions are significant among the reactions of sodium whose presence has a significant impact on NO reduction, they do not show the largest sensitivity factors. This reflects the nature of these reactions as moderating the fast-reacting radical species, rather than reacting directly with the high concentration, slowly reacting species such as NO and NH_3.

In both Cases 1 and 3, Reactions (326-327) both proceed in the reverse direction, thus boosting the radical pool by converting H_2O to OH and H. In Case 1, their rates diminish rapidly after about 0.1 s following the end of N-agent addition, while in Case 3 they also diminish with time but less

rapidly, as is the case for most of the other significant reactions. These observations are consistent with the correlations between radical and NO/NH$_3$ histories discussed above.

8.4.2 Effect of Sodium Promotion in AR-Lean

Effect of Injection Temperature. To better understand the effect of co-injecting sodium with Nagent in AR-Lean, the kinetic models (ODF and SENKIN) have been used to predict behavior at different injection locations with and without sodium. The modeling approach for these calculations are similar to those for the results just presented for AR-Rich. Many of the input parameters are the same: SR$_2$=0.99, and mixing time 0.03 s for all injections. The temperature profile is -300 K/s to a final exit temperature of about 600 K. The chief difference is that in this case the OFA injection location is varied, and the delay time for the start of NH$_3$ injection is 0.1 s after the start of OFA injection in all cases. This is consistent with results shown earlier (for example, Figure 8.2.16) which indicate an optimum delay time at about 0.1 s.

The amount of NH$_3$ added was fixed at 394 ppm for all cases presented here. This corresponds to NSR=1.0 for OFA injection at 1400 K. At higher injection temperatures, the resulting NSR will be slightly lower, and vice versa, due to the corresponding change in NO at the injection point. Over the range of OFA injection temperatures considered, NSR ranges between 0.9 and 1.5. Adjusting the NH$_3$ injection to a uniform NSR would not be expected to change the trends in the results presented here.

Figure 8.4.10 shows the impact of promotion on the exit NO for each case. The predominant effect of sodium injection is a horizontal shift in the curves. For temperatures higher than about 1330 K, including the promoter has a beneficial effect on final NO, but at lower temperatures the addition of sodium actually increased NO relative to AR-Lean at the same conditions without sodium.

The trend in exit NH$_3$ is similar to that for SNCR. For injection temperatures higher than a few degrees above the optimum for NO reduction, exit NH$_3$ is negligible. As injection temperature decreases to temperatures just below the optimum, NH$_3$ increases rapidly, asymptotically approaching the injected concentration. As for SNCR, practical AR-Lean systems should be designed to ensure temperatures on the high side of the optimum value for NO reduction alone, to avoid ammonia slip.
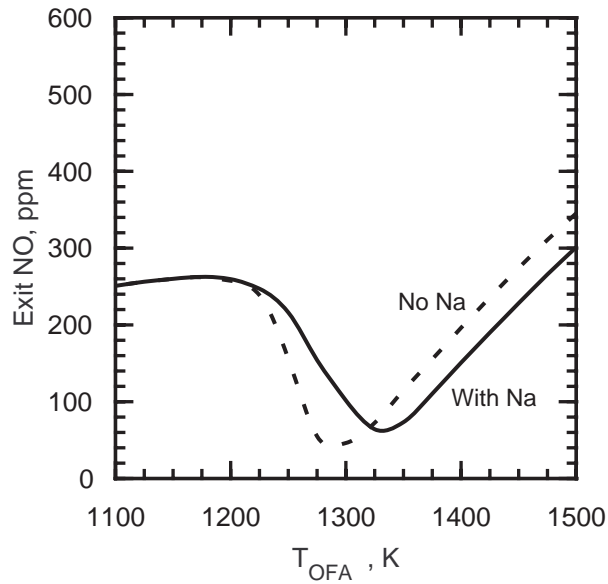
Figure 8.4.10. Effect of promoter on NO exit concentrations for AR-Lean.

The next step is to understand why this upward temperature shift is predicted. For this purpose, four cases were selected for additional analysis, for two injection temperatures with and without promoter. The two conditions selected are designed to maximize the difference due to promotion, negative in one case (lower injection temperature) and positive in the other. The cases selected are presented in Table 8.4.2, along with predicted concetrations at specific locations. Cases 1 and 2 represent OFA injection at 1280 K (near the optimum for unpromoted AR-Lean). Cases 3 and 4 represent OFA injection at 1380 K (near the optimum for promoted AR-Lean). Cases 1 and 3 inject 50 ppm Na_2CO_3 with the NH_3, which Cases 2 and 4 add no sodium.

Figure 8.4.11 shows the kinetic curves for some of the most important species for Cases 1 and 2, to show the effect of sodium for OFA injection at 1280 K. The most notable difference between these two cases is the faster initial decay rates in the presence of sodium for a number of species including NO, NH_3, CO, OH, NO_2, and N_2O (the latter two decaying substantially with promoter but persisting in ppm levels without it). On the other hand, NO, NH_3, and H_2 persist in higher levels in the presence of promoter, consistent with the reduced performance predicted for 1280 K OFA injection. Furthermore, note that after initial conversion to NaOH, sodium is reconverted to Na_2CO_3 in Case 1, effectively eliminating it's effectiveness for reactions involving radicals.

Table 8.4.2. Results of AR-Lean at Different Injection Temperatures, with and without sodium.

Case	1	2	3	4
Injection Conditions				
T at start of OFA injection (K)	1280	1280	1380	1380
T at start of NH_3 injection (K)	1250	1250	1350	1350
Na_2CO_3 added (ppm)	50	0	50	0
Concentrations (ppm)				
Just Before NH_3 added				
NO	353.	353.	388.	388.
OH	9.4	9.4	17.8	17.8
H	0.001	0.001	0.003	0.003
0.03 s after start of NH_3 Addition				
(End of Mixing Zone)				
NO	269.	254.	242.	232.
NH_3	303.	290.	187.	160.
OH	2.	3.2	15.	22.
H	0.007	0.015	0.033	0.068
0.1 s after start of NH_3 Addition				
NO	196.	119.	141.	167.
NH_3	224.	141.	27.	2.
OH	0.8	2.9	10.	18.
H	0.002	0.005	0.003	0.004
Exit (at 600 K)				
NO	146.	52.	121.	165.
NH_3	173.	64.	0.02	0.
NO_2	0.01	7.	1.	1.
N_2O	<0.001	7.	0.01	4.

Notes: Delay time is 0.1s from start of OFA injection in all cases.

                For all cases, mixing time is 30 ms for all injected streams, and $SR_2 = 0.99$.

                394 ppm NH3 added in all cases (NSR = 1.0 to 1.1)

                Na_2CO_3, when added, is always premixed with the added NH_3.

                Temperature profile is -300 K/s from start of reburn fuel addition at 1700 K.

                Initial (primary zone) NO before reburn fuel injection is 606 ppm for all cases.

50 ppm Na$_2$CO$_3$ added with NH$_3$

NH$_3$ added without sodium
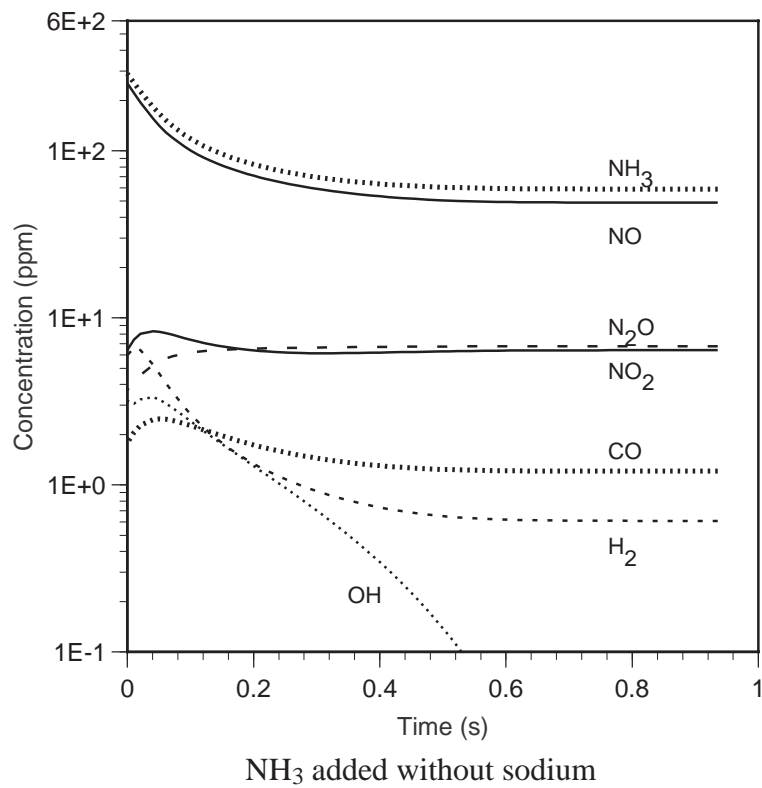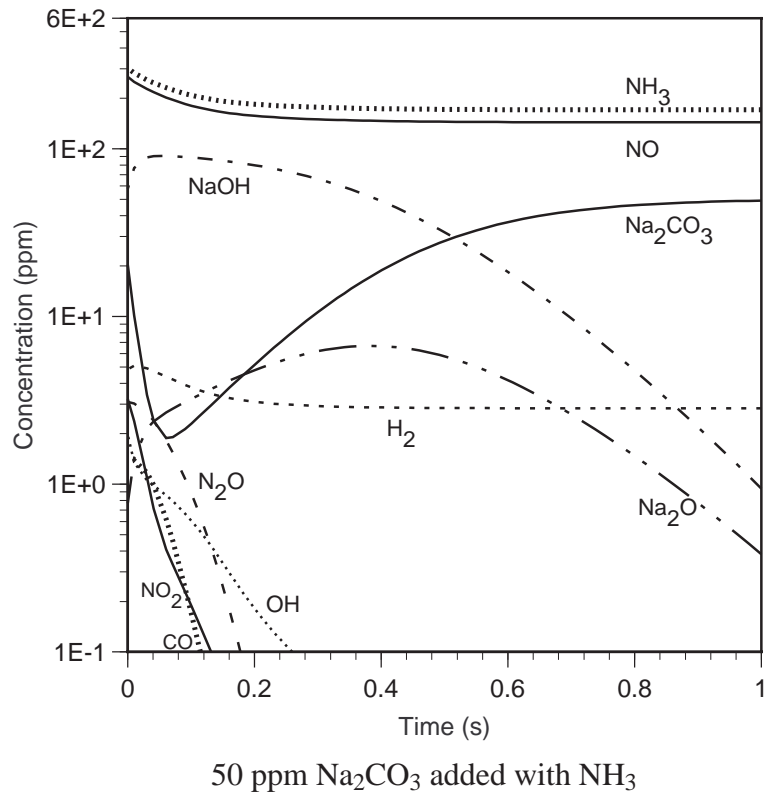
Figure 8.4.11. AR-Lean kinetic curves with 30 ms mixing from the point of NH$_3$ injection, which is 0.1 s after OFA injection at 1280 K.

Figure 8.4.12 shows the kinetic curves for Cases 3 and 4, to show the effect of sodium for OFA injection at 1380 K. These curves show faster decay for many species (notably excepting NH_3 and H_2) in the presence of promoter. The initial decay rate for NO appears to be similar with and without promoter for about the first 20 ms. The difference in NO appears to occur over the time span from about 20 to 200 ms, during which NO decay continues (albeit at a reduced rate) with promoter, but essentially stops without it. These time scales appear to reflect the difference in decay time of NH_3. As previously discussed for AR-Rich, an important element in the sodium promotion mechanism is persistence in the availability of the N-agent (or intermediate species generated by it).

The NO concentration immediate after the end of N-agent injection (0.03 s) is better without promoter, for both injection temperatures. At the lower temperature, the gap widens, while at the higher temperature the promoter eventually results in lower NO and TFN at the exit. As for the optimum case in AR-Rich, the beneficial effect in sodium addition lies in the prolonging of significant NO reduction rates over a longer interval in the NH_3 reaction zone.

Sensitivity Analysis. The ODF results immediately following the end of N-agent mass addition was used as the initial condition for SENKIN sensitivity calculations. This analysis provides further insight into the source of the differences between these cases.

Comparing the NO contribution and sensitivity factors, it is seen that reactions 280, 281 and 282 are the most significant reactions in all cases. All of these reactions involve NH_2+NO, with final products NNH+OH for Reaction (280) and N_2+H_2O for Reactions (281-282).

Other reactions with significant sensitivity effects include reaction (38) and (202):

$$H + O_2 \quad <=> \quad O + OH \tag{38}$$

$$NH_2 + OH \quad <=> \quad NH + H_2O \tag{202}$$

Reaction (38) has a negative influence at the lower temperature and (after an initial negative transient) a positive influence on NO at the higher temperature. Reaction (202) has a notable positive sensitivity effect on NO at the higher temperature, as it competes with other NH_2 reactions (280-282) which

50 ppm Na$_2$CO$_3$ added with NH$_3$

NH$_3$ added without sodium
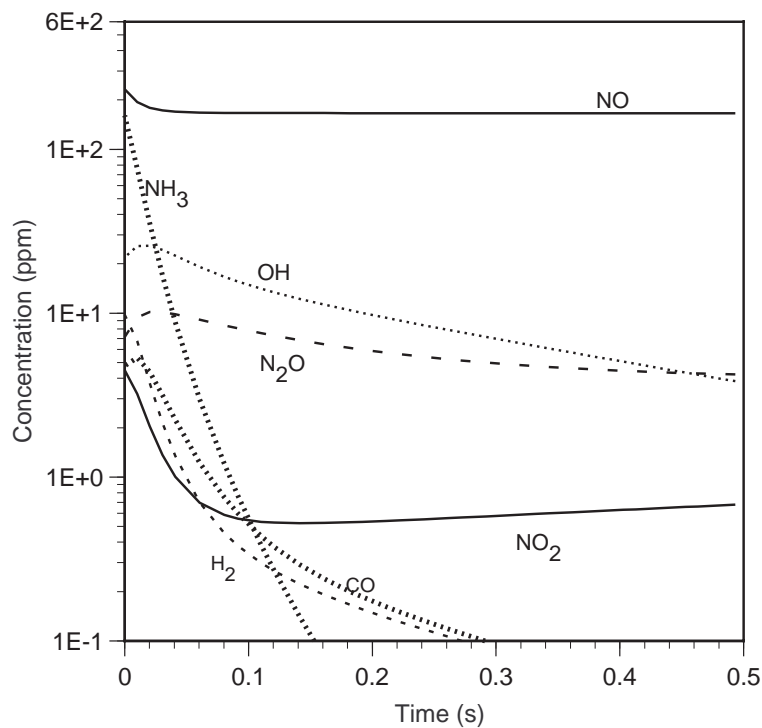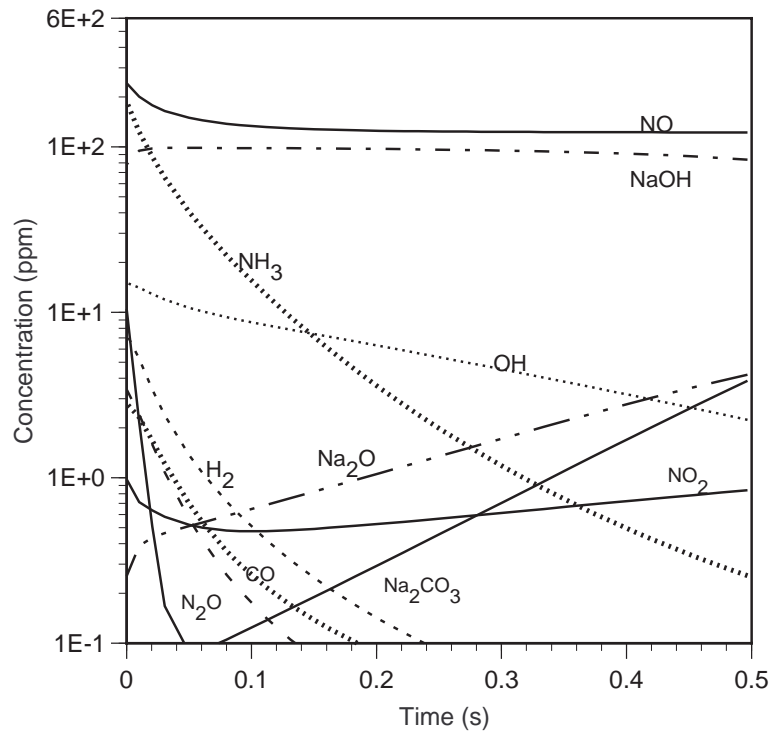
Figure 8.4.12. AR-Lean kinetic curves with 30 ms mixing from the point of NH$_3$ injection, which is 0.1 s after OFA injection at 1380 K.

8-81

remove NO, and at the same time converts NH_2 to less reactive NH.

The importance of radicals in the NO removal mechanism begins with the removal of NH_3, which is dominated by Reaction (277):

$$NH_3 + OH \quad <=> \quad NH_2 + H_2O \tag{277}$$

Therefore, the availability of OH controls the rate of NH_3 reaction. It is NH_2 which predominates in reactions (280-281) which remove NO, and so control of the rate of NH_3 affects the availability of NH_2.

For both cases with sodium, the Na reactions with the largest contribution effect for NO is (323)

$$NaO + NO = Na + NO_2 \tag{323}$$

The contribution to NO is positive, indicating that the reaction is proceeding in reverse. The sodium reaction with the greatest sensitivity is (326)

$$NaOH + H = Na + H_2O \tag{326}$$

. In fact, reaction (326) is also the most significant sodium reaction for several other species, including NH_3 and NH_2. Reaction (326) shows positive sensitivity for NO at all times in Case 1, while for Case 3, it peaks positive at about 20 ms, then declines and goes negative. In other words, NO formation is favored by Reaction (326) in Case 1, but NO destruction is favored by Reaction (326) for most of Case 3. This is consistent with the positive and negative influence of the presence of sodium in those cases.

Having identified reactions with major contribution and sensitivity influences, a more complete picture of the role of sodium may be drawn. The initial steps of the sodium mechanism can be summarized by Reactions (317-319):

$$Na_2CO_3 \quad <=> \quad Na_2O + CO_2 \tag{317-318}$$

$$Na_2O + H2O \quad <=> \quad 2\ NaOH \tag{319}$$

Since Reaction (317) is the only one involving Na_2CO_3, it is seen that Na_2CO_3 is ineffective at managing the radical pool, adding to the ineffectiveness of sodium at later times in Case 1, when Na_2CO_3 is the dominant species.

When NaOH is available, it reacts predominantly through Reaction (326) to remove H:

$$NaOH + H \quad <=> \quad Na + H_2O \tag{326}$$

If reaction (327)

$$Na+OH+M<=>NaOH+M \tag{327}$$

is running in the same direction, it works with Reaction (326) to either recombine H + OH into H_2O, or in reverse to increase these radicals. In Case 3, both reactions move forward, while in Case 1 they oppose each other. In both cases, the rate of (326) is larger in magnitude. Its main importance may lie in the indirect influence of the OH concentration through other reactions such as Reaction (38):

$$H + O_2 \quad <=> \quad O + OH \tag{38}$$

By reducing the concentration of H, Reaction (326) slows Reaction (38) and therefore reduces the availability of OH. Other sodium reactions affect the radical pool, but to a lesser extent than (326). However, at the higher temperature the OH concentration is much higher, resulting in more rapid and complete NH_3 destruction than at the lower temperature, where a significant NH_3 concentration persists.

When NH_3 removal is incomplete (as for 1280 K OFA injection), the reduction of NH_3 at early times is all that contributes to NO removal, so faster NH_3 removal during that time period is more beneficial to NO reduction. When NH_3 removal is complete (as for 1380 K OFA injection), then

spreading it out over a longer time provides a more consistent stream of reactants to reduce NO, and so is able to do so more effectively. The role of sodium in slowing NH_3 removal rates appears to be the primary difference in the behavior for 1280 K versus 1380 K OFA injection.

8.5 Summary of Modeling Studies

The GRI-Mech combustion mechanism has been extended based on literature and experimental data to include SNCR chemistry, as well as reactions involving compounds of Na, S, and Cl. The sodium mechanism has been used to evaluate the performance of AR-Rich and AR-Lean scenarios, promoted by Na_2CO_3.

The individual AR injection processes have been investigated using one-dimensional chemical kinetics models, to determine their behavior over time and as a result of parametric variations. Analysis of sensitivity and contribution factors identifies specific reactions in the mechanism which affect the results.

Analysis of the basic reburning process revealed an initial fast NO reduction zone followed by a longer, slower NO reduction zone. This provides an opportunity for improvement through AR-Rich, by enhancing the rate of reaction in the latter zone.

The effect of ammonia in both AR-Rich and AR-Lean was investigated. In both cases, it is possible to optimize NO reduction with respect to the injection temperature and/or delay time of N-agent injection. Optimization of the amount of N-agent is also important to system performance. The quantity must be adequate for the degree of NO reduction but more is not necessarily better. Designing the injection system to promote uniform mixing should help minimize the quantity of N-agent needed but the performance also depends on the characteristic time of mixing. The NSR and mixing time both affect the net NO reduction as well as the net concentration of other TFN species. In most cases, the trend is toward better performance at longer mixing times, which implies that the results at full scale should be able to at least match pilot scale experimental results. The chief drawback of larger scales is increased potential unmixedness of the reburn fuel, as well as N-agents with flue gas. This may create zones with too high and too low SR_2 that will reduce AR performance.

The effect of promoters was also investigated. First, the effect and influence of various types of promoting species, including radicals, was considered. Later, more attention was paid to the use of specific promoters of current interest for field implementation, notably Na_2CO_3. In AR-Rich the effect of Na_2CO_3 is to broaden the range of injection locations with good NO reduction performance. In AR-Lean, the primary effect is to shift the optimum in NO reduction to higher temperatures.

Sodium promotion can improve AR-Rich performance by sustaining the radical pool when it is needed. As for unpromoted AR, this effect is most pronounced in systems with long characteristic mixing times, and so promoted advanced reburning continues to show promise for commercial implementation. Similarly, sodium promotion can improve AR-Lean, in this case by limiting the radical pool to moderate the reaction rate of NH_3.

In both AR-Rich and AR-Lean, it should be noted that optimization involves managing both the concentrations of important species (such as NH_3 and OH), and their rate of removal. Generally, concentrations and rates which are too high are undesirable as well as those which are too low. In general, optimum solutions tend to be those with slow but steady NO removal using as much of the reaction zone as possible.

9.0 DESIGN METHODOLOGY AND APPLICATION

This task was included in the project to provide a conduit for translation of the analytical and experimental SGAR configurations into practical full scale designs. The task includes the extension of EER's reburning design methodology to AR and SGAR configurations and the evaluation of SGAR economics and market potential for US utility boilers. The original work scope for this task was based on use of a hypothetical case study. However, it was hoped that an initial AR demonstration could be developed in parallel with Phase I (outside the scope of this DOE project) and could be used to evaluate some of the elements of SGAR during the later portion of Phase I and in Phase II.

EER has been successful in developing an initial AR demonstration project. In 1995 EER installed the original AR configuration (now termed AR-Lean) on a 105 MW tangentially fired boiler. Accordingly, this unit was used as the basis for extending the design methodology. Testing is being conducted in three phases during the summer of 1996, 97, and 98. In this task, this unit was used as a case study for extending the reburn design methodology to SGAR. It also was used to test some elements of the various SGAR configurations during summer 1997. If the project proceeds through Phase II, additional elements will be tested in 1998.

The following section describes the extension of EER's reburning design methodology to AR and SGAR. The general approach is outlined and then applied to the 105 MW tangentially fired demonstration unit. Section 9.2 discusses the application of AR-Lean to this unit which was conducted as part of a separate project, and the initial testing of some SGAR elements. Finally, Section 9.3 discusses the application of SGAR to the US utility industry including the regulatory drivers, economics and market potential.

9.1 AR Design Methodology

9.1.1 General Approach

EER's general methodology for application of AR technologies to utility boilers is shown in Figure 9.1.1. The design methodology uses various experimental and analytical tools to develop the injector specifications and operating characteristics of the AR system with the objective of meeting specific process requirements for optimum emissions control performance while maintaining boiler operation and performance at normal levels. The primary elements of the methodology consist of:

- Collection of system design and operating data to quantify the characteristics of the

full-scale system, and to obtain data for use in model set up and calibration. This information typically includes the range of typical operation, specific unit limitations that should be taken into account in the design, and emissions controls requirements.

- Heat transfer modelling of the unit to predict the boiler's thermal characteristics as functions of various input and operational variables. This analysis is focussed on studying the impacts of the process on boiler performance, and on identification of possible remedies for any adverse impacts which are expected to occur.

- Isothermal flow modelling of the unit to simulate the full-scale furnace flow field, and to optimize the injection parameters of the reburning/AR systems. A key objective of the flow model studies is to develop injection systems which provide rapid and uniform mixing of the reburning fuel, OFA, and N-agents.

- Development of performance predictions for full-scale applications of the reburning process using process and kinetic models developed from the results of subscale tests and the fundamental chemistry involved in the process. Model predictions under ideal mixing conditions are used in conjunction with the results of isothermal model mixing studies to assess the impacts of mixing on reburning/AR performance.
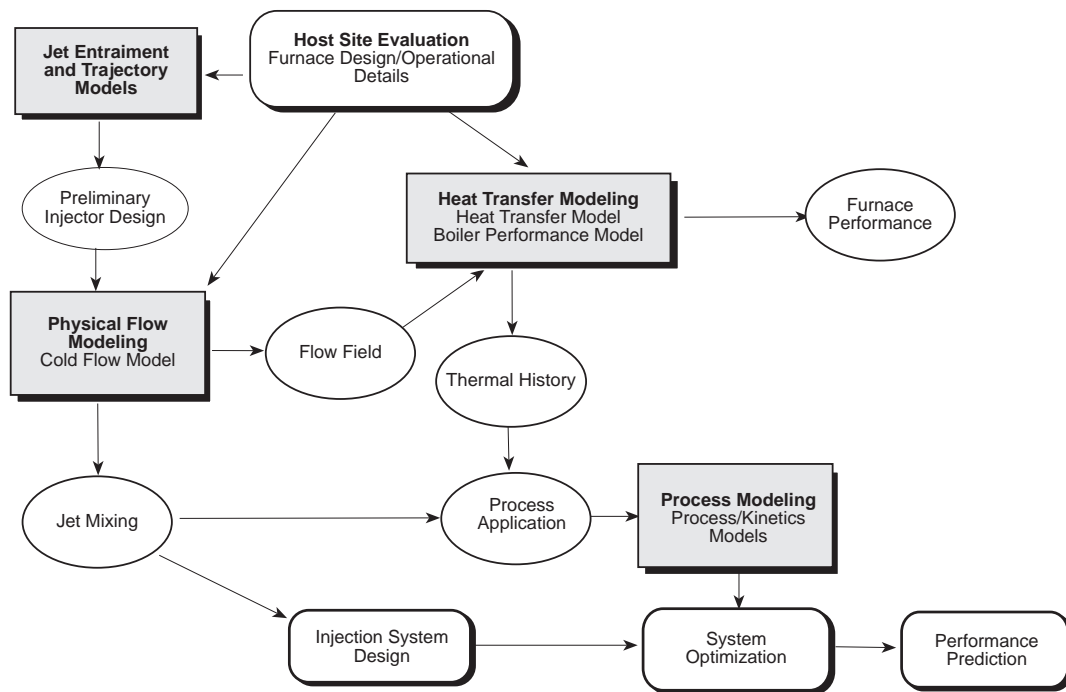
Figure 9.1.1 Generalized design methodology for AR technologies.

This design methodology has been used to scale up and apply reburning and AR technologies to utility boilers. In this task of the project,the methodology was updated to take into account the specific requirements of the AR systems. To demonstrate the applicability of the final methodology, it was applied to a typical 100 MW coal-fired utility boiler with tangentially firing burners, resulting in development of conceptual designs for several second generation AR systems, and predictions of their impacts on boiler NO_x emissions and operating performance.

9.1.2 Case Study Boiler Characteristics

The boiler used for the case study analysis was NYSEG's Greenridge 105 MWe unit manufactured by Combustion Engineering. The boiler is a tangentially fired, radiant, single drum unit typical of pre-NSPS boilers. A schematic detailing the major components of the boiler is shown in Figure 9.2.1. The boiler is rated for 97.52 kg/s of superheated steam and 73.21 kg/s of reheat steam. Superheated steam temperature control is provided by means of burner tilt control and desuperheater sprays. Reheat outlet steam temperature is primarily maintained by means of burner tilt control.
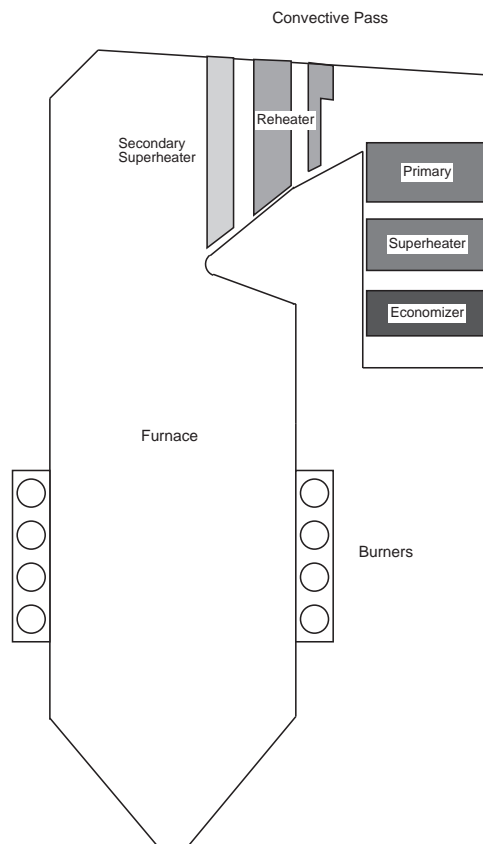
Figure 9.1.2 Schematic of case study boiler.

The unit is currently fired with the eastern bituminous coal which has a higher heating value of 29.94 J/kg. Four bowl type mills pulverize the coal to a maximum fineness of 83 percent through a #200 U.S.S. sieve. The pulverized coal is transported by heated primary air at a temperature of 344 K to one of four rows of coal burners on each corner of the boiler. Each pulverizer serves a row of burners for a total of sixteen burners on the unit. The burners have tilting mechanisms with a maximum range of ±27° from the horizontal. Heated secondary air at a temperature of 533 K is supplied to the furnace windbox which distributes the air to the burner air registers. At each corner, the fuel and air nozzles are directed along lines tangent to an imaginary circle located in the center of the furnace. The fuel and air streams combine to form a single swirling "fireball" in the furnace area. The resulting swirl action effectively mixes the fuel and air, resulting in near complete combustion of the fuel. Exiting the furnace, the hot combustion gases pass through a secondary superheater, reheater, primary superheater, economizer, and two regenerative air heaters.

For baseline operation of the unit at full load (104 MW), NO_x emissions are 512 ppm, dry, corrected to 3% O_2. Corresponding CO emissions at these conditions are 4 ppm, dry, corrected to 3% O_2. As boiler load drops, the firing intensity of each level of burners is reduced resulting in lower NO_x with a slight increase in CO emissions. As the boiler load is reduced further, the top row of burners are taken out of service resulting in increased firing rate for the remaining burners and the excess air is increased, resulting in an increase in NO_x emissions. Unburned carbon-in-ash is less than 4 percent over this load range.

9.1.3 Heat Transfer Analysis

A heat transfer analysis of the case study boiler was performed to identify appropriate locations for injection of the streams involved in SGAR processes (i.e, reburning fuel, OFA, and N-agents), and to assess the impacts of the process on unit performance. The heat transfer analysis consisted of setting up a two-dimensional heat transfer model simulation of the radiant furnace and a one-dimensional model simulation of the convective pass sections. The model was calibrated against available field data and design and operating data. The results of the furnace predictions for baseline operating conditions was used to identify appropriate locations for the reburning fuel, OFA, and reagent streams associated with the SGAR processes. Next, a parametric study of the impacts of the SGAR processes on boiler performance was performed. The models used in the analysis and the results of the study are summarized below.

For this study, EER's two-dimensional furnace combustion and heat transfer code (2DHT) was applied to evaluate thermal characteristics in a radiation-dominated boiler furnace. A key element

of this code is the radiation submodel for calculating radiative heat exchange between all volume and surface zones in the boiler furnace. This submodel is based on a semi-stochastic method derived from pure Monte-Carlo techniques, and considers radiative species of CO_2, H_2O, ash, char, and soot as non-gray components. The furnace code has submodels to handle coal devolatilization, as well as char and fuels (gas, liquid, volatiles) combustion. Coal particles are divided into ten different classes of size, and devolatilized according to a one-step Arrhenius rate law. Volatile packets are assigned statistically distributed lifetimes, and each packet reacts completely at the end of its assigned lifetime. Char oxidation is described by a global rate equation which considers diffusion and chemical reaction rates.

Other unique features of the furnace code include: (a) Directly calculates radiative heat exchange between upper-furnace radiant heat exchangers and the lower-furnace flame zones; (b) Handles complicated boundary conditions as usually occurs in large-scale utility boilers or combustors, such as variation of ash deposition, steam temperature, and wall emissivity. The code is decoupled from the solution of the momentum conservation equation. Therefore, the flow field is prescribed by the user, based on the results of isothermal flow modeling, experience in modeling boilers of similar design, or from computational fluid dynamics codes. The furnace code can handle furnaces fired with gas, liquid, and solid fuels with the option of introducing over- and under-fired air streams. The furnace code has built-in submodels to simulate various forms of burner fuel co-firing and reburning with gaseous, liquid and solid fuels.

EER's boiler performance model (BPM) was used to calculate boiler steam-side heat balance for all heat exchanger surfaces in the flue gas pass of the boiler. For boiler sections not modeled by the furnace code, such as the backpass convective tube-banks and the air heater, the boiler performance model calculated a heat balance for both the steam or air and the gas sides. For sections that were included in the domain of the furnace code, it is not necessary for the boiler performance model to recalculate the gas-side heat balance.

The boiler performance model is basically a one-dimensional heat transfer model which solves the coupled energy balance equations of the boiler steam and gas sides. The model uses computerized functions for enthalpy calculations of all flue gas components and steam/water, and is coupled with the outputs of the furnace heat transfer code, which in turn incorporates the input of boilerspecific information such as heat fluxes and gas temperatures for the boiler performance model. The boiler performance model predicts steam and gas sides properties including steam temperatures, steam flow rates, attemperation flows and flue gas temperatures for a given set of feedwater inlet temperatures, boundary conditions and steam-cycle pressure distributions throughout the boiler.

The boiler efficiency is calculated based on the ASME heat loss method.

To set up the furnace code to simulate the boiler performance under baseline operation and with retrofit of the SGAR processes, the furnace was first divided into a computational grid for input to the model. Figure 9.1.3 illustrates how the three-dimensional boiler is represented in the furnace code as an axisymmetric cylindrical grid, and how the boiler furnace was divided into 26 layers in the direction of the gas flow. The length and radius of each section up to the nose plane were chosen such that the volume, furnace height, and cross-sectional area were matched to those of the corresponding section in the full-scale unit. For the sections above the nose plane until the exit of the low temperature reheater section, the ratio of heat sink surface to zonal volume was preserved. This geometric transformation was performed to maintain the heat transfer similarity between the model and the actual boiler. Since the momentum conservation equation was not solved in the furnace heat transfer code, the flow field was prescribed using flow patterns acquired from an isothermal flow modeling study.
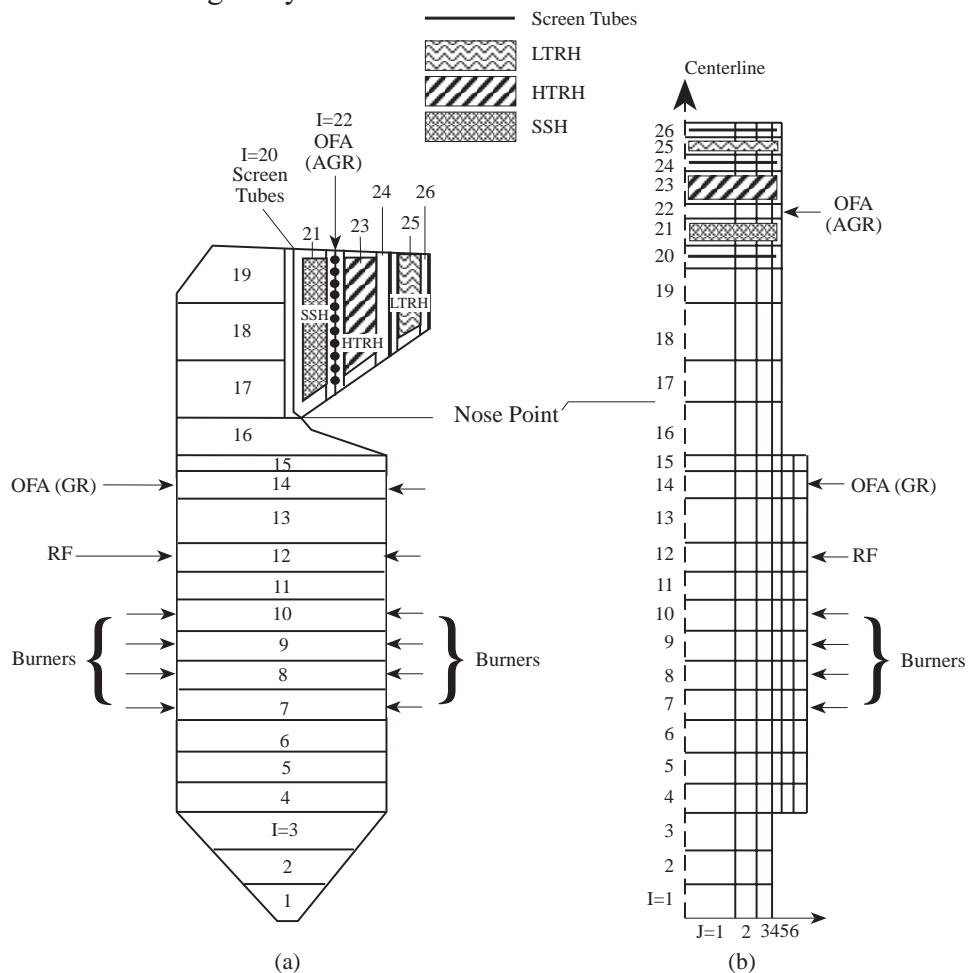
Figure 9.1.3 Furnace heat transfer model set up.

Since it is not possible to fully describe a complicated three-dimensional object using only two dimensions, and since some model parameters cannot be easily assessed without comprehensive boiler data, the model was initially calibrated against existing data to verify that the models were properly simulating the boiler performance at full load with two levels of tilt. The model was calibrated against field data collected by EER in a previous project and boiler design data provided by the boiler owner. The field data include flue gas temperatures, unburned fixed carbon-in-ash value, steam generation, attemperation flows, and water/steam temperatures for the major heat transfer components.

Mean gas temperatures predicted by the furnace code for the furnace section before the exit of low-temperature reheater section are shown in Figure 9.1.4, where burner locations, nose plane and upper-furnace heat exchanger sections are labeled. The plot identifies the first few banks of the convective pass simulated in the furnace code: secondary superheater (SSH), hightemperature reheater (HTRH), and low-temperature reheater (LTRH). The predicted mean gas temperatures basically fall in the range of the measured data, except for the temperatures at the nose plane. The differences between predicted gas temperatures and measurement at the nose plane are believed to be primarily due to the temperature stratification, since no measurement close to the center of the plane was taken. Therefore, these differences are considered within the prediction accuracy.
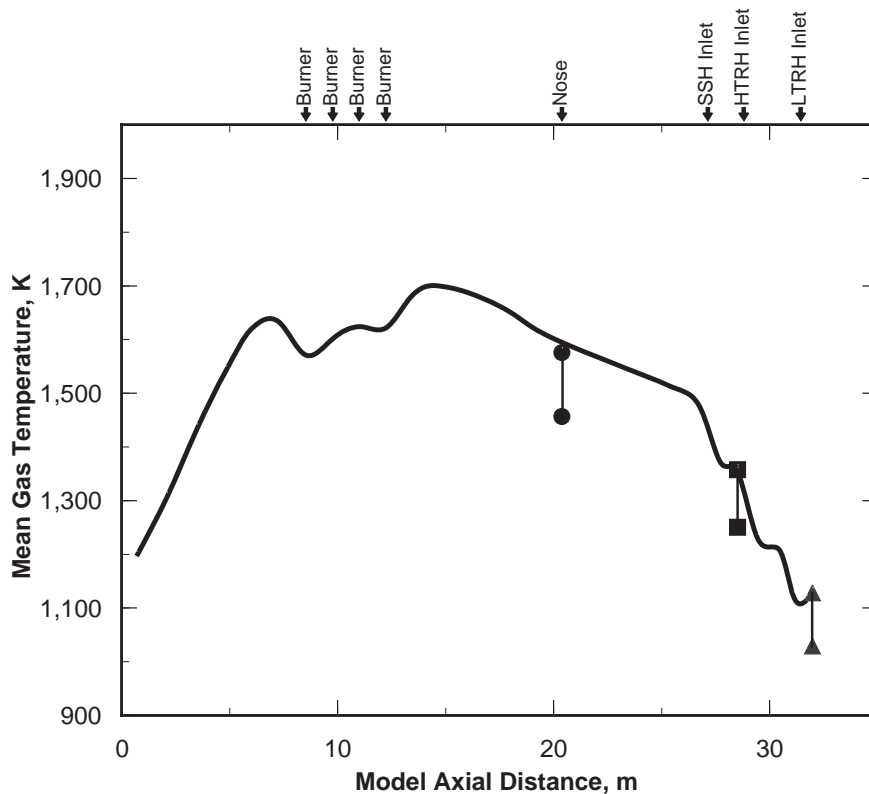
Figure 9.1.4 Comparison of predicted and measured furnace gas temperatures.

Three processes are being considered for application to the case study boiler: AR-Lean, AR-Rich, and MIAR. The results of the pilot scale studies (Section 7) indicate that optimum performance of the AR-Lean process requires injection of the OFA and N-agent at approximately 1300 K. For the AR-Rich process, the OFA is injected at this temperature, but the N-agent is injected upstream at a temperature of about 1370 K. For optimum performance of the MIAR process, the OFA is again injected at close to 1300 K, but the N-agent is divided into two streams and injected at temperatures of 1300 K and 1370 K, which correspond to the point of OFA introduction and to a plane upstream of the overfire air. In each of these processes, the reburning fuel is injected in the lower furnace above the main burners.

Figure 9.1.5 shows the bulk mean temperatures predicted in the upper furnace of the case study boiler by the heat transfer model. As shown in this figure, the optimum location for overfire air injection for each of the AR processes occurs within the first tube bank of the reheater, and the optimum location for reagent injection for AR-Rich and MIAR occurs between the secondary superheater and the reheater. Therefore, one approach for implementation of these processes on this boiler would be to inject the fuel-rich reagent into the cavity between the secondary superheater and reheater and the overfire air into the cavity between the reheater tube banks. As shown in Figures 9.1.4 and 9.1.5, the temperature in the reheater cavity is on the order of 1,120 K, which is expected to be too cold for overfire air injection and for injection of reagent in the AR-Lean and MIAR processes. Installation of OFA/N-agent injection systems in this region would also interfere with the plant sootblowing equipment in this region.
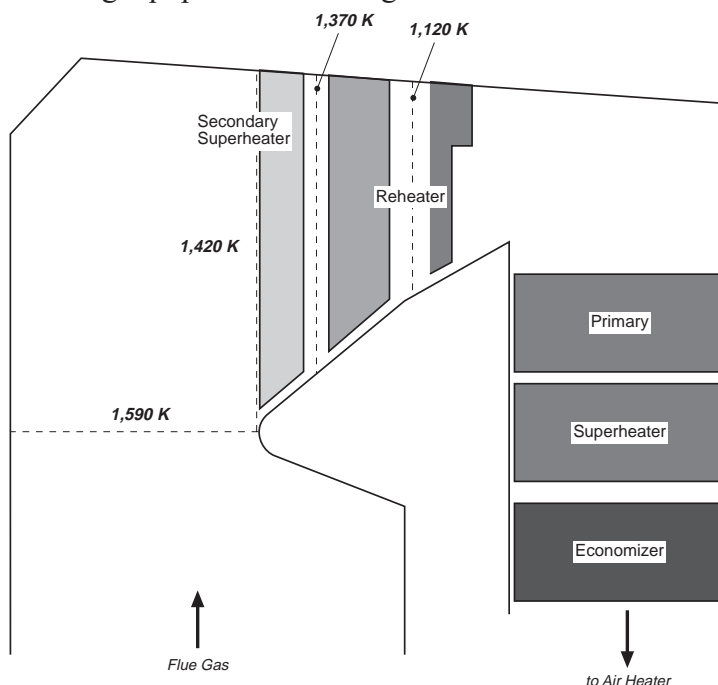
Figure 9.1.5 Predicted bulk mean temperatures in upper furnace of case study boiler.

The preferred approach for implementation of the OFA and N-agents stages of the AR processes on the case study boiler is shown in Figure 9.1.6. For the AR-Lean process, natural gas is injected in the furnace, and OFA and N-agent are injected into the cavity in between the secondary superheater platen and the first reheater platen. This location is on the high side of the optimum temperature, but should be adequate to ensure burnout of the carbon monoxide in the flue gases during AR-Lean operation. For the AR-Rich process, natural gas is injected in the furnace, Nagent is injected upstream of the secondary superheater, and OFA is injected into the cavity in between the secondary superheater platen and the first reheater platen. Injection of both of these streams at a higher than optimum temperature represents a compromise between practical implementation of the process on the case study boiler, and achieving optimum performance. Implementation of the MIAR process on the case study boiler consists of natural gas injection into the furnace, reagent injection upstream of the secondary superheater, and OFA and N-agent injection into the cavity in between the secondary superheater platen and the first reheater platen.

(a) AR-Lean

(b) AR-Rich

(c) MIAR
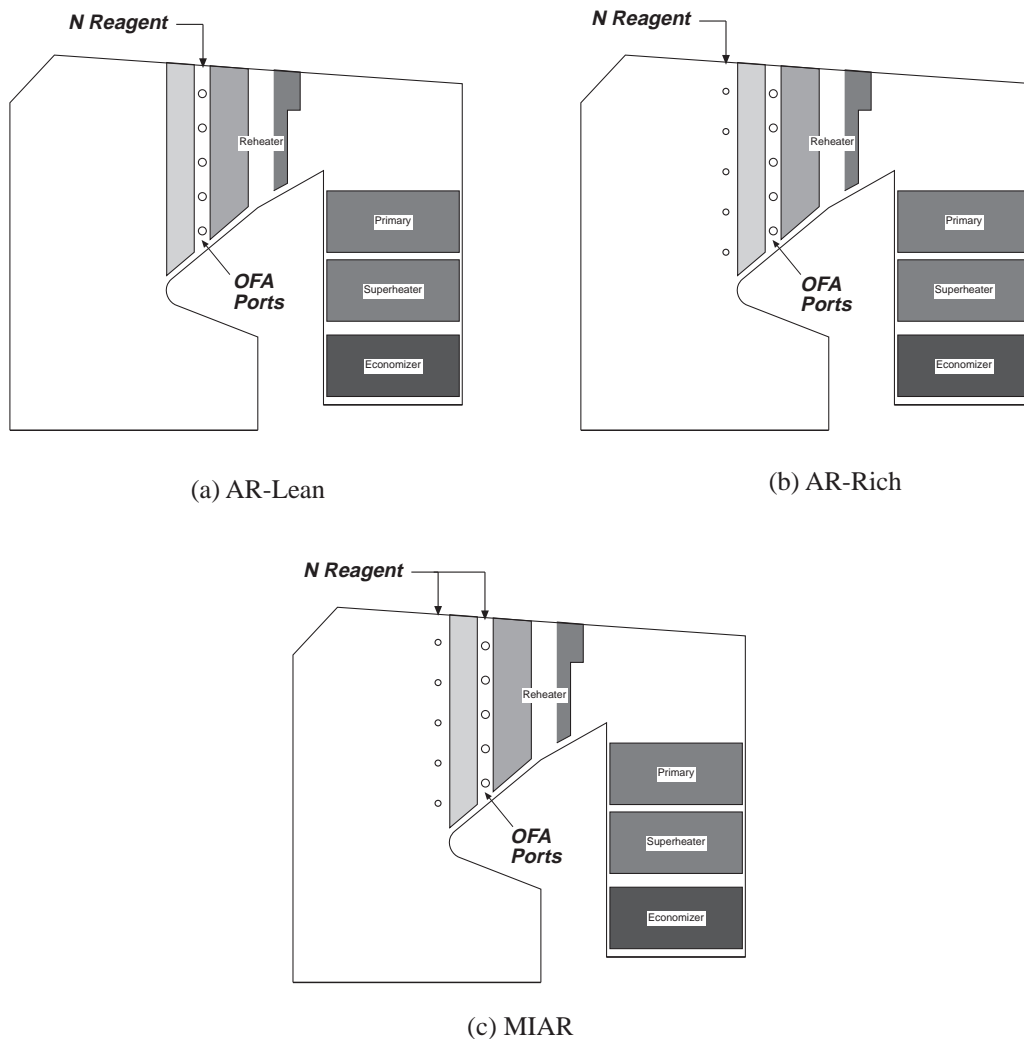
Figure 9.1.6 Implementation of AR technologies on case study boiler.

To study the impacts of the AR process configurations shown in Figure 9.1.6 on unit performance and efficiency, a parametric study was performed using the heat transfer models. Injection of the N-agent was assumed to have a negligible impact on boiler performance, therefore, the analysis was concentrated on evaluating the effects of stoichiometric ratio changes in conjunction with OFA injection into the secondary superheater/reheater cavity. In the analysis, the reburning fuel was assumed to be natural gas. The primary operating variables under study were the zone stoichiometries and the burner tilt settings. Two sets of zone stoichiometries were evaluated. The first set of zone stoichiometries consisted of using stoichiometric ratios (SR) of 1.1, 0.99, and 1.15 for, respectively, the primary (SR_1), reburning (SR_2), and burnout zones (SR_3). This set of zone stoichiometries represents assumed operating conditions for optimum NO_x reduction performance with each of the AR processes. The second set of zone stoichiometries consisted of using stoichiometric ratios of 1.2, 1.05, and 1.2 for, respectively, the primary, reburning, and burnout zones. This set of zone stoichiometries represents operating conditions assumed to reduce the impacts of AR on carbon in ash and boiler thermal performance. Both of these cases were ran with the burner tilt at its baseline or normal setting. A final case was run with the burner tilt set higher than the normal setting to assess the ability to minimize the impacts of the AR processes on boiler performance by modifying boiler operation. For comparison, the model was also used to predict the impacts of basic reburning on boiler performance as well. The thermal performance impacts evaluated in this study include furnace exit gas temperature (FEGT), unburned fixed carbon in ash, main and reheat steam temperatures, and attemperation requirements. The FEGT is defined as the mean flue gas temperature located at the nose plane.

Figures 9.1.7 and 9.1.8 show the predicted impacts of gas reburning and advanced reburning processes on furnace exit gas temperature and carbon in ash. For implementation of gas reburning, the model predicts a slight decrease in furnace exit gas temperature, and an increase in carbon loss. The change in furnace exit gas temperature with reburning is due to a slight modification of the boiler heat absorption distribution. Carbon loss is expected to increase by close to 3.5% over baseline conditions with reburning due to operation of the burners at a lower than baseline excess air level. In the proposed AR process configurations, the overfire air is injected into the secondary superheater/ reheater cavity. This reduces the mass loading to the furnace at the nose plane by approximately 20% in comparison to basic reburning. As shown in Figure 9.1.7, the reduction in mass loading in the furnace results in an increase in furnace exit gas temperatures with AR operation. For baseline AR operation (i.e, primary SR ~ 1.1, reburning SR ~ 0.99), delaying the addition of OFA until the convective pass is predicted to increase carbon loss by approximately 9% over normal reburning operation. Increasing the primary zone stoichiometry from 1.1 to 1.2 while maintaining close to 10% reburning fuel, results in an increase in furnace exit gas temperature, but reduces the impact of

OFA injection into the convective pass on carbon loss. For the case of AR operation with 20% excess air in the burners, carbon loss is expected to increase by only 1.5% over reburning operation.
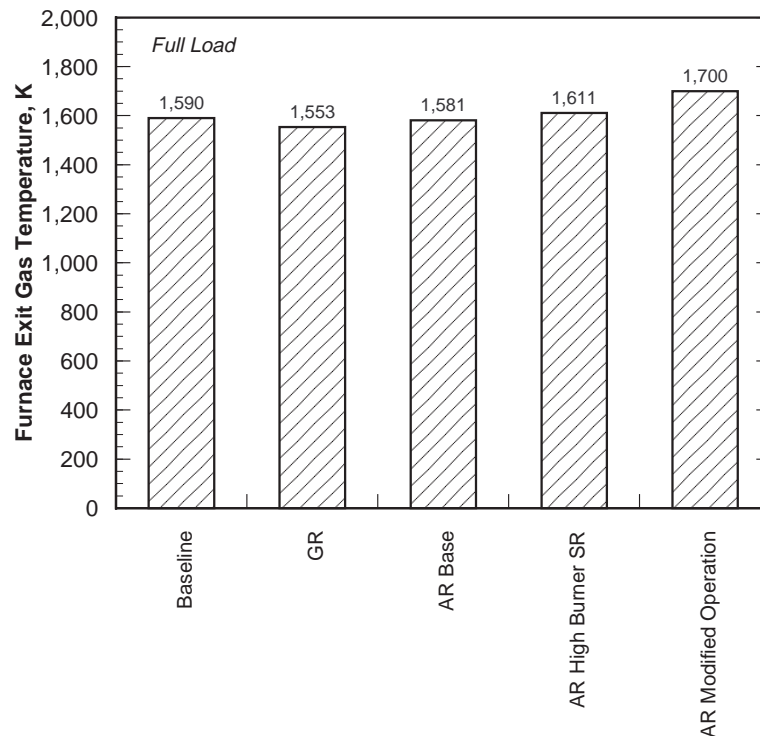
Figure 9.1.7 Projected impacts of AR processes on furnace exit gas temperature.
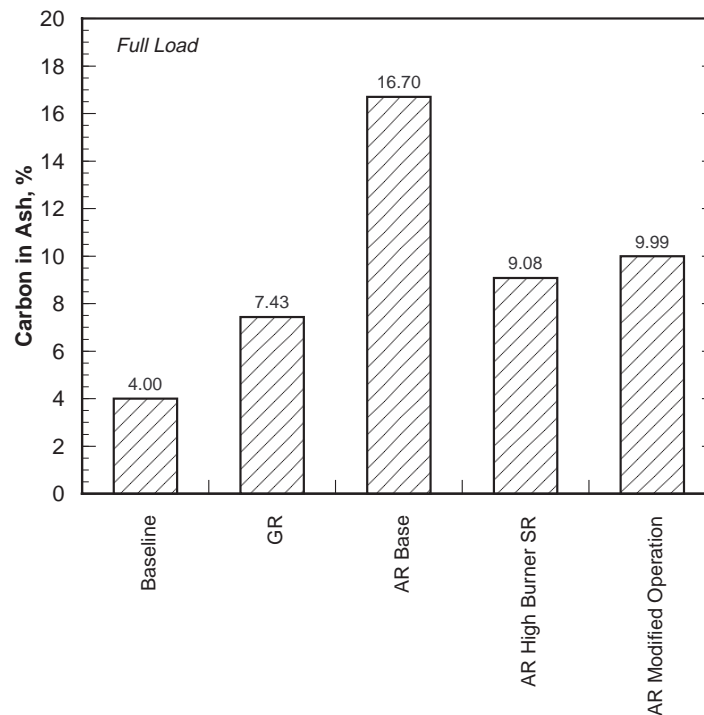
Figure 9.1.8 Projected impacts of AR processes on carbon in ash.

For baseline AR process operation, carbon loss is expected to increase over basic reburning operation, however, the impact of the additional carbon loss on boiler efficiency is small, as shown in Figure 9.1.9, in comparison to the effects of basic gas reburning alone. The use of gas reburning is expected to reduce boiler efficiency by close to 1.25%. This reduction is primarily due to the change in hydrogen/carbon ratio of the fuel. The use of natural gas increases the boiler heat loss efficiency due to an increase in water vapor in the flue gas in comparison to operation with coal. For operation with AR, Figure 9.1.9 shows that the heat loss efficiency is close to that for operation with basic reburning and is higher or lower depending upon the process and boiler operating conditions.
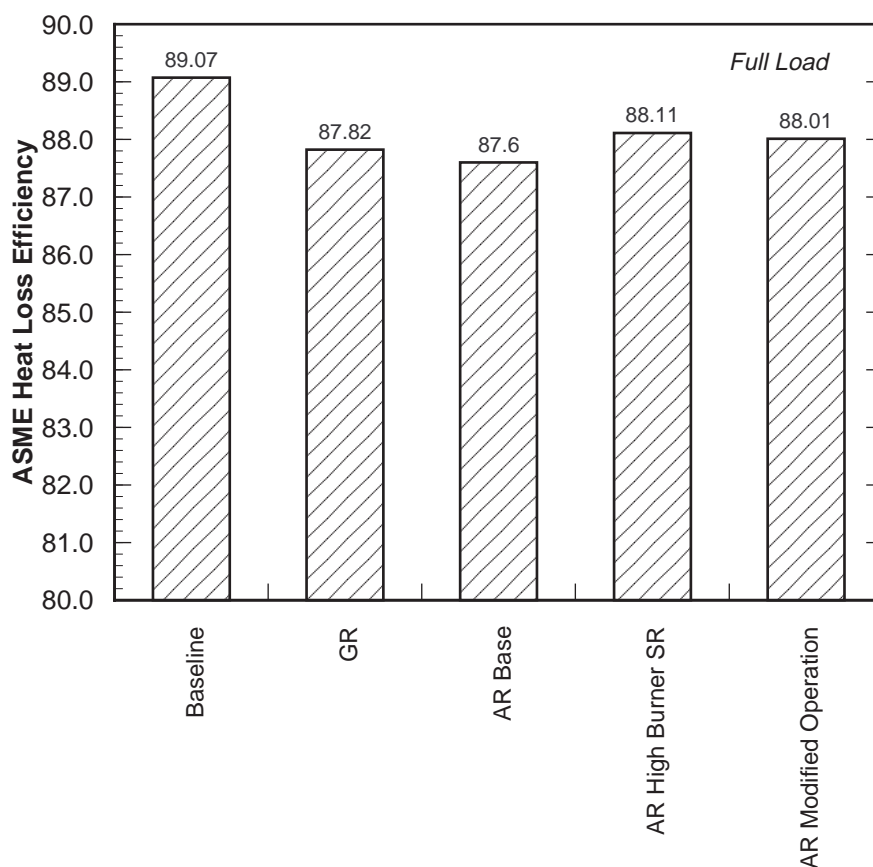
Figure 9.1.9 Projected impacts of AR processes on ASME heat loss efficiency.

The impacts of operation with basic reburning and AR processes on main and reheat steam temperatures at full load are shown in Figure 9.1.10. For the gas reburning case, the model main and reheat steam temperatures can be maintained close to normal levels using the same degree of burner tilt as that used for normal operation. For baseline AR process operation, the predicts that main and reheat steam temperatures will decrease below normal operation when burner tilt is maintained at its normal full load set point. This decrease is primarily due to the reduced mass loading across the secondary superheater section, as compared to the mass loading with basic

reburning. Although the mass loading after the OFA ports is restored close to that for basic reburning, the reheat steam temperatures for AR process operation are still lower than those for basic reburning due to the quenching effect of the overfire air that is introduced into the secondary superheater/ reheater cavity. As shown in Figure 9.1.10, increasing the primary zone stoichiometry improves the main and reheat steam temperatures. This improvement is due to slight increases in furnace exit gas temperature and overall mass loading to the boiler. Alternatively, increasing the burner tilt when operating the AR system would also be expected to restore main and reheat steam temperatures back to normal conditions, as shown by the AR Modified Operation case in Figure 9.1.10.
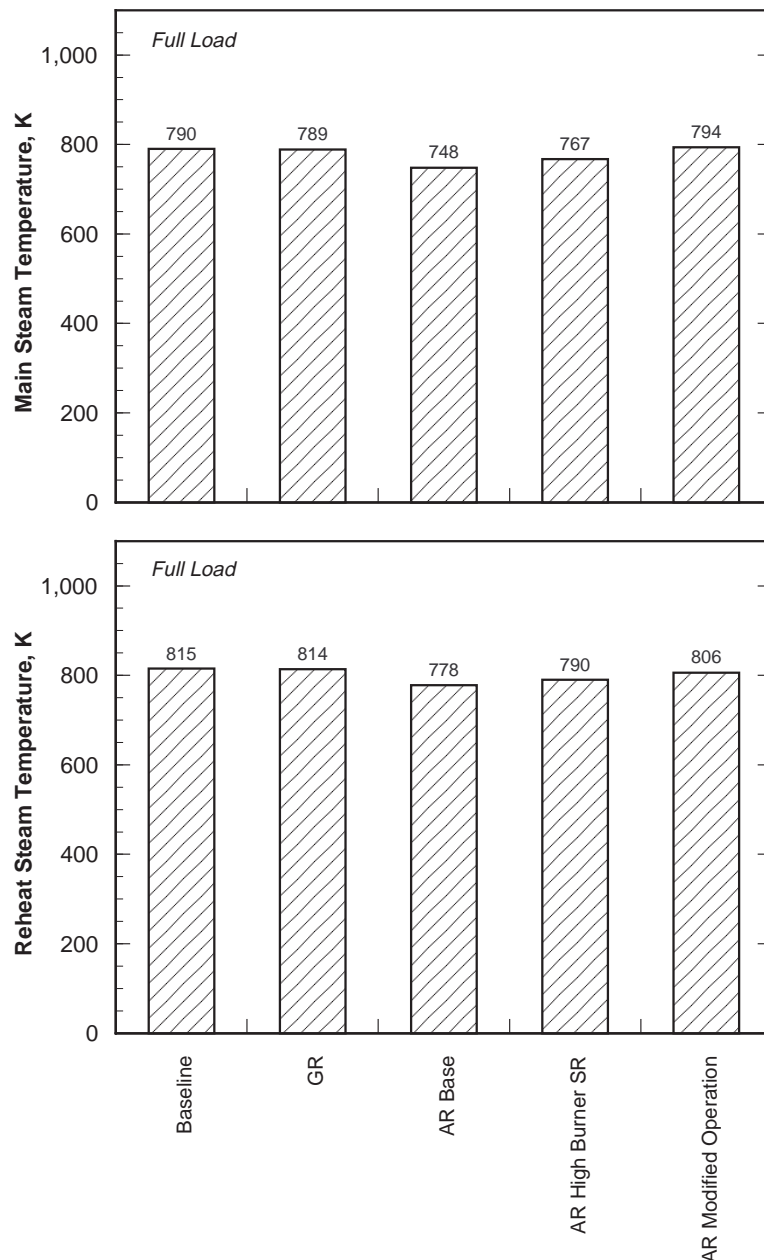
Figure 9.1.10 Projected impacts of AR processes on steam temperatures.

In summary, thermal performance models were used to evaluate the impacts of implementing AR processes on the thermal performance of a nominally 100 MW tangentially fired boiler. For implementation of AR-Lean, AR-Rich, or MIAR processes on this boiler, the reburning fuel would be injected into the lower furnace and the overfire air would be injected into the upper furnace in a cavity between the first two tube banks of the convective pass. The model results indicate that the this configuration is expected to increase carbon loss and reduce main and reheat steam temperatures in comparison to baseline or gas reburning operation. Changes in the operating settings of the AR process can be used to mitigate some of the increase in carbon loss. However, the overall boiler efficiency for operation with an AR system is similar to that for operation with a basic gas reburning system. Changes in the operating settings of the AR process or in the boiler operating settings can be used to mitigate the impacts of AR on main and reheat steam temperatures. It should be noted that the results of this analysis are specific to the boiler configuration evaluated and should not be generalized to other boiler designs.

9.1.4 Injection System Studies

To assist in the design of injection systems for the reburning fuel and overfire air used in implementation of the AR processes, a physical model of the case study boiler was constructed. The model was a 1:12 geometric scale replica of the boiler furnace from the hopper to the primary superheater. Following construction of the model, flow visualization was performed to study the characteristics of the furnace flow field. Next, simulated injection system were installed on the model. Jet penetration and mixing studies were performed to develop injection systems which resulted in optimum dispersion of the advanced reburning process streams. The results of these studies are summarized below.

The major characteristics of the case study boiler flow field under baseline conditions are shown in Figure 9.1.11. During baseline operation, the burners are tilted -15° with respect to the horizontal. It should be noted that the natural swirl for the tangentially fired unit is counter clockwise. The two planes represented in the figure are with respect to the right-hand side wall. Flow in the near field is front to back and is supplied from the left-hand side burner packs. As the flow approaches the nose elevation, gases flow from the front wall and enter the convective sections without contributing much mass to the recirculations zones in the upper furnace. Flow in the far plane is supplied from the right-hand side burner packs. The flow field on the far plane is more heavily effected by the nose and provides some mass in the upper furnace recirculation zones. From the right-hand side, gases flow under the nose and enter the far plane from back to front. Gases are then distributed into the center and left side portions of the convective pass entrance. Some mass is entrained into the

upper furnace recirculation zone. The characteristics of the flow field are typical of a tangentially fired boiler. Because of the firing orientation, the flow entering the superheater is biased toward the upper right-hand side wall. This is also considered typical of tangentially fired boilers.

Near Plane   **Far Plane**
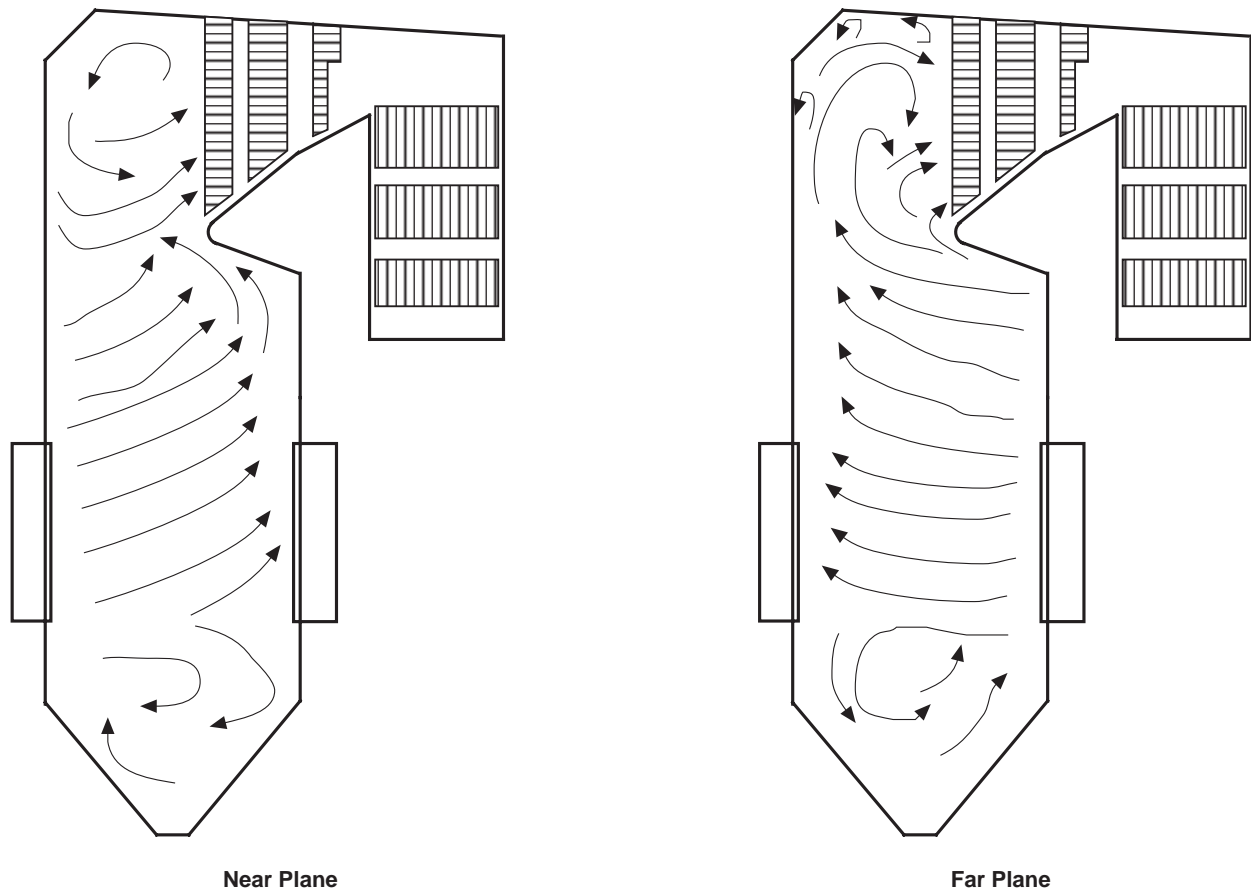
Figure 9.1.11 Baseline flow field characteristics.

Next, the flow model was used to study the design of injection systems for effective distribution of the reburning fuel into the lower furnace and overfire air into the convective pass. Various configurations were valuated for both systems. The configurations were first screened using smoke visualization to determine jet penetration and dispersion of the smoke fluid throughout the furnace. The more promising design options were then selected for more detailed characterization using tracer dispersion measurements. In this technique, a small amount of tracer gas was added to the stream of interest and the extent of dispersion of the tracer evaluated across a plane downstream of the injection location. The results were then evaluated in terms of the local stoichiometric ratio at full scale to determine how effectively the system was mixing the stream of interest into the flue gas. Various injector configurations were tested until an optimum configuration was identified. The

optimum configurations identified for the reburning fuel and overfire air within the constraints of the boiler geometry are described below.

For the reburning fuel, the nozzles in the optimum configuration were arranged with two highvelocity natural gas injectors in each corner. The firing circle of the reburning fuel jets was set opposite that of the burners. This allowed the jets to penetrate into the flue gas at a steeper angle and increased the mixing rate of the reburning fuel. The dispersion profile for this configuration is shown in Figure 9.1.12. The contour lines represent constant reburning zone stoichiometry. The figure shows that reasonably good distribution of the reburning fuel into the flue gas was achieved over most of the boiler cross section without the reburning fuel jets over penetrating into the center recirculation zone. Coverage near the corners was reduced, but this is not expected to greatly influence the performance of the injection system.
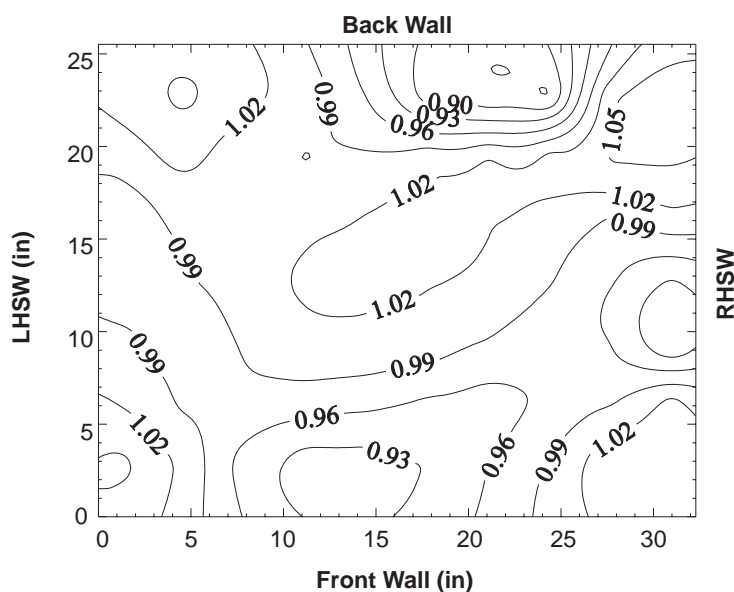
Figure 9.1.12 Dispersion pattern for preferred reburning fuel injector configuration.

For the overfire air, the injector arrangement in the optimum configuration consisted of ports located on the sidewalls of the furnace designed to effectively distributed overfire air across the width and height of plane at the entrance to the reheater, and a centrally located lance designed to cover the center portion of the plane. Measurements without this lance showed that the center region was poorly treated. The dispersion profile for this configuration is shown in Figure 9.1.13. The contour lines represent constant burnout zone stoichiometry. As shown in this figure, this injection configuration provides for good distribution of the overfire air at this location.
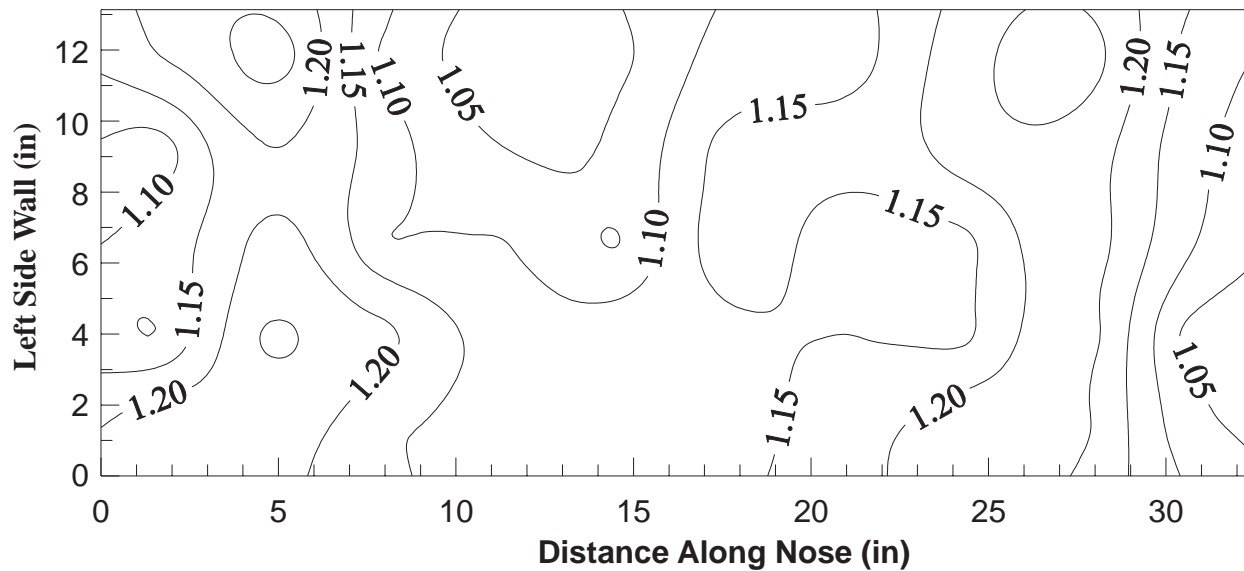
Figure 9.1.13 Dispersion pattern for preferred overfire air port configuration.

For injection of the nitrogen-based reagent in the AR processes, the approach used to inject the reagent depends upon the process used. For the AR-Lean process, the preferred approach would be to inject the reagent with the overfire air stream thereby allowing the momentum of the air jets to transport and mix the reagent with the flue gas. For the AR-Rich process, the regent would need to be injected in front of the secondary superheater either from lances placed into the gas flow or from high-velocity wall jets. For the MIAR process, a portion of the reagent would be injected with the overfire air, and a portion would be injected using lances or wall jets. For the case study boiler, injection of the reagent along with the overfire air would be an effective means of mixing the reagent into the flue gas. As shown in Figure 9.1.13, good mixing of the overfire air can be achieved with a design that consists of wall injectors and an in-furnace distribution header. Therefore, it is expected that any reagent injected with the overfire air would be mixed well into the flue gas.

Effective distribution of reagent into the flue gases entering the secondary superheater on the case study boiler is complicated by the complex structure of the flue gas flow in this region. Although wall jets have been effectively used for injection of SNCR agents on utility boilers, it is not believed that this approach is applicable to the features of the flow field shown in Figure 9.1.11. In addition, the use of air to assist with injection of the reagent would be detrimental to the process and the use of steam would be undesirable from a boiler performance standpoint. Therefore, for this application, the use of lances inserted into the flow would be the preferred means of injecting reagent for the AR-Rich and MIAR processes. It should be noted that lance-based SNCR systems have been used successfully in a number of utility applications. For the case study boiler, design calculations suggest that a lance system consisting of five lances inserted into the gas flow from each sidewall in front of

the secondary superheater could achieve adequate distribution of the reagent. Each lance would be equipped with approximately six nozzles for reagent atomization. The nozzles would need to generate droplets with a size less than 100 microns in order to ensure rapid droplet evaporation.

In summary, the results of injection system analysis indicate that good mixing of the process streams necessary to implement advanced reburning (AR-Lean, AR-Rich, and MIAR) on the case study boiler can be achieved. Natural gas can be injected from each wall in a pattern which achieves good distribution of the reburning fuel. Overfire air injection into a cavity in the convective pass, needed for implementation of each of the AR processes under consideration, can be achieved using high pressure wall jets. For the AR-Lean and MIAR processes, these ports can also be used to inject the reagent. Injection of reagent into the upper furnace, needed for the AR-Rich and MIAR processes, can be achieved using a lance-based system.

9.1.5 Full Scale Performance Prediction

This section of the report presents the results of an analysis of the potential NO_x reduction levels which are expected to be achievable by the application of the SGAR processes to the case study boiler. The NO_x projections presented herein were developed based upon the boiler emissions characteristics (i.e., sensitivity towards load, excess air and boiler operating conditions), the results of the flow model studies, and the estimated thermal characteristics of the boiler. These projections were developed by applying EER's process models and database on performance of SGAR processes at pilot scale to the information generated in this study. The NO_x projections attempt to take into account all of the various parameters (temperature, residence time, stoichiometry, initial NO_x level, reburning fuel and reagent mixing, etc.) which are believed to have the most significant influence on the performance of the reburning process.

Baseline NO_x emissions for the case study boiler at full load are approximately 340 ppm, 3% O_2. For the use of 10% natural gas as a reburning fuel, NO_x emissions could be reduced to 187 ppm, which represents a reduction in baseline emissions of 45%. By applying AR-Lean, EER projects that NO_x emissions could be reduced to approximately 74 ppm, which represents a reduction in baseline emissions of 78%. The use of AR-Rich and MIAR on this unit is expected to result in NO_x emissions levels of respectively, 45 and 30 ppm. For AR-Rich, this emissions level corresponds to 87% control from baseline conditions, and for MIAR, it corresponds to 91% control. Additional NO_x reduction can be achieved with the use of promoters. These estimates of the potential NO_x control levels achievable with the implementation of AR processes on the case study boiler are expected to be representative of the levels which could potentially be achieved with a properly designed and operating reburning system on the unit used in the study. The performance achievable

on other units would be sensitive to the NO_x emissions and operating characteristics of the boiler, and would need to be evaluated on a site specific basis.

9.2 AR Application

This subsection discusses the conversion of the process design presented in the previous subsection into retrofit hardware for the AR-Lean system and discusses the results of initial AR-Lean tests as well as tests of some of the SGAR components.

The unit is Greenidge Unit 4, which is owned and operated by New York State Electric and Gas (NYSEG). All of NYSEG's units are located within the North East Ozone Transport Region (NEOTR) and as a result are subject to Title 1 NO_x control requirements. (See subsection 9.3 for additional information on the regulations.) NYSEG's compliance plan involves a system-wide daily cap on NO_x emissions. After considering a number of alternatives, NYSEG decided to utilize reburning and AR-Lean for NO_x control at Greenidge. EER installed the gas reburning system as part of a commercial project with guaranteed performance. The upgrade to AR-Lean was conducted as a cooperatively funded demonstration project with the support of NYSEG and a number of cofunding organizations including the Electric Power Research Institute, Empire State Electric Energy Research Corporation, Gas Research Institute, Gaz de France, New York State Energy Research & Development Authority, and Orange & Rockland Utilities.

The AR-Lean process design specifications for the location and size of the reburning gas, furnace overfire air, and convective pass overfire air (discussed in the previous section) were utilized to prepare an engineering retrofit design. Figure 9.2.1 is an isometric view of the unit showing the arrangement of the gas reburning and AR-Lean components external to the furnace.

N-AGENT INJECTORS
AND CARRIER AIR
(PENDENT)

GR OVERFIRE AIR
INJECTORS
(4 CORNERS)

N-AGENT INJECTORS
AND CARRIER AIR
(SIDEWALLS)

GAS INJECTORS
(4 CORNERS)

GR OVERFIRE
AIR DUCT

N-AGENT
SUPPLY

EXISTING BURNERS
(4 CORNERS)
(4 BURNERS EACH)

NATURAL GAS
SUPPLY

FROM NH$_3$
CONVERTER

AGR OVERFIRE AIR
BOOSTER FAN

AQUEOUS AMMONIA
STORAGE TANK
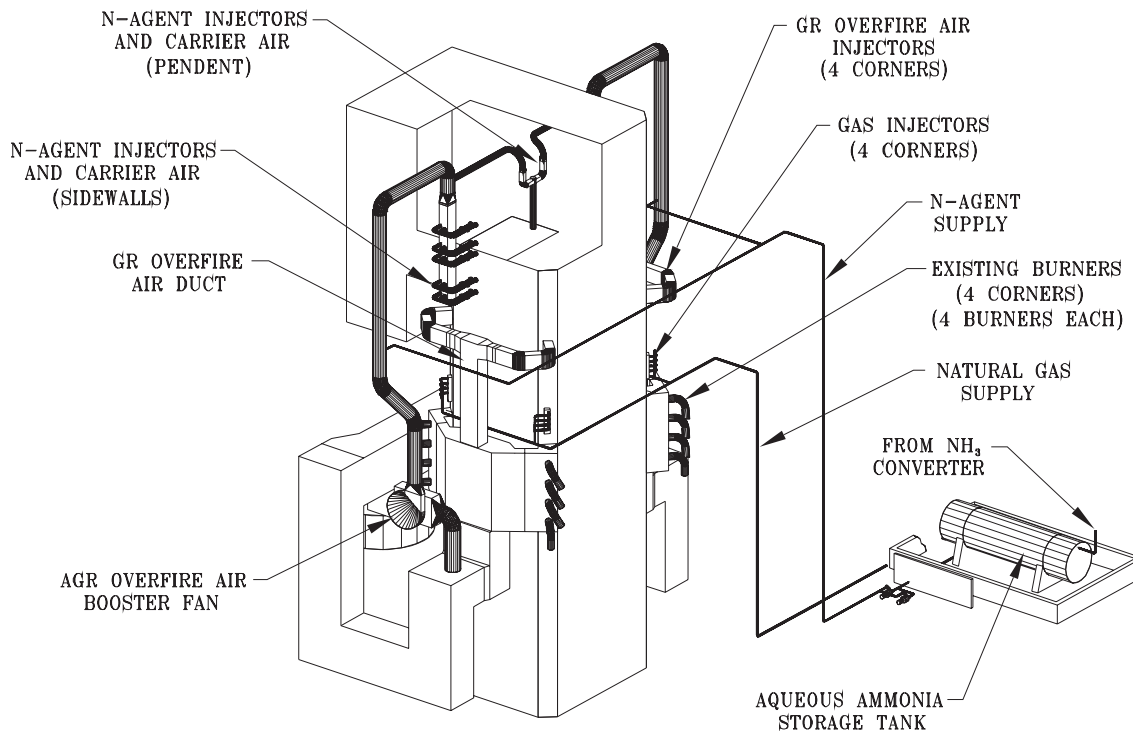
Figure 9.2.1 Isometric view of Greenridge Unite 4 showing gas reburning and AR-Lean components external to the boiler.

The gas injectors were corner mounted and consisted of multiple injectors in each corner with a surrounding cooling air passage. The multiple gas injector approach allows independent control of the quantity of reburn fuel and the injection velocity. The natural gas valve train included pressure reduction, double block and bleed shutoff control, and flowrate control valves.

The furnace OFA ports were corner mounted above the reburn injectors but below the furnace nose. The OFA for these ports was supplied by takeoffs from the top of the burner windbox. Although this tangentially fired unit operates at a relatively low windbox to furnace pressure differential, the differential was sufficient to achieve the design air injection velocities. The overfire air flow was controlled by dampers.

To achieve the required rapid and complete mixing of the convective pass OFA with the furnace gases in the narrow space between the convective surfaces, air was injected from side wall ports as well as a header in the center extending downward from the boiler penthouse. The windbox to furnace pressure differential was insufficient to produce the design point velocity. To boost the pressure, two fans were installed between the windbox and the convective pass overfire air supply headers.

Aqueous ammonia was used for the N-agent. It was produced on site from anhydrous ammonia. A variable speed positive displacement pump provided flow control. The N-agent was piped to pressure atomizers located in the convective pass overfire air headers on each side of the unit downstream of the booster fans. To provide enhanced control of the N-agent injection distribution, this system was subsequently modified with separate injectors in each wall port and in each air supply duct feeding the central header.

The gas reburning and AR-Lean components were integrated with the unit's WDPF Level 4 control system. This includes 140 input/outputs fully integrated with the combustion control system. The gas reburning and AR-Lean systems can be controlled remotely from the boiler control room and are fully automated. A series of permissives and trips ensure safe operation.

The gas reburning and AR-Lean systems were designed to provide the flexibility to adjust NO_x to meet NYSEG's system-wide NO_x cap. The initial NO_x reduction is from leakage air through the furnace and convective pass overfire air ports which provides a degree of staging.

The gas reburning system is brought into operation for the second increment of NO_x reduction. This involves, (1) ramping up the gas injection rate, (2) reducing the coal firing rate to compensate for the gas, (3) decreasing the combustion air supplied to the burners to maintain lower furnace stoichiometry, and (4) injecting combustion air through the furnace overfire air ports to maintain the overall stoichiometry at near baseline. The gas injection rate is the primary variable controlling NO_x reduction. The coal firing rate and air flows are adjusted to the design point burner and overall stoichiometries. NO_x is decreased as the gas injection rate is ramped up.

A transition is made to AR-Lean for the final increment of NO_x reduction. This involves (1) decreasing the gas injection rate, (2) increasing the coal firing rate, (3) increasing the combustion air supplied to the burners to maintain lower furnace stoichiometry, (4) switching the OFA from the furnace to the convective pass ports, (5) adjusting the OFA flowrate to maintain the overall stoichiometry at near baseline, and (6) injecting the N-agent through the convective pass overfire air ports. The N-agent injection rate is the primary variable controlling NO_x reduction. The gas, coal and combustion air flowrates are adjusted to produce near stoichiometric conditions in the reburn zone and design point burner and overall stoichiometries. NO_x is decreased as the N-agent injection rate is ramped up.

NO_x emissions for gas reburning and AR-Lean are shown in Figure 9.2.2 as a function of the reburning gas percentage. The baseline NO_x emissions for the unit prior to the equipment retrofit

were 0.62 lb/106 Btu. Leakage air through the furnace and convective pass overfire air ports provided air staging and reduced NO_X to 0.46 lb/106 Btu. In the normal gas reburning mode, additional overfire air was added through the furnace overfire air ports as the reburning gas was injected. As shown in Figure 9.2.2, NO_X decreased as the gas injection rate increased down to 0.22 lb/106 Btu which represents a NO_X control level of 62 percent. CO emissions were typically under 30 ppm.
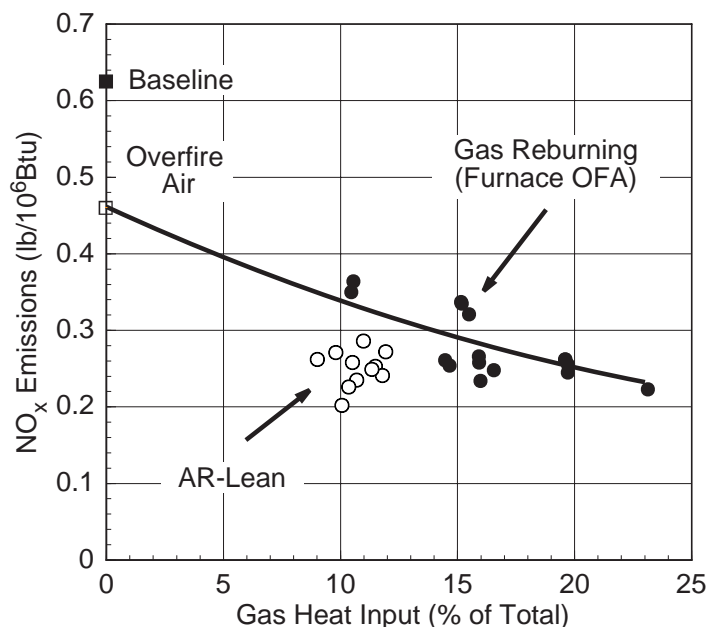
Figure 9.2.2 Gas reburning and AR-Lean NO_X data, Greenridge Unit 4.

Since the gas reburning portion of the system was a commercial system, a guarantee test was conducted with the following result at 15% gas injection.

Parameter	Measured Performance	Commercial Guarantee	Units
NO_X	0.286	0.300	lb/106 Btu
CO	17	60	ppm

Initial testing of AR-Lean was conducted in summer 1996. The initial tests focused on establishing the operating conditions without ammonia injection. This involved the first five steps listed above. The system was set up to control the CO level at the point of convective pass overfire air introduction. Under these conditions, NO_X was reduced slightly to about 0.30 lb/106 Btu. This was a consequence of the moving the overfire air injection to the convective pass which extended the reburning zone. The convective pass overfire air system was effective in controlling stack CO emissions to levels comparable to baseline.

The next test series involved ramping up the N-agent injection (step six in the list above). As the N-agent injection was increased, NO_x decreased, as expected. Figure 9.2.2 shows the AR-Lean NO_x data superimposed on the gas reburning data illustrating the lower NO_x emissions achieved at nominally 10% gas firing. In these AR-Lean tests, minimum NO_x was constrained by NH_3 emissions to 0.19 lb/106 Btu. This was unexpected and was traced to non-uniform conditions in the reburning zone as discussed below.

In conventional N-agent injection without reburning, the temperature window is narrow: injection within the window reduces NO_x with minimum NH_3 emissions; injection on the hot side of the temperature window may increase NO_x but with minimal NH_3 emissions; injection on the cold side of the temperature window achieves less NO_x reduction and produces NH_3 emissions. With AR-Lean, CO oxidation occurs in parallel with the NH_3 reactions effectively broadening the temperature window on the cold side. During these AR-Lean tests, the CO level in the reburning zone was in the range expected to broaden the temperature window to lower temperatures, on the order of several thousand ppm. CO measured in the boiler exhaust was typically less than 50 ppm indicating excellent CO burnout. While the overall CO levels and burnout were on design, probe measurements in the upper furnace showed considerable CO stratification. In some regions the furnace gases had low CO and excess O_2. In other areas while CO was on design, O_2 was also present indicating streamwise stratification or poor micro-mixing. This stratification accounts for the NO_x emission reduction and NH_3 emissions. That portion of the furnace flow with low CO and excess O_2 was not producing the temperature window broadening and this resulted in excess NH_3 emissions limiting the maximum NH_3 injection rate and hence NO_x reduction.

These Greenidge tests have revealed an important AR issue: the uniformity of conditions in the reburning zone is important to the optimization of the AR process. In small scale tests, the furnace flow is fairly well mixed so that this stratification effect is not significant. However, stratification may be the limiting factor in full scale applications.

Once this stratification effect was understood, additional tests were conducted at Greenidge to improve performance. The focus of testing in summer 1997 was on adjusting the AR-Lean system to provide more uniform reburn zone conditions. This included: (1) burner balancing, (2) modification of the gas injectors to reduce stratification and enhance the micro-mixing of the fuel and air so as to avoid regions of excessively rich or lean conditions, and (3) reduction of leakage air through the furnace overfire air ports. In addition, the N-agent injectors were modified to allow the tailoring of the distribution of the N-agent among the convective pass overfire air injectors. These changes have resulted in improved performance and additional NO_x reduction with lower NH_3 slip.

In addition to these AR-Lean tests, opportunity was taken to obtain larger scale data on several of the SGAR components. It should be noted that the Greenidge unit was set up only for AR-Lean and the furnace penetrations available in the unit were not optimum for the other SGAR configurations. A series of tests were conducted in Summer 1997 to evaluate the following SGAR components:

- N-agent injection downstream of the overfire air In these tests, the gas reburning system was operated in the normal mode using the furnace overfire air. The N-agent was injected through a series of lances on the front wall above the overfire air ports. Based on the process design studies, it was expected that these temporary N-agent injectors would not produce a uniform distribution of N-agent across the furnace and that the furnace temperature would be too hot for effective SNCR operation. The tests confirmed these predictions. Only modest NO_x reduction was achieved and NH_3 slip was minimal.

- N-agent Injection into the reburn zone This SGAR component was tested by operating the system in the AR-Lean configuration using the convective pass overfire air ports. The N-agent was injected through the same furnace lances described above. While this injection location was not optimum, it provided some initial data on AR-Rich conditions. These tests will continue through fall 1997.

- Multiple N-agent injection Limited tests were also conducted with injection both through the furnace lances and through the convective pass injectors. Again, the tests do not represent an optimum MIAR configuration. However, they allow a preliminary evaluation of multiple injection and the ability to stratify the N-agent injection for the stratified furnace flow conditions.

If this project proceeds to Phase II, these large scale tests will continue in summer 1998. Alternate injection arrangements and promoters are expected to be tested.

9.3 Economic and Market Analysis

This section discusses the economics of NO_x control via AR and the potential market for the AR technologies in the US for compliance under the 1990 CAAA. The following subsection 9.3.1 discusses the market drivers and the nominal NO_x control requirements to meet existing and projected regulations (see also Section 3.1). Then, Section 9.3.2 outlines an economic methodology for comparing cost effectiveness of conventional and AR technologies and defines two representative

applications, cyclone and wall-fired boilers. The methodology was uses to compare the costs of conventional NO_x controls (SNCR, SCR and OFA) with the costs of reburning based technologies including basic reburning and the full range of AR technologies being developed in this project. Subsection 9.3.3 discusses the cost and performance of each NO_x control technology and Subsection 9.3.4 presents the results. The results show a considerable economic advantage for the AR technologies particularly for deep NO_x control with cost savings in the range of 50%. The resulting market for these AR technologies is discussed in Subsection 9.3.5.

9.3.1 NO_x Control Drivers

The Clean Air Act Amendment of 1990 (CAAA), established the framework for NO_x emission regulations to mitigate ozone non-attainment areas and acid rain. Over the last seven years, EPA has developed most of the specific NO_x regulations authorized by the CAAA. The most stringent NO_x controls are required in ozone non-attainment areas or areas which transport pollutants into ozone non-attainment areas. In the Northeast, EPA has defined the Northeast Ozone Transport Region (NEOTR) consisting of Pennsylvania and the States North and East. In that zone, NO_x reductions of up to 75% are required by 2003 with the potential for even deeper controls depending on the results of modeling over the next few years. EPA is now considering expanding the NEOTR to include Texas and all states North and East. In this 37 state region, it is projected that NO_x emissions may need to be reduced by as much as 85%.

As these specific regulations have developed, the trend has been towards cost effective emission controls. Rather than setting specific limits for each plant, in many areas the regulations have been established to provide the flexibility to over-control on some units and under-control on others if that approach is cost effective. This can be of considerable advantage since the cost of NO_x control for some units (particularly smaller units) may be much higher than for others, on a $/ton basis. This bubbling approach depends on the availability of NO_x control technologies which can achieve NO_x reductions greater than the nominal control levels (75-85%) with low costs.

The NO_x control requirements developed by EPA to date were based on the current National Ambient Air Quality Standards (NAAQS). EPA has issued revised NAAQS for ozone and fine particulate which are substantially lower. Since NO_x is a precursor of both pollutants, achieving the new NAAQS will require even greater NO_x reductions.

Therefore, the goal established by DOE for this project, 95% NO_x control down to 0.06 lb/10^6 Btu, is appropriate. NO_x control technologies which meet this goal will only be employed if their costs

are competitive with conventional controls on a \$/ton basis. At present, the only commercial NO_x control technology capable of achieving such deep NO_x control is SCR. The advantage of the AR technologies being developed on this project is that they can provide the deep NO_x control of SCR at a considerable cost reduction.

9.3.2 Methodology and Cases Evaluated

To evaluate the cost effectiveness of the AR technologies, an economic analysis has been conducted using the EPRI Technology Assessment Guide (TAG) methodology, which is widely used in the utility industry to evaluate advanced emission control technologies. The TAG methodology calculates the total levelized annual costs including capital and operating cost components. This can be expressed in terms of \$/ton of NO_x controlled. The total installed cost (capital cost) of the NO_X control technology is estimated and distributed over the operating life in a series of uniform annual costs by applying a Capital Recovery Factor (CRV). The CRV depends on the operating life, time value of money, depreciation, etc. In this analysis, a CRV of 0.131 was utilized. This is equivalent to simple amortization at an annual interest rate of 10% over a 15 year operating life. The annual operating costs for the technology are calculated for the first year and then levelized over the life of the technology by applying an annual levelization factor. In this TAG analysis, a constant dollar approach was utilized so that the levelization factor is 1.0.

AR technologies can be applied to all types of combustion systems including the three most common utility boilers (wall, tangential and cyclone fired). Two applications have been selected for the economic evaluation: A cyclone fired boiler and a dry bottom wall fired unit equipped with low NO_x burners.

Reburning applications on cyclones are particularly attractive for several reasons:
1. <u>The baseline NO_x levels are high.</u> Since NO_x is a reactant in the reburning reactions, high baseline NO_x increases the rate of NO_x reduction. Thus, the cost of NO_x control for units with high baseline NO_x is low for reburning based technologies.

2. <u>Furnace temperatures are high.</u> High furnace temperatures improve reburning NO_x control since the reduction reactions are kinetically limited.

3. <u>No other combustion modification NO_x controls.</u> Low NO_x burners and OFA ports cannot be used with cyclones. This makes reburning based controls SNCR, and SCR the only alternatives.

In contrast to the cyclone application, dry bottom wall fired units can be equipped with low NO_X burners and OFA. In fact, Title 4 of the CAAA mandates that "Low NO_x Burner Technology" be applied to all dry bottom wall fired units by 2000 with a NO_x requirement of 0.46 lb/10^6 Btu.

The assumptions utilized in the analysis and those specific to the two applications (cyclone and wall-fired) are summarized in Table 9.3.1.

Table 9.3.1. Economic data.

Parameter	Units		
Unit Specifications			
Unit Capacity	MW		200
Capacity Factor	%		65
Heat Rate	Btu/KWH		10,000
Fuels data			
Coal Sulfur	lb/10^6 Btu		1.2
Coal Heating Value	Btu/lb		12,000
Coal cost	$/$10^6$ Btu		1.50
Gas cost	$/$10^6$ Btu		2.5
Coal ash content	%		10
Unit costs			
Value of SO_2 Reduction	$/ton		125
Ash Disposal Cost	$/ton		10
Economic Factors			
Capital Recovery Factor			0.131
Escalation	Constant dollar		
Boiler Data			
Firing Configuration		Cyclone	Wall-Fired
Baseline NO_x controls		None	Low NO_x Burners
Baseline NO_x	lb/10^6 Btu	1.2	0.46

9.3.3 Technology Specific Inputs

The NO_x control technologies selected for evaluation are presented in Table 9.3.2. The reburning technologies were evaluated using both gas and coal as reburning fuels. The key technology specific

assumptions are presented in Table 9.3.3 and are discussed further below.

The performance of SNCR is highly site specific. A typical performance in full scale applications with modest ammonia slip is in the range of 40% NO_x reduction with injection of an N-agent at NSR=1.5. The capital cost was based on discussions with SNCR vendors. The N-agent was Nalco Fuel Tech NO_XOut A, a commercially available aqueous urea solution.

Table 9.3.2. Evaluated NO_x control technologies.

Technology	NO_x Reduction (%)	Application	
		Cyclone	Wall
Conventional NO_x Controls			
Overfire Air	25		X
Selective Non-Catalytic Reduction (SNCR)	40	X	X
Selective Catalytic Reduction (SCR)	80	X	X
Selective Catalytic Reduction (SCR)	90	X	X
Reburning NO_x Controls			
Basic Reburning	60	X	X
Advanced Reburning—Rich (AR-Rich)	80	X	X
Advanced Reburning—Lean (AR-Lean)	80	X	X
Promoted Advanced Reburning—Lean (PAR-Lean)	90	X	X
Promoted Advanced Reburning—Rich (PAR-Rich)	90	X	X
Multiple Injection Advanced Reburning (MIAR)	95	X	X

Table 9.3.3. NO_x control technology data.

	Units	OFA	SNCR	Basic Reburn	AR R/L	PAR R/L	MIAR	SCR 80%	SCR 95%
NO_X									
NO_x Reduction	%		40	60	80	90	95	80	95
Cyclone Final NO_X	lb/10^6		0.72	0.48	0.24	0.12	0.06	0.24	0.06
Wall Fired Final NOx		0.35	0.28	0.18	0.09	0.05	0.02	0.05	0.02
SO_2 Control (via gas)	%	0	0	15	10	10	10	0	0
Capital Cost									
Gas Reburning	$/kw			15	20/22	20/22	27		
Coal Reburning	$/kw			25	30/32	30/32	37		
Conventional	$/kw	10	5					80	109
Reburning fuel firing	%			15	10	10	10		
Catalyst Life	Years							4	4

Costs and performance for SCR were obtained from an EPA report (Phase II NO_x Control, 1996) which presented DOE estimates for a high sulfur coal fired unit of 200 MW capacity with initial NO_x of 1.0 lb/10^6 Btu and 80% NO_x reduction. These conditions were scaled to those utilized here. Reburning costs and performance were based on EER's extensive data base and the projected performance of AR systems developed in this project. For the coal reburning systems, costs were included for the pulverizers to produce the fine-grind (micronized) coal necessary to minimize carbon loss. There is no incremental fuel cost (except for efficiency penalty) since the normal plant coal is used for reburning. For gas reburning systems, no pulverizers are required, but the gas cost is greater than coal. A differential of 1.00 $/$10^6$ Btu was assumed. It is assumed that coal and gas reburning technologies can achieve comparable NO_x reduction.

9.3.4 Economic Results

Figures 9.3.1 and 9.3.2 show the results of the economic comparison as plots of the total annual cost of NO_x reduction versus percentage NO_x reduction. Lines of constant unit cost of NO_x control ($/ton of NO_x reduced) are also plotted as fans. As discussed above, the unit cost of NO_x control is the appropriate figure of merit since utilities will apply controls to a number of units, bubbling to achieve the lowest total cost.

Figure 9.3.1 shows the cyclone results. The conventional NO_x controls, SNCR and SCR have the highest unit cost of NO_x control in the range of 800-1100 $/ton. The reburning based technologies are considerably lower in cost. Based on the assumptions used for this study, the costs for coal as the reburning fuel are lower than for gas. However, it should be noted that site specific considerations may favor gas in some situations. Factors favoring gas include a low gas-coal cost differential, problems related to carbon loss which are more significant with coal as the reburning fuel, and space limitations which make pulverizer installation expensive, difficult or impossible.

Figure 9.3.2 shows the wall fired results. Since the baseline NO_x is lower than for the cyclone application (0.46 versus 1.2 lb/10^6 Btu), the unit cost of NO_x control is higher. As with the cyclone results, the reburn technologies have a considerable cost advantage. OFA has been included for this application (it cannot be applied to cyclone fired units). While the total annual cost of OFA is low, the low NO_x reduction (25%) results in higher unit cost of NO_x control than all except the SCR technologies. The lower baseline NO_x for this application reduces the amount of N-agent required improving the unit cost of NO_x control for SNCR.
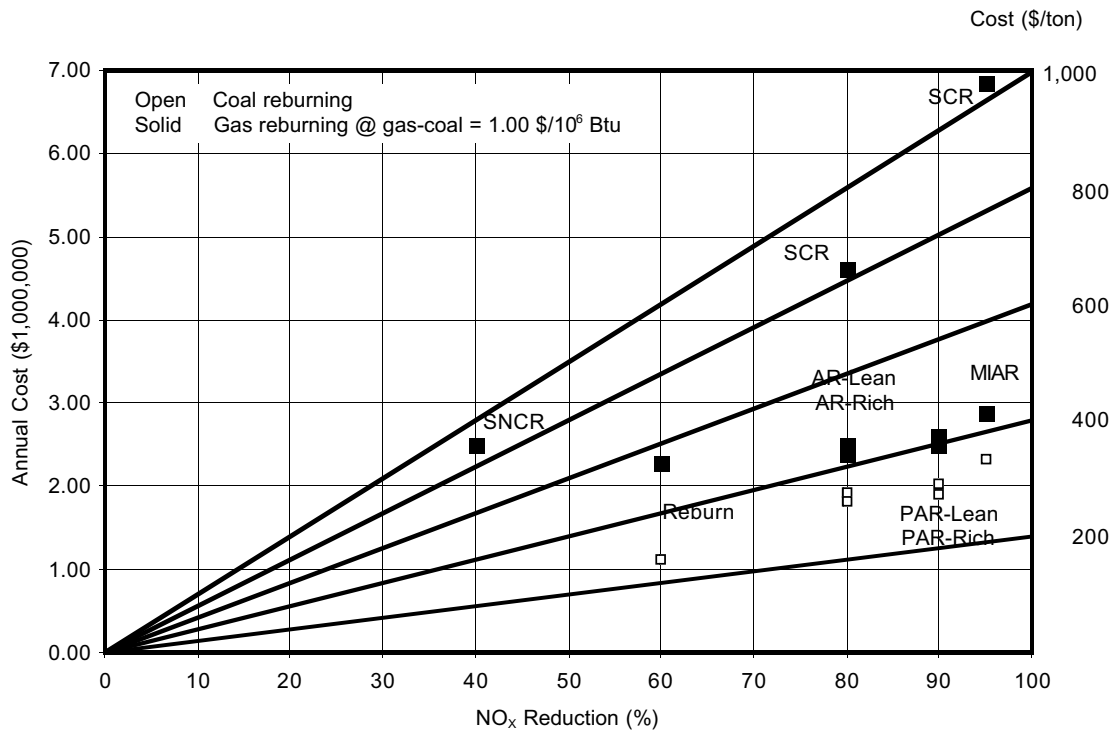
Figure 9.3.1. Cyclone fired boiler NO$_X$ economics.
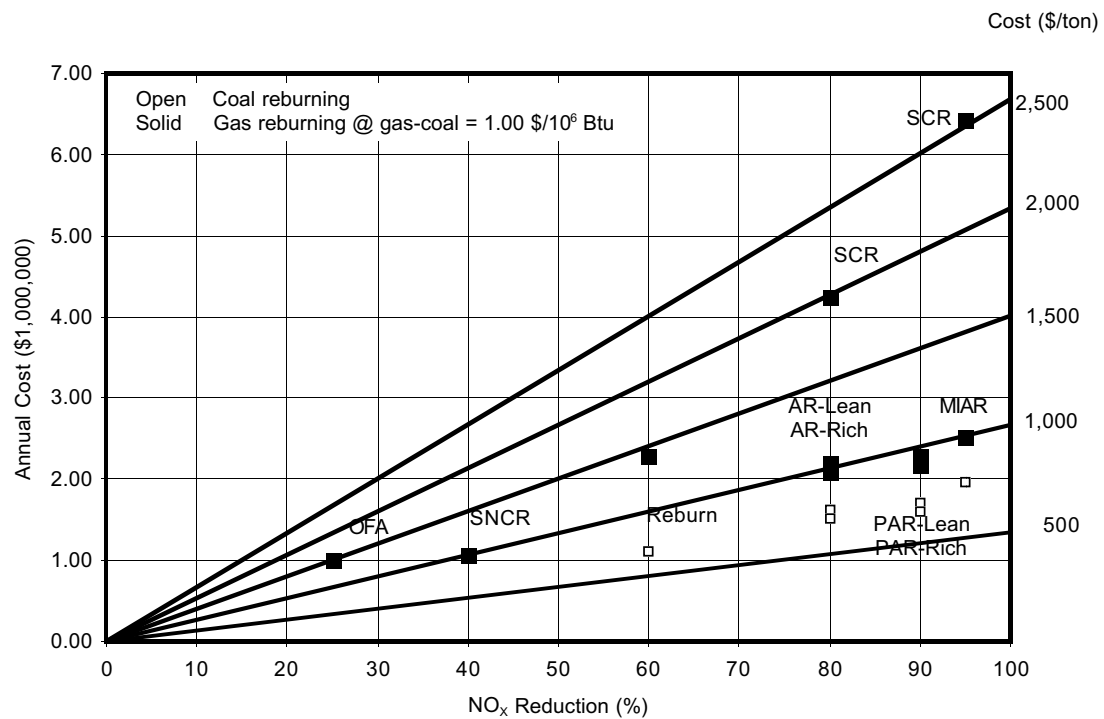
Figure 9.3.2. Wall fired boiler NO$_X$ economics.

These results show the significant economic advantage of the technologies developed on this project for the projected NO_x control market characterized by deep NO_x control and the potential for bubbling. For example, in the cyclone application, the total annual cost of SNCR is comparable to MIAR, but MIAR provides more than twice the NO_x reduction.

Table 9.3.4 compares the deep control techniques for 80 and 95% NO_x reduction. Both the coal and gas reburning based AR technologies have considerable cost advantages over SCR in the range of 48 to 69%. Under conditions of this analysis, 80% NO_x reduction via AR is 1.9-2.9 times less expensive than SCR, and 95% AR NO_x reduction is 2.0-3.2 times less expensive than SCR.

Table 9.3.4. Comparing cost effectiveness for deep NO_x control.

		Cyclone, Baseline NO_x 1.2 lb/10^6 Btu				Wall, Baseline NO_x 0.46 lb/10^6 Btu			
NO_x Control		80%		95%		80%		95%	
AR Technology		AR-Rich		MIAR		AR-Rich		MIAR	
		10^6 $/yr	$/ton NO_x	10^6 $/yr	$/ton NO_x	10^6 $/yr	$/ton NO_x	10^6 $/yr	$/ton NO_x
Costs									
	SCR	4.61	836	6.84	1,034	4.26	2,011	6.41	2,527
	AR (gas reburning)	2.39	433	2.88	440	2.08	986	2.52	1,000
	AR (coal reburning)	1.81	328	2.33	355	1.51	712	1.96	780
Cost Reduction									
	AR (gas reburning)	48		58		51		61	
	AR (coal reburning)	61		66		65		69	

9.3.5 Market Assessment

The size of the market for AR technologies has been estimated by considering the existing and projected CAAA regulations, the power plants affected by the regulations, and industry projections for the mix of NO_x control technologies necessary for cost effective compliance with these regulations. The results are presented in Table 9.3.5 and are discussed below.

Table 9.3.5. Estimated market for AR technologies.

	Units	NEOTR	OTAG Expansion	Total
States		10	27	37
Boiler Capacity				
Total	1,000 MW	70.40	305.70	376.10
Coal Fired Portion	%	36.93	50.00	
Coal Fired Capacity	1,000 MW	26.00	152.85	178.85
Projected Deep Controls				
Portion of Coal Fired		38.00	67.00	
Total Capacity To Be Retrofitted	1,000 MW	9.88	102.41	112.29
AGR Market				
Unit AGR Cost	$/kw	30.00	30.00	
Total Market (100% penetration)				
Capacity	1,000 MW	9.88	102.41	112.29
Installed Cost	$1,000,000	296.40	3,072.29	3,368.69
Potential Penetration				
Estimated Penetration	%	50.00	50.00	
Capacity	1,000 MW	4.94	51.20	56.14
Installed Cost	$1,000,000	148.20	1,536.14	1,684.34

At present, NO_x control regulations requiring reductions of up to 75% have been established in the NEOTR. A recent study conducted by ICF Kaiser evaluated the alternatives for cost effective NO_x control compliance in this region. It was projected that 9,880 MW of coal fired units will be retrofitted for deep NO_x control, assumed to be SCR. This is the AR market potential and corresponds to $296 million at the mean installed cost for AR of 30 $/kw (range 22-37 $/kw). Although AR is projected to be considerably more cost effective than SCR, a number of factors will reduce AR's market penetration such as the lack of full scale operating experience at the time the retrofit decision is required. If the market is shared equally between SCR and AR, AR will be installed on 4,900 MW at a total cost of $148 million.

EPA is now considering expanding the NEOTR to the 37 state OTAG region. NO_x reductions as high as 85% are being discussed for units in this region. A recent study of NO_x control alternatives in this area was conducted by Hewson and Stamberg (1995) using an approach similar the ICF Kaiser study. Using similar assumptions, the total market for deep NO_x control in the expansion region is 102,000 MW corresponding to $3.07 billion. If the market is shared equally between SCR and AR, AR will be installed on 51,000 MW at a total cost of $1.54 billion. The total market is the sum of the NEOTR and expansion region.

The total market is the sum of the NEOTR and expansion region and is as shown in Table 9.3.6.

Table 9.3.6. Total estimated AR market.

	Capacity (1,000 MW)	Installed Cost ($ billion)
Total Market	112	3.4
Projected Penetration, 50%	56	1.7

Economic analysis demonstrates a considerable economic advantage for the AR technologies. In particular, for deep NO_x control in the 80-95% range the cost savings are at least 50% in comparison with SCR. NO_x reduction efficiency of 80% via AR is 1.9-2.9 times less expensive than SCR, and 95% AR NO_x reduction is 2.0-3.2 times less expensive than SCR. The resulting market for AR technologies is estimated to be about $1.7 billion.

9.4 Design Methodology and Application: Conclusions

In this task, a design methodology, which consists of various computational and analytical models, was generalized for use with SGAR technologies. This methodology was then applied to develop conceptual designs for application of three AR concepts—AR-Lean, AR-Rich, and MIAR to a typical 100 MW tangentially fired utility boiler, and to predict the impacts of the AR systems on boiler performance and NO_x emissions.

The design methodology uses various experimental and analytical tools to develop the injector specifications and operating characteristics of the AR system with the objective of meeting specific process requirements for optimum emissions control performance while maintaining boiler operation and performance at normal levels.

Thermal performance models were used to evaluate the impacts of implementing AR processes on the thermal performance of a nominally 100 MW tangentially fired boiler. For implementation of AR-Lean, AR-Rich, or MIAR processes on this boiler, the reburning fuel would be injected into the lower furnace and the overfire air would be injected into the upper furnace in a cavity between the first two tube banks of the convective pass. The model results indicate that the this configuration is expected to increase carbon loss and reduce main and reheat steam temperatures in comparison to baseline or gas reburning operation. Changes in the operating settings of the AR process can be used to mitigate some of the increase in carbon loss. However, the overall boiler efficiency for operation with an AR system is similar to that for operation with a basic gas reburning system. Changes in the operating settings of the AR process or in the boiler operating settings can be used

to mitigate the impacts of AR on main and reheat steam temperatures. It should be noted that the results of this analysis are specific to the boiler configuration evaluated and should not be generalized to other boiler designs. The results of injection system analysis indicate that good mixing of the process streams necessary to implement advanced reburning (AR-Lean, AR-Rich, and MIAR) on the case study boiler can be achieved. Natural gas can be injected from each wall in a pattern which achieves good distribution of the reburning fuel. Overfire air injection into a cavity in the convective pass, needed for implementation of each of the AR processes under consideration, can be achieved using high pressure wall jets. For the AR-Lean and MIAR processes, these ports can also be used to inject the reagent. Injection of reagent into the upper furnace, needed for the AR-Rich and MIAR processes, can be achieved using a lance-based system. The overall boiler efficiency for operation with AR systems is similar to that for operation with a basic gas reburning system. Full scale NO_x reduction level is predicted to be above 90% and can be additionally increased with the use of promoters.

The original work scope was based on applying the design methodology to a hypothetical case study; however, it was hoped that an initial AR demonstration could be developed in parallel with Phase I (outside the scope of this DOE project) to allow application to a real unit and evaluation of some of the SGAR elements. EER was successful in developing an initial AR demonstration project. In 1995 EER installed AR-Lean on a 105 MW tangentially fired boiler. Initial AR testing was conducted in 1996-97 and will continue through 1998. This unit was used as the basis for extending the design methodology. AR-Lean tests on the boiler showed that stratification within the reburn zone could adversely affect the performance. Regions of inadequate CO in the reburning zone reduced the N-agent NOx control and caused NH3 slip. While modifications were successful in reducing stratification, this experience shows the importance of mixing and scale up, two factors to be evaluated in Phase II. In addition to these AR-Lean tests, opportunity was taken to obtain preliminary larger scale data on several of the SGAR components, including N-agent injection into the reburning zone, N-agent injection downstream of the reburning zone in an SNCR mode, and N-agent injection into the reburning zone and with the overfire air.

Economic analysis demonstrates a considerable economic advantage of AR technologies in comparison with existing commercial NOx control techniques, such as basic reburning, SNCR, and SCR. Particularly for deep NOx control, AR results in 2-3 times lower costs (in $/ton of NOx removed) than SCR for the same level of NOx control. The market for AR technologies is estimated to be above $1.5 billion.

10.0 CONCLUSIONS

1. This project is developing novel AR concepts for high efficiency and low cost NO_x control from coal fired utility boilers. AR technologies are based on a combination of basic reburning and N-agent/promoter injection. All Phase I project objectives have been met or exceeded, and it was demonstrated that the AR technologies can provide effective NO_x control for coal fired combustors. Three technologies were originally envisioned for development: AR-Lean, AR-Rich, and MIAR. Along with these, three additional technologies were identified during the project: reburning plus promoted SNCR, AR-Lean plus promoted SNCR, and AR-Rich plus promoted SNCR. These six SGAR configurations differ primarily in the N-agent/promoter injection components. Various components can be selected to tailor the SGAR system to site specific boiler design and NO_x control requirements.

2. Bench scale combustion tests in the 20 kW facility demonstrated NO_x reduction of 86%, 88%, and 91% for AR-Lean, AR-Rich, and MIAR, respectively. These levels of NO_x control can be achieved with only 15 ppm Na_2CO_3 in flue gas. Pilot scale studies in the 200 kW combustion facility demonstrated the ability of the AR technologies to achieve NO_x reductions of 95+% during gas firing and 90+% during coal firing. Byproduct emissions were found to be lower than those generated by commercial reburning and SNCR technologies. Sodium compounds promote NO_x reduction more effectively during gas firing than coal firing; however, NO_x control without sodium addition is more effective for coal than for gas firing. The maximum NO_x reductions achieved by the SGAR configurations were 95-98% during gas firing and 90-95% during coal firing.

3. A flow system decomposition study revealed that the primary gas-phase decomposition products of Na_2CO_3 are Na atoms, NaOH and CO_2. The observed decomposition rate of Na_2CO_3 can be described kinetically in terms of two irreversible Na_2CO_3

$\rightarrow Na_2O + CO_2$ and $Na_2O + CO_2 \rightarrow Na_2CO_3$ and one reversible $Na_2O + H_2O <=> 2NaOH$ chemical reactions. The corresponding rate coefficients were measured or estimated to describe the rate of Na_2CO_3 decomposition in the temperature range of 900-1190 K. Extrapolating the results to higher temperatures shows that Na_2CO_3 decomposition at temperatures over 1400 K produces NaOH and CO_2 very quickly . NaOH then decomposes more slowly. Experiments show no chemical reaction between Na_2CO_3 decomposition products and H_2, CO, CH_4 or NO at 1150 K. This confirms that sodium has little or no reactivity with major flue gas components in the absence of ammonia.

4. A detailed reaction mechanism was developed to model the AR chemical processes. The mechanism (355 reactions of 65 species) includes the following submechanisms: GRI-Mech-2.11, SNCR chemistry, sodium chemistry with Na_2CO_3 decomposition reactions, SO_2/SO_3 reactions, and interaction of HCl with flue gas components. Kinetic modeling provided insight into the controlling factors of the process and qualitatively described the observed reaction trends. The following factors mainly define the efficiency of AR systems: equivalence ratio in the reburning zone, process streams injection temperatures (reburning fuel, N-agents, promoters, and OFA), concentrations of N-agents and promoters, delay times for injection of N-agents into the reburning and burnout zones, and characteristic mixing times of the injection streams with flue gas. The modeling predicted and explained the NO_x reduction enhancement of sodium promotion under both fuel-rich and fuel-lean conditions. The promotion effect is most pronounced in systems with long characteristic mixing times which are typical of full scale industrial and utility boilers. A sensitivity analysis revealed the most significant elementary reactions affecting formation and destruction of NO and other N-containing compounds in the reburning and burnout zones.

5. The AR design methodology was upgraded by using experiments and analytical models to include the second generation improvements. This work took advantage of a full scale application of the original AR configuration in progress on a 105 MW tangentially fired boiler

outside the scope of this project. The upgraded methodology was used to prepare process designs for three SGAR concepts on the 105 MW boiler and to predict the impacts of the SGAR systems on boiler performance and NO_x emissions. Some elements of SGAR were tested in the boiler. These tests showed that the large scale stratification in the furnace gases affected the NO_x reduction and ammonia slip associated with N-agent injection. These mixing-related issues will be addressed in Phase II in the 10 x 10^6 Btu/hr tests and limited additional boiler tests.

6. An economic analysis was conducted to compare the cost effectiveness of SGAR and SCR using the EPRI Technology Assessment Guide methodology for two representative Title 1 CAAA applications: a cyclone fired boiler and a wall fired boiler equipped with low NO_x burners. The total cost of NO_x control (combining capital and operating cost components) for the SGAR systems was 48-69% less than for SCR depending on the specific application. The requirements for NO_x control under the CAAA were evaluated. The key drivers are the current ozone non- attainment areas, the potential to expand those regions to the eastern half of the US and the recent tightening of the National Ambient Air Quality Standards for ozone and fine particulate which will require additional NO_x control nationwide. The market for AR technologies was estimated to be above $1.5 billion.

7. Additional work is needed in Phase II to move the technology to a demonstration stage. In particular, the following steps are necessary to optimize and scale up the SGAR technologies:

• Identify alternative promoters based on the promotion mechanisms developed in Phase I.
• Identify and test coal mineral compounds responsible for the increased NO_x reduction in AR-Rich and MIAR with coal firing (about 10% higher than for gas firing).
• Optimize mixing (reburn fuel, N-agents, OFA) via combined chemistry/mixing models.
• Optimize N-agent injection to maximize NO_x reduction with negligible ammonia slip.
• Evaluate the effect of N-agent/promoter mixing times representative of full scale.

- Optimize SGAR with new promoters and mixing regimes at 1×10^6 Btu/hr scale.

- Scale up and confirm the design methodology via 10×10^6 Btu/hr Proof-of- Concept tests and limited component tests during the ongoing boiler AR tests.

- Update the economic and market analysis to confirm the advantages of SGAR.

11.0 ACKNOWLEDGMENTS

12.0 REFERENCES

Ager, J.W., III and Howard, C.J. (1987). Gas Phase Kinetics of the Reactions of NaO with H_2, D_2, H_2O, and D_2O, J. Chem. Phys., V. 87, p. 921.

Ager, J.W., III and Talcott, C.L., Howard, C.J. (1986). Gas Phase Kinetics of the Reactions of Na and NaO with O_3 and N_2O, J. Chem. Phys., V. 85, p. 5584.

Arand, J.K., Muzio, L.J. and Sotter, J.G., U.S. Patent 4,208,386, June 17, 1980.

Armitage, J. W. and Cullis, C. F. (1971). Studies of the Reaction between Nitrogen Dioxide and Sulfur Dioxide, Combust. Flame, V. 16, p. 125.

Atkinson, R., Baulch, D.L., Cox, R.A., Hampson, R.F., Jr., Kerr, J.A. and Troe, J. (1992). Evaluated Kinetic and Photochemical Data for Atmospheric Chemistry, J. Phys. Chem. Ref. Data, V. 21, pp. 1125-1568.

Bailar, J.C. Jr., Emeleus, H.J. Nyholm, R. and Trotman-Dickenson, A.F. (1973). Comprehensive Inorganic Chemistry, Pergamon Press.

Ball, M.C., Snelling, C.M., Strachan, A.N. and Strachan, R.M. (1992). Thermal Decomposition of Solid Sodium Sesquicarbonate, $Na_2CO_3.NaHCO_3.2H_2O$. J. Chem. Soc. Faraday Trans. 88, pp. 631-636.

Barin, I. (1989). Thermodynamic Data of Pure Substances, VCH Verlagsgesellschaft mbH, D-6940 Weinheim, Germany.

Baulch, D.L., Duxbury, J., Grant, S.J. and Montague, D.C. (1981). Evaluated Kinetic Data for High Temperature Reactions. Volume 4. Homogeneous Gas Phase Reactions of Halogen- and Cyanide-Containing Species, J. Phys. Chem. Ref. Data, V. 10, Suppl. 1, 1-1.

Bowman, C.T. (1996). In Physical and Chemical Aspects of Combustion: A Tribute to Irvine Glassman (F.L. Dryer, R.F. Sawyer, Eds), Gordon and Breach.

Bowman, C.T., Hanson, R.K., Davidson, D.F., Gardiner, W.C.Jr., Lissianski, V.V., Smith, G.P., Golden, D.M., Frenklach, M., Wang, H. and Goldenberg, M. (1995). http://www.gri.org.

Carabetta, R. and Kaskan, W.E. (1968). The Oxidation of Sodium, Potassium, and Cesium in Flames. J. Phys. Chem. 72, No. 7, pp. 2483-2489.

Chase, M.W. Jr., Davies, C.A., Downey, J.R. Jr., Frurip, D.J., McDonald, R.A. and Syverud, A.N. (1985). JANAF Thermochemical Tables, Third Edition. Journal of Physical and Chemical Reference Data, 14, Suppl. 1.

Chen, S.L., Ho, L., Cole, J.A and Seeker, W.R., 1989, "An Investigation to Define the Physical/Chemical Constraints Which Limit NO_x Emission Reduction Achievable by Reburning", EER Final Report, DOE contract No. DE-AC22-86PC91025.

Chen, S.L., Lyon, R.K. and Seeker, W.R. (1991). Environ. Progress, V. 10, P. 182, August, 1991.

Chen, S.L., Seeker, W.R., Lyon, R.K. and Ho, L. (1993). N_2O Decomposition Catalyzed in the Gas Phase by Sodium, 205th ACS National Meeting, Denver, CO, March 28 - April 2, 1993.

Cohen, N. (1996) J. Phys. Chem. Ref. Data 25, 1411.

Cotton, D.H. and Jenkins, D.R. (1971). Trans. Faraday Soc. 67, 730, 1971.

DeMore, W.B., Golden, D.M., Hampson, R.F., Howard, C.J., Kurylo, M.J., Molina, M.J., Ravishankara, A.R. and Sander, S.P. (1987). Chemical Kinetics and Photochemical Data for Use in Stratospheric Modeling, Evaluation Number 8, JPL Publication 87-41, 1.

Ebbinghaus, B.B. (1993). Thermodynamics of Gas Phase Chromium Species, Combust. Flame, 93, pp. 119-137.

Feitelberg, A.S. (1994). CET89 for the Macintosh: A Chemical Equilibrium and Transport Properties Calculator. General Electric Company.

Fenimore, C.P. (1973). Two Modes of Interaction of NaOH and SO_2 in Gases From Fuel-Lean H_2-Air Flames, 14th Symposium (Intern.) on Combustion, The Combustion Institute, Pittsburgh, pp. 955-963.

Frenklach, M., Wang, H., Bowman, C.T., Hanson, R.K., Smith, G.P., Golden, D.M., Gardiner, W.C., and Lissianski, V. (1994). An Optimized Kinetics Model for Natural Gas Combustion, 25th International Symposium on Combustion, Irvine, California, Work-In-Progress Poster Session 3, Number 26.

Galwey, A.K. and Hood, W.J. (1979). Thermal Decomposition of Sodium Carbonate Perhydrate in the Solid State. J. Phys. Chem. 83, pp. 1810-1815.

Gardiner, W.C. Jr., Walker, B.F. and Wakefield, C.B. (1981). In Shock Waves in Chemistry, A. Lifshitz., Ed.; Marcel Dekker: New York; p. 319.

Glarborg, P., Dam-Johansen, K. and Kristensen, P.G. (1993). Reburning Rich-Lean Kinetics, Final Report to GRI, Contract No. 5091-260-2126.

Heda, P.K. Dollimore, D., Alexander, K.S., Chen, D., Law, E. and Bicknell, P. (1995). A Method of Assessing Solid State Reactivity Illustrated by Thermal Decomposition Experiments on Sodium Bicarbonate. Thermochimica Acta 255, pp. 255-272.

Hewson, T.A. and Stamberg, J.B. (1995) Evaluation of Proposed 37 State Seasonal NO_x Control Program. Compliance Costs and Issues, Report by Energy Ventures Analysis, Inc., Arlington, VA.

Hildenbrand, D.L. And Murad, E. (1970). Dissociation Energy of NaO(g) and the Heat of Atomization of Na_2O(g), J. Chem. Phys. 53, 3403-3408.

Ho, L. Chen, S.L., Seeker, W.R. and Maly, P.M. (1993). U.S. Patent No. 5,270,025.

Husain, D. and Plane, J.M.C. (1982). Kinetic Investigation of the Reaction Between Na + O_2 + M by Time-Resolved Atomic Resonance Absorption Spectroscopy. J. Chem. Soc. Faraday Trans. 2 78, pp. 163-178.

Husain, D. and Marshall, P. (1986). Determination of Absolute Rate Data for the Reactions of Atomic Sodium with CH_3F, CH_3Cl, CH_3Br, HCl, and HBr as a Function of Temperature by Time-Resolved Atomic Resonance Spectroscopy, Int. J. Chem. Kinet., V. 18, p. 83.

Hynes, A.J., Steinberg, M. and Schofield, K., The Chemical Kinetics and Thermodynamics of Sodium Species in Oxygen-Rich Hydrogen Flames, J. Chem. Phys. 80, 1984, pp. 2585-2597.

Jensen, D.E. and Jones, G.A. (1982). Kinetics of Flame Inhibition by Sodium, J. Chem. Soc. Faraday Trans. 1, V. 78, p. 2843.

Kaskan, W.E. (1971). The Reaction of Alkali Atoms in Lean Flames. 10th Symposium (International) on Combustion, The Combustion Institute, pp.4 1-45.

Kee, R.J., Rupley, F.M. and Miller, J.A. (1992). Chemkin II: a Fortran Chemical Kinetics Package for the Analysis of Gas Phase Chemical Kinetics, Sandia National Laboratories, Report SAND89-8009.

Lay, T.H., Bozzelli, J.W., Dean, A.M., and Ritter, E.R. (1995) J. Phys. Chem. 99, 14514.

Lutz, A.E., Kee, R.J. and Miller, J.A. (1987). SENKIN: a Fortran Program for Predicting Gas Phase Chemical Kinetics with Sensitivity Analysis, Sandia National Laboratories Report No.

SAND87-8248.

Lyon, R. K. U.S. Patent 3,900,554, August 19, 1975.

Lyon, R.K. and Hardy, J.E. (1986). Ind. Eng. Chem. Fundam. 25, 19.

Mallard, W.G., Westley, F., Herron, J.T., Hampson, R.F., and Frizzell, D.H. (1994). NIST Chemical Kinetics Database: Version 6.0, National Institute of Standards and Technology, Gaithersburg, MD.

Marshall, P., Narayan, A.S., and Fontijn, A. (1990) J. Phys. Chem. 94, 2998.

McBride, B.J., Gordon, S., and Reno, M.A. (1993). Coefficients for Calculating Thermodynamic and Transport Properties of Individual Species, NASA Technical Memorandum 4513, October, 1993.

McBride, B.J., M.A. Reno, and S. Gordon (1994), CET93 and CETPC: An Interim Updated Version of the NASA Lewis Computer Program for Calculating Complex Chemical Equilibria with Applications, NASA Lewis Research Center, Cleveland, Ohio, NASA technical Memorandum 4557; program distributed by COSMIC, NASA's Software Technology Center, The University of Georgia, GA.

McEwan, M.J. and Phillips, L.F. (1965). Trans. Faraday Soc. 62, p. 1717.

Miller, J.A. and Bowman, C.T. (1989). Mechanism and Modeling of Nitrogen Chemistry in Combustion, Progr. Energy Combust. Sci., 15, 287-338.

Mitani, T. and Nioka, T. (1984). Extinction Phenomenon of Premixed Flames with Alkali Metal Compounds. Combust. Flame 55, pp. 13-21.

Partridge, H., Bauschlichter, C.W., Jr., Sodupe, M. and Langhoff, S.R. (1992). Chem. Phys. Lett., V. 195, p. 200.

Perry, R.A. and Miller, J.A. (1995). An Exploratory Investigation of the Use of Alkali Metals in Nitrous Oxide Control. Int. J. Chem. Kinetics 28, pp. 217-234.

Phase II NO_x Controls for the MARAMA and NESCAUM Regions, EPA-453/R-96-002, 1996.

Plane, J.M.C. and Rajasekhar, B. (1989). Kinetic Study of the Reactions $Na + O_2$ and $Na + N_2O$ over an Extended Temperature Range, J. Phys. Chem., V. 93, p. 3135.

Plane, J.M.C. and Husain, D. (1986). Determination of the Absolute Rate Constant for the

Reaction O+NaO = Na+O$_2$ by Time-Resolved Atomic Chemiluminescence, J. Chem. Soc. Faraday Trans. 2, V. 82, p. 2047.

Plane, J.M.C. (1991) Int. Reviews Phys. Chem. 10, 55.

Plane, J.M.C. (1992). A Comparison Between the Oxidation Reactions of the Alkali and Alkaline Earth Atoms, Gas-Phase Metal Reactions, ed. A. Fontijn, Elsevier Science Publ., Amsterdam, Netherlands, pp. 29-56.

Schofield, K., and Steinberg, M. (1992) J. Phys. Chem. 96, 715.

Seeker, W.R., Proc. of the Reburning Workshop, Orenas Slott, Sweden, Nov. 26-27, 1990.

Seeker, W.R., Chen, S.L. and Kramlich, J.C., 1992, "Advanced Reburning for Reduction of NO$_x$ Emissions in Combustion Systems", U.S. Patent 5,139,755.

Shi, Y. and Marshall, P. (1991). A Kinetic Study of the Recombination Reaction Na + SO$_2$ + Ar, J. Phys. Chem., V. 95, p. 1654.

Silver, J.A. and Kolb, C.E. (1986). Gas-Phase Reaction Rate of Sodium Superoxide with Hydrochloric Acid, J. Phys. Chem., V. 90, p. 3267.

Silver, J.A., Stanton, A.C., Zahniser, M.S. and Kolb, C.E. (1984). Gas-Phase Reaction Rate of Sodium Hydroxide with Hydrochloric Acid, J. Phys. Chem., V. 88, p. 3123.

Smith, O. I., Tseregounis, S. and Wang, S-N. (1982). High-Temperature Kinetics of the Reactions of SO$_2$ and SO$_3$ with Atomic Oxygen, Int. J. Chem. Kinet., V. 14, p. 679.

Srinivasachar, S., Helble, J.J., Ham, D.O. and Domazetis, G. (1990). A Kinetic Description of Vapor Phase Alkali Transformations in Combustion Systems. Progr. Energy Combust. Sci. 16, pp. 303-309.

Steinberg, M. and Schofield, K. (1990). The Chemistry of Sodium with Sulfur in Flames, Prog. Energy Combust. Sci., Vol. 16, pp. 311-317.

Terai, R., Sugae, I., Hayami, R. (1968). Kinetics and Mechanism of the Solid State Reaction of Alkali Carbonate and Silica. Zairyo, 17(177) 527.

United States Environmental Protection Agency. (1977). Process Measurement Procedures - Sulfuric Acid Emissions.

Wendt, J.O.L., Sterling, C.V. and Matovich, M.A. (1973). 14th Symposium (International) on

Combustion, P. 897, 1973.

Westley, F., Frizzell, D.H., Herron, J.T., Hampson, R.F. and Mallard, W.G. (1994). NIST Chemical Kinetics Database, version 5.0. NIST.

Wu, Y.-L. and Shih, S.-M. (1993). Instrinsic Kinetics of the Thermal Decomposition of Sodium Bicarbonate. Thermochimica Acta 223, pp. 177-186.

Zamansky, V.M. and Borisov, A.A. (1992). Promotion of High-Temperature Self-Ignition, Prog. Energy Combust. Sci., V. 18, pp. 297-325.

Zamansky, V.M. and Maly, P.M. (1996a). Second Generation Advanced Reburning for High Efficiency NOx Control, EER 1st Quarterly Report, DOE Contract No. DE-AC22-95PC95251, January, 1996.

Zamansky, V.M. (1996). Second Generation Advanced Reburning for High Efficiency NOx Control, EER 2nd Quarterly Report, DOE Contract No. DE-AC22-95PC95251, April, 1996.

Zamansky, V.M. and Maly, P.M. (1996b). Second Generation Advanced Reburning for High Efficiency NOx Control, EER 3d Quarterly Report, DOE Contract No. DE-AC22-95PC95251, July, 1996.

Zamansky, V.M. and Maly, P.M. (1996c). Second Generation Advanced Reburning for High Efficiency NOx Control, EER 4th Quarterly Report, DOE Contract No. DE-AC22-95PC95251, October, 1996.

Zamansky, V.M. and Maly, P.M. (1997a). Second Generation Advanced Reburning for High Efficiency NOx Control, EER 5th Quarterly Report, DOE Contract No. DE-AC22-95PC95251, January, 1997.

Zamansky, V.M. et al. (1997b). Second Generation Advanced Reburning for High Efficiency NOx Control, EER 6th Quarterly Report, DOE Contract No. DE-AC22-95PC95251, April, 1997.

Appendix 1. Reaction Mechanism in Chemkin/Senkin Interpreter Format

```
CHEMKIN INTERPRETER OUTPUT: CHEMKIN-II Version 3.1 Feb. 1993; DOUBLE PRECISION
                        --------------------
                        ELEMENTS    ATOMIC
                        CONSIDERED  WEIGHT
                        --------------------
                        1. O        15.9994
                        2. H        1.00797
                        3. C        12.0112
                        4. N        14.0067
                        5. AR       39.9480
                        6. S        32.0640
                        7. NA       22.9898
                        8. CL       35.4530
                        --------------------
-------------------------------------------------------------------------------
                         C
                       P H
                       H A
                       A R
SPECIES                S G MOLECULAR TEMPERATURE   ELEMENT COUNT
CONSIDERED             E E WEIGHT    LOW    HIGH    O  H  C  N  AR S  NA CL
-------------------------------------------------------------------------------
  1. H2               G 0    2.01594 200.0 3500.0   0  2  0  0  0  0  0  0
  2. H                G 0    1.00797 200.0 3500.0   0  1  0  0  0  0  0  0
  3. O                G 0   15.99940 200.0 3500.0   1  0  0  0  0  0  0  0
  4. O2               G 0   31.99880 200.0 3500.0   2  0  0  0  0  0  0  0
  5. OH               G 0   17.00737 200.0 3500.0   1  1  0  0  0  0  0  0
  6. H2O              G 0   18.01534 200.0 3500.0   1  2  0  0  0  0  0  0
  7. HO2              G 0   33.00677 200.0 3500.0   2  1  0  0  0  0  0  0
  8. H2O2             G 0   34.01474 200.0 3500.0   2  2  0  0  0  0  0  0
  9. C                G 0   12.01115 200.0 3500.0   0  0  1  0  0  0  0  0
 10. CH               G 0   13.01912 200.0 3500.0   0  1  1  0  0  0  0  0
 11. CH2              G 0   14.02709 200.0 3500.0   0  2  1  0  0  0  0  0
 12. CH2(S)           G 0   14.02709 200.0 3500.0   0  2  1  0  0  0  0  0
 13. CH3              G 0   15.03506 200.0 3500.0   0  3  1  0  0  0  0  0
 14. CH4              G 0   16.04303 200.0 3500.0   0  4  1  0  0  0  0  0
 15. CO               G 0   28.01055 200.0 3500.0   1  0  1  0  0  0  0  0
 16. CO2              G 0   44.00995 200.0 3500.0   2  0  1  0  0  0  0  0
 17. HCO              G 0   29.01852 200.0 3500.0   1  1  1  0  0  0  0  0
 18. CH2O             G 0   30.02649 200.0 3500.0   1  2  1  0  0  0  0  0
 19. CH2OH            G 0   31.03446 200.0 3500.0   1  3  1  0  0  0  0  0
 20. CH3O             G 0   31.03446 300.0 3000.0   1  3  1  0  0  0  0  0
 21. CH3OH            G 0   32.04243 200.0 3500.0   1  4  1  0  0  0  0  0
 22. C2H              G 0   25.03027 200.0 3500.0   0  1  2  0  0  0  0  0
 23. C2H2             G 0   26.03824 200.0 3500.0   0  2  2  0  0  0  0  0
 24. C2H3             G 0   27.04621 200.0 3500.0   0  3  2  0  0  0  0  0
 25. C2H4             G 0   28.05418 200.0 3500.0   0  4  2  0  0  0  0  0
 26. C2H5             G 0   29.06215 200.0 3500.0   0  5  2  0  0  0  0  0
 27. C2H6             G 0   30.07012 200.0 3500.0   0  6  2  0  0  0  0  0
 28. HCCO             G 0   41.02967 300.0 4000.0   1  1  2  0  0  0  0  0
 29. CH2CO            G 0   42.03764 200.0 3500.0   1  2  2  0  0  0  0  0
 30. HCCOH            G 0   42.03764 200.0 5000.0   1  2  2  0  0  0  0  0
 31. N                G 0   14.00670 200.0 6000.0   0  0  0  1  0  0  0  0
 32. NH               G 0   15.01467 200.0 6000.0   0  1  0  1  0  0  0  0
 33. NH2              G 0   16.02264 200.0 6000.0   0  2  0  1  0  0  0  0
 34. NH3              G 0   17.03061 200.0 6000.0   0  3  0  1  0  0  0  0
 35. NNH              G 0   29.02137 200.0 6000.0   0  1  0  2  0  0  0  0
 36. NO               G 0   30.00610 200.0 6000.0   1  0  0  1  0  0  0  0
 37. NO2              G 0   46.00550 200.0 6000.0   2  0  0  1  0  0  0  0
 38. N2O              G 0   44.01280 200.0 6000.0   1  0  0  2  0  0  0  0
 39. HNO              G 0   31.01407 200.0 6000.0   1  1  0  1  0  0  0  0
 40. CN               G 0   26.01785 200.0 6000.0   0  0  1  1  0  0  0  0
 41. HCN              G 0   27.02582 200.0 6000.0   0  1  1  1  0  0  0  0
 42. H2CN             G 0   28.03379 300.0 4000.0   0  2  1  1  0  0  0  0
 43. HCNN             G 0   41.03252 300.0 5000.0   0  1  1  2  0  0  0  0
 44. HCNO             G 0   43.02522 300.0 5000.0   1  1  1  1  0  0  0  0
 45. HOCN             G 0   43.02522 300.0 5000.0   1  1  1  1  0  0  0  0
 46. HNCO             G 0   43.02522 300.0 5000.0   1  1  1  1  0  0  0  0
 47. NCO              G 0   42.01725 200.0 6000.0   1  0  1  1  0  0  0  0
 48. N2               G 0   28.01340 300.0 5000.0   0  0  0  2  0  0  0  0
 49. AR               G 0   39.94800 300.0 5000.0   0  0  0  0  1  0  0  0
 50. N2H2             G 0   30.02934 300.0 5000.0   0  2  0  2  0  0  0  0
 51. SO2              G 0   64.06280 300.0 5000.0   2  0  0  0  0  1  0  0
 52. SO3              G 0   80.06220 300.0 5000.0   3  0  0  0  0  1  0  0
 53. HSO3             G 0   81.07017 300.0 2000.0   3  1  0  0  0  1  0  0
```

```
-----------------------------------------------------------------------
 54. HCL          G 0  36.46097  300.0 2000.0  0  1  0  0  0  0  0  1
 55. CL           G 0  35.45300  300.0 2000.0  0  0  0  0  0  0  0  1
 56. CL2          G 0  70.90600  300.0 2000.0  0  0  0  0  0  0  0  2
 57. NAO2         G 0  54.98860  300.0 2000.0  2  0  0  0  0  0  1  0
 58. NASO2        G 0  87.05260  300.0 2000.0  2  0  0  0  0  1  1  0
 59. NA2SO3       L 0 126.04180  300.0 2000.0  3  0  0  0  0  1  2  0
 60. NA2SO4       G 0 142.04120  300.0 2000.0  4  0  0  0  0  1  2  0
 61. NACL         G 0  58.44280  300.0 2000.0  0  0  0  0  0  0  1  1
 62. NAOH         G 0  39.99717  300.0 2000.0  1  1  0  0  0  0  1  0
 63. NA           G 0  22.98980  300.0 2000.0  0  0  0  0  0  0  1  0
 64. NAO          G 0  38.98920  300.0 2000.0  1  0  0  0  0  0  1  0
 65. NA2CO3       G 0 105.98895  300.0 2000.0  3  0  1  0  0  0  2  0
 66. NA2O         S 0  61.97900  300.0 2000.0  1  0  0  0  0  0  2  0
-----------------------------------------------------------------------
```

$$(k = A\ T^{**}b\ \exp(-E/RT))$$

	REACTIONS		A	b	E

NOTE: A units mole-cm-sec-K, E units cal/mole

!GRI-Mech 2.11

```
  1. 2O+M<=>O2+M                                   1.20E+17  -1.0      0.0
        H2           Enhanced by   2.400E+00
        H2O          Enhanced by   1.540E+01
        CH4          Enhanced by   2.000E+00
        CO           Enhanced by   1.750E+00
        CO2          Enhanced by   3.600E+00
        C2H6         Enhanced by   3.000E+00
        AR           Enhanced by   8.300E-01
  2. O+H+M<=>OH+M                                   5.00E+17  -1.0      0.0
        H2           Enhanced by   2.000E+00
        H2O          Enhanced by   6.000E+00
        CH4          Enhanced by   2.000E+00
        CO           Enhanced by   1.500E+00
        CO2          Enhanced by   2.000E+00
        C2H6         Enhanced by   3.000E+00
        AR           Enhanced by   7.000E-01
  3. O+H2<=>H+OH                                    5.00E+04   2.7   6290.0
  4. O+HO2<=>OH+O2                                  2.00E+13   0.0      0.0
  5. O+H2O2<=>OH+HO2                                9.63E+06   2.0   4000.0
  6. O+CH<=>H+CO                                    5.70E+13   0.0      0.0
  7. O+CH2<=>H+HCO                                  8.00E+13   0.0      0.0
  8. O+CH2(S)<=>H2+CO                               1.50E+13   0.0      0.0
  9. O+CH2(S)<=>H+HCO                               1.50E+13   0.0      0.0
 10. O+CH3<=>H+CH2O                                 8.43E+13   0.0      0.0
 11. O+CH4<=>OH+CH3                                 1.02E+09   1.5   8600.0
 12. O+CO+M<=>CO2+M                                 6.02E+14   0.0   3000.0
        H2           Enhanced by   2.000E+00
        O2           Enhanced by   6.000E+00
        H2O          Enhanced by   6.000E+00
        CH4          Enhanced by   2.000E+00
        CO           Enhanced by   1.500E+00
        CO2          Enhanced by   3.500E+00
        C2H6         Enhanced by   3.000E+00
        AR           Enhanced by   5.000E-01
 13. O+HCO<=>OH+CO                                  3.00E+13   0.0      0.0
 14. O+HCO<=>H+CO2                                  3.00E+13   0.0      0.0
 15. O+CH2O<=>OH+HCO                                3.90E+13   0.0   3540.0
 16. O+CH2OH<=>OH+CH2O                              1.00E+13   0.0      0.0
 17. O+CH3O<=>OH+CH2O                               1.00E+13   0.0      0.0
 18. O+CH3OH<=>OH+CH2OH                             3.88E+05   2.5   3100.0
 19. O+CH3OH<=>OH+CH3O                              1.30E+05   2.5   5000.0
 20. O+C2H<=>CH+CO                                  5.00E+13   0.0      0.0
 21. O+C2H2<=>H+HCCO                                1.02E+07   2.0   1900.0
 22. O+C2H2<=>OH+C2H                                4.60E+19  -1.4  28950.0
 23. O+C2H2<=>CO+CH2                                1.02E+07   2.0   1900.0
 24. O+C2H3<=>H+CH2CO                               3.00E+13   0.0      0.0
 25. O+C2H4<=>CH3+HCO                               1.92E+07   1.8    220.0
 26. O+C2H5<=>CH3+CH2O                              1.32E+14   0.0      0.0
 27. O+C2H6<=>OH+C2H5                               8.98E+07   1.9   5690.0
 28. O+HCCO<=>H+2CO                                 1.00E+14   0.0      0.0
```

```
                                                            (k = A T**b exp(-E/RT))
        REACTIONS                                           A         b        E
29. O+CH2CO<=>OH+HCCO                                     1.00E+13    0.0    8000.0
30. O+CH2CO<=>CH2+CO2                                     1.75E+12    0.0    1350.0
31. O2+CO<=>O+CO2                                         2.50E+12    0.0   47800.0
32. O2+CH2O<=>HO2+HCO                                     1.00E+14    0.0   40000.0
33. H+O2+M<=>HO2+M                                        2.80E+18   -0.9       0.0
        O2              Enhanced by     0.000E+00
        H2O             Enhanced by     0.000E+00
        CO              Enhanced by     7.500E-01
        CO2             Enhanced by     1.500E+00
        C2H6            Enhanced by     1.500E+00
        N2              Enhanced by     0.000E+00
        AR              Enhanced by     0.000E+00
34. H+2O2<=>HO2+O2                                        3.00E+20   -1.7       0.0
35. H+O2+H2O<=>HO2+H2O                                    9.38E+18   -0.8       0.0
36. H+O2+N2<=>HO2+N2                                      3.75E+20   -1.7       0.0
37. H+O2+AR<=>HO2+AR                                      7.00E+17   -0.8       0.0
38. H+O2<=>O+OH                                           8.30E+13    0.0   14413.0
39. 2H+M<=>H2+M                                           1.00E+18   -1.0       0.0
        H2              Enhanced by     0.000E+00
        H2O             Enhanced by     0.000E+00
        CH4             Enhanced by     2.000E+00
        CO2             Enhanced by     0.000E+00
        C2H6            Enhanced by     3.000E+00
        AR              Enhanced by     6.300E-01
40. 2H+H2<=>2H2                                           9.00E+16   -0.6       0.0
41. 2H+H2O<=>H2+H2O                                       6.00E+19   -1.2       0.0
42. 2H+CO2<=>H2+CO2                                       5.50E+20   -2.0       0.0
43. H+OH+M<=>H2O+M                                        2.20E+22   -2.0       0.0
        H2              Enhanced by     7.300E-01
        H2O             Enhanced by     3.650E+00
        CH4             Enhanced by     2.000E+00
        C2H6            Enhanced by     3.000E+00
        AR              Enhanced by     3.800E-01
44. H+HO2<=>O+H2O                                         3.97E+12    0.0     671.0
45. H+HO2<=>O2+H2                                         2.80E+13    0.0    1068.0
46. H+HO2<=>2OH                                           1.34E+14    0.0     635.0
47. H+H2O2<=>HO2+H2                                       1.21E+07    2.0    5200.0
48. H+H2O2<=>OH+H2O                                       1.00E+13    0.0    3600.0
49. H+CH<=>C+H2                                           1.10E+14    0.0       0.0
50. H+CH2(+M)<=>CH3(+M)                                   2.50E+16   -0.8       0.0
        Low pressure limit:  0.32000E+28 -0.31400E+01  0.12300E+04
        TROE centering:      0.68000E+00  0.78000E+02  0.19950E+04  0.55900E+04
        H2              Enhanced by     2.000E+00
        H2O             Enhanced by     6.000E+00
        CH4             Enhanced by     2.000E+00
        CO              Enhanced by     1.500E+00
        CO2             Enhanced by     2.000E+00
        C2H6            Enhanced by     3.000E+00
        AR              Enhanced by     7.000E-01
51. H+CH2(S)<=>CH+H2                                      3.00E+13    0.0       0.0
52. H+CH3(+M)<=>CH4(+M)                                   1.27E+16   -0.6     383.0
        Low pressure limit:  0.24770E+34 -0.47600E+01  0.24400E+04
        TROE centering:      0.78300E+00  0.74000E+02  0.29410E+04  0.69640E+04
        H2              Enhanced by     2.000E+00
        H2O             Enhanced by     6.000E+00
        CH4             Enhanced by     2.000E+00
        CO              Enhanced by     1.500E+00
        CO2             Enhanced by     2.000E+00
        C2H6            Enhanced by     3.000E+00
        AR              Enhanced by     7.000E-01
53. H+CH4<=>CH3+H2                                        6.60E+08    1.6   10840.0
54. H+HCO(+M)<=>CH2O(+M)                                  1.09E+12    0.5    -260.0
        Low pressure limit:  0.13500E+25 -0.25700E+01  0.14250E+04
        TROE centering:      0.78240E+00  0.27100E+03  0.27550E+04  0.65700E+04
        H2              Enhanced by     2.000E+00
        H2O             Enhanced by     6.000E+00
        CH4             Enhanced by     2.000E+00
        CO              Enhanced by     1.500E+00
        CO2             Enhanced by     2.000E+00
        C2H6            Enhanced by     3.000E+00
        AR              Enhanced by     7.000E-01
55. H+HCO<=>H2+CO                                         7.34E+13    0.0       0.0
56. H+CH2O(+M)<=>CH2OH(+M)                                5.40E+11    0.5    3600.0
```

A-3

REACTIONS			A	b	E
Low pressure limit:	0.12700E+33	-0.48200E+01	0.65300E+04		
TROE centering:	0.71870E+00	0.10300E+03	0.12910E+04	0.41600E+04	
H2	Enhanced by	2.000E+00			
H2O	Enhanced by	6.000E+00			
CH4	Enhanced by	2.000E+00			
CO	Enhanced by	1.500E+00			
CO2	Enhanced by	2.000E+00			
C2H6	Enhanced by	3.000E+00			
57. H+CH2O(+M)<=>CH3O(+M)			5.40E+11	0.5	2600.0
Low pressure limit:	0.22000E+31	-0.48000E+01	0.55600E+04		
TROE centering:	0.75800E+00	0.94000E+02	0.15550E+04	0.42000E+04	
H2	Enhanced by	2.000E+00			
H2O	Enhanced by	6.000E+00			
CH4	Enhanced by	2.000E+00			
CO	Enhanced by	1.500E+00			
CO2	Enhanced by	2.000E+00			
C2H6	Enhanced by	3.000E+00			
58. H+CH2O<=>HCO+H2			2.30E+10	1.1	3275.0
59. H+CH2OH(+M)<=>CH3OH(+M)			1.80E+13	0.0	0.0
Low pressure limit:	0.30000E+32	-0.48000E+01	0.33000E+04		
TROE centering:	0.76790E+00	0.33800E+03	0.18120E+04	0.50810E+04	
H2	Enhanced by	2.000E+00			
H2O	Enhanced by	6.000E+00			
CH4	Enhanced by	2.000E+00			
CO	Enhanced by	1.500E+00			
CO2	Enhanced by	2.000E+00			
C2H6	Enhanced by	3.000E+00			
60. H+CH2OH<=>H2+CH2O			2.00E+13	0.0	0.0
61. H+CH2OH<=>OH+CH3			1.20E+13	0.0	0.0
62. H+CH2OH<=>CH2(S)+H2O			6.00E+12	0.0	0.0
63. H+CH3O(+M)<=>CH3OH(+M)			5.00E+13	0.0	0.0
Low pressure limit:	0.86000E+29	-0.40000E+01	0.30250E+04		
TROE centering:	0.89020E+00	0.14400E+03	0.28380E+04	0.45569E+05	
H2	Enhanced by	2.000E+00			
H2O	Enhanced by	6.000E+00			
CH4	Enhanced by	2.000E+00			
CO	Enhanced by	1.500E+00			
CO2	Enhanced by	2.000E+00			
C2H6	Enhanced by	3.000E+00			
64. H+CH3O<=>H+CH2OH			3.40E+06	1.6	0.0
65. H+CH3O<=>H2+CH2O			2.00E+13	0.0	0.0
66. H+CH3O<=>OH+CH3			3.20E+13	0.0	0.0
67. H+CH3O<=>CH2(S)+H2O			1.60E+13	0.0	0.0
68. H+CH3OH<=>CH2OH+H2			1.70E+07	2.1	4870.0
69. H+CH3OH<=>CH3O+H2			4.20E+06	2.1	4870.0
70. H+C2H(+M)<=>C2H2(+M)			1.00E+17	-1.0	0.0
Low pressure limit:	0.37500E+34	-0.48000E+01	0.19000E+04		
TROE centering:	0.64640E+00	0.13200E+03	0.13150E+04	0.55660E+04	
H2	Enhanced by	2.000E+00			
H2O	Enhanced by	6.000E+00			
CH4	Enhanced by	2.000E+00			
CO	Enhanced by	1.500E+00			
CO2	Enhanced by	2.000E+00			
C2H6	Enhanced by	3.000E+00			
AR	Enhanced by	7.000E-01			
71. H+C2H2(+M)<=>C2H3(+M)			5.60E+12	0.0	2400.0
Low pressure limit:	0.38000E+41	-0.72700E+01	0.72200E+04		
TROE centering:	0.75070E+00	0.98500E+02	0.13020E+04	0.41670E+04	
H2	Enhanced by	2.000E+00			
H2O	Enhanced by	6.000E+00			
CH4	Enhanced by	2.000E+00			
CO	Enhanced by	1.500E+00			
CO2	Enhanced by	2.000E+00			
C2H6	Enhanced by	3.000E+00			
AR	Enhanced by	7.000E-01			
72. H+C2H3(+M)<=>C2H4(+M)			6.08E+12	0.3	280.0
Low pressure limit:	0.14000E+31	-0.38600E+01	0.33200E+04		
TROE centering:	0.78200E+00	0.20750E+03	0.26630E+04	0.60950E+04	
H2	Enhanced by	2.000E+00			
H2O	Enhanced by	6.000E+00			
CH4	Enhanced by	2.000E+00			
CO	Enhanced by	1.500E+00			
CO2	Enhanced by	2.000E+00			
C2H6	Enhanced by	3.000E+00			
AR	Enhanced by	7.000E-01			
73. H+C2H3<=>H2+C2H2			3.00E+13	0.0	0.0

```
                                                       (k = A T**b exp(-E/RT))
   REACTIONS                                           A          b          E

 74. H+C2H4(+M)<=>C2H5(+M)                            1.08E+12    0.5     1820.0
     Low pressure limit:  0.12000E+43 -0.76200E+01  0.69700E+04
     TROE centering:      0.97530E+00  0.21000E+03  0.98400E+03  0.43740E+04
        H2           Enhanced by    2.000E+00
        H2O          Enhanced by    6.000E+00
        CH4          Enhanced by    2.000E+00
        CO           Enhanced by    1.500E+00
        CO2          Enhanced by    2.000E+00
        C2H6         Enhanced by    3.000E+00
        AR           Enhanced by    7.000E-01
 75. H+C2H4<=>C2H3+H2                                 1.32E+06    2.5    12240.0
 76. H+C2H5(+M)<=>C2H6(+M)                            5.21E+17   -1.0     1580.0
     Low pressure limit:  0.19900E+42 -0.70800E+01  0.66850E+04
     TROE centering:      0.84220E+00  0.12500E+03  0.22190E+04  0.68820E+04
        H2           Enhanced by    2.000E+00
        H2O          Enhanced by    6.000E+00
        CH4          Enhanced by    2.000E+00
        CO           Enhanced by    1.500E+00
        CO2          Enhanced by    2.000E+00
        C2H6         Enhanced by    3.000E+00
        AR           Enhanced by    7.000E-01
 77. H+C2H5<=>H2+C2H4                                 2.00E+12    0.0        0.0
 78. H+C2H6<=>C2H5+H2                                 1.15E+08    1.9     7530.0
 79. H+HCCO<=>CH2(S)+CO                               1.00E+14    0.0        0.0
 80. H+CH2CO<=>HCCO+H2                                5.00E+13    0.0     8000.0
 81. H+CH2CO<=>CH3+CO                                 1.13E+13    0.0     3428.0
 82. H+HCCOH<=>H+CH2CO                                1.00E+13    0.0        0.0
 83. H2+CO(+M)<=>CH2O(+M)                             4.30E+07    1.5    79600.0
     Low pressure limit:  0.50700E+28 -0.34200E+01  0.84350E+05
     TROE centering:      0.93200E+00  0.19700E+03  0.15400E+04  0.10300E+05
        H2           Enhanced by    2.000E+00
        H2O          Enhanced by    6.000E+00
        CH4          Enhanced by    2.000E+00
        CO           Enhanced by    1.500E+00
        CO2          Enhanced by    2.000E+00
        C2H6         Enhanced by    3.000E+00
        AR           Enhanced by    7.000E-01
 84. OH+H2<=>H+H2O                                    2.16E+08    1.5     3430.0
 85. 2OH(+M)<=>H2O2(+M)                               7.40E+13   -0.4        0.0
     Low pressure limit:  0.23000E+19 -0.90000E+00 -0.17000E+04
     TROE centering:      0.73460E+00  0.94000E+02  0.17560E+04  0.51820E+04
        H2           Enhanced by    2.000E+00
        H2O          Enhanced by    6.000E+00
        CH4          Enhanced by    2.000E+00
        CO           Enhanced by    1.500E+00
        CO2          Enhanced by    2.000E+00
        C2H6         Enhanced by    3.000E+00
        AR           Enhanced by    7.000E-01
 86. 2OH<=>O+H2O                                      3.57E+04    2.4    -2110.0
 87. OH+HO2<=>O2+H2O                                  2.90E+13    0.0     -500.0
 88. OH+H2O2<=>HO2+H2O                                1.75E+12    0.0      320.0
     Declared duplicate reaction...
 89. OH+H2O2<=>HO2+H2O                                5.80E+14    0.0     9560.0
     Declared duplicate reaction...
 90. OH+C<=>H+CO                                      5.00E+13    0.0        0.0
 91. OH+CH<=>H+HCO                                    3.00E+13    0.0        0.0
 92. OH+CH2<=>H+CH2O                                  2.00E+13    0.0        0.0
 93. OH+CH2<=>CH+H2O                                  1.13E+07    2.0     3000.0
 94. OH+CH2(S)<=>H+CH2O                               3.00E+13    0.0        0.0
 95. OH+CH3(+M)<=>CH3OH(+M)                           6.30E+13    0.0        0.0
     Low pressure limit:  0.27000E+39 -0.63000E+01  0.31000E+04
     TROE centering:      0.21050E+00  0.83500E+02  0.53980E+04  0.83700E+04
        H2           Enhanced by    2.000E+00
        H2O          Enhanced by    6.000E+00
        CH4          Enhanced by    2.000E+00
        CO           Enhanced by    1.500E+00
        CO2          Enhanced by    2.000E+00
        C2H6         Enhanced by    3.000E+00
 96. OH+CH3<=>CH2+H2O                                 5.60E+07    1.6     5420.0
 97. OH+CH3<=>CH2(S)+H2O                              2.50E+13    0.0        0.0
 98. OH+CH4<=>CH3+H2O                                 1.00E+08    1.6     3120.0
 99. OH+CO<=>H+CO2                                    4.76E+07    1.2       70.0
100. OH+HCO<=>H2O+CO                                  5.00E+13    0.0        0.0
101. OH+CH2O<=>HCO+H2O                                3.43E+09    1.2     -447.0
102. OH+CH2OH<=>H2O+CH2O                              5.00E+12    0.0        0.0
```

```
                                                      (k = A T**b exp(-E/RT))
    REACTIONS                                         A          b          E

103. OH+CH3O<=>H2O+CH2O                               5.00E+12   0.0        0.0
104. OH+CH3OH<=>CH2OH+H2O                             1.44E+06   2.0     -840.0
105. OH+CH3OH<=>CH3O+H2O                              6.30E+06   2.0     1500.0
106. OH+C2H<=>H+HCCO                                  2.00E+13   0.0        0.0
107. OH+C2H2<=>H+CH2CO                                2.18E-04   4.5    -1000.0
108. OH+C2H2<=>H+HCCOH                                5.04E+05   2.3    13500.0
109. OH+C2H2<=>C2H+H2O                                3.37E+07   2.0    14000.0
110. OH+C2H2<=>CH3+CO                                 4.83E-04   4.0    -2000.0
111. OH+C2H3<=>H2O+C2H2                               5.00E+12   0.0        0.0
112. OH+C2H4<=>C2H3+H2O                               3.60E+06   2.0     2500.0
113. OH+C2H6<=>C2H5+H2O                               3.54E+06   2.1      870.0
114. OH+CH2CO<=>HCCO+H2O                              7.50E+12   0.0     2000.0
115. 2HO2<=>O2+H2O2                                   1.30E+11   0.0    -1630.0
     Declared duplicate reaction...
116. 2HO2<=>O2+H2O2                                   4.20E+14   0.0    12000.0
     Declared duplicate reaction...
117. HO2+CH2<=>OH+CH2O                                2.00E+13   0.0        0.0
118. HO2+CH3<=>O2+CH4                                 1.00E+12   0.0        0.0
119. HO2+CH3<=>OH+CH3O                                2.00E+13   0.0        0.0
120. HO2+CO<=>OH+CO2                                  1.50E+14   0.0    23600.0
121. HO2+CH2O<=>HCO+H2O2                              1.00E+12   0.0     8000.0
122. C+O2<=>O+CO                                      5.80E+13   0.0      576.0
123. C+CH2<=>H+C2H                                    5.00E+13   0.0        0.0
124. C+CH3<=>H+C2H2                                   5.00E+13   0.0        0.0
125. CH+O2<=>O+HCO                                    3.30E+13   0.0        0.0
126. CH+H2<=>H+CH2                                    1.11E+08   1.8     1670.0
127. CH+H2O<=>H+CH2O                                  1.71E+13   0.0     -755.0
128. CH+CH2<=>H+C2H2                                  4.00E+13   0.0        0.0
129. CH+CH3<=>H+C2H3                                  3.00E+13   0.0        0.0
130. CH+CH4<=>H+C2H4                                  6.00E+13   0.0        0.0
131. CH+CO(+M)<=>HCCO(+M)                             5.00E+13   0.0        0.0
     Low pressure limit:  0.26900E+29 -0.37400E+01  0.19360E+04
     TROE centering:      0.57570E+00  0.23700E+03  0.16520E+04  0.50690E+04
         H2            Enhanced by    2.000E+00
         H2O           Enhanced by    6.000E+00
         CH4           Enhanced by    2.000E+00
         CO            Enhanced by    1.500E+00
         CO2           Enhanced by    2.000E+00
         C2H6          Enhanced by    3.000E+00
         AR            Enhanced by    7.000E-01
132. CH+CO2<=>HCO+CO                                  3.40E+12   0.0      690.0
133. CH+CH2O<=>H+CH2CO                                9.46E+13   0.0     -515.0
134. CH+HCCO<=>CO+C2H2                                5.00E+13   0.0        0.0
135. CH2+O2<=>OH+HCO                                  1.32E+13   0.0     1500.0
136. CH2+H2<=>H+CH3                                   5.00E+05   2.0     7230.0
137. 2CH2<=>H2+C2H2                                   3.20E+13   0.0        0.0
138. CH2+CH3<=>H+C2H4                                 4.00E+13   0.0        0.0
139. CH2+CH4<=>2CH3                                   2.46E+06   2.0     8270.0
140. CH2+CO(+M)<=>CH2CO(+M)                           8.10E+11   0.5     4510.0
     Low pressure limit:  0.26900E+34 -0.51100E+01  0.70950E+04
     TROE centering:      0.59070E+00  0.27500E+03  0.12260E+04  0.51850E+04
         H2            Enhanced by    2.000E+00
         H2O           Enhanced by    6.000E+00
         CH4           Enhanced by    2.000E+00
         CO            Enhanced by    1.500E+00
         CO2           Enhanced by    2.000E+00
         C2H6          Enhanced by    3.000E+00
         AR            Enhanced by    7.000E-01
141. CH2+HCCO<=>C2H3+CO                               3.00E+13   0.0        0.0
142. CH2(S)+N2<=>CH2+N2                               1.50E+13   0.0      600.0
143. CH2(S)+AR<=>CH2+AR                               9.00E+12   0.0      600.0
144. CH2(S)+O2<=>H+OH+CO                              2.80E+13   0.0        0.0
145. CH2(S)+O2<=>CO+H2O                               1.20E+13   0.0        0.0
146. CH2(S)+H2<=>CH3+H                                7.00E+13   0.0        0.0
147. CH2(S)+H2O(+M)<=>CH3OH(+M)                       2.00E+13   0.0        0.0
     Low pressure limit:  0.27000E+39 -0.63000E+01  0.31000E+04
     TROE centering:      0.15070E+00  0.13400E+03  0.23830E+04  0.72650E+04
         H2            Enhanced by    2.000E+00
         H2O           Enhanced by    6.000E+00
         CH4           Enhanced by    2.000E+00
         CO            Enhanced by    1.500E+00
         CO2           Enhanced by    2.000E+00
         C2H6          Enhanced by    3.000E+00
148. CH2(S)+H2O<=>CH2+H2O                             3.00E+13   0.0        0.0
149. CH2(S)+CH3<=>H+C2H4                              1.20E+13   0.0     -570.0
```

A-6

```
                                                         (k = A T**b exp(-E/RT))
      REACTIONS                                          A           b        E

150. CH2(S)+CH4<=>2CH3                                    1.60E+13    0.0     -570.0
151. CH2(S)+CO<=>CH2+CO                                   9.00E+12    0.0        0.0
152. CH2(S)+CO2<=>CH2+CO2                                 7.00E+12    0.0        0.0
153. CH2(S)+CO2<=>CO+CH2O                                 1.40E+13    0.0        0.0
154. CH2(S)+C2H6<=>CH3+C2H5                               4.00E+13    0.0     -550.0
155. CH3+O2<=>O+CH3O                                      2.68E+13    0.0    28800.0
156. CH3+O2<=>OH+CH2O                                     3.60E+10    0.0     8940.0
157. CH3+H2O2<=>HO2+CH4                                   2.45E+04    2.5     5180.0
158. 2CH3(+M)<=>C2H6(+M)                                  2.12E+16   -1.0      620.0
     Low pressure limit:  0.17700E+51 -0.96700E+01  0.62200E+04
     TROE centering:      0.53250E+00  0.15100E+03  0.10380E+04  0.49700E+04
         H2               Enhanced by    2.000E+00
         H2O              Enhanced by    6.000E+00
         CH4              Enhanced by    2.000E+00
         CO               Enhanced by    1.500E+00
         CO2              Enhanced by    2.000E+00
         C2H6             Enhanced by    3.000E+00
         AR               Enhanced by    7.000E-01
159. 2CH3<=>H+C2H5                                        4.99E+12    0.1    10600.0
160. CH3+HCO<=>CH4+CO                                     2.65E+13    0.0        0.0
161. CH3+CH2O<=>HCO+CH4                                   3.32E+03    2.8     5860.0
162. CH3+CH3OH<=>CH2OH+CH4                                3.00E+07    1.5     9940.0
163. CH3+CH3OH<=>CH3O+CH4                                 1.00E+07    1.5     9940.0
164. CH3+C2H4<=>C2H3+CH4                                  2.27E+05    2.0     9200.0
165. CH3+C2H6<=>C2H5+CH4                                  6.14E+06    1.7    10450.0
166. HCO+M<=>H+CO+M                                       1.87E+17   -1.0    17000.0
         H2               Enhanced by    2.000E+00
         H2O              Enhanced by    1.120E+01
         CH4              Enhanced by    2.000E+00
         CO               Enhanced by    1.500E+00
         CO2              Enhanced by    2.000E+00
         C2H6             Enhanced by    3.000E+00
167. HCO+O2<=>HO2+CO                                      7.60E+12    0.0      400.0
168. CH2OH+O2<=>HO2+CH2O                                  1.80E+13    0.0      900.0
169. CH3O+O2<=>HO2+CH2O                                   4.28E-13    7.6    -3530.0
170. C2H+O2<=>HCO+CO                                      5.00E+13    0.0     1500.0
171. C2H+H2<=>H+C2H2                                      4.07E+05    2.4      200.0
172. C2H3+O2<=>HCO+CH2O                                   3.98E+12    0.0     -240.0
173. C2H4(+M)<=>H2+C2H2(+M)                               8.00E+12    0.4    88770.0
     Low pressure limit:  0.70000E+51 -0.93100E+01  0.99860E+05
     TROE centering:      0.73450E+00  0.18000E+03  0.10350E+04  0.54170E+04
         H2               Enhanced by    2.000E+00
         H2O              Enhanced by    6.000E+00
         CH4              Enhanced by    2.000E+00
         CO               Enhanced by    1.500E+00
         CO2              Enhanced by    2.000E+00
         C2H6             Enhanced by    3.000E+00
         AR               Enhanced by    7.000E-01
174. C2H5+O2<=>HO2+C2H4                                   8.40E+11    0.0     3875.0
175. HCCO+O2<=>OH+2CO                                     1.60E+12    0.0      854.0
176. 2HCCO<=>2CO+C2H2                                     1.00E+13    0.0        0.0
177. N+NO<=>N2+O                                          3.50E+13    0.0      330.0
178. N+O2<=>NO+O                                          2.65E+12    0.0     6400.0
179. N+OH<=>NO+H                                          7.33E+13    0.0     1120.0
180. N2O+O<=>N2+O2                                        1.40E+12    0.0    10810.0
181. N2O+O<=>2NO                                          2.90E+13    0.0    23150.0
182. N2O+H<=>N2+OH                                        4.40E+14    0.0    18880.0
183. N2O+OH<=>N2+HO2                                      2.00E+12    0.0    21060.0
184. N2O(+M)<=>N2+O(+M)                                   1.30E+11    0.0    59620.0
     Low pressure limit:  0.62000E+15  0.00000E+00  0.56100E+05
         H2               Enhanced by    2.000E+00
         H2O              Enhanced by    6.000E+00
         CH4              Enhanced by    2.000E+00
         CO               Enhanced by    1.500E+00
         CO2              Enhanced by    2.000E+00
         C2H6             Enhanced by    3.000E+00
         AR               Enhanced by    7.000E-01
185. HO2+NO<=>NO2+OH                                      2.11E+12    0.0     -480.0
```

```
                                                                (k = A T**b exp(-E/RT))
        REACTIONS                                                A        b          E

186. NO+O+M<=>NO2+M                                            1.06E+20   -1.4       0.0
        H2            Enhanced by    2.000E+00
        H2O           Enhanced by    6.000E+00
        CH4           Enhanced by    2.000E+00
        CO            Enhanced by    1.500E+00
        CO2           Enhanced by    2.000E+00
        C2H6          Enhanced by    3.000E+00
        AR            Enhanced by    7.000E-01
187. NO2+O<=>NO+O2                                             3.90E+12    0.0    -240.0
188. NO2+H<=>NO+OH                                             1.32E+14    0.0     360.0
189. NH+O<=>NO+H                                               5.00E+13    0.0       0.0
190. NH+H<=>N+H2                                               3.20E+13    0.0     330.0
191. NH+OH<=>HNO+H                                             2.00E+13    0.0       0.0
192. NH+OH<=>N+H2O                                             2.00E+09    1.2       0.0
193. NH+O2<=>HNO+O                                             4.61E+05    2.0    6500.0
194. NH+O2<=>NO+OH                                             1.28E+06    1.5     100.0
195. NH+N<=>N2+H                                               1.50E+13    0.0       0.0
196. NH+H2O<=>HNO+H2                                           2.00E+13    0.0   13850.0
197. NH+NO<=>N2+OH                                             2.16E+13   -0.2       0.0
198. NH+NO<=>N2O+H                                             4.16E+14   -0.5       0.0
199. NH2+O<=>OH+NH                                             7.00E+12    0.0       0.0
200. NH2+O<=>H+HNO                                             4.60E+13    0.0       0.0
201. NH2+H<=>NH+H2                                             4.00E+13    0.0    3650.0
202. NH2+OH<=>NH+H2O                                           9.00E+07    1.5    -460.0
203. NNH<=>N2+H                                                3.30E+08    0.0       0.0
     Declared duplicate reaction...
204. NNH+M<=>N2+H+M                                            1.30E+14   -0.1    4980.0
        H2            Enhanced by    2.000E+00
        H2O           Enhanced by    6.000E+00
        CH4           Enhanced by    2.000E+00
        CO            Enhanced by    1.500E+00
        CO2           Enhanced by    2.000E+00
        C2H6          Enhanced by    3.000E+00
        AR            Enhanced by    7.000E-01
     Declared duplicate reaction...
205. NNH+O2<=>HO2+N2                                           5.00E+12    0.0       0.0
206. NNH+O<=>OH+N2                                             2.50E+13    0.0       0.0
207. NNH+O<=>NH+NO                                             7.00E+13    0.0       0.0
208. NNH+H<=>H2+N2                                             5.00E+13    0.0       0.0
209. NNH+OH<=>H2O+N2                                           2.00E+13    0.0       0.0
210. NNH+CH3<=>CH4+N2                                          2.50E+13    0.0       0.0
211. H+NO+M<=>HNO+M                                            8.95E+19   -1.3     740.0
        H2            Enhanced by    2.000E+00
        H2O           Enhanced by    6.000E+00
        CH4           Enhanced by    2.000E+00
        CO            Enhanced by    1.500E+00
        CO2           Enhanced by    2.000E+00
        C2H6          Enhanced by    3.000E+00
        AR            Enhanced by    7.000E-01
212. HNO+O<=>NO+OH                                             2.50E+13    0.0       0.0
213. HNO+H<=>H2+NO                                             4.50E+11    0.7     660.0
214. HNO+OH<=>NO+H2O                                           1.30E+07    1.9    -950.0
215. HNO+O2<=>HO2+NO                                           1.00E+13    0.0   13000.0
216. CN+O<=>CO+N                                               7.70E+13    0.0       0.0
217. CN+OH<=>NCO+H                                             4.00E+13    0.0       0.0
218. CN+H2O<=>HCN+OH                                           8.00E+12    0.0    7460.0
219. CN+O2<=>NCO+O                                             6.14E+12    0.0    -440.0
220. CN+H2<=>HCN+H                                             2.10E+13    0.0    4710.0
221. NCO+O<=>NO+CO                                             2.35E+13    0.0       0.0
222. NCO+H<=>NH+CO                                             5.40E+13    0.0       0.0
223. NCO+OH<=>NO+H+CO                                          2.50E+12    0.0       0.0
224. NCO+N<=>N2+CO                                             2.00E+13    0.0       0.0
225. NCO+O2<=>NO+CO2                                           2.00E+12    0.0   20000.0
226. NCO+M<=>N+CO+M                                            8.80E+16   -0.5   48000.0
        H2            Enhanced by    2.000E+00
        H2O           Enhanced by    6.000E+00
        CH4           Enhanced by    2.000E+00
        CO            Enhanced by    1.500E+00
        CO2           Enhanced by    2.000E+00
        C2H6          Enhanced by    3.000E+00
        AR            Enhanced by    7.000E-01
227. NCO+NO<=>N2O+CO                                           2.85E+17   -1.5     740.0
228. NCO+NO<=>N2+CO2                                           5.70E+18   -2.0     800.0
```

	REACTIONS			A	b	E
229.	HCN+M<=>H+CN+M			1.04E+29	-3.3	126600.0
	H2	Enhanced by	2.000E+00			
	H2O	Enhanced by	6.000E+00			
	CH4	Enhanced by	2.000E+00			
	CO	Enhanced by	1.500E+00			
	CO2	Enhanced by	2.000E+00			
	C2H6	Enhanced by	3.000E+00			
	AR	Enhanced by	7.000E-01			
230.	HCN+O<=>NCO+H			1.11E+04	2.6	4980.0
231.	HCN+O<=>NH+CO			2.77E+03	2.6	4980.0
232.	HCN+O<=>CN+OH			2.13E+09	1.6	26600.0
233.	HCN+OH<=>HOCN+H			1.10E+06	2.0	13370.0
234.	HCN+OH<=>HNCO+H			4.40E+03	2.3	6400.0
235.	HCN+OH<=>NH2+CO			1.60E+02	2.6	9000.0
236.	H+HCN+M<=>H2CN+M			1.40E+26	-3.4	1900.0
	H2	Enhanced by	2.000E+00			
	H2O	Enhanced by	6.000E+00			
	CH4	Enhanced by	2.000E+00			
	CO	Enhanced by	1.500E+00			
	CO2	Enhanced by	2.000E+00			
	C2H6	Enhanced by	3.000E+00			
	AR	Enhanced by	7.000E-01			
237.	H2CN+N<=>N2+CH2			6.00E+13	0.0	400.0
238.	C+N2<=>CN+N			6.30E+13	0.0	46020.0
239.	CH+N2<=>HCN+N			2.86E+08	1.1	20400.0
240.	CH+N2(+M)<=>HCNN(+M)			3.10E+12	0.1	0.0

Low pressure limit: 0.13000E+26 -0.31600E+01 0.74000E+03
TROE centering: 0.66700E+00 0.23500E+03 0.21170E+04 0.45360E+04

	H2	Enhanced by	2.000E+00			
	H2O	Enhanced by	6.000E+00			
	CH4	Enhanced by	2.000E+00			
	CO	Enhanced by	1.500E+00			
	CO2	Enhanced by	2.000E+00			
	C2H6	Enhanced by	3.000E+00			
	AR	Enhanced by	7.000E-01			
241.	CH2+N2<=>HCN+NH			1.00E+13	0.0	74000.0
242.	CH2(S)+N2<=>NH+HCN			1.00E+11	0.0	65000.0
243.	C+NO<=>CN+O			1.90E+13	0.0	0.0
244.	C+NO<=>CO+N			2.90E+13	0.0	0.0
245.	CH+NO<=>HCN+O			5.00E+13	0.0	0.0
246.	CH+NO<=>H+NCO			2.00E+13	0.0	0.0
247.	CH+NO<=>N+HCO			3.00E+13	0.0	0.0
248.	CH2+NO<=>H+HNCO			3.10E+17	-1.4	1270.0
249.	CH2+NO<=>OH+HCN			2.90E+14	-0.7	760.0
250.	CH2+NO<=>H+HCNO			3.80E+13	-0.4	580.0
251.	CH2(S)+NO<=>H+HNCO			3.10E+17	-1.4	1270.0
252.	CH2(S)+NO<=>OH+HCN			2.90E+14	-0.7	760.0
253.	CH2(S)+NO<=>H+HCNO			3.80E+13	-0.4	580.0
254.	CH3+NO<=>HCN+H2O			9.60E+13	0.0	28800.0
255.	CH3+NO<=>H2CN+OH			1.00E+12	0.0	21750.0
256.	HCNN+O<=>CO+H+N2			2.20E+13	0.0	0.0
257.	HCNN+O<=>HCN+NO			2.00E+12	0.0	0.0
258.	HCNN+O2<=>O+HCO+N2			1.20E+13	0.0	0.0
259.	HCNN+OH<=>H+HCO+N2			1.20E+13	0.0	0.0
260.	HCNN+H<=>CH2+N2			1.00E+14	0.0	0.0
261.	HNCO+O<=>NH+CO2			9.80E+07	1.4	8500.0
262.	HNCO+O<=>HNO+CO			1.50E+08	1.6	44000.0
263.	HNCO+O<=>NCO+OH			2.20E+06	2.1	11400.0
264.	HNCO+H<=>NH2+CO			2.25E+07	1.7	3800.0
265.	HNCO+H<=>H2+NCO			1.05E+05	2.5	13300.0
266.	HNCO+OH<=>NCO+H2O			4.65E+12	0.0	6850.0
267.	HNCO+OH<=>NH2+CO2			1.55E+12	0.0	6850.0
268.	HNCO+M<=>NH+CO+M			1.18E+16	0.0	84720.0
	H2	Enhanced by	2.000E+00			
	H2O	Enhanced by	6.000E+00			
	CH4	Enhanced by	2.000E+00			
	CO	Enhanced by	1.500E+00			
	CO2	Enhanced by	2.000E+00			
	C2H6	Enhanced by	3.000E+00			
	AR	Enhanced by	7.000E-01			
269.	HCNO+H<=>H+HNCO			2.10E+15	-0.7	2850.0
270.	HCNO+H<=>OH+HCN			2.70E+11	0.2	2120.0
271.	HCNO+H<=>NH2+CO			1.70E+14	-0.8	2890.0
272.	HOCN+H<=>H+HNCO			2.00E+07	2.0	2000.0
273.	HCCO+NO<=>HCNO+CO			2.35E+13	0.0	0.0

	(k = A T**b exp(-E/RT))		
REACTIONS	A	b	E
274. CH3+N<=>H2CN+H	6.10E+14	-0.3	290.0
275. CH3+N<=>HCN+H2	3.70E+12	0.1	-90.0
276. NH3+H<=>NH2+H2	5.40E+05	2.4	9915.0
277. NH3+OH<=>NH2+H2O	5.00E+07	1.6	955.0
278. NH3+O<=>NH2+OH	9.40E+06	1.9	6460.0

!End GRI-Mech 2.1

!Bowman's SNCR mechanism

279. NH2+O=NO+H2	5.00E+12	0.0	0.0
280. NH2+NO=NNH+OH	2.80E+13	-0.6	0.0
281. NH2+NO=N2+H2O	1.30E+16	-1.2	0.0

Declared duplicate reaction...

| | | | |
| 282. NH2+NO=N2+H2O | -2.80E+13 | -0.6 | 0.0 |

Declared duplicate reaction...

283. NNH+NO=N2+HNO	5.00E+13	0.0	0.0
284. NNH+NH2=N2+NH3	5.00E+13	0.0	0.0
285. NNH+NH=N2+NH2	5.00E+13	0.0	0.0
286. NNH+O=N2O+H	1.00E+14	0.0	0.0
287. HNO+NH2=NH3+NO	2.00E+13	0.0	1000.0
288. HNO+HNO=N2O+H2O	3.95E+12	0.0	5000.0
289. HNO+NO=N2O+OH	2.00E+12	0.0	26000.0
290. NH2+NH=N2H2+H	1.50E+15	-0.5	0.0
291. NH+NH=N2+H+H	2.50E+13	0.0	0.0
292. NH2+N=N2+H+H	7.20E+13	0.0	0.0
293. N2H2+M=NNH+H+M	5.00E+16	0.0	50000.0

H2O	Enhanced by	1.500E+01
O2	Enhanced by	2.000E+00
N2	Enhanced by	2.000E+00
H2	Enhanced by	2.000E+00

294. N2H2+H=NNH+H2	5.00E+13	0.0	1000.0
295. N2H2+O=NH2+NO	1.00E+13	0.0	0.0
296. N2H2+O=NNH+OH	2.00E+13	0.0	1000.0
297. N2H2+OH=NNH+H2O	1.00E+13	0.0	1000.0
298. N2H2+NO=N2O+NH2	3.00E+12	0.0	0.0
299. N2H2+NH=NNH+NH2	1.00E+13	0.0	1000.0
300. N2H2+NH2=NH3+NNH	1.00E+13	0.0	1000.0
301. NH2+NH2=N2H2+H2	5.00E+11	0.0	0.0
302. NH2+O2=HNO+OH	4.50E+12	0.0	25000.0
303. NCO+NO2=N2O+CO2	5.80E+14	-0.7	0.0
304. NH+HNCO=NH2+NCO	3.00E+13	0.0	23700.0
305. NH2+HNCO=NH3+NCO	1.00E+12	0.0	6955.0
306. HO2+HNCO=NCO+H2O2	3.00E+11	0.0	29000.0
307. NH3+HO2=NH2+H2O2	3.00E+11	0.0	22000.0
308. NH2+NO2=N2O+H2O	2.84E+18	-2.2	0.0
309. NH+NO2=N2O+OH	1.00E+13	0.0	0.0
310. NH2+NH2=NH+NH3	5.00E+13	0.0	10000.0
311. NH2+HO2=NH3+O2	4.30E+13	0.0	0.0
312. NO2+SO2=NO+SO3	6.31E+12	0.0	27000.0

!End of Bowman's SNCR mechanism

!Reactions of sulfur oxides

313. SO2+O+M=SO3+M	1.45E+16	0.0	2000.0
314. SO2+OH+M=HSO3+M	2.12E+25	-3.3	0.0
315. HSO3+O2=HO2+SO3	7.83E+11	0.0	656.0
316. O+SO3=SO2+O2	1.32E+12	0.0	6100.0

!Reactions of sodium

317. NA2CO3=>NA2O+CO2	2.54E+06	0.0	25820.0
318. NA2O+CO2=>NA2CO3	1.11E+05	0.0	-15000.0
319. NA2O+H2O<=>2NAOH	9.18E+12	0.0	3120.0
320. NA+N2O=NAO+N2	1.69E+14	0.0	3159.0
321. NAO+H2O=NAOH+OH	1.32E+13	0.0	0.0
322. NAO+O=NA+O2	2.23E+14	0.0	0.0
323. NAO+NO=NA+NO2	9.04E+13	0.0	0.0
324. NAO+H2=NAOH+H	1.25E+13	0.0	0.0
325. NA+O2+M=NAO2+M	1.74E+21	-1.3	0.0

H2O	Enhanced by	5.000E+00
CO2	Enhanced by	3.000E+00
CO	Enhanced by	2.000E+00
H2	Enhanced by	2.000E+00

326. NAOH+H=NA+H2O	5.00E+13	0.0	0.0
327. NA+OH+M=NAOH+M	1.82E+21	-1.0	0.0
328. NAO+OH=NAOH+O	2.00E+13	0.0	0.0
329. NAO+HO2=NAOH+O2	5.00E+13	0.0	0.0
330. NAO+H2=NA+H2O	3.13E+12	0.0	0.0

REACTIONS	A	b	E
331. NAO+CO=NA+CO2	1.00E+14	0.0	0.0
332. H+NAO2=HO2+NA	2.00E+14	0.0	0.0
333. NAO+H=NA+OH	2.00E+14	0.0	0.0
334. NAO+OH=NA+HO2	3.00E+13	0.0	0.0
335. NA+HO2=NAOH+O	1.00E+14	0.0	0.0
336. NAO2+H=NAO+OH	5.00E+13	0.0	0.0
337. NAO2+OH=NAOH+O2	2.00E+13	0.0	0.0
338. NAO+HO2=NAO2+OH	5.00E+13	0.0	0.0
339. NAO2+H=NAOH+O	1.00E+14	0.0	0.0
340. NAO2+CO=NAO+CO2	1.00E+14	0.0	0.0
341. NAO2+O=NAO+O2	1.00E+14	0.0	0.0
342. NAO+NH3=NAOH+NH2	1.00E+13	0.0	0.0
343. NAOH+SO2=NASO2+OH	1.00E+13	0.0	35400.0
344. NA+SO2=NASO2	1.21E+14	0.0	0.0
345. NASO2+NAO2=NA2SO4	1.00E+14	0.0	0.0
346. NASO2+NAO=NA2SO3	1.00E+14	0.0	0.0

!Reactions of chlorine

	A	b	E
347. NAO+HCL=NACL+OH	1.69E+14	0.0	0.0
348. NA+HCL=NACL+H	2.41E+14	0.0	130.0
349. NAOH+HCL=NACL+H2O	1.69E+14	0.0	0.0
350. NAO2+HCL=NACL+HO2	1.39E+14	0.0	0.0
351. CL+H2=HCL+H	1.45E+13	0.0	4370.0
352. H+CL2=CL+HCL	8.59E+13	0.0	1170.0
353. CL+CL+M=CL2+M	2.23E+14	0.0	-1800.0
354. O+HCL=CL+OH	6.87E+12	0.0	6697.0
355. CL+H2O=OH+HCL	1.68E+13	0.0	17230.0

Appendix 2. Thermodynamic database for Reaction Mechanism in Chemkin Format

Nomenclature (from Kee et al., 1991):

Thermodynamic properties for each species are calculated from polynomial fits to the specific heat at constant pressure:

$$C^o_p/R = a_1 + a_2 T + a_3 T^2 + a_4 T^3 + a_5 T^4$$

$$H^o/RT = a_1 + (a_2/2)T + (a_3/3)T^2 + (a_4/4)T^3 + (a_5/5)T^4 + (a_6/T)$$

$$S/R = a_1 \ln(T) + a_2 T + (a_3/2)T^2 + (a_4/3)T^3 + (a_5/4)T^4 + a_7$$

These coefficients are stored for two temperature intervals, one between a low temperature and a common temperature, the second between the common temperature and the high temperature. The second line of the database (before any species data) contains the lowest, highest, and default common temperatures. The data for each species occupies four lines (with the line number at the right margin, in column 80) and contains the following information (see Kee et al., 1991 for detailed format information):

Line 1:   Species Name
Date (not used in the code)
up to four atomic symbols and formula
phase of species (S, L, or G for solid, liquid, or gas, respectively)
low temperature
high temperature
common temperature (or blank for default)
fifth atomic symbols and formula (if needed)

Line 2:   Coefficients a1 through a5, for the upper temperature interval

Line 3:   Coefficients a6, a7 for the upper temperature interval and
a1, a2, a3 for the lower temperature interval

Line 4:   Coefficients a4, a5, a6, a7 for the lower temperature interval

```
THERMO
300.        5000.       1000.
NA2O               81092NA  2O   1          S 0300.00   2000.00 1000.00      1
 0.08804423E+02 0.03253428E-01-0.03530522E-05-0.04324117E-08 0.01394574E-11    2
-0.05257507E+06-0.04209654E+03 0.04776964E+02 0.01483269E+00-0.01052247E-03    3
 0.01278469E-07 0.01046187E-10-0.05155651E+06-0.02156737E+03                   4
NAO2               D=37.2NA  1O   2    0     G  300.000  2000.000 1000.00      1
  .24373729D+01  .11708054D-01 -.12465450D-04  .60394798D-08 -.10877028D-11    2
 -.68349080D+04  .15175355D+02  .24373729D+01  .11708054D-01 -.12465450D-04    3
  .60394798D-08 -.10877028D-11 -.68349080D+04  .15175355D+02                   4
HCL                42189CL  1H   1          G  300.000  2000.000 1000.00      1
  .37039792D+01 -.12852596D-02  .24168090D-05 -.12493998D-08  .21730232D-12    2
 -.12167451D+05  .16516317D+01  .37039792D+01 -.12852596D-02  .24168090D-05    3
 -.12493998D-08  .21730232D-12 -.12167451D+05  .16516317D+01                   4
CL                 42189CL  1          G  300.000  2000.000 1000.00      1
  .21819488D+01  .23933914D-02 -.34824719D-05  .19618096D-08 -.38542551D-12    2
  .13858705D+05  .68500574D+01  .21819488D+01  .23933914D-02 -.34824719D-05    3
  .19618096D-08 -.38542551D-12  .13858705D+05  .68500574D+01                   4
CL2                42189CL  2          G  300.000  2000.000 1000.00      1
  .33474856D+01  .35465402D-02 -.41020340D-05  .21051260D-08 -.39180420D-12    2
 -.11234604D+04  .68564007D+01  .33474856D+01  .35465402D-02 -.41020340D-05    3
  .21051260D-08 -.39180420D-12 -.11234604D+04  .68564007D+01                   4
NASO2              EST-VZNA  1S   2    0G  300.000  2000.000 1000.00      1
  .10564578D+02  .12021251D-02  .23902747D-05 -.21589178D-08  .52044716D-12    2
 -.49517463D+05 -.45542840D+02  .10564578D+02  .12021251D-02  .23902747D-05    3
 -.21589178D-08  .52044716D-12 -.49517463D+05 -.45542840D+02                   4
NA2SO4             80792NA  2O   4S         G  300.000  2000.000 1000.00      1
  .45889397D+01  .38040129D-01 -.41096543D-04  .20017107D-07 -.36046429D-11    2
 -.12705639D+06  .58915156D+01  .45889397D+01  .38040129D-01 -.41096543D-04    3
  .20017107D-07 -.36046429D-11 -.12705639D+06  .58915156D+01                   4
NA2SO3             BAR 77NA  2S   1O   3    0L  300.000  2000.000 1000.00      1
  .21890427D+02  .00000000D+00  .00000000D+00  .00000000D+00  .00000000D+00    2
 -.13847832D+06 -.11136788D+03  .21890427D+02  .00000000D+00  .00000000D+00    3
  .00000000D+00  .00000000D+00 -.13847832D+06 -.11136788D+03                   4
NACL               81092CL  1NA  1          G  300.000  2000.000 1000.00      1
  .38609970D+01  .21586897D-02 -.25630874D-05  .13632700D-08 -.26045355D-12    2
 -.23047048D+05  .50924911D+01  .38609970D+01  .21586897D-02 -.25630874D-05    3
  .13632700D-08 -.26045355D-12 -.23047048D+05  .50924911D+01                   4
NAOH               J12/70NA  1O   1H   100  0G  300.000  2000.000 1000.00      1
  .45711116D+01  .61346093D-02 -.76237353D-05  .43706135D-08 -.89064713D-12    2
 -.25359026D+05 -.95321963D-01  .45711116D+01  .61346093D-02 -.76237353D-05    3
  .43706135D-08 -.89064713D-12 -.25359026D+05 -.95321963D-01                   4
NA                 L 4/93NA  100  000  000  0G  300.000  2000.000 1000.00      1
  .25010442D+01  .00000000D+00  .00000000D+00  .00000000D+00  .00000000D+00    2
  .12157060D+05  .42385793D+01  .25010442D+01  .00000000D+00  .00000000D+00    3
  .00000000D+00  .00000000D+00  .12157060D+05  .42385793D+01                   4
```

A-12

```
NAO               J12/67NA  1O   100 000   0G    300.000  2000.000 1000.00      1
  .36192660D+01  .29441938D-02 -.35206654D-05  .18827273D-08 -.36198896D-12    2
  .88821327D+04  .62033018D+01  .36192660D+01  .29441938D-02 -.35206654D-05    3
  .18827273D-08 -.36198896D-12  .88821327D+04  .62033018D+01                   4
NA2CO3(S)         J 3/66NA  2C   1O   3   0S    300.000  2000.000 1000.00      1
  .12014036D+02 -.50536347D-02  .25519440D-04 -.13688606D-07  .27714728D-11    2
 -.13815566D+06 -.48715125D+02  .12014036D+02 -.50536347D-02  .25519440D-04    3
 -.13688606D-07  .27714728D-11 -.13815566D+06 -.48715125D+02                   4
NA2CO3(L)         J 3/66NA  2C   1O   3   0L    300.000  2000.000 1000.00      1
  .22796238D+02  .00000000D+00  .00000000D+00  .00000000D+00  .00000000D+00    2
 -.14229112D+06 -.11622189D+03  .22796238D+02  .00000000D+00  .00000000D+00    3
  .00000000D+00  .00000000D+00 -.14229112D+06 -.11622189D+03                   4
NA2CO3            BENSONNA  2C   1O   3   0G    300.000  2000.000 1000.00      1
  .56157861D+01  .25916438D-01  .25963740D-05 -.15866667D-07  .51192999D-11    2
 -.13627651D+06 -.21019356D+02  .56157861D+01  .25916438D-01  .25963740D-05    3
 -.15866667D-07  .51192999D-11 -.13627651D+06 -.21019356D+02                   4
HSO3              T 3/96H   1S   1O   3   0G    300.000  2000.00  1000.00      1
  .29221355D+01  .24537632D-01 -.28258748D-04  .14728290D-07 -.28007910D-11    2
 -.48042084D+05  .12532987D+02  .29221355D+01  .24537632D-01 -.28258748D-04    3
  .14728290D-07 -.28007910D-11 -.48042084D+05  .12532987D+02                   4
SO2               121286S   1O   2       G    0300.00   5000.00  1000.00      1
 0.05254498E+02 0.01978545E-01-0.08204226E-05 0.15763830E-09-0.11204512E-13    2
-0.03756885E+06-0.11460563E+01 0.02911438E+02 0.08103022E-01-0.06906710E-04    3
 0.03329015E-07-0.08777121E-11-0.03687881E+06 0.11117403E+02                   4
SO3               121286S   1O   3       G    0300.00   5000.00  1000.00      1
 0.07050668E+02 0.03246560E-01-0.14088974E-05 0.02721535E-08-0.01942364E-12    2
-0.05020667E+06-0.11064426E+02 0.02575282E+02 0.15150916E-01-0.12298717E-04    3
 0.04240257E-07-0.05266812E-11-0.04894410E+06 0.12195116E+02                   4
CH3O2       L184      C  1H   3O   2      G    300.000  5000.00  1000.00      1
 0.66812963E 01 0.80057271E-02-0.27188507E-05 0.40631365E-09-0.21927725E-13    2
 0.52621851E 03-0.99423847E 01 0.20986490E 01 0.15786357E-01 0.75683261E-07    3
-0.11274587E-07 0.56665133E-11 0.20695879E 04 0.15007068E 02                   4
CH3O2H      BENSON/Vit C  1H   4O   2     G    300.000  2000.000 1000.00      1
  .70880631D+02 -.34336913D+00  .54005126D-03 -.32136525D-06  .65219886D-10    2
 -.24541521D+05 -.29072672D+03  .70880631D+02 -.34336913D+00  .54005126D-03    3
 -.32136525D-06  .65219886D-10 -.24541521D+05 -.29072672D+03                   4
CH2*        L S/93C   1H   2  00   00G    200.000  3500.000  1000.000         1
 2.29203842E+00 4.65588637E-03-2.01191947E-06 4.17906000E-10-3.39716365E-14    2
 5.09259997E+04 8.62650169E+00 4.19860411E+00-2.36661419E-03 8.23296220E-06    3
-6.68815981E-09 1.94314737E-12 5.04968163E+04-7.69118967E-01 9.93967200E+03    4
HNO2              120186H   1N   1O   2   G    0200.00   6000.00  1000.00      1
 0.57900059E+01 0.36505061E-02-0.12902803E-05 0.20751067E-09-0.12300051E-13    2
-0.11563080E+05-0.40550308E+01 0.32100428E+01 0.81300665E-02 0.16621031E-05    3
-0.95328431E-08 0.48700696E-11-0.10700764E+05 0.98200995E+01                   4
HNO3              121286H   1N   1O   3   G    0300.00   5000.00  1000.00      1
 0.07003844E+02 0.05811493E-01-0.02333788E-04 0.04288814E-08-0.02959385E-12    2
-0.01889952E+06-0.10478628E+02 0.13531850E+01 0.02220024E+00-0.01978811E-03    3
 0.08773908E-07-0.16583844E-11-0.16587346E+06 0.01851868E+03                   4
H2O2+             120186H   2O   2       G    0300.00   5000.00  1000.00      1
 0.04573167E+02 0.04336136E-01-0.14746888E-05 0.02348903E-08-0.14316536E-13    2
-0.01800696E+06 0.05011369E+01 0.03388753E+02 0.06569226E-01-0.14850125E-06    3
-0.04625805E-07 0.02471514E-10-0.01766314E+06 0.06785363E+02                   4
O           L 1/90O   1  00   00   00G    200.000  3500.000  1000.000         1
 2.56942078E+00-8.59741137E-05 4.19484589E-08-1.00177799E-11 1.22833691E-15    2
 2.92175791E+04 4.78433864E+00 3.16826710E+00-3.27931884E-03 6.64306396E-06    3
-6.12806624E-09 2.11265971E-12 2.91222592E+04 2.05193346E+00 6.72540300E+03    4
O2          TPIS89O   2  00   00   00G    200.000  3500.000  1000.000         1
 3.28253784E+00 1.48308754E-03-7.57966669E-07 2.09470555E-10-2.16717794E-14    2
-1.08845772E+03 5.45323129E+00 3.78245636E+00-2.99673416E-03 9.84730201E-06    3
-9.68129509E-09 3.24372837E-12-1.06394356E+03 3.65767573E+00 8.68010400E+03    4
H           L 7/88H   1  00   00   00G    200.000  3500.000  1000.000         1
 2.50000001E+00-2.30842973E-11 1.61561948E-14-4.73515235E-18 4.98197357E-22    2
 2.54736599E+04-4.46682914E-01 2.50000000E+00 7.05332819E-13-1.99591964E-15    3
 2.30081632E-18-9.27732332E-22 2.54736599E+04-4.46682853E-01 6.19742800E+03    4
H2          TPIS78H   2  00   00   00G    200.000  3500.000  1000.000         1
 3.33727920E+00-4.94024731E-05 4.99456778E-07-1.79566394E-10 2.00255376E-14    2
-9.50158922E+02-3.20502331E+00 2.34433112E+00 7.98052075E-03-1.94781510E-05    3
 2.01572094E-08-7.37611761E-12-9.17935173E+02 6.83010238E-01 8.46810200E+03    4
```

A-13

```
OH                RUS 78O   1H   1    00    00G   200.000  3500.000  1000.000      1
 3.09288767E+00 5.48429716E-04 1.26505228E-07-8.79461556E-11 1.17412376E-14       2
 3.85865700E+03 4.47669610E+00 3.99201543E+00-2.40131752E-03 4.61793841E-06       3
-3.88113333E-09 1.36411470E-12 3.61508056E+03-1.03925458E-01 8.81310600E+03       4
H2O               L 8/89H   2O   1    00    00G   200.000  3500.000  1000.000      1
 3.03399249E+00 2.17691804E-03-1.64072518E-07-9.70419870E-11 1.68200992E-14       2
-3.00042971E+04 4.96677010E+00 4.19864056E+00-2.03643410E-03 6.52040211E-06       3
-5.48797062E-09 1.77197817E-12-3.02937267E+04-8.49032208E-01 9.90409200E+03       4
HO2               L 5/89H   1O   2    00    00G   200.000  3500.000  1000.000      1
 4.01721090E+00 2.23982013E-03-6.33658150E-07 1.14246370E-10-1.07908535E-14       2
 1.11856713E+02 3.78510215E+00 4.30179801E+00-4.74912051E-03 2.11582891E-05       3
-2.42763894E-08 9.29225124E-12 2.94808040E+02 3.71666245E+00 1.00021620E+04       4
H2O2              L 7/88H   2O   2    00    00G   200.000  3500.000  1000.000      1
 4.16500285E+00 4.90831694E-03-1.90139225E-06 3.71185986E-10-2.87908305E-14       2
-1.78617877E+04 2.91615662E+00 4.27611269E+00-5.42822417E-04 1.67335701E-05       3
-2.15770813E-08 8.62454363E-12-1.77025821E+04 3.43505074E+00 1.11588350E+04       4
C                 L11/88C   1    00    00    00G   200.000  3500.000  1000.000      1
 2.49266888E+00 4.79889284E-05-7.24335020E-08 3.74291029E-11-4.87277893E-15       2
 8.54512953E+04 4.80150373E+00 2.55423955E+00-3.21537724E-04 7.33792245E-07       3
-7.32234889E-10 2.66521446E-13 8.54438832E+04 4.53130848E+00 6.53589500E+03       4
CH                TPIS79C   1H   1    00    00G   200.000  3500.000  1000.000      1
 2.87846473E+00 9.70913681E-04 1.44445655E-07-1.30687849E-10 1.76079383E-14       2
 7.10124364E+04 5.48497999E+00 3.48981665E+00 3.23835541E-04-1.68899065E-06       3
 3.16217327E-09-1.40609067E-12 7.07972934E+04 2.08401108E+00 8.62500000E+03       4
CH2               L S/93C   1H   2    00    00G   200.000  3500.000  1000.000      1
 2.87410113E+00 3.65639292E-03-1.40894597E-06 2.60179549E-10-1.87727567E-14       2
 4.62636040E+04 6.17119324E+00 3.76267867E+00 9.68872143E-04 2.79489841E-06       3
-3.85091153E-09 1.68741719E-12 4.60040401E+04 1.56253185E+00 1.00274170E+04       4
CH2(S)            L S/93C   1H   2    00    00G   200.000  3500.000  1000.000      1
 2.29203842E+00 4.65588637E-03-2.01191947E-06 4.17906000E-10-3.39716365E-14       2
 5.09259997E+04 8.62650169E+00 4.19860411E+00-2.36661419E-03 8.23296220E-06       3
-6.68815981E-09 1.94314737E-12 5.04968163E+04-7.69118967E-01 9.93967200E+03       4
CH3               L11/89C   1H   3    00    00G   200.000  3500.000  1000.000      1
 2.28571772E+00 7.23990037E-03-2.98714348E-06 5.95684644E-10-4.67154394E-14       2
 1.67755843E+04 8.48007179E+00 3.67359040E+00 2.01095175E-03 5.73021856E-06       3
-6.87117425E-09 2.54385734E-12 1.64449988E+04 1.60456433E+00 1.03663400E+04       4
CH4               L 8/88C   1H   4    00    00G   200.000  3500.000  1000.000      1
 7.48514950E-02 1.33909467E-02-5.73285809E-06 1.22292535E-09-1.01815230E-13       2
-9.46834459E+03 1.84373180E+01 5.14987613E+00-1.36709788E-02 4.91800599E-05       3
-4.84743026E-08 1.66693956E-11-1.02466476E+04-4.64130376E+00 1.00161980E+04       4
CO                TPIS79C   1O   1    00    00G   200.000  3500.000  1000.000      1
 2.71518561E+00 2.06252743E-03-9.98825771E-07 2.30053008E-10-2.03647716E-14       2
-1.41518724E+04 7.81868772E+00 3.57953347E+00-6.10353680E-04 1.01681433E-06       3
 9.07005884E-10-9.04424499E-13-1.43440860E+04 3.50840928E+00 8.67100000E+03       4
CO2               L 7/88C   1O   2    00    00G   200.000  3500.000  1000.000      1
 3.85746029E+00 4.41437026E-03-2.21481404E-06 5.23490188E-10-4.72084164E-14       2
-4.87591660E+04 2.27163806E+00 2.35677352E+00 8.98459677E-03-7.12356269E-06       3
 2.45919022E-09-1.43699548E-13-4.83719697E+04 9.90105222E+00 9.36546900E+03       4
HCO               L12/89H   1C   1O   1    00    00G   200.000  3500.000  1000.000      1
 2.77217438E+00 4.95695526E-03-2.48445613E-06 5.89161778E-10-5.33508711E-14       2
 4.01191815E+03 9.79834492E+00 4.22118584E+00-3.24392532E-03 1.37799446E-05       3
-1.33144093E-08 4.33768865E-12 3.83956496E+03 3.39437243E+00 9.98945000E+03       4
CH2O              L 8/88H   2C   1O   1    00    00G   200.000  3500.000  1000.000      1
 1.76069008E+00 9.20000082E-03-4.42258813E-06 1.00641212E-09-8.83855640E-14       2
-1.39958323E+04 1.36563230E+01 4.79372315E+00-9.90833369E-03 3.73220008E-05       3
-3.79285261E-08 1.31772652E-11-1.43089567E+04 6.02812900E-01 1.00197170E+04       4
CH2OH             GUNL93C   1H   3O   1    00    00G   200.000  3500.000  1000.000      1
 3.69266569E+00 8.64576797E-03-3.75101120E-06 7.87234636E-10-6.48554201E-14       2
-3.24250627E+03 5.81043215E+00 3.86388918E+00 5.59672304E-03 5.93271791E-06       3
-1.04532012E-08 4.36967278E-12-3.19391367E+03 5.47302243E+00 1.18339080E+04       4
CH3O              121686C   1H   3O   1    00    00G   300.00   3000.00   1000.000   1
 0.03770799E+02 0.07871497E-01-0.02656384E-04 0.03944431E-08-0.02112616E-12       2
 0.12783252E+03 0.02929575E+02 0.02106204E+02 0.07216595E-01 0.05338472E-04       3
-0.07377636E-07 0.02075610E-10 0.09786011E+04 0.13152177E+02                     4
CH3OH             L 8/88C   1H   4O   1    00    00G   200.000  3500.000  1000.000      1
 1.78970791E+00 1.40938292E-02-6.36500835E-06 1.38171085E-09-1.17060220E-13       2
-2.53748747E+04 1.45023623E+01 5.71539582E+00-1.52309129E-02 6.52441155E-05       3
-7.10806889E-08 2.61352698E-11-2.56427656E+04-1.50409823E+00 1.14352770E+04       4
C2H               L 1/91C   2H   1    00    00G   200.000  3500.000  1000.000      1
 3.16780652E+00 4.75221902E-03-1.83787077E-06 3.04190252E-10-1.77232770E-14       2
 6.71210650E+04 6.63589475E+00 2.88965733E+00 1.34099611E-02-2.84769501E-05       3
 2.94791045E-08-1.09331511E-11 6.68393932E+04 6.22296438E+00 1.04544720E+04       4
C2H2              L 1/91C   2H   2    00    00G   200.000  3500.000  1000.000      1
 4.14756964E+00 5.96166664E-03-2.37294852E-06 4.67412171E-10-3.61235213E-14       2
 2.59359992E+04-1.23028121E+00 8.08681094E-01 2.33615629E-02-3.55171815E-05       3
 2.80152437E-08-8.50072974E-12 2.64289807E+04 1.39397051E+01 1.00058390E+04       4
C2H3              L 2/92C   2H   3    00    00G   200.000  3500.000  1000.000      1
 3.01672400E+00 1.03302292E-02-4.68082349E-06 1.01763288E-09-8.62607041E-14       2
 3.46128739E+04 7.78732378E+00 3.21246645E+00 1.51479162E-03 2.59209412E-05       3
-3.57657847E-08 1.47150873E-11 3.48598468E+04 8.51054025E+00 1.05750490E+04       4
```

A-14

```
C2H4              L 1/91C   2H   4    00   00G   200.000  3500.000  1000.000    1
 2.03611116E+00 1.46454151E-02-6.71077915E-06 1.47222923E-09-1.25706061E-13    2
 4.93988614E+03 1.03053693E+01 3.95920148E+00-7.57052247E-03 5.70990292E-05    3
-6.91588753E-08 2.69884373E-11 5.08977593E+03 4.09733096E+00 1.05186890E+04    4
C2H5              L12/92C   2H   5    00   00G   200.000  3500.000  1000.000    1
 1.95465642E+00 1.73972722E-02-7.98206668E-06 1.75217689E-09-1.49641576E-13    2
 1.28575200E+04 1.34624343E+01 4.30646568E+00-4.18658892E-03 4.97142807E-05    3
-5.99126606E-08 2.30509004E-11 1.28416265E+04 4.70720924E+00 1.21852440E+04    4
C2H6              L 8/88C   2H   6    00   00G   200.000  3500.000  1000.000    1
 1.07188150E+00 2.16852677E-02-1.00256067E-05 2.21412001E-09-1.90002890E-13    2
-1.14263932E+04 1.51156107E+01 4.29142492E+00-5.50154270E-03 5.99438288E-05    3
-7.08466285E-08 2.68685771E-11-1.15222055E+04 2.66682316E+00 1.18915940E+04    4
CH2CO             L 5/90C   2H   2O   1    00G   200.000  3500.000  1000.000    1
 4.51129732E+00 9.00359745E-03-4.16939635E-06 9.23345882E-10-7.94838201E-14    2
-7.55105311E+03 6.32247205E-01 2.13583630E+00 1.81188721E-02-1.73947474E-05    3
 9.34397568E-09-2.01457615E-12-7.04291804E+03 1.22156480E+01 1.17977430E+04    4
HCCO              SRIC91H   1C   2O   1    00G   300.00   4000.00   1000.000    1
 0.56282058E+01 0.40853401E-02-0.15934547E-05 0.28626052E-09-0.19407832E-13    2
 0.19327215E+05-0.39302595E+01 0.22517214E+01 0.17655021E-01-0.23729101E-04    3
 0.17275759E-07-0.50664811E-11 0.20059449E+05 0.12490417E+02                   4
HCCOH             SRI91C   2O   1H   2    00G   300.000  5000.000  1000.000    1
 0.59238291E+01 0.67923600E-02-0.25658564E-05 0.44987841E-09-0.29940101E-13    2
 0.72646260E+04-0.76017742E+01 0.12423733E+01 0.31072201E-01-0.50866864E-04    3
 0.43137131E-07-0.14014594E-10 0.80316143E+04 0.13874319E+02                   4
H2CN              41687H   2C   1N   1    00G   300.00   4000.000  1000.000     1
 0.52097030E+01 0.29692911E-02-0.28555891E-06-0.16355500E-09 0.30432589E-13    2
 0.27677109E+05-0.44444780E+01 0.28516610E+01 0.56952331E-02 0.10711400E-05    3
-0.16226120E-08-0.23511081E-12 0.28637820E+05 0.89927511E+01 0.00000000E+00    4
HCN               L 7/88H   1C   1N   1    00G   200.000  6000.000  1000.000    1
 0.38022392E+01 0.31464228E-02-0.10632185E-05 0.16619757E-09-0.97997570E-14    2
 0.14910512E+05 0.15754601E+01 0.22589886E+01 0.10051170E-01-0.13351763E-04    3
 0.10092349E-07-0.30089028E-11 0.15215853E+05 0.89164419E+01 0.16236675E+05    4
HNO               And93 H   1N   1O   1    00G   200.000  6000.000  1000.000    1
 0.29792509E+01 0.34944059E-02-0.78549778E-06 0.57479594E-10-0.19335916E-15    2
 0.11750582E+05 0.86063728E+01 0.45334916E+01-0.56696171E-02 0.18473207E-04    3
-0.17137094E-07 0.55454573E-11 0.11548297E+05 0.17498417E+01 0.12271667E+05    4
N                 L 6/88N   1    00   00   00G   200.000  6000.000  1000.000    1
 0.24159429E+01 0.17489065E-03-0.11902369E-06 0.30226245E-10-0.20360982E-14    2
 0.56133773E+05 0.46496096E+01 0.25000000E+01 0.00000000E+00 0.00000000E+00    3
 0.00000000E+00 0.00000000E+00 0.56104637E+05 0.41939087E+01 0.56850012E+05    4
NNH               T07/93N   2H   1    00   00G   200.000  6000.000  1000.000    1
 0.37667544E+01 0.28915082E-02-0.10416620E-05 0.16842594E-09-0.10091896E-13    2
 0.28650697E+05 0.44705067E+01 0.43446927E+01-0.48497072E-02 0.20059459E-04    3
-0.21726464E-07 0.79469539E-11 0.28791973E+05 0.29779410E+01 0.30009828E+05    4
N2O               L 7/88N   2O   1    00   00G   200.000  6000.000  1000.000    1
 0.48230729E+01 0.26270251E-02-0.95850874E-06 0.16000712E-09-0.97752303E-14    2
 0.80734048E+04-0.22017207E+01 0.22571502E+01 0.11304728E-01-0.13671319E-04    3
 0.96819806E-08-0.29307182E-11 0.87417744E+04 0.10757992E+02 0.98141680E+04    4
NH                And94 N   1H   1    00   00G   200.000  6000.000  1000.000    1
 0.27836928E+01 0.13298430E-02-0.42478047E-06 0.78348501E-10-0.55044470E-14    2
 0.42120848E+05 0.57407799E+01 0.34929085E+01 0.31179198E-03-0.14890484E-05    3
 0.24816442E-08-0.10356967E-11 0.41880629E+05 0.18483278E+01 0.40758266E+05    4
NH2               And89 N   1H   2    00   00G   200.000  6000.000  1000.000    1
 0.28347421E+01 0.32073082E-02-0.93390804E-06 0.13702953E-09-0.79206144E-14    2
 0.22171957E+05 0.65204163E+01 0.42040029E+01-0.21061385E-02 0.71068348E-05    3
-0.56115197E-08 0.16440717E-11 0.21885910E+05-0.14184248E+00 0.22851617E+05    4
NH3               J 6/77N   1H   3    00   00G   200.000  6000.000  1000.000    1
 0.26344521E+01 0.56662560E-02-0.17278676E-05 0.23867161E-09-0.12578786E-13    2
-0.65446958E+04 0.65662928E+01 0.42860274E+01-0.46605230E-02 0.21718513E-04    3
-0.22808887E-07 0.82638046E-11-0.67417285E+04-0.62537277E+00-0.55202866E+04    4
NO                RUS 78N   1O   1    00   00G   200.000  6000.000  1000.000    1
 0.32606056E+01 0.11911043E-02-0.42917048E-06 0.69457669E-10-0.40336099E-14    2
 0.99209746E+04 0.63693027E+01 0.42184763E+01-0.46389760E-02 0.11041022E-04    3
-0.93361354E-08 0.28035770E-11 0.98446230E+04 0.22808464E+01 0.10976594E+05    4
NO2               L 7/88N   1O   2    00   00G   200.000  6000.000  1000.000    1
 0.48847542E+01 0.21723956E-02-0.82806906E-06 0.15747510E-09-0.10510895E-13    2
 0.23164983E+04-0.11741695E+00 0.39440312E+01-0.15854290E-02 0.16657812E-04    3
-0.20475426E-07 0.78350564E-11 0.28966179E+04 0.63119917E+01 0.41124702E+04    4
HCNO              BDEA94H   1N   1C   1O   1G   300.000  5000.000  1382.000     1
 6.59860456E+00 3.02778626E-03-1.07704346E-06 1.71666528E-10-1.01439391E-14    2
 1.79661339E+04-1.03306599E+01 2.64727989E+00 1.27505342E-02-1.04794236E-05    3
 4.41432836E-09-7.57521466E-13 1.92990252E+04 1.07332972E+01                   4
HOCN              BDEA94H   1N   1C   1O   1G   300.000  5000.000  1368.000     1
 5.89784885E+00 3.16789393E-03-1.11801064E-06 1.77243144E-10-1.04339177E-14    2
-3.70653331E+03-6.18167825E+00 3.78604952E+00 6.88667922E-03-3.21487864E-06    3
 5.17195767E-10 1.19360788E-14-2.82698400E+03 5.63292162E+00                   4
HNCO              BDEA94H   1N   1C   1O   1G   300.000  5000.000  1478.000     1
 6.22395134E+00 3.17864004E-03-1.09378755E-06 1.70735163E-10-9.95021955E-15    2
-1.66599344E+04-8.38224741E+00 3.63096317E+00 7.30282357E-03-2.28050003E-06    3
-6.61271298E-10 3.62235752E-13-1.55873636E+04 6.19457727E+00                   4
```

A-15

```
NCO               EA 93 N   1C   1O   1   00G   200.000  6000.000  1000.000     1
 0.51521845E+01 0.23051761E-02-0.88033153E-06 0.14789098E-09-0.90977996E-14     2
 0.14004123E+05-0.25442660E+01 0.28269308E+01 0.88051688E-02-0.83866134E-05     3
 0.48016964E-08-0.13313595E-11 0.14682477E+05 0.95504646E+01 0.21347373E+05     4
CN                HBH92 C   1N   1   00   00G   200.000  6000.000  1000.000     1
 0.37459805E+01 0.43450775E-04 0.29705984E-06-0.68651806E-10 0.44134173E-14     2
 0.51536188E+05 0.27867601E+01 0.36129351E+01-0.95551327E-03 0.21442977E-05     3
-0.31516323E-09-0.46430356E-12 0.51708340E+05 0.39804995E+01 0.52954172E+05     4
HCNN              SRI/94C   1N   2H   1   00G   300.000  5000.000  1000.000     1
 0.58946362E+01 0.39895959E-02-0.15982380E-05 0.29249395E-09-0.20094686E-13     2
 0.53452941E+05-0.51030502E+01 0.25243194E+01 0.15960619E-01-0.18816354E-04     3
 0.12125540E-07-0.32357378E-11 0.54261984E+05 0.11675870E+02                    4
N2                121286N   2              00G   300.000  5000.000  1000.000     1
 0.02926640E+02 0.14879768E-02-0.05684760E-05 0.10097038E-09-0.06753351E-13     2
-0.09227977E+04 0.05980528E+02 0.03298677E+02 0.14082404E-02-0.03963222E-04     3
 0.05641515E-07-0.02444854E-10-0.10208999E+04 0.03950372E+02                    4
AR                120186AR  1              00G   300.000  5000.000  1000.000     1
 0.02500000E+02 0.00000000E+00 0.00000000E+00 0.00000000E+00 0.00000000E+00     2
-0.07453750E+04 0.04366000E+02 0.02500000E+02 0.00000000E+00 0.00000000E+00     3
 0.00000000E+00 0.00000000E+00-0.07453750E+04 0.04366000E+02                    4
N2H2              121286N   2H   2         00G   300.000  5000.000  1000.000     1
 0.03371185E+02 0.06039968E-01-0.02303853E-04 0.04062789E-08-0.02713144E-12     2
 0.02418172E+06 0.04980585E+02 0.16179994E+01 0.13063122E-01-0.01715711E-03     3
 0.16056079E-07-0.06093638E-10 0.02467526E+06 0.13794670E+02                    4
C2N2              121286C   2N   2         00G   300.000  5000.000  1000.000     1
 0.06548002E+02 0.03984707E-01-0.16342164E-05 0.03038596E-08-0.02111069E-12     2
 0.03490716E+06-0.09735790E+02 0.04265459E+02 0.11922569E-01-0.13420142E-04     3
 0.09192297E-07-0.02778941E-10 0.03547887E+06 0.01713212E+02                    4
H2NO              102290H   2N   1O   1    00G   300.000  4000.00   1500.000     1
 0.05673346E+02 0.02298837E-01-0.01774446E-05-0.01103482E-08 0.01859762E-12     2
 0.05569325E+05-0.06153540E+02 0.02530590E+02 0.08596035E-01-0.05471030E-04     3
 0.02276249E-07-0.04648073E-11 0.06868030E+05 0.01126651E+03                    4
END
```

A-16

Appendix 3. Thermodynamic database for sodium compounds.

(Heats of formation, entropies, and thermal conductivities at different temperatures in kcal/cal/mol/K Units)

SPECIES	HF(298)	S (298)	CP300	CP500	CP800	CP1000	CP1500	CP2000	COMMENTS
ELEMENTS									
Na2CO3	-265.20	37.14	26.31	34.89	43.69	46.46	45.11	45.33	BENSON
NA 2 C 1 O 3 0 G									
NAO2	-11.30	63.69	9.90	11.65	12.86	13.18	13.57	13.72	D=37.2
NA 1 O 2 0 G									
NASO2	-92.00	30.00	22.03	22.90	24.17	24.88	26.02	27.00	EST-VZ
NA 1 S 1 O 2 0 G									
Na	25.64	36.74	4.97	4.97	4.97	4.97	4.97	4.97	L 4/93
NA 1. 0. 0. G									
Na+	145.63	35.36	4.97	4.97	4.97	4.97	4.97	4.97	J12/83
NA 1. E -1. 0. G									
NaALF4	-439.99	82.44	24.91	28.56	30.37	30.86	31.36	31.58	J12/79
NA 1. AL 1. F 4. 0. G									
NaBO2	-155.00	68.66	13.96	16.07	17.72	18.32	19.06	19.43	J 6/71
NA 1. B 1. O 2. 0. G									
NaBr	-34.40	57.65	8.69	8.92	9.04	9.10	9.21	9.31	J 9/64
NA 1. BR 1. 0. 0. G									
NaCN	22.53	58.17	12.01	12.71	13.40	13.75	14.26	14.53	J3/66
NA 1. C 1. N 1. 0. G									
NaCL	-43.36	54.92	8.56	8.85	9.00	9.06	9.17	9.26	J12/64
NA 1. CL 1. 0. 0. G									
NaF	-69.42	52.01	8.19	8.68	8.92	9.01	9.14	9.25	J12/68
NA 1. F 1. 0. 0. G									
NaF2-	-160.00	59.92	13.14	14.13	14.57	14.69	14.80	14.85	J12/68
NA 1. F 2. E 1. 0. G									
NaH	29.70	45.02	7.24	7.91	8.54	8.77	9.09	9.30	J 3/63
NA 1. H 1. 0. 0. G									
NaI	-21.30	59.52	8.77	8.95	9.06	9.12	9.23	9.34	L 6/72
NA 1. I 1. 0. 0. G									
NaO	20.00	54.77	8.41	8.80	9.00	9.08	9.21	9.33	J12/67
NA 1. O 1. 0. 0. G									
NaO-	-29.00	51.98	8.39	8.79	9.00	9.08	9.22	9.34	J12/67
NA 1. O 1. E 1. 0. G									
NaOH	-47.26	54.60	11.59	12.39	12.82	13.07	13.63	14.03	J12/70
NA 1. O 1. H 1. 0. G									
NaOH+	162.00	57.99	11.80	12.48	12.86	13.11	13.66	14.05	J12/71
NA 1. O 1. H 1. E -1. G									
Na2	33.95	55.03	8.98	9.16	9.38	9.41	8.43	7.91	J12/83
NA 2. 0. 0. 0. G									
Na2C2N2	-2.10	82.97	25.78	27.35	28.77	29.48	30.50	31.05	J 3/66
NA 2. C 2. N 2. 0. G									
Na2CL2	-135.29	77.78	18.85	19.49	19.72	19.77	19.83	19.85	J12/64
NA 2. CL 2. 0. 0. G									
Na2F2	-202.30	68.69	16.99	18.69	19.38	19.56	19.72	19.80	J12/68
NA 2. F 2. 0. 0. G									
Na2O	-9.90	62.43	13.27	14.19	14.60	14.71	14.81	14.86	L10/74
NA 2. O 1. 0. 0. G									
Na2O2H2	-145.20	73.47	18.99	22.24	25.16	26.38	28.36	29.56	J12/70
NA 2. O 2. H 2. 0. G									
Na2SO4	-247.04	82.90	25.32	31.12	34.64	35.67	36.76	37.25	J 6/78
NA 2. S 1. O 4. 0. G									
Na(cr)	.00	12.26	6.76	11.32	45.19	100.09	.00	.00	CODA89
NA 1. 0. 0. 0. C									
Na(L)	.58	13.80	7.77	7.32	6.92	6.88	7.62	9.58	CODA89
NA 1. 0. 0. 0. C									
NaALO2(b)	-271.02	15.93	21.70	22.39	23.60	24.45	26.59	28.62	J 3/63
NA 1. AL 1. O 2. 0. C									
NaBr(s)	-86.38	20.75	12.31	13.11	13.99	14.60	16.57	19.63	J 9/64
NA 1. BR 1. 0. 0. C									
NaBr(L)	-81.10	24.94	14.90	14.90	14.90	14.90	14.90	14.90	J 9/64
NA 1. BR 1. 0. 0. C									
NaCN(s)	-21.67	28.31	16.39	16.44	16.51	16.37	11.78	-10.59	J 3/66
NA 1. C 1. N 1. 0. C									
NaCN(L)	-20.94	28.20	19.00	19.00	19.00	19.00	19.00	19.00	J 3/66
NA 1. C 1. N 1. 0. C									
NaCL(s)	-98.26	17.24	12.08	12.88	14.17	15.50	12.44	-23.81	J 9/64
NA 1. CL 1. 0. 0. C									
NaCL(L)	-95.37	16.07	21.34	19.72	17.95	17.14	16.04	15.79	J 9/64
NA 1. CL 1. 0. 0. C									
NaF(s)	-137.52	12.25	11.23	12.26	13.31	14.22	17.00	13.15	J12/68
NA 1. F 1. 0. 0. C									
NaF(L)	-134.21	10.30	20.07	19.14	18.00	17.41	16.38	15.85	J12/68
NA 1. F 1. 0. 0. C									
NaI(s)	-68.80	23.54	12.50	13.16	13.98	14.51	15.46	13.65	J 9/63

```
NA 1. I 1.    0.    0. C
 NaI(L)     -64.45    27.07    15.50  15.50  15.50  15.50  15.50  15.50    J 9/63
NA 1. I 1.    0.    0. C
 NaOH(a)   -101.78    15.45    14.28  18.02  18.68 -12.90 ****** ******    J12/70
NA 1. O  1. H  1.    0. C
 NaOH(L)    -99.51    18.34    19.98  20.52  20.33  20.02  19.36  18.70    J12/70
NA 1. O  1. H  1.    0. C
 NaO2(s)    -62.30    27.70    17.26  19.21  22.14  24.10  28.98  33.87    J 6/63
NA 1. O  2.    0.    0. C
 Na2CO3(I) -270.26    33.17    26.59  33.99  50.76  58.60 -38.57 ******    J 3/66
NA 2. C  1. O  3.    0. C
 Na2CO3(II)-267.47    38.25    24.74  28.46  36.65  42.83  58.99  77.14    J 3/66
NA 2. C  1. O  3.    0. C
 Na2CO3(L) -269.25    27.15    45.30  45.30  45.30  45.30  45.30  45.30    J 3/66
NA 2. C  1. O  3.    0. C
 NA2CRO4(1)-317.60    44.40    34.19  40.88  50.92  57.61  74.34  91.07    BAR 77
NA 2. CR 1. O  4.    0. S
 NA2CRO4(2)-315.79    46.19    39.54  42.01  45.70  48.17  54.34  60.50    BAR 77
NA 2. CR 1. O  4.    0. S
 NA2CRO4(L)-313.57    44.43    48.90  48.90  48.90  48.90  48.90  48.90    BAR 77
NA 2. CR 1. O  4.    0. L
 NA2CR2O4(S-418.40    38.81    42.82  47.20  50.30  51.99  55.82  59.50    BAR 77
NA 2. CR 2. O  4.    0. S
 NA2FE2O4(S-318.00    42.20    49.61  50.88  52.79  54.06  57.24  60.42    BAR 73
NA 2. FE 2. O  4.    0. S
 Na2O(c)    -99.90    17.93    16.54  19.45  21.83  22.69  18.43 -47.25    J 6/68
NA 2. O  1.    0.    0. C
 Na2O(a)    -45.04   130.88   ****** -85.47  -8.96  15.33  25.82 148.68    J 6/68
NA 2. O  1.    0.    0. C
 Na2O(L)    -89.11    21.90    25.00  25.00  25.00  25.00  25.00  25.00    J 6/68
NA 2. O  1.    0.    0. C
 Na2O2(a)  -122.66    22.66    21.37  24.80  27.66  28.92  22.51 -35.13    J 6/68
NA 2. O  2.    0.    0. C
 Na2O2(b)  -122.33    21.87    27.15  27.15  27.15  27.15  27.15  27.15    J 6/68
NA 2. O  2.    0.    0. C
 Na2S(1)    -87.50    23.00    19.80  20.50  21.53  22.19  95.76 131.76    J 3/78
NA 2. S  1.    0.    0. C
 Na2S(2)   *******  *******   ****** ****** ****** ****** -44.25 ******    J 3/78
NA 2. S  1.    0.    0. C
 Na2S(L)    -78.47    28.74    22.00  22.00  22.00  22.00  22.00  22.00    J 3/78
NA 2. S  1.    0.    0. C
 NA2SO3(S) -260.38    34.90    28.72  30.80  33.92  36.00  41.20  46.40    BAR 77
NA 2. S  1. O  3.    0. S
 NA2SO3(L) -262.21    26.54    43.50  43.50  43.50  43.50  43.50  43.50    BAR 77
NA 2. S  1. O  3.    0. L
 Na2SO4(V) -331.69    35.75    30.71  38.18  74.07 167.97    .00    .00    J 6/78
NA 2. S  1. O  4.    0. C
 Na2SO4(IV)-331.65    35.81    31.25  37.98  46.22  50.48    .00    .00    J 6/78
NA 2. S  1. O  4.    0. C
 Na2SO4(I) -330.03    38.30    38.01  40.63  44.76  47.87  55.45  62.80    J 6/78
NA 2. S  1. O  4.    0. C
 Na2SO4(L)    .00      .00      .00    .00    .00    .00  47.09  47.09    J 6/78
NA 2. S  1. O  4.    0. C
 NA2SIO3(S)-373.19    27.21    26.85  33.41  37.78  40.09  43.41 -68.88    BAR 73
NA 2. SI 1. O  3.    0. S
 NA2SIO3(L)-365.98    25.96    42.38  42.38  42.38  42.38  42.38  42.38    BAR 73
NA 2. SI 1. O  3.    0. L
 NA2SI2O5(2-602.57    15.20    70.00  70.00  70.00  70.00  70.00  70.00    BAR77
NA 2. SI 2. O  5.    0. S
 NA2SI2O5(3-602.42    15.35    70.00  70.00  70.00  70.00  70.00  70.00    BAR77
NA 2. SI 2. O  5.    0. S
 NA2SI2O5(L-587.49    32.96    62.43  62.43  62.43  62.43  62.43  62.43    BAR77
NA 2. SI 2. O  5.    0. L
 NA2TIO3(1)-376.70    29.10    31.40  35.54  41.76  45.91  56.27  66.64    BAR 77
NA 2. TI 1. O  3.    0. S
 NA2TIO3(2)-376.08    30.31    31.05  34.45  39.55  42.95  51.45  59.95    BAR 77
NA 2. TI 1. O  3.    0. S
 NA2TIO3(L)-366.66    29.39    46.90  46.90  46.90  46.90  46.90  46.90    BAR 77
NA 2. TI 1. O  3.    0. L
 NA2V2O6(S)-550.39    54.43    48.05  57.82  61.31  62.42  63.91  64.91    BAR 73
NA 2. V  2. O  6.    0. S
 Na3ALF6(b)-785.68    69.00    43.24  50.29  61.17  68.63  88.06 112.65    J12/79
NA 3. AL 1. F  6.    0. C
 Na3ALF6(L)-792.45    34.31    94.52  94.52  94.52  94.52  94.52  94.52    J12/79
NA 3. AL 1. F  6.    0. C
 NA4SIO4(S)-503.50    46.80    44.18  47.73  53.05  56.60  65.47  74.34    BAR 77
NA 4. SI 1. O  4.    0. S
 NA4SIO4(L)-498.61    40.46    62.00  62.00  62.00  62.00  62.00  62.00    BAR 77
NA 4. SI 1. O  4.    0. L
 NA4V2O7(S)-701.39    76.13    65.37  76.22  81.33  83.52  87.71  91.41    BAR 73
```

```
NA 4. V  2. O  7.    0. S
 NA6SI2O7(S-856.30    83.32    73.34   83.73   94.75  101.60  118.20  134.60           BAR 73
NA 6. SI 2. O  7.    0. S
 NA6V2O8(S)-845.10    90.63    82.69   94.62  101.35  104.62  111.51  117.91           BAR 73
NA 6. V  2. O  8.    0. S
```